Dissecting the Role of TGFß in Pancreatic Ductal Adenocarcinoma

by
DALE M. WATT

September 2021

A thesis submitted for the degree of Doctor of Philosophy in the Institute of Cancer Sciences, College of Medical, Veterinary, and Life Sciences, The University of Glasgow

CRUK Beatson Institute
Garscube Estate
Switchback Road
Glasgow
G61 1BD
United Kingdom

Abstract

Pancreatic Cancer is a disease of unmet clinical need with near uniform lethality. Genome sequencing of patient tumour samples has highlighted the transforming growth factor beta (TGFß) signalling pathway to be one of the most dysregulated in pancreatic ductal adenocarcinoma (PDAC). TGFß is proposed to drive tumour suppression through blockade of cell proliferation, while also having the capacity to induce epithelial mesenchymal transition (EMT) aiding cell escape and drug resistance. Further, it has potent effects as an immune suppressor and as an activator of fibroblasts, particularly pertinent in PDAC due to the abundance of cancer-associated fibroblast (CAF) infiltrate and extracellular matrix (ECM) deposition. Therefore, using a dual recombinase (DR) mouse model of PDAC I interrogated the function of TGFß across multiple cell types at both tumour initiating time points and in established tumours.

I have demonstrated that TGFß is a potent tumour suppressor, with deletion of the essential receptor component *Alk5* accelerating oncogenic *Kras*^{G12D}-driven tumourigenesis in pre-neoplastic pancreatic lesions, with development of PDAC noted. This novel model develops only pancreatic tumours and replicates the stepwise acquisition of genetic permutations observed in the progression of human disease, through the tamoxifen-controlled deletion of *Alk5* in adult pancreas tissue. Previous *Alk5* deleted models developed squamous stomach and skin tumours complicating their use in studying PDAC.

Altered biology was detected between the *Alk5* deletion driven tumours compared to *Pdx1-Flippase; FSF-Kras*$^{G12D/+}$*; Trp53*$^{frt/+}$ (KPF) mouse tumours, highlighted through RNA sequencing of bulk tumour. Deletion of *ALK5,* or other components of the TGFß signalling pathway, alongside oncogenic *KRAS,* is present in a large subset of PDAC patients, with the *Alk5* depleted model potentially re-capitulating these tumours, thereby providing a pre-clinical model to test therapeutics. For instance, Gene Set Enrichment Analysis (GSEA) highlighted elevated p53 pathway enrichment and decreased enrichment of EMT genes in the *Alk5* deleted model. Deletion of *Alk5* in the cancer epithelium of established tumours in the KPF mice reduced the metastatic burden, although did not affect survival, with deletion of *Tgfb1* showing similar findings. These

findings may be indicative of the pro-tumourigenic role of TGFß signalling in EMT.

Stromal targeted therapies have had mixed efficacy in PDAC, with pre-clinical findings failing to be translated into human trials. I show that depletion of *Alk5* or *Tgfb1* across all CAFs, or in restricted population of myofibroblasts (myCAF) in established tumours does not affect survival. Although, deletion of *Tgfb1* in the restricted myCAF population, but not across all fibroblasts, does alter the CAF population, reducing the abundance of myCAFs specifically. These findings indicated a dependence on fibroblast-derived, TGFß mediated paracrine stromal crosstalk for maintaining myCAF populations in PDAC.

Neutrophils have been shown to play a role in the metastatic cascade of PDAC, with depletion reducing metastatic burden. TGFß has been proposed to polarize neutrophils to a tumour promoting phenotype. I therefore investigated the neutrophil specific deletion of *Alk5,* in the KPF mice, observing no change in survival, but with alterations in metastasis noted. Neutrophil maturity was decreased in *Alk5* deleted neutrophils, although further experimentation is required to confirm and clarify the relevance of these findings.

Collectively, my data has elucidated the dual role of TGFß signalling in initiating and established tumour stages, while highlighting a stromal programming role of fibroblast produced TGFß1 and implicating TGFß signalling as a modulator of neutrophil maturity.

Table of Contents

List of Tables

List of Figures

Acknowledgements

I would like to first thank my supervisor Jennifer Morton, for her help, guidance, and continuous support over the last four years. Without this, I would not have been able to develop the skills, knowledge or desire to continue to pursue a career in science.

To the R10 lab group, both current and past members, thank you for being a kind, supportive, knowledgeable and most of all an encouraging lab to be part of. Saadia Karim for the invaluable help in multiple techniques, Karen Pickering for all the help with IF imaging, Mathias Tesson for constant scientific dialogue, Peter Repisca and Kay Kong for all the bioinformatics assistance, Loveena Rishi Delori for all matters flow cytometry and of course my fellow PhD students Laura Lapienytė and Curtis Rink for going through the process together.

Thank you to CRUK for funding my PhD project and to the University of Glasgow for facilitating my degree.

Without the Core facilities provided in the Beatson this work would not have been possible. Thank you to Colin Nixon and the whole Histology team for dealing with countless requests and always being happy to help. To Billy Clark and the Molecular Technology Services team for performing the RNA sequencing. To all of the staff in the Biological Service Unit, without your continuous hard work the bulk of the Animal model work would not be possible. The Core services team that keep the institute running and making life easier for everyone in the labs. To Tom Gilbey and the flow cytometry team as well as John MacKey, your vast knowledge was essential in experimental designs.

Finally, I would like to thank my family. To my parents I cannot put in words how much you mean but I can say your encouragement, love and support has allowed me to get where I am. To my brothers, thank you for always being there and finally I have the evidence to prove who the best is. To my partner Evanna, without you I would never have finished my thesis. You have been there for me through everything and all I can say is I love you. Lastly, to my daughter Freya, you brought a special spark into my life and you will never know how much happiness you bring to me while constantly inspiring me to be better.

Author's Declaration

I confirm that the contents of this thesis are my own work throughout. Where I have received assistance, I have acknowledged the individuals. This work has not been submitted elsewhere.

Definitions/Abbreviations

ADM - Acinar-to-Ductal Metaplasia

AKT - Protein Kinase B

apCAF - Antigen Presenting CAF

αSMA - Alpha Smooth Muscle Actin

BM - Bone Marrow

CAF - Cancer Associated Fibroblast

CCNG1 - Cyclin G1

CDK - Cyclin Dependent Kinase

CSF1R - Colony Stimulating Factor 1 Receptor

CXCL - CXC Motif Ligand

CXCR - CXC Chemokine receptor

CyTOF - Cytometry by Time of Flight

DR - Dual Recombinase

ECM - Extracellular Matrix

EGF - Epidermal Growth Factors

EMT - Epithelial Mesenchymal Transition

ERK - MEK Extracellular Signal Regulated Kinase

F - 5-fluorouracil

FACS - Fluorescence-activated Cell Sorting

FAMMM - Familial Atypical Multiple Mole Melanoma Syndrome

FAP - Fibroblast Activation Protein

Flp - Flippase

FMO - Fluorescence Minus One

FOL - Folinic Acid

FSF - FRT-Stop-FRT

GAP - GTPase Activating Proteins

G-CSF - Granulocyte Colony Stimulating Factor

GDP - Guanosine Diphosphate

GEF - Guanine Nucleotide Exchange Factors

GFAP - Glial Fibrillary Acidic Protein

GFP - Green Fluorescent Protein

GM-CSF - Granulocyte Macrophage Colony Stimulating Factor

GSEA - Gene Set Enrichment Analysis

GTP - Guanosine Triphosphate

H&E - Haematoxylin & Eosin

HS - Histoscore

HSC - Haematopoietic Stem Cells

iCAF - Inflammatory CAF

IHC - Immunohistochemistry

IL - Interleukin

IPMN - Intraductal Papillary Mucinous Neoplasm

IRIN - Irinotecan

KAF - *Pdx1-Flp; FSF-Kras$^{G12D/+}$; Alk5$^{fl/fl}$*

KF - *Pdx1-Flp; FSF-Kras$^{G12D/+}$;*

KIC - *Ptf1a-Cre; Kras$^{LSL-G12D/+}$; Ink4a$^{fl/fl}$*

KPC - *Pdx1-Cre; Kras$^{LSL-G12D/+}$; LSL-Trp53$^{R172H/+}$*

KPF - *Pdx1-Flippase; FSF-Kras$^{G12D/+}$; Trp53$^{Frt/+}$*

KPF^{C} - *KPF; Col1a2-CreER*

KPF^{G} - KPF; *Gli-CreER*

KPF^{L}- KPF; *Ly6G-Cre*

KP$^{fl/fl}$C - *Pdx1-Cre; Kras$^{LSL-G12D/+}$; Trp53$^{fl/fl}$*

KSC - *Pdx1-Cre; Kras$^{LSL-G12D/+}$; Smad4$^{fl/fl}$*

KTC - *Ptf1a-Cre; Kras$^{LSL-G12D/+}$; Tgfbr2fl$^{/fl}$*

KTF - *Pdx1-Flp; FSF-Kras$^{G12D/+}$; Tgfb1$^{fl/fl}$*

LIF - Leukaemia Inhibitory Factor

LTBP - Latent TGFß Binding Protein

MAPK - Mitogen Activated Protein Kinase

MCN – Mucinous Cystic Neoplasms

MDM2 - Mouse Double Minute 2

MEF - Mouse Embryonic Fibroblasts

MEK - MAPK kinase

MMP – Matrix MetalloproteinaseMPO - Myeloperoxidase

MSC - Mesenchymal Stem Cells

mTOR - Mechanistic Target of Rapamycin

myCAF - Myofibroblast

NET - Neutrophil Extracellular Trap

NK - Natural Killer

OX - Oxaliplatin

PanIN - Pancreatic Intraepithelial Neoplasia

PDAC - Pancreatic Ductal Adenocarcinoma

PI3K - Phosphoinositide 3 Kinase

PIP2 - Phosphatidylinositol 4,5-bisphosphate

PIP3 - Phosphatidylinositol 4,5-trisphosphate

PP2A - Protein Phosphatase 2A

PSC - Pancreatic Stellate Cells

PTEN - Phosphatase and Tensin Homology

RAF - Rapidly Accelerated Fibrosarcoma

RalGEF - Ral Guanine Nucleotide Exchange Factors

RB - Retinoblastoma

SARA - SMAD Anchor for Receptor Activation

SBE - SMAD Binding Elements

scRNAseq - Single Cell RNA Sequencing

SGF - Sarcoma Growth Factors

SHH - Sonic Hedgehog

TAN - Tumour Associated Neutrophil

TGFβ - Transforming Growth Factor Beta

TGFBR1 – TGFβ Receptor 1

TME - Tumour Microenvironment

TNF - Tumour Necrosis Factor

Chapter 1 Chapter 1 – Introduction

1.1 The pancreas

1.1.1 The normal pancreas structure and function

The pancreas is an abdominal organ, which has essential functions in aiding digestion and modulating blood sugar levels. The pancreas has both exocrine and endocrine functions dictated by the acinar cell compartment and islets of Langerhans respectively, which form in a process known as branching morphogenesis (Sznurkowska et al., 2018) (**Figure. 1**). The acinar cells make up roughly 80% of the pancreas and are responsible for the production of digestive enzymes such as amylase, chymotrypsin, elastase, lipase and trypsin. These pancreatic juices drain, via intercalated ducts found in acinar beds, into the main pancreatic duct, which runs the length of the pancreas. These ducts are also responsible for the secretion of a buffer composed of water, bicarbonate and chloride. This main duct combines with the common bile duct at the ampulla of Vater and releases its contents into the duodenum (Campbell and Verbeke, 2013; Hezel et al., 2006).

The islet of Langerhans contain alpha (α), beta (ß), gamma (γ), delta (δ) and epsilon (ϵ) cells which produce glucagon, insulin, pancreatic polypeptide, somatostatin and ghrelin respectively. The central function of the islets is control of blood glycaemia through α-cell released glucagon and ß-cell released insulin. Somatostatin works to regulate insulin, glucagon and ghrelin secretion, pancreatic polypeptide controls exocrine pancreas secretions and ghrelin is involved in inducing hunger (Xavier, 2018).

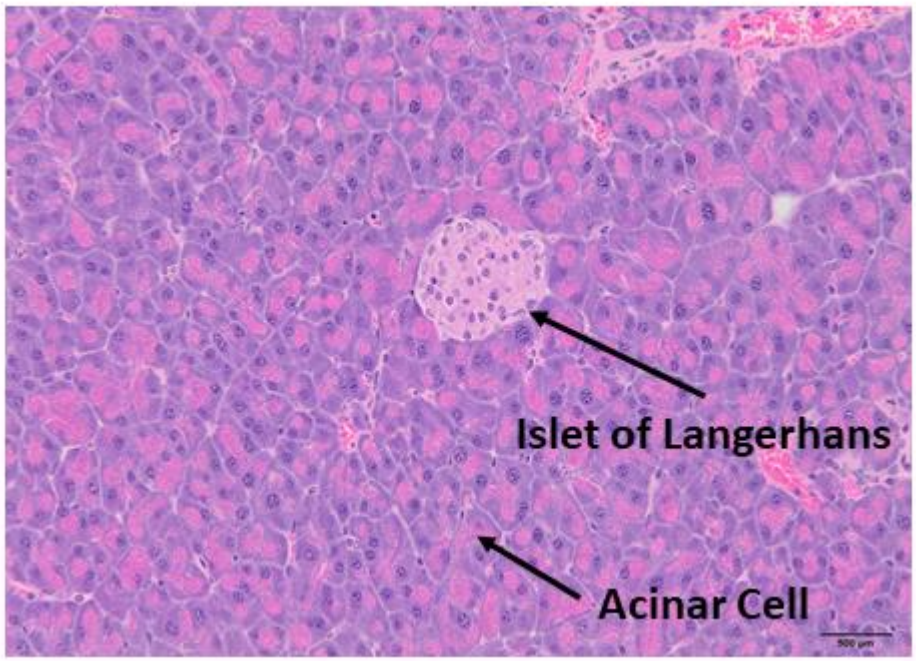

Figure 1 Histology of the mouse pancreas
Representative image of an H&E stained slide of normal pancreatic tissue showing normal acinar tissue and an islet of Langerhans.

1.2 Pancreatic Cancer

1.2.1 Subtypes of Pancreatic cancer

There are multiple types of pancreatic cancer; however, the most common subtype is pancreatic ductal adenocarcinoma (PDAC), which accounts for 90% of cases. Cancer of the neuroendocrine lineage is the next most frequent observed in around 10% of cases (Kleeff et al., 2016). PDAC develops most commonly from pre-neoplastic lesions termed pancreatic intraepithelial neoplasia (PanIN), although it can also arise from intraductal papillary mucinous neoplasms (IPMNs) or mucinous cystic neoplasms (MCNs) (Hezel et al., 2006).

1.2.2 Epidemiology of PDAC

Pancreatic cancer is the 10th most common cancer in the UK; however, it is the 5th most common cause of cancer related death, with near uniform lethality (CancerResearchUK). Around 20% of patients survive the first year post diagnosis, with a 5-year survival rate of around 8% (Rawla et al., 2019). Incidence of pancreatic cancer increases with age, with 47% of patients older than 75 years of age and males accounting for 51% of cases. Over the last 50 years, there has been very little improvement of long-term survival in pancreatic cancer yet incidence has increased and by 2030 PDAC is predicted to become the third leading cause of cancer related mortality (Ferlay et al., 2016).

1.2.2.1 Non-Modifiable risk factors

PDAC is slightly more prevalent within males (51% of cases) with a 1.8% (1 in 53) lifetime risk of pancreatic cancer diagnosis in males (meaning that 1 out of 53 men will develop PDAC in their lifetime) and a 1.7% risk in females (1 in 57) (CancerResearchUK, 2018; Smittenaar et al., 2016), this is further supported by the SEER data set, which indicates a 1.7% lifetime risk of diagnosis with PC in the US (SEER, 2018). Younger female patients (<49 years of age) have a greater 5-year survival than their male counterparts (26.3% vs 17.2%), with 71% of early onset pancreatic cancer being found in males (Ntala et al., 2018). An equivalent net survival of <10% was noted for all patients regardless of gender >49 years of age. Interestingly, elevated expression of X-linked genes was observed within

female patients, although the relevance of this requires further study (Principe and Rana, 2020).

As alluded to above age has a major bearing on pancreatic cancer mortality, with 51% of deaths occurring in patients >75 years of age, with the peak in the 85-89 age bracket. This is more likely due to the median age of diagnosis at 70 years of age, with most cases diagnosed between 65-74 years of age (Principe and Rana, 2020) and PDAC occurring in less than 10% of patients under the age of 50. One study noted no difference in survival between early and late onset patients (Ntala et al., 2018). However, in a larger data set the 5-year survival of 20-40 year olds diagnosed with pancreatic cancer was 44.7% over 3 times greater than 5-year survival of patients >40 years of age (Wang et al., 2020). Patients diagnosed with later stages had worse prognosis with the 5-year survival of those at stage 1A 31.7% falling to 0.5% when diagnosed at stage IV (Bengtsson et al., 2020).

1.2.2.2 Familial disposition

With late stage diagnosis of PDAC significantly worse for survival, active efforts to identify high-risk patients for routine screening could potentially increase early diagnosis and improve patient outcome (Klein, 2012). There was nearly a two-fold increase in risk of pancreatic cancer when there is a family history of the disease (Jacobs et al., 2010; Permuth-Wey and Egan, 2009). Chronic pancreatitis confers a 16-fold increase in risk of pancreatic cancer when followed up 2 years after exhibiting pancreatitis, with this risk falling to an 8-fold risk when patients are followed 5 years on (Kirkegard et al., 2017). Hereditary pancreatitis specifically, caused by mutation of the *PRSS1* gene, confers a 53-fold greater risk of developing pancreatic cancer in affected patients (Haddad et al., 2011). Mutations in *BRAC1* and *BRAC2* confer a 2 fold to 9 fold risk respectively (Haddad et al., 2011) with Familial Atypical Multiple Mole Melanoma Syndrome (FAMMM) patients having a 34-fold increased risk of developing pancreatic cancer due to mutations in *CDKN2A*, a potent tumour suppressor frequently mutated in sporadic pancreatic cancer.

1.2.2.3 Modifiable risk factors

Modifiable risk factors such as smoking have been attributed to 22% of pancreatic cancer cases (Brown et al., 2018) with risk correlating with higher daily cigarette consumption and duration of history of smoking. Cessation of smoking continued to show an increased risk 10 years after quitting, however by 20 years the risk was no different from that of non-smokers (Bosetti et al., 2012). Obesity was linked to 12% of cases with risk correlating with increased body mass index (Brown et al., 2018; Kyrgiou et al., 2017). Alcohol consumption of greater than 3 units per day also increased the risk of developing pancreatic cancer, with no risk for consumption below that level (Wang et al., 2016). Further, red meat consumption in males but not females was associated with increased risk of pancreatic cancer (Zhao et al., 2017).

1.2.3 Therapeutic intervention in PDAC

Although there are multiple treatment modalities for PDAC most are broadly ineffective at curing disease. Pancreatic cancer is commonly discovered following emergency presentation, in 46% of cases, with stage IV disease most frequently diagnosed (~50% of cases). Symptoms of pancreatic cancer are persistent abdominal or back pain, weight loss, indigestion with jaundice the most notable symptom (CancerResearchUK). In recent years there has been a drive to improve understanding of pancreatic cancer symptoms in order to promote early diagnosis with the aim of increasing long-term survival (PCUK).

The most effective treatment strategy is surgical resection, termed a pancreaticoduodenectomy (Whipple procedure), which involves removal of the pancreatic head and duodenum, gallbladder and occasionally part of the stomach (Whipple et al., 1935). Surgical removal of the primary tumour has been shown to lead to a 5-year survival of 30% of when combined with gemcitabine and capecitabine adjuvant chemotherapy (*Neoptolemos, 2018*). However, surgery is available to only 15-20% of pancreatic cancer patients, those with non-metastatic and/or non-locally-invasive disease and with no encasement of major vessels (Bockhorn et al., 2014), highlighting the benefits of detecting disease at an earlier stage. Although removal of the primary tumour improves outcomes, recurrence occurs in up to 80% of cases, often caused by metastasis to distal

sites or local reoccurrence (Moletta et al., 2019). Therefore, although the Whipple procedure is the best therapy for PDAC, it is by no means curative.

Many patients also present with borderline resectable disease, which involves contact with major blood vessels making surgical intervention more complex (Isaji et al., 2018). Patients will often, therefore require neoadjuvant chemotherapy as either the sole treatment for the tumour or to attempt to reduce tumour mass to allow surgical removal of the primary tumour. The main drug combinations used as the standard for care in PDAC are Gemcitabine, Capecitabine, FOLFIRINOX and nAb-Paclitaxel.

Gemcitabine is a nucleoside analogue that was shown to have a positive impact on reducing cancer cell growth in *in vivo* models (Hertel et al., 1990). It was the first drug to show efficacy in pancreatic cancer extending survival by 1 month while improving quality of life, when compared to 5-fluorouracil (Burris et al., 1997), and consequently became the standard of care. Subsequently clinical trials have shown that the neoadjuvant combination of gemcitabine with capecitabine, which blocks DNA synthesis, improved survival in locally advanced and metastatic PDAC (median survival 6.2 vs 7.1 months) (Cunningham et al., 2009). Further, adjuvant therapy of gemcitabine and capecitabine, following surgical resection, resulted in an improved median survival of 28 months when compared to 25.5 months of gemcitabine treatment alone (Neoptolemos et al., 2017).

A combination of folinic acid (FOL), 5-fluorouracil (F), irinotecan (IRIN) and oxaliplatin (OX), termed FOLFIRINOX, was shown in a clinical trial of metastatic pancreatic cancer to be superior to gemcitabine with a median survival of 11.1 months versus 6.8 months with an improved quality of life at 6 months post treatment although with more associated toxicities (Conroy et al., 2011). It was therefore recommended as the first line therapy for metastatic disease although in younger healthier patients more capable of tolerating the side effects. Subsequently it was shown that FOLFIRINOX is also superior to gemcitabine alone as an adjuvant therapy following surgical resection (median overall survival 54.4 months vs 35.0 months) (Conroy et al., 2018).

Albumin bound paclitaxel (nAb-Paclitaxel), a cytoskeletal targeted drug that blocks cell division, was shown to improve survival when used in combination with gemcitabine extending survival by roughly 2 months (Goldstein et al., 2015; Von Hoff et al., 2013).

Overall, the approved frontline therapies are largely ineffective in terms of providing long-term survival, failing to provide curative therapy in the majority of cases or to combat metastatic disease effectively. The treatments covered above document over 20 years of research during which time survival in the UK has changed very little, yet understanding of the disease has continued to improve. Therefore, PDAC is described as a disease of unmet clinical need and many clinical trials and pre-clinical studies are ongoing to provide better therapeutic options. For instance, the Precision-Panc trial based in Glasgow provides an umbrella study, which involves stratified therapies using patient cancer genomics (Dreyer et al., 2020a). For example, research led work has highlighted a subset of PDAC patients, which could be responsive to DNA damaging therapy (Dreyer et al., 2021).

Promising work from pre-clinical mouse model systems could also be developed into clinical trials, with macrophage depletion through Colony Stimulating Factor 1 Receptor (CSF1R) (Candido et al., 2018) extending survival and CXC Chemokine receptor 2 (CXCR2) small molecule inhibition reducing metastatic burden (Steele et al., 2016).

Stromal targeting presents another therapeutic avenue with promising results in mouse models of PDAC published (Olive et al., 2009), however, their promise failed to translate to patients (Kim et al., 2014; Van Cutsem et al., 2020). Subsequent modelling highlighted divergent functions of fibroblast populations (Lee et al., 2014; Oezdemir et al., 2014; Rhim et al., 2014), with further understanding required of the stromal composition in order to provide effective targets. This is discussed in more detail later in this chapter.

1.2.4 Genetics of PDAC

Pancreatic cancer progresses from pre-neoplastic lesions, most commonly from PanINs but also from IPMNs or MCNs. PanINs have been well characterised and

are graded through stages 1 to 3. PanIN-1 are characterised by columnar epithelial cells with basally orientated nuclei. Upon loss of their nuclear polarity and alterations in nuclear size, they can be classified as PanIN-2. The final step to PanIN-3 is defined by the formation of papillae bridging the lumen, cribriforming, and budding of cells into the lumen of the duct (Hruban et al., 2008).

The underlying genetic mutations which occur in PDAC have been well documented through multiple studies sequencing human tumour samples (Aguirre et al., 2017; Bailey et al., 2016; Collisson et al., 2011). The most common mutation occurring in over 95% of PDAC cases involves the oncogenic transformation of the *KRAS* gene, with tumour suppressors *CDKN2A*, *TP53* and *SMAD4,* lost in ~95%, 50-75% and 50% of cases respectively, occurring next most frequently. There is also an array of low penetrance mutations in various other genes, with multiple signalling pathways dysregulated that are important for carcinogenesis (Collisson et al., 2019). It has been shown that PanINs acquired their genetic permutations in a stepwise manner. Oncogenic activation of *KRAS* occurs first driving development of PanIN-1, with p16 and p19, the protein encoded by *CDKN2A*, lost in early PanIN-1 and PanIN-2 lesions. The tumour suppressors *TP53* and *SMAD4* are then most frequently lost in late stage PanIN-3 lesions (Feldmann et al., 2007).

1.2.4.1 Oncogenic KRAS

Normally RAS proteins cycle from an inactive, guanosine diphosphate (GDP) bound state, to an active, guanosine triphosphate (GTP) bound state, with the aid of guanine nucleotide exchange factors (GEFs) and GTPase activating proteins (GAPs) at each stage respectively. In its GDP bound state KRAS can be found in lipid rafts at the internal cellular membrane and upon receptor membrane activation GDP, via GEF activity, dissociates allowing for the binding of GTP, thereby activating KRAS (Feig, 1999).

Point mutations in exon 2 (codon 12) are the most commonly detected in PDAC (70-95% of cases). The most frequent point mutations result in the conversion of wild-type glycine to either an aspartic acid (G12D), to valine (G12V) or arginine (G12R) in 40%, 33% and 15% of codon 12 mutated cases respectively. Other point

mutations can occur in codons 11, 13, 61 or 146 within the same exon, although at a less frequent rate. Although these mutations ultimately culminate in a more active KRAS protein they are not all made equal, with evidence suggesting that patients with G12D alterations have a worse survival than G12V or G12R, and that specific codon mutations may predict efficacy of treatment options or potential for KRAS inhibition (Canon et al., 2019; Haigis, 2017).

The activated GTP bound form of KRAS has the potential to interact with over 80 proteins, with the ultimate outcome resulting in a transformed cell with greater fitness for survival and proliferation. The most common downstream effectors are the RAF/MEK/ERK pathway, the PI3K/PTEN/AKT pathway and the RalGEFs (**Figure 2**). Rapidly accelerated fibrosarcoma (RAF) is recruited and activated by GTP bound KRAS, this results in phosphorylation of mitogen-activated protein kinase (MAPK) kinase (MEK) 1/2 which subsequently activates MEK-extracellular signal regulated kinase (ERK) 1/2. This culminates in an increase in proliferation and survival, thus boosting tumorigenesis (Pettazzoni et al., 2015). Phosphoinositide 3 kinase (PI3K) is activated by RAS driving phosphatidylinositol 4,5-biphosphate (PIP_2) to phosphatidylinositol 4,5-triphosphate (PIP_3) which is then able to recruit, phosphorylate and activate protein kinase B (AKT). AKT is then able to stimulate mechanistic target of rapamycin (MTOR) signalling. Phosphatase and tensin homology (PTEN) is a negative regulator of this pathway via the dephosphorylation of PIP_3 to PIP_2, and has been shown to be a potent tumour suppressor (Kennedy et al., 2011; Ying et al., 2011). The Ral guanine nucleotide exchange factors (RalGEFs) are able to activate RalA and RalB. RalA has been shown to enhance anchorage independent growth and RalB is thought to be involved in metastasis (Buscail et al., 2020; Mann et al., 2016).

Further, oncogenic KRAS has been shown to alter the tumour microenvironment. An oncogenic *Kras*^{G12D}, under the control of doxycycline, in a mouse model of pancreatic cancer highlighted that continuous oncogenic stimulation was required for the maintenance of both PanIN lesions as well as for the recruited stromal infiltrate (Collins et al., 2012). Additionally, oncogenic *Kras* was shown to drive immunosuppression in a MYC and BRAF dependent manner thereby hindering anti-tumour immunity and facilitating immune evasion (Ischenko et al., 2021).

These selected examples highlight a picture of oncogenic transformed KRAS cells having an increased capacity for survival and enhanced proliferation. Although, it has been shown that elevated levels of RAS signalling can impose a senescence phenotype that would inhibit the progression from PanIN lesions to frank PDAC (Acosta et al., 2013; Morton et al., 2010). Therefore, additional mutations are required to overcome this senescence and drive PDAC formation.

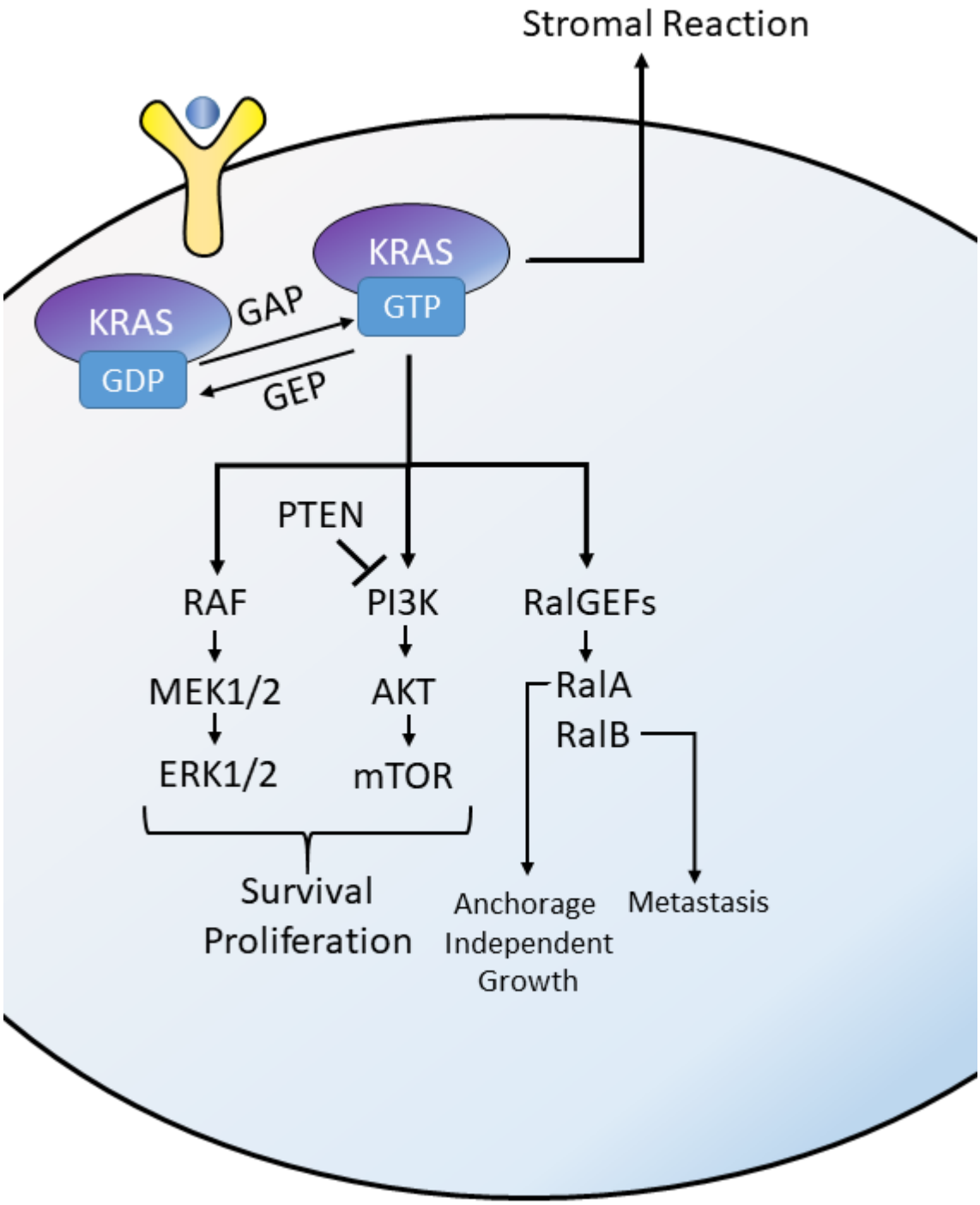

Figure 2 Mutant KRAS signalling drives initiation and survival of PDAC
Schematic outline of the KRAS signalling pathway with activation of downstream signalling components that drive initiation, maintenance and stromal recruitment in PDAC.

1.2.4.2 Tumour suppressor CDKN2A

CDKN2A is deleted or epigenetically silenced in roughly 80-95% of PDAC. Mouse modelling of *Cdkn2a* deletion has shown it was insufficient to drive PDAC on its own, but combined with oncogenic *Kras*, tumorigenesis was initiated (Aguirre et al., 2003). Within human disease, it is frequently lost during PanIN progression (Feldman, 2007). It encodes two proteins $p16^{INK4A}$ and $p14^{ARF}$, both of which have

tumour suppressive function. Cyclin dependent kinase (CDK) 4 and CDK6 phosphorylate retinoblastoma (RB), permitting progression into the S phase of the cell cycle; however, $p16^{INK4A}$ inhibits CDK4 and CDK6, thereby blocking cell cycle progression. Further, $p14^{ARF}$ is tumour suppressive through sequestration of the well-known p53 negative regulator mouse double minute 2 (MDM2) (Bardeesy and DePinho, 2002; Wu et al., 1993).

1.2.4.3 Tumour suppressor P53

TP53 is one of the most well-known and well-characterised tumour suppressor genes across all types of cancer. It is the most frequently mutated gene across all cancers and is mutated in ~42% of cases (Kandoth et al., 2013), and specifically in PDAC where it is mutated 50% of the time. Mutations in *TP53* are detected from PanIN2 stages onwards in PDAC, highlighting the importance of losing functional p53 early in disease progression (Feldman, 2007). The p53 protein is a central figure in maintaining cell fitness and is frequently termed the "guardian of the genome". Activation of p53, by the stabilization of the protein, occurs following the detection of cellular stress such as DNA damage, hypoxia and oncogenic activation. In response to this stress, p53 is able to drive cell cycle arrest, promote DNA repair or even drive apoptotic cell death (Hafner et al., 2019). Within PDAC *TP53* can be mutated or deleted, with mouse models showing mutation of *Trp*53 ($Trp53^{R172H}$) combined with oncogenic *Kras* generates a more invasive and metastatic PDAC model than *Trp53* deletion (Morton et al., 2010).

p53 controls the expression of many genes and has for instance been shown to increase the transcription of a non-canonical cyclin, Cyclin G1 (CCNG1) (Okamoto and Beach, 1994). CCNG1 was described as non-canonical as it does not oscillate with the cell cycle as other cell cyclin molecules do (Horne et al., 1996). It was shown to interact with protein phosphatase 2A (PP2A) (Okamoto et al., 1996), with radiation of mouse embryonic fibroblasts (MEFs) increasing expression of CCNG1 via p53 transactivation and MEFs lacking CCNG1 being more sensitive to radiation (Kimura et al., 2001). Interestingly, overexpression of CCNG1 in p53 proficient human colorectal cancer cells increased cell growth, with elevated sensitivity to cisplatin (Smith et al., 1997). Subsequently, it was shown that a complex of PP2A and CCNG1 was able to dephosphorylate and

activate MDM2 (Kimura and Nojima, 2002). MDM2 has also been shown to be induced by p53 and acts as a negative regulator of P53 function (Barak et al., 1993; Wu et al., 1993) by blocking both its transcriptional capability (Momand et al., 1992; Oliner et al., 1993) and marking it for degradation (Haupt et al., 1997).

1.2.4.4 Tumour suppressor SMAD4

SMAD4 is a central mediator of the transforming growth factor beta (TGFβ) signalling family, which will be discussed further within this chapter. Upon activation of the TGFβ signalling pathway, intracellular SMAD4 is required for transcription of genes. Originally termed deleted in pancreatic cancer 4, *SMAD4* is mutated in ~50% of PDAC cases (Hahn et al., 1996). The TGF-β signalling pathway is responsible for inducing cell cycle arrest, growth suppression and senescence (Seoane et al., 2004; Seoane et al., 2001; Staller et al., 2001), therefore mutations in this signalling pathway, including receptors upstream of SMAD4, are common to overcome this tumour suppressor function. Loss of SMAD4 IHC staining in patient biopsies is an indicator of the switch from benign pancreatic tissue to invasive carcinoma (McCarthy and Chetty, 2018). Mutations upstream of SMAD4 in TGFβ Receptor 1 (TGFBR1) and TGFBR2 are also prevalent in PDAC (Collisson et al., 2019), with mouse modelling of deletion of these TGFβ signalling components accelerating oncogenic *Kras* driven pancreatic cancer (Acosta et al., 2013; Bardeesy et al., 2006; Ijichi et al., 2006).

1.2.4.5 Transcriptomic subtypes of pancreatic cancer

Transcriptional analysis of PDAC patient samples has highlighted molecular subtypes of the disease. It was initially shown in a combined study of patient samples, with human and mouse cell lines, that three subsets of PDAC can be defined, as classical, quasimesenchymal and exocrine-like. Patients with classical subtype tumours had a better survival following tumour resection than patients with the quasimesenchymal subtype. Interestingly, cell lines classified as either classical or quasimesenchymal subtype, showed subtype-specific responses to gemcitabine, with the quasimesenchymal cell lines being more sensitive on average (Collisson et al., 2011). A virtual dissection of a PDAC gene expression microarray has digitally distinguished expression of tumour, stromal

and normal genes and has also elucidated tumour specific subtypes of PDAC. Tumour specific gene expression highlighted two PDAC subtypes, Classical and Basal-like, with patients stratified as Basal-like having poorer prognosis (Moffitt et al., 2015). With the Classical and Basal-like subtypes confirmed in RNA extracted from paraffin embedded PDAC patient tissue (Puleo et al., 2018). Further genomic analysis by *Bailey et al.*, defined four subtypes of PDAC termed, squamous, pancreatic progenitor, immunogenic and aberrantly differentiated endocrine exocrine (ADEX), with ten signalling pathways, including TGFβ, with components frequently mutated. Squamous subtypes were characterised with inflammation, metabolic reprogramming, TGFβ signalling, hypoxia and MYC activation gene networks. Progenitor subtypes were enriched for pancreatic transcription factors, such as PDX1, with apomucins expressed preferentially in this subtype. The immunogenic subtype was similar to the pancreatic progenitor however, there was significant immune infiltration with elevated antigen processing, $CD4^+$ T cells and $CD8^+$ T cell pathways. The ADEX subtype had both exocrine and endocrine pathways upregulated. Patients characterised with the squamous subtype had the worse prognosis (Bailey et al., 2016).

It has also been shown that high levels of SMAD4 and GATA6 mRNA associate with the classical subtype, with epigenetic silencing of GATA6, measured through 5 methylcytosine (5mc), associated with the squamous subtype. Restoration of SMAD4 in tumour cells from *Pdx1-Cre; LSL-Kras^{G12D}; Ink4a/Arf$^{fl/fl}$; Smad4$^{fl/fl}$* mice caused a shift away from the squamous subtype, with SMAD4 shown to increase ten-eleven translocation 2 (TET2). TET2 hydroxylates 5mc to 5 hydroxymethylcytosine (5hmc) thereby removing epigenetic silencing of GATA6 with GATA6 5hmc associated with the classical subtype (Eyres et al., 2021).

The capacity to stratify patients in this way can prove key to target therapy appropriately and to those patients predicted to be sensitive.

1.3 Tumour stroma

1.3.1 Fibroblasts

A major feature of PDAC is the dense stromal reaction, which can compose up to 90% of the whole tumour (McCarroll et al., 2014). An abundance of cancer-

associated fibroblasts (CAFs) are observed within the PDAC TME and are major producers of the ECM. Over 90% of the ECM, composed predominantly of collagens, has been shown to be produced by stromal cells with the complexity of the ECM increasing throughout disease progression (Tian et al., 2019). CAFs were revealed to accumulate in early PanIN lesions, in a mouse modelling experiment using tetracycline inducible oncogenic *Kras*. Upon 'switching off' of oncogenic *Kras,* however, neoplastic regions and the stromal infiltrate would resolve (Collins et al., 2012), highlighting the intrinsic links between malignant transformation and fibroblast accumulation and reminiscent of the role of normal fibroblasts in wound healing (Dekoninck and Blanpain, 2019).

Fibroblasts and CAFs have been shown in both 2D (Begum et al., 2019) and 3D spheroid cultures (Dominguez et al., 2020; Ohlund et al., 2017), to promote the proliferation of cancer cells. Orthotopic tumours exhibit elevated growth when co-injected with pancreatic stellate cells (PSCs, discussed below) (Bachem et al., 2005) or CAFs (Hwang et al., 2008), alongside increased ECM deposition and metastasis. They have been shown to participate in reciprocal crosstalk with tumour cells, with the Jørgensen lab highlighting that $Kras^{G12D}$ transformed cells regulate the PSC secretome through SHH signalling, which in turn resulted in elevated AKT activation in tumour cells through secreted IGF1 and GAS6 (Tape et al., 2016). Further, cancer cell conditioned media increased the production of ECM proteins by PSCs (Bachem et al., 2005), particularly pertinent given evidence showing this dense stroma can sequester therapeutic agents and limit drug penetrance (Jacobetz et al., 2013; Olive et al., 2009). Further, stimulation by factors such as PDGF (Apte et al., 1999) and TGFß (Schneider et al., 2001; Shek et al., 2002) caused increased ECM production by CAFs. Additionally, CAF conditioned media was able to convey resistance to gemcitabine and radiation, while promoting proliferation and invasion of cancer cells (Hwang et al., 2008). PSC production of CXCL12, for instance, was shown to promote cancer cell invasion and proliferation through CXCR4 (Gao et al., 2010), with PSCs able to increase cancer cell epithelial-mesenchymal transition (EMT) (Kikuta et al., 2010).

Collectively these data suggest that PSCs have a generally pro-tumorigenic function in PDAC and prompted investigation of therapeutic intervention

directed towards CAFs and ECM products. For instance targeting of SHH, a driver of pancreatic desmoplasia (Bailey et al., 2008), was interrogated in mouse models of PDAC (Olive et al., 2009). This resulted in a depletion of stroma, with improved vascularisation, which enhanced intra-tumoural drug delivery culminating in extended survival in pre-clinical models. Further, elevated interstitial pressure resulting in the collapse of vasculature was shown to be driven by hyaluronan (Jacobetz et al., 2013), with enzymatic targeting of hyaluronan normalising interstitial pressure, improving microvasculature and enhancing the efficacy of gemcitabine in PDAC mouse models (Provenzano et al., 2012). However, translation to the clinic of these two agents was disappointing with clinical trials discontinued. SHH inhibition decreased patient stromal content and downstream SHH targets, but was not more beneficial than gemcitabine alone (Kim et al., 2014), whilst hyaluronan depletion in combination with nAb Paclitxel and gemcitabine, in patients stratified by high hyaluronan levels, showed no additive benefit (Van Cutsem et al., 2020).

Therefore, studies in pre-clinical models were undertaken to attempt to understand the reasons behind the failure of these promising therapies. Deletion of *Shh* in *Ptf1a1-Cre; LSL-Kras^{G12D}* mice accelerated PanIN progression with elevated proliferation noted in these early lesions (Lee et al., 2014). Further, in both *Ptf1a-Cre; LSL-Kras^{G12D}; Trp53$^{fl/+}$ (Lee et al., 2014)* and *Pdx1-Cre; LSL-Kras^{G12D}; Trp53$^{fl/+}$ (Rhim et al., 2014)* models of pancreatic cancer, epithelial driven deletion of *Shh* resulted in reduced survival, with SHH response genes decreased and the stroma depleted. Long-term pharmaceutical inhibition of SHH signalling also mirrored the findings in the genetic models, with survival significantly reduced, differing from the results shown in the first pre-clinical trial (Olive et al., 2009). Further, depletion of αSMA positive cells, in the *Ptf1a-Cre; LSL-Kras^{G12D}; Tgfbr2$^{fl/fl}$* model resulted in decreased stromal content and collagen deposition culminating in reduced survival (Oezdemir et al., 2014). Poorly differentiated tumours were shown to predominate upon stromal ablation, with metastasis elevated. Vasculature was elevated in the SHH inhibited models, however, anti-VEGFR2 increased survival (Rhim et al., 2014). Collectively, these studies highlighted that the PDAC stroma can act to restrain tumour progression, through inhibiting growth and driving the formation of more

well differentiated tumours, although it should be noted that in the conditional models, *Shh* was deleted prior to PanIN formation.

Clarity upon the function of PDAC stroma is required, as reports have conflicted as to its role in restricting or promoting tumour progression. Over recent years, advances have been made in examining intra and inter-tumoural heterogeneity of fibroblasts to address this issue.

1.3.1.1 Source of cancer associated fibroblasts

Within PDAC, the source of CAFs has yet to be fully clarified, although the current consensus proposes the activation and expansion of resident pancreatic stellate cell (PSCs) populations by factors released by neoplastic cells. The initial isolation of PSCs was from rat pancreas (Apte et al., 1998) before confirmation of their presence within the human pancreas (Vonlaufen et al., 2010). They were described as having a polygonal or stellate shape in culture with lipid drops, which were positive for vitamin A. Within the pancreas, cells positive for the PSC markers, desmin and glial fibrillary acidic protein (GFAP), were found in periacinar regions, with the expression of these markers by PSC confirmed *in vitro*. However, prolonged culture resulted in loss of vitamin A-containing lipid droplets and the acquisition of αSMA expression, which was not seen in tissue resident PSCs in the normal rat pancreas, denoting a loss of their quiescent state. This loss of quiescence has also been reported within PDAC, with staining of serial sections of human tumour tissue highlighting GFAP, desmin and αSMA positive cells embedded in a dense collagen matrix (Apte et al., 2004). It was shown that PSCs could produce collagen, laminin, fibronectin and hyaluronan while TGFß stimulation increased PSC activation and collagen production (Apte et al., 1999; Lu et al., 2019). Further, *in vitro* culture with human PDAC cell line conditioned media enhanced production of ECM proteins, with neutralisation of TGFß1 inhibiting this fibrotic response. Co-injection of PSCs alongside pancreatic cancer cell lines in xenograft models accelerated tumour growth (Bachem et al., 2005) further, emphasising the supportive role activated PSCs play in the developing tumour.

CAFs have also been demonstrated to be derived from mesenchymal stem cells (MSCs), with a population expressing fibroblast specific markers αSMA, fibroblast

activation protein (FAP) and vimentin alongside MSC markers CD90, CD49a, CD44 and CD73 (Waghray et al., 2016). Previous studies highlighted the presence of MSCs around the normal pancreatic ductal epithelium and within perivascular regions of the pancreas, which retained the capacity to differentiate into chondrocytes, adipocytes and osteoblasts (Crisan et al., 2008; Mathew et al., 2016; Seeberger et al., 2006). The MSC derived CAFs had the capacity to secrete cytokines such as IL6, IL10, CXCL8 and TGFβ, but most intriguingly the authors demonstrated they were the exclusive producers of granulocyte macrophage colony stimulating factor (GM-CSF) which enhanced the invasion of cancer cells (Waghray et al., 2016). It was also shown that MSCs harvested from pancreatic tumours could enhance recruitment of macrophages and polarize them to an arginase1 and CD206 high alternatively activated state (Mathew et al., 2016).

More recently, through transplantation of green fluorescent protein (GFP) positive bone marrow (BM) into an autochthonous model of PDAC, a population of BM derived CAF like cells has been discovered. This population was shown to be GFP, podoplanin and F4/80 positive, denoting BM origin as well as expressing known fibroblast and macrophage markers, and was retained when MSCs were depleted. These cells were able to produce multiple cytokines, for example, IL-6 and IL-10, while in culture, and could be αSMA positive or negative. They were found positioned towards the invasive front within PDAC and could enhance cell invasion *in vitro* (Iwamoto et al., 2021).

Compounding these studies was a recent publication that explored the differential expansion of pancreatic fibroblasts within the developing PDAC. The presence of both fibroblasts and PSCs (positive for lipid droplets) was noted in the normal pancreas while lineage tracing of Hoxb6 and Gli1 positive fibroblasts marked these distinct subsets throughout the parenchyma, or in perivascular regions, respectively. As the tumour progressed $Gli1^+$ fibroblast populations expanded and contributed to the αSMA positive population of fibroblasts, whereas $Hoxb6^+$ fibroblasts failed to contribute to the active CAF population. The authors also allude to further subpopulations, with $Gli1^+Hoxb6^+$ fibroblasts also failing to expand and CD105 expression observed on a subset of both $Gli1^+$ and $Hoxb6^+$ fibroblasts (Garcia et al., 2020).

Collectively, these studies highlight that within the normal pancreas there exists a heterogeneous population of fibroblasts, with some having the capacity for divergent expansion upon tumour development, alongside populations that can be derived from infiltrating cells. Recently, understanding of the stromal heterogeneity has been appreciated; however, clarity is still required to recognise how these populations may affect the developing TME.

1.3.1.2 Fibroblast subtypes

Studies have highlighted the existence of multiple subtype classifications within PDAC through sequencing of human samples, highlighting the existence of both low and high penetrance mutations (Aguirre et al., 2017; Bailey et al., 2016; Collisson et al., 2011). However, the predominant focus has been on sequencing of bulk tumours, therefore specific understanding of tumour-associated fibroblasts has been lacking. The existence of inter-tumoural heterogeneity was initially elucidated from work by *Moffitt et al.*, via 'virtual microdissection'. They divided bulk RNA sequencing data into stromal or cancer cell specific signatures via comparison to a stromal defining gene set. From this, they were able to highlight the existence of either an 'activated' or a 'normal' stroma, alongside a 'classical' or 'basal-like' tumour cell signature. Within the 'normal' stroma, there was enrichment of vimentin, desmin and αSMA, which denoted PSCs, whereas, the 'activated' stroma showed enrichment for ECM remodelling markers, such as matrix metalloproteinase 9 (MMP9) and MMP11, immune cell recruitment genes, CCL18 and CCL13, as well as FAP. There was no correlation between the cancer cell subtype and stromal cell subtype, however, regardless of cancer cell subtype the 'activated' stroma correlated with a poorer survival (Moffitt et al., 2015). Interestingly high levels of FAP have also been noted to correlate with poor patient survival (Cohen et al., 2008).

Subsequently, the 'classical' and 'basal-like' cancer cell definitions were confirmed on RNA extracted from formalin-fixed paraffin embedded PDAC tissue with high tumour cellularity. However, when including samples with low tumour cellularity, three further subsets were identified based upon the TME derived signatures. The 'immune-classical' subtype had a signature denoting high infiltration of immune cells such as T cells, B cell and natural killer (NK) cells, but lacked fibroblast infiltration. The 'desmoplastic' and 'stroma-activated'

subtypes were both enriched for fibroblasts and endothelial cells but diverged on immune cell representation, with 'stroma-activated' demonstrating a low immune cell signature. The 'pure basal-like' subtypes, derived from the high cellularity cancer cell samples, marked patients with the worse prognosis (Puleo et al., 2018).

Further heterogeneity of the stromal components was shown via RNA sequencing of laser capture micro-dissection of stromal regions of PDAC. The authors of this study defined stromal subtypes as 'immune-rich', with enrichment of chemokine signalling and haematopoietic lineage markers, or 'ECM-rich', with enrichment for collagens, integrin-1 signalling and factors associated with ECM organisation. The tumour epithelium in this study continued to be defined as 'classical' or 'basal-like', with the 'ECM-rich' stroma shown to more frequently associate with the 'basal-like' epithelium which correlated with the worst survival of the combinations (Maurer et al., 2019).

Collectively these findings demonstrate the heterogeneity present within the stromal infiltrate of PDAC and that bulk analysis of the stroma could predict patient prognosis. They highlight that stromal composition varies across PDAC patients; however, the limitations of these studies mean intra-tumoural variation could not be detected. Further, the utilisation of bulk RNA, either from the total tumour or from all stroma limits the ability to investigate CAF specific function. Consequently, multiple studies have utilised techniques such as *in vitro* CAF culturing, single cell RNA sequencing (scRNAseq) and cytometry by time of flight (CyTOF) to dissect CAF heterogeneity at population or single cell resolution.

Sequencing of low passage *in vitro* cultured human PDAC derived CAFs revealed four distinct subpopulations, highlighting both inter and intra-tumoural heterogeneity. The authors were able to define specific markers for three of the subtypes, periostin for 'A', podoplanin for 'B' and myosin-11 for 'C'. They noted spatially distinct staining, with periostin staining located at both the invasive edge and centre of tumours, whereas, only staining in the central regions of tumours was observed with podoplanin and myosin-11 (Neuzillet et al., 2019). Interestingly, a subsequent study demonstrated that podoplanin was a pan-fibroblast maker (Elyada et al., 2019). Multiple CAF subtypes could be derived

from a single patient sample signifying intra-tumoural CAF heterogeneity within PDAC. Additionally, using their dominant subtype, patients could be stratified from analysis of bulk tumour sequencing data. Subtype 'A' was the most dominantly expressed across a PDAC cohort, was more proliferative and expressed less αSMA than other subtypes. Subtype 'D' denoted the poorest prognosis while subtype 'C' had the longest survival when stratified by gene expression signature. However, immunohistochemical analysis found that patients with high periostin and low myosin-11 and podoplanin expression (denoting subtype 'A') had shorter survival. Co-culture of these CAFs with pancreatic cell lines highlighted that subtype 'A' is less pro-tumourigenic, inducing less cancer cell invasion and proliferation while conveying less protection from gemcitabine. Intriguingly, stellate cell education by cancer cell conditioned media promoted an increase in subtypes 'B' and 'C' at the expense of 'A', the αSMA low population (Neuzillet et al., 2019). Other work, has shown that 2D culture of PSC drives towards a myofibroblastic αSMA high phenotype (Ohlund et al., 2017), indicating that care must be taken with culture conditions when investigating the biology of *ex vivo* CAFs.

Work from the Tuveson lab has been particularly insightful into the intra-tumoural heterogeneity of CAFs. Their work has documented the existence of three distinct subpopulations named 'myCAFs', 'iCAFs' and 'apCAFs', with initial organoid and *in vivo* work defining myofibroblasts (myCAFs) and inflammatory CAFs (iCAFs). The expression of αSMA was used to differentiate between the two populations, with 'myCAFs' expressing high αSMA and found proximal to cancer cells, whereas, 'iCAFs' had low αSMA expression and were observed distal to tumour cells. As their name suggests, iCAFs were found to secrete chemokines and cytokines such as CXCL1, CXCL2, LIF, IL-6 and IL-11, with myCAFs responsible for ECM deposition and expressing TGFβ response genes. The appropriate stimulation of PSCs *in vitro* could promote either subtype. For instance, iCAFs only required cancer cell conditioned media, whereas myCAFs required 2D culture or close contact with cancer cells in co-culture. However, most intriguing was the plasticity of the CAFs, which could be altered to either subtype by adjusting culture conditions (Ohlund et al., 2017).

The mechanisms dictating these subpopulations were found to be tumour secreted TGFß and IL-1 driving myCAFs and iCAFs, respectively. TGFß was shown, *in vitro*, to drive a myofibroblast phenotype in PSCs, with active TGFß signalling through Smad2/3 shown in myCAFs *in vivo*. Stimulation of PSCs with IL1α induced an iCAF phenotype with upregulation of *Il1a*, *Il6* and leukaemia inhibitory factor (*Lif*) at the expense of myCAF markers, *Acta2* and *Ctgf*. Inhibition of JAK or deletion of STAT3 in PSCs abrogated the iCAF phenotype, with the authors concluding that signalling via IL-1 induces a JAK/STAT cascade to drive iCAF formation. Interestingly, the iCAF phenotype was inhibited by the TGFß induced downregulation of IL1 receptor (IL1R1), pointing to TGFß exerting dominant control over CAF identity (Tjomsland et al., 2016). The study also highlighted that inhibition of JAK/STAT signalling via use of JAK inhibitors caused an increase in the 'myCAF' subtype while decreasing the 'iCAFs', whereas, TGFBR inhibition does not affect the subtype composition, potentially due to the reduced proliferative capacity of 'iCAFs', but does reduce αSMA expression and collagen deposition. This raises the interesting potential of therapies either deliberately or non-intentionally skewing fibroblast composition (Biffi et al., 2019).

Through single cell RNA sequencing, of both human and mouse PDAC, the same lab confirmed the existence of both the myCAF and iCAF populations, while defining a new antigen presenting CAF (apCAF) population. The apCAFs were shown to express CD74 and MHCII and were capable of presenting the OVA antigen to OVA specific T cells resulting in increased T cell activation markers even though they lacked co-stimulatory molecules CD80, CD86 and CD40 found in professional antigen presenting cells (Elyada et al., 2019). Collectively, these experiments effectively illustrate intra-tumoural heterogeneity of CAFs, with both functional and spatial information aiding the conclusion that they represent bona fide CAF subpopulations.

Additional studies utilising single cell sequencing have further confirmed intra-tumoural heterogeneity. Sequencing of the normal pancreas, PanIN bearing pancreas, and PDAC from both the *Pdx1*$^{Cre/+}$*; Kras*$^{LSL\text{-}G12D/+}$*; Trp53*$^{fl/fl}$ (KP$^{fl/fl}$C) and *Ptf1a*$^{Cre/+}$*; Kras*$^{LSL\text{-}G12D/+}$*; Ink4a*$^{fl/fl}$ (KIC) models demonstrated the existence of three fibroblast populations. These populations were found in the normal

pancreas, before expanding in the PanIN-bearing pancreas, and finally converging into two populations within PDAC. It was noted that these populations mirrored 'myCAFs' and 'iCAFs' with 'FB3' expressing *Acta2* and *Tagln* and 'FB1' expressing *Pdgfra* and *Il6*. The 'apCAF' markers MHCII and CD74 were not exclusive to either population but were enriched in the 'FB3' subset (Hosein et al., 2019).

The 'myCAF/iCAF' classification was further confirmed by work from *Steele et al.*, as they analysed a published scRNAseq data set from PDAC (Peng et al., 2019). Intriguingly, the authors went on to highlight further subdivision, particularly of the 'myCAF' subtype, by showing enrichment of sonic hedgehog (SHH) signalling in some but not all 'myCAFs'. Expression of *Gli1*, a SHH transcriptional target, was predominantly expressed in αSMA and podoplanin dual positive fibroblasts, representative of the 'myCAFs'. Short-term inhibition of hedgehog signalling decreased *Gli1* expression leading to a reduction in 'myCAFs' while increasing 'iCAFs'. This shift in CAF populations was also shown to inhibit cytotoxic T cell infiltration while promoting T regulatory cell accumulation in the tumour (Steele et al., 2021).

Single cell sequencing of podoplanin and PDGFRα positive fibroblasts was performed by the Turley lab (Dominguez et al., 2020), highlighting fibroblast heterogeneity in the normal pancreas and within PDAC. Normal fibroblasts could be distinguished by their expression of dipeptidyl peptidase-4 (DPP4) and Ly6C or endoglin (CD105), with a $CD105^+$ fibroblast population also shown to exist in the normal pancreas in a subsequent CyTOF study (Hutton et al., 2021). The $CD105^+$ population was associated with higher expression of ECM structural proteins such as collagens, whereas the $Ly6C^+$ population showed high expression of genes encoding proteins associated with ECM attachment. Interestingly, the authors suggest the normal fibroblasts give rise to two distinct CAF populations in tumours, which recapitulate the 'myCAF' and 'iCAF' subpopulations described previously, with the CD105+ fibroblasts giving rise to 'myCAFs', the $Ly6C^+$ cells generating 'iCAFs', and TGFß and IL1 dictating fate, respectively. The 'myCAF' population expanded and composed the majority of CAFs in the tumour with upregulation of a TGFß induced gene *Lrrc15* noted (Dominguez et al., 2020).

Continuing on the vein of CD105 expression, a recent study utilising CyTOF to examine the stromal component of PDAC highlighted two distinct fibroblast populations present within the normal and tumour tissue in both mouse and human. As described by *Dominguez et al,* the $CD105^+$ population were most abundant with $CD105^-$ populations more proliferative. These populations appeared distinct from the 'myCAF' and 'iCAF' definitions, with variable expression of definitive markers, such as αSMA, across both the $CD105^+$ and $CD105^-$ CAFs. However, $CD105^+$ CAFs were enriched for TGFβ signalling with $CD105^-$ enriched for IL6, TNFα and JAK2 signalling. Interestingly, *Lrrc15* and *Dpp4* were not enriched in either population, but *Ly6C* was enriched in the $CD105^-$ cells. Under appropriate stimulation *in vitro,* either 'myCAF' or 'iCAF' genes could be elevated in both populations, however, *Eng* was only expressed in the $CD105^+$ population and was unaffected by treatment, indicating a 'locked' state. The expression of 'apCAF' markers appears enriched within the $CD105^-$ population; however, stimulation with IFNγ could increase their expression in both populations, with inhibition observed following exposure to TGFβ1. Subcutaneous co-injection of PDAC cells lines with either $CD105^+$, $CD105^-$ or a mixed population of fibroblasts highlighted that only $CD105^-$ fibroblasts restrained tumour growth and improved survival. The tumour restriction was mediated through the adaptive immune system and was lost in dendritic cell or immunodeficient mouse models. Deletion of CD105 in $CD105^+$ fibroblasts could reduce the transcriptional response to TGFβ1 but did not replicate the tumour suppression noted in $CD105^-$ fibroblasts, indicating that CD105 is strong marker of distinct fibroblast populations, but its loss is not sufficient for conveying anti-tumourigenic fibroblast function (Hutton et al., 2021).

Combined, these studies effectively demonstrate both inter and intra tumour heterogeneity within fibroblast populations. The utilisation of multiple techniques is key in defining these populations. For example, the tissue dissociation required in single cell techniques could potentially affect the transcriptome, so validation and function data are necessary to verify discoveries. What is apparent throughout the publications is that there is still a lack of a consensus on *bona fide* markers to define set populations. Improving understanding of the complexity may allow new vulnerabilities to be exposed in patients.

1.3.1.3 Education of CAF influenced by PDAC genetics

Further complexity is imbued by the impact that genetics of PDAC have on the TME. A stiffer fibrosis, including elevated fibronectin and tenascin C was found in *SMAD4* deficient patients and this correlated with poorer survival. Mouse modelling with *Tgfbr2* deficient PDAC models highlighted a similar ECM stiff phenotype in comparison to the KPC model. Mechanosignalling through increased ß1 integrin and elevated pSTAT3 levels promoted this amplified tissue tension (Laklai et al., 2016).

The loss of epithelial ROBO2 has been reported in PDAC to result in the upregulation of ROBO1 within the stroma, with mutations in ROBO pathway genes frequently observed in human disease (Biankin et al., 2012). The deletion of *Robo2* in mouse pancreatic epithelium culminated in elevated expression of Wnt signalling genes, alongside increased *Tgfb1* and *Tgfbr2*. In acute pancreatitis models, the epithelial deletion of *Robo2* drove elevated fibrosis, collagen deposition, T cell accumulation and TGFß signalling activation with increased pSMAD2 , a phenotype which could be reversed by TGFßR inhibition (Pinho et al., 2018). Interestingly ROBO1 expression in patients correlated with the *Moffitt et al,* 'activated-stroma' definition, which denotes poor prognosis (Moffitt et al., 2015).

Differing mutations within the same gene also affected the biology of CAFs. For instance, CAFs derived from KPC tumours with $Trp53^{R172H}$ mutation created an environment that was more collagen dense than that created by their $KP^{fl}C$ tumour counterparts. Further, KPC educated CAFs increased the invasion of $KP^{fl}C$ cancer cells, which have reduced metastatic potential (Morton et al., 2010), by creation of a stiffer matrix and through secreted perlecan, which was elevated in the KPC CAFs and within the stroma of KPC tumours (Vennin et al., 2019). TNFα was shown to heighten $KP^{fl}C$ educated CAF perlecan expression, which is interesting given the role of TNFα in driving the iCAF phenotype (Biffi et al., 2019). More recently, gain of function p53 mutations were shown to correlate with elevated deposition of ECM thereby excluding cytotoxic CD8 T cells (Maddalena et al., 2021). Further, the 'stroma-activated' signature, described by *Puleo et al,* appears enriched in samples that are p53 mutated, which is

particularly interesting given this subtype was described as having a low immune signature (Puleo et al., 2018).

This adds a layer of complexity to comprehending CAF subtypes with the predominance of work focussing on the KPC model, which reflects the p53 gain of function patient subtype. However, interrogation of KPC, KIC and $KP^{fl/fl}C$ late stage tumours has reflected a similar clustering of CAFs as presented by the Tuveson lab (Elyada et al., 2019; Hosein et al., 2019) suggesting that the overarching classification of CAFs is not drastically affected by the genetics. It is still important to note that CAF subtypes across the full spectrum of PDAC genetic drivers has yet to be examined.

1.3.1.4 Therapeutic intervention and CAFs

Extensive work has been conducted to elucidate new targets for therapy in PDAC, give the failure of front line therapies. The exciting avenue of patient stratification may expose new vulnerabilities based on subsets of disease. The intriguing developments in the fibroblasts field could also provide new targets to either reprogram the TME or influence 'bad' or 'good' actors in disease.

Early insights suggested that exclusion of chemotherapy in PDAC was caused by the dense fibrotic stroma and proposed depletion of ECM and/or CAFs as a potential treatment modality. Work on SHH pathway inhibition (Olive et al., 2009), or hyaluronan depletion (Provenzano et al., 2012) showed promise in preclinical trials but failed to translate in patients (Kim et al., 2014; Van Cutsem et al., 2020), particularly disappointing in the hyaluronan depletion trial which made use of stratification to target patients with high hyaluronan. Subsequent work emphasised the tumour-restraining role of the stroma with αSMA^{+} cell depletion and chronic inhibition or epithelial deletion of SHH generating more poorly differentiated and aggressive tumours (Lee et al., 2014; Oezdemir et al., 2014; Rhim et al., 2014). Intriguingly, undifferentiated tumours are more 'basal-like', with this poor prognosis subtype shown to have improved survival when stroma signatures are present (Puleo et al., 2018). Further understanding of why the above-mentioned stromal depletion studies failed could be gleaned from the enrichment of SHH in a subset of 'myCAFs'. SHH pathway inhibition was therefore predicted to predominantly affect this 'myCAF' subpopulation causing

an increased ‘iCAF’ to ‘myCAF’ ratio (Steele et al., 2021), with ‘iCAFs’ shown to secrete cachexia linked cytokines, such as IL-6 (Biffi et al., 2019), which are predictive of a worse survival (Rupert et al., 2021). Further, stromal specific blockade of TGFßR2 in mouse models culminated in reduced IL-6 with therapeutic benefit. Fibroblasts with high IL-6 were shown to express the most *Tgfbr2*, with non-canonical TGFß signalling via JunD elevating IL-6 and LIF (Huang et al., 2019). Although the ‘iCAF’ phenotype was antagonised by TGFß signalling, iCAFs also had elevated *Tgfbr2* expression (Elyada et al., 2019). Thus, depletion of ‘myCAFs’ through SHH inhibition could promote the inappropriate stimulation of ‘iCAFs’ via TGFß and the subsequent secretion of cytokines associated with poor prognosis.

Therefore, alteration of CAF function may provide more promising results than total/subtype specific CAF ablation. For instance, KPC educated CAFs produce more perlecan, with CAF targeted deletion of perlecan in a co-transplanted orthotopic model improving sensitivity to a combination therapy of gemcitabine and abraxane (nab-Paclitaxel) (Vennin et al., 2019). However, conflicting results have been obtained when disrupting CAFs ability to produce collagen I. In a dual recombinase mouse model of PDAC, deletion of collagen I from αSMA^{+} fibroblasts, but not fibroblast specific protein 1 positive fibroblasts, accelerated tumourigenesis and the development of immune-suppressed poorly differentiated tumours (Chen et al., 2021). In contrast, Losartan, an angiotensin inhibitor, shown to inhibit collagen and TGFß1 production by CAFs resulting in reduced fibrosis in tumour models and enhanced drug delivery (Chauhan et al., 2013; Diop-Frimpong et al., 2011) show promise in a clinical trial (Murphy et al., 2019). This provides an interesting insight into timing of intervention; tumours developing in collagen I deficient stroma show a worse prognosis, yet collagen I ablation in established tumours was beneficial. This is key factor to consider when developing pre-clinical mouse models.

Further, front-line therapies have been shown to impact on the TME and the CAFs within. With CAFs already shown to enhance cancer cell resistance to gemcitabine (Hwang et al., 2008), conditioned media from gemcitabine-resistant cell lines stimulated altered CAF cytokine secretion, which could be mostly abrogated by TGFß signalling inhibition. Additionally, long-term gemcitabine

treatment elevated immune checkpoint gene expression and TGFβ1 ligand availability in the TME, and generated CAFs resistant to gemcitabine. Treatment of pre-clinical models with a TGFβ receptor inhibitor in combination with anti-PDL1 and gemcitabine improved survival (Principe et al., 2020). This could prove particularly interesting, with dual TGFβ inhibition and immunotherapy combinations synergising in other cancers (Mariathasan et al., 2018; Tauriello et al., 2018) and in a small population of PDAC patients (Strauss et al., 2018), and a TGFβR inhibitor in combination with gemcitabine providing a 1 month survival benefit in non-resectable patients (Melisi et al., 2018). Of further interest, given the alternate phenotype of $CD105^{+}$ vs $CD105^{-}$ CAFs (Hutton et al., 2021), long term gemcitabine treated KPC tumours had elevated CD105, which did not occur in the cancer cell lines.

Therefore, when conducting clinical trials, noting alterations to the TME, particularly within CAF populations, could prove beneficial, not only to understand the biology better but also to expose vulnerabilities that could indicate promising potential combinations or second line therapies.

1.3.2 Immune cells

A hallmark of PDAC is a restricted infiltration of the adaptive immune system but a relative abundance of innate immune cells, primarily with extensive macrophage penetrance, with this demonstrated within mouse models of PDAC (Lee et al., 2016).

Significant macrophage infiltration in stromal regions of PDAC has been observed with alternately activated macrophages expressing high levels of CD206 associated with worse patient outcomes (Vayrynen et al., 2021). Expansion of embryonically derived tissue resident macrophages shape the developing TME of PDAC by developing a pro-fibrotic phenotype and promoting PDAC progression (Zhu et al., 2017). Subsequently, macrophages positive for CSF1R were shown to be important for maintenance of PDAC in mouse models, by suppressing T cells and driving a squamous cancer subtype, with depletion of these macrophages extending survival in a genetically engineered mouse model (Candido et al., 2018).

PDAC is generally poorly infiltrated by T cells, as a result of the immunosuppressive stroma (Vonderheide and Bear, 2020). Treg cells were shown, in patient samples, to reside in close proximity to tumours cells and persist through PanIN to PDAC stages, while $CD8^+$ T cells were sparse. However, although elevated circulating Tregs correlates with poor survival in PDAC, depletion of Tregs in early disease states drives worsening of disease (Zhang et al., 2020).

1.4 TGFβ signalling pathway

1.4.1 The discovery and history of the TGFβ signalling pathway

1.4.1.1 The discovery of the TGF-β ligands

In 1978, work carried out in the Todaro lab discovered polypeptides, of three different weights secreted from Moloney murine sarcoma virus-transformed cells. Fibroblast assays using these polypeptides showed they were able to induce overgrowth in monolayers and anchorage independent growth in agar and they were subsequently termed sarcoma growth factors (SGFs) due to cancer transforming properties (Delarco and Todaro, 1978). Further work in 1980 isolated peptides from transformed cells, which were shown to have similar transforming properties in fibroblast assays to SGFs, and these were termed transforming growth factors (TGFs) (Roberts et al., 1980; Todaro et al., 1980). Continued work on these peptides resulted in multiple publications in the early 1980s which highlighted that these TGFs required de novo protein synthesis for their transforming properties (Ozanne et al., 1980), that they can be produced by non-neoplastic cells (Assoian et al., 1983; Roberts et al., 1981) and that they could be split into two independent fractions based on their requirement for epidermal growth factor (EGF) (Anzano et al., 1982b; Moses et al., 1981). These two fractions were termed TGFα and TGFß, with TGFα shown to compete with EGF for EGF receptors, whereas TGFß did not (Anzano et al., 1982a).

Platelet derived TGFß allowed for purification of larger quantities of the ligand, subsequently shown to exist as a dimer of two identical 12.5kDa subunits (Assoian et al., 1983). Cloning of the gene highlighted a pro-TGFß structure, which requires cleavage to generate its mature form (Derynck et al., 1985). The defined crystal structure of TGFß2 confirmed a disulphide bond between

residues 77 of each monomer linking them to form a dimeric structure (Daopin et al., 1992). It was subsequently shown that there are three isoforms of TGFß found in mice and humans.

1.4.1.2 Discovery of the TGF-β receptors

Work by Massague et al. in 1982 revealed that labelled SGF bound to the EGF receptor as well as to an unknown 60kDa receptor, with binding blocked by excess TGF but not EGF (Massague et al., 1982). Research highlighted that the labelled TGFß was bound to a receptor complex of 280kDa as well as a lower affinity receptor of 70kDa (Massague and Like, 1985). This receptor complex existed as an oligomer (Massague, 1985), with work from *Tucker et al*. and *Frolik et al*. confirming similar findings (Frolik et al., 1984; Tucker et al., 1984a).

Significant time was spent identifying the structure of the TGF-ß receptors with cloning of TGFßR2 revealing it was a serine/threonine kinase of roughly 60kDa with the capacity to auto-phosphorylate itself (Lin et al., 1992). TGFßR1, termed ALK5 henceforth, was also found to be a serine/threonine kinase with a similar structure to TGFßR2, with the receptors capable of forming a complex (Franzen et al., 1993).

Work from *Boyd et al.*, and *Laiho et al.*, showed, via the development of cell lines resistant to the growth arresting effects of TGFß1 and TGFß2, that both ALK5 and TGFßR2 were required for sensitivity to TGFß signalling (Boyd and Massague, 1989; Laiho et al., 1990). This was confirmed by *Wrana et al*, via transfection of TGFßR2 into the resistant cell lines. They showed TGFß response only in the presence of ALK5 and that ALK5 was unable to bind a mutated TGFßR2, with the functional kinase domain of TGFßR2 required to propagate downstream signalling (Wrana et al., 1992). These data confirmed that TGFßR2 and ALK5 form a complex upon ligand binding, and that kinase activity is required to initiate intracellular signalling cascades.

Also highlighted in the tagged TGFß studies was a larger molecule of 280kDa, which was shown to exist in greater abundance than the lower weight ALK5 or TGFßR2. Work showed that this type III receptor bound to TGFß2 with greater affinity than TGFß1, whereas, ALK5 and TGFßR2 bind with less affinity to TGFß2

(Moustakas et al., 1993). TGFβR3 was cloned and shown to be a transmembrane protein, called betaglycan, with a short cytoplasmic tail, various sites for glycosylation, as well as sites for chondroitin sulphate and heparin sulphate binding and a cleavage site allowing for a soluble form of the protein to exist (Lopezcasillas et al., 1991). Interestingly, the sequence showed large areas of homology, in particular in the cytoplasmic and transmembrane regions, to the protein endoglin (Gougos and Letarte, 1990), which was subsequently shown to bind TGFβ1 and TGFβ2 (Cheifetz et al., 1992). This indicated that betaglycan and endoglin could support signalling via the recruitment of TGFβ to the receptor complex.

1.4.2 The TGFβ signalling cascade

1.4.2.1 Intracellular propagation of TGFβ signalling

Following receptor ligation TGFβ signalling is propagated by intracellular receptor SMADs (R-SMAD), such as SMAD2 and SMAD3. SMAD Anchor for Receptor Activation (SARA) is able to bind both SMAD2 and SMAD3 and recruits SMAD2 to the TGFβR complex (Tsukazaki et al., 1998). ALK5 phosphorylation of SMAD2 (pSMAD2) occurs at the receptor complex promoting release of pSMAD2 from SARA and subsequently a SMAD4:pSMAD2 complex forms (Abdollah et al., 1997). SMAD3 was also shown to be phosphorylated by the receptor complex (Liu et al., 1997) and able to interact with SMAD4 (Wu et al., 1997). SMAD molecules are continuously shuttling from the cytoplasm to the nucleus (Pierreux et al., 2000) however, following TGFβ stimulation SMADs accumulate in the nucleus peaking at 45 minutes and are retained there for roughly 5 hours, with dephosphorylated R-SMADs dissociating from SMAD4 within the nucleus and shuttling back to the cytoplasm (Inman et al., 2002; Xu et al., 2002) (**Figure 3**). Additional binding partners, such as YAP/TAZ, enhance retention of SMADs in the nucleus with knockdown of YAP/TAZ or activation of the hippo pathway, which sequesters YAP/TAZ in the cytoplasm, increasing SMAD egress from the nucleus following TGFβ stimulation (Labibi et al., 2020). TAZ has been shown to be capable of binding phosphorylated SMAD2/3 in complex with SMAD4 upon TGFβ stimulation (Varelas et al., 2008). Furthermore, high density cell culturing, which activates the Hippo pathway, culminated in cytoplasmic sequestering of YAP/TAZ and decreased nuclear pSMAD2/3, thus inhibiting TGFβ signalling function (Varelas et

al., 2010), indicative of cross talk with additional signalling pathways affecting TGFß signalling potential. Acute stimulation of cells with TGFß results in rapid internalisation of the receptor molecules rendering cells refractory to subsequent stimulation for around 12-24 hours (Vizan et al., 2013). Within the nucleus, SMAD complexes bind motifs such as SMAD binding elements (SBEs) (Dennler et al., 1998; Jonk et al., 1998) with SMAD3 and an isoform of SMAD2 able to directly bind DNA (Yagi et al., 1999), although with low affinity (Shi et al., 1998). Therefore, additional binding partners are recruited such as Foxh1 (Chen et al., 1996) or c-Fos and c-Jun (Zhang et al., 1998) which expands TGFß induced transcriptional control. The crystal structure of SMAD2 and SMAD3 highlighted multiple hydrophobic patches which facilitate interactions with binding partners (Miyazono et al., 2018).

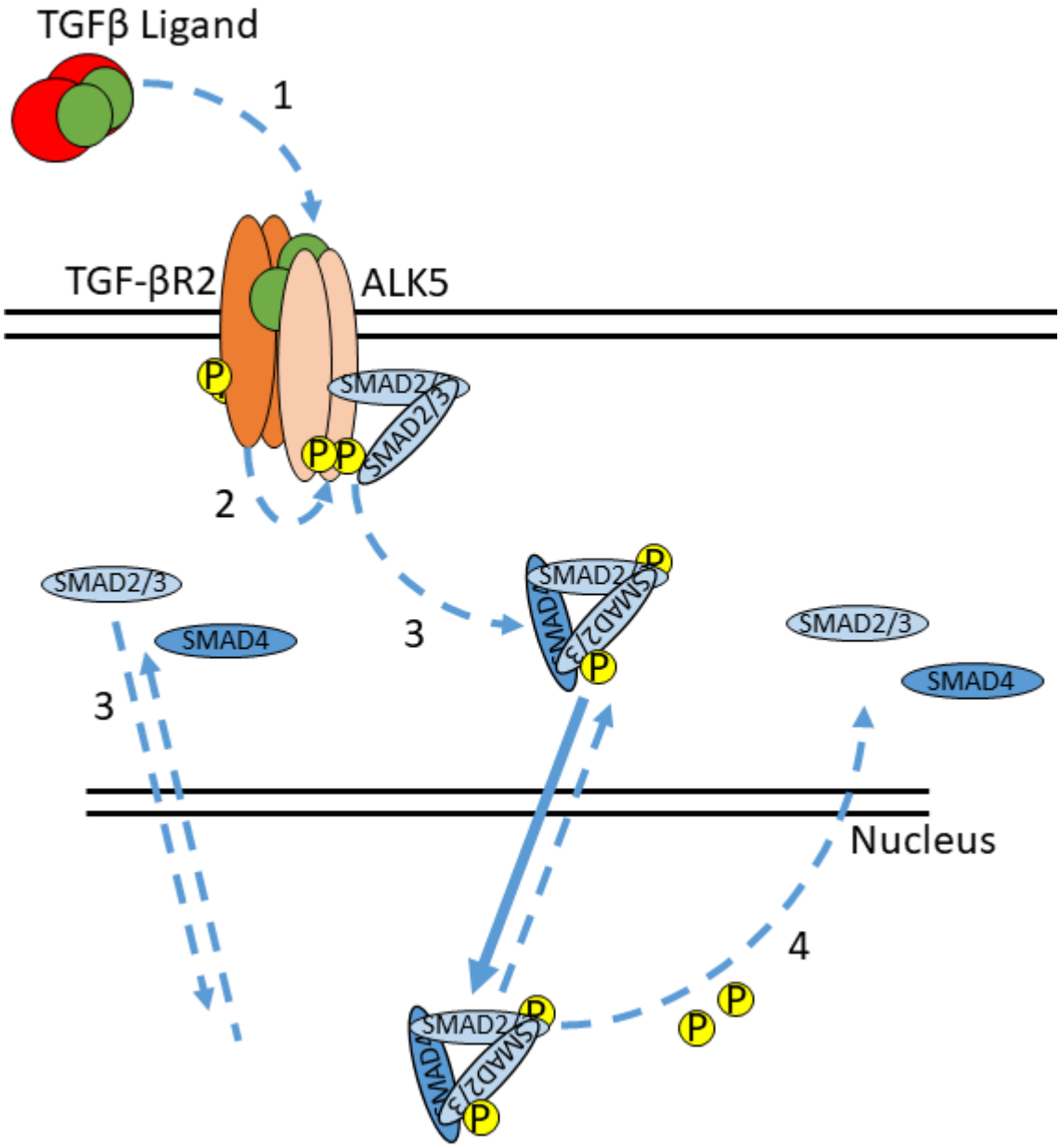

Figure 3 TGFβ signalling pathway
Schematic outline of the TGFβ signalling pathway. 1) Latent TGFβ is released with the active dimer binding to TGFBR2 and ALK5 at the cell surface. 2) TGFβ-bound, constitutively phosphorylated TGFBR2 recruits, binds and phosphorylates ALK5. 3) The receptor complex propagates down-stream signalling through the phosphorylation of SMAD2/3, at their C-termini, which forms a complex with SMAD4. SMAD molecules constantly shuttle between cytoplasm and nucleus in steady state, but upon the formation of the pSMAD2/3:SMAD4 complex SMADs are concentrated and retained in the nucleus for longer. In the nucleus the SMAD complex and additional binding partners can repress or induce gene expression depending on contextual cues. 4) SMAD2/3 are de-phosphorylated in the nucleus and return to the cytoplasm where they can undergo additional cycles of activating phosphorylation through the TGFβ receptor complex if ligand remains available.

1.4.2.2 TGFβ signalling control

Control of TGFß signalling involves multiple mechanisms. TGFß is secreted in a latent bound form (Pircher et al., 1986). TGFß is cleaved within the cell by furin, however, the latency associated protein remains non-covalently attached upon secretion, termed pro-TGFß, retaining TGFß in an inactive form (Gentry and Nash, 1990). This pro-TGFß interacts with Latent TGFß binding protein (LTBP) bound to the ECM and upon protein cleavage mature TGFß can be released (Taipale et al., 1994). Upon application of force, TGFß was also released in its mature form with this dependent upon LTBP binding to the ECM (Buscemi et al., 2011). Interestingly, recent work has suggest that latent TGFß can be activated through $\alpha_V\beta_8$ integrin interaction which precludes the necessity for release of mature TGFß (Campbell et al., 2020). This was dependent on LTBP1 (Annes et al., 2004), with GARP (glycoprotein A repetitions predominant), expressed on T regulatory cells (Tregs) facilitating presentation of LTBP bound TGFß to the $\alpha_v\beta_8$ integrin thus driving immunosuppression (Lienart et al., 2018).

Further, SMAD7 is an important protein in controlling active TGFß signalling. It was shown to bind directly to ALK5 and thereby block interactions with SMAD2/3 (Hayashi et al., 1997). Additionally, SMAD7 interacts with ubiquitin ligase Smurf2 thereby recruiting it to the receptor complex targeting TGFßR for degradation (Kavsak et al., 2000). As well as inducing receptor degradation the SMAD7-Smurf2 complex was able to cause proteasomal degradation of SARA (Wojtowicz et al., 2020). TGFß controls its own signalling through induction of SMAD7 (Huang et al., 2020).

1.4.3 Functions of TGFβ in cancer

1.4.3.1 Tumour suppressive function

TGFß has been convincingly shown to have cytostatic functions in cells (Tucker et al., 1984b), with cell lines resistant to TGFß growth suppression lacking receptor expression (Laiho et al., 1990). TGFß was shown to inhibit the ID (Inhibitors of differentiation) proteins, which drive proliferation and regulate cancer stem cells, through induction and formation of SMAD ATF3 complexes (Kang et al., 2003). For instance ID2 has been shown to override the tumour suppressive function of RB (Lasorella et al., 2014), with TGFß shown to inhibit

ID2 expression and sustain this through induction of MAD expression which prevents MYC from binding to the *ID2* promoter (Siegel et al., 2003). Interestingly, in TGFß signalling proficient tumours, *ID1* expression becomes uncoupled from TGFß suppression and therefore sustained expression of *ID1* can promote carcinogenesis (Huang et al., 2020). Further, TGFß signalling has been shown to induce inhibitors of cyclin dependent kinases (CDK), thereby blocking cell cycle progression. TGFß induced inhibition of Myc also culminates in reduced suppression of p21 and p15 (Staller et al., 2001), with p21 and p15 known CDK inhibitors. Additionally, SMADs binding with FoxO can induce expression of p21 from the *CDKN1A* gene (Seoane et al., 2004) and p15 from the *CDKN2B* gene (Gomis et al., 2006). Following hepatic injury, elevated TGFß ligand secretion can induce p21 senescence with the inhibition of TGFß reducing measurable p21 expression and observed to enhance tissue regeneration (Bird et al., 2018). Further, TGFß signalling can induce apoptosis by driving expression of death-associated protein kinase (Jang et al., 2002), as well as inducing pro-apoptotic Bim binding to Bcl-X_L (Ohgushi et al., 2005).

1.4.3.2 Epithelial mesenchymal transition in cancer

TGFß is often referred to as a double-edged sword due to having both tumour suppressive and tumour promoting activity. Epithelial mesenchymal transition (EMT) is the loss of epithelial cell polarity with the promotion of a mesenchymal phenotype, increasing cell invasiveness (Yang et al., 2020). EMT has been shown to be potently driven by TGFß signalling, with TGFß initially shown to promote EMT in heart endothelial cells (Potts and Runyan, 1989). Decreased expression of epithelial markers, E-cadherin and zonula-occludens 1 (ZO1), alongside increased mesenchymal markers, vimentin and fibronectin, and an altered cuboidal to spindle like cell morphology was shown following TGFß stimulation of mammary epithelial cells, with this switch dependent on TGFß receptor expression (Miettinen et al., 1994). A complex of SMAD3, SMAD4 and SNAIL1 was able to bind and repress genes important for maintaining epithelial phenotype, such as E-cadherin, claudin-3 and occludin (Vincent et al., 2009). TGFßR2 was further shown to bind and phosphorylate Par6, a protein important for epithelial polarity and tight junction formation, to induce EMT (Ozdamar et al., 2005).

The expression of mesenchymal markers SNAIL, TWIST and SLUG was noted in the majority of human pancreatic patient tissue (Hotz et al., 2007), with EMT shown to contribute to drug resistance in PDAC cell lines (Arumugam et al., 2009). TGFß driven EMT has also been shown to be important for metastasis of cancer cells (Oft et al., 1998), with *Rhim et al*, showing that mesenchymal marker expression could be observed in PanIN lesions, with cell dissemination preceding tumour development. The authors show that from PanIN II stage onwards, yellow fluorescent protein labelled KPC cells can be seen in the stroma with acquisition of fibroblast like morphology, suggesting invasion across the basement membrane. KPC cells were also detected in the circulating blood and as single cells in the liver, indicative of an invasive capacity of KPC cells preceding frank carcinoma development (Rhim et al., 2012). Although deletion of *Twist* or *Snai1* in the KPC model had no impact on metastatic dissemination, the models were less resistant to gemcitabine therapy (Zheng et al., 2015).

It has been suggested that lethal EMT can be driven through TGFß signalling in a SMAD4 dependent manner, with Sox4 driving pro-apoptotic Bim (David et al., 2016). However, it has been shown that RAS signalling cooperates with TGFß through RAS responsive element binding protein 1 to bind to multiple genes involved in EMT such as *Snai1*, *Twist1* and *Zeb1 (Su et al., 2020)*. A combination of mutant p53 and RAS in combination with TGFß signalling has been shown to form a mutant p53/p63/SMAD2 complex that increases metastasis (Adorno et al., 2009). Further, stimulation of 3D organoid cultures of $Kras^{G12D}$ expressing pancreatic cells with TGFß ligands induced a partial mesenchymal state with elevated mesenchymal gene expression and increased proliferation (Handler et al., 2018). Subsequent, *in vitro* studies have observed increased tube forming cell morphology following TGFß stimulation of PDAC organoids, with elevated *Snai1* and *Cdh2* noted (Yamaguchi et al., 2019), while prolonged exposure to TGFß promoted stable EMT, which increased drug resistance and enhanced cell stemness (Katsuno et al., 2019).

1.4.3.3 Immune modulation of TGFβ

TGFß has also been highlighted as potent inhibitor of multiple cell types within the immune system (Batlle and Massague, 2019). For instance TGFß was proposed to alter neutrophil activation (Fridlender et al., 2009), discussed in

more detail later in this chapter, as well as inhibiting natural killer (NK) cell function (Lazarova and Steinle, 2019). Macrophages are proposed to exist in a spectrum of polarized states with TGFß signalling in part driving alternately activated macrophages which are tumour promoting (Orecchioni et al., 2019). TGFß signalling in macrophages was shown to promote the expression of immune suppressive cytokines, such as IL-10, at the expense of inflammatory cytokines, IL-12 and TNFα through SNAIL mediated repression, while elevating expression of the alternately activated macrophage marker CD206 (Zhang et al., 2016).

TGFß can also drive the prototypical immunosuppressive T cell, the Treg (Zheng et al., 2002b), potentially through induction of the Treg canonical transcription factor, Foxp3 (Chen et al., 2003). TGFß is also involved in the development of IL-17 producing T helper cells (Th17), through inhibition of SOCS3, thereby prolonging STAT3 activation (Qin et al., 2009). Further, T cell inhibition, particularly of cytotoxic $CD8^+$ T cells has been shown. For instance, adoptive transfer of *Alk5* deficient $CD8^+$ T cells into KC mice reduces neoplastic burden with increased PanIN cell death observed (Principe et al., 2016). Whole body haploinsufficiency of *Alk5* in the KC mouse model also decreased Treg infiltration, while elevating CD8 T cell infiltration and expression of cytotoxic granzyme (Principe et al., 2016). TGFß signalling, has also been, shown to inhibit PD-L1 expression on cancer cells, however, therefore inhibition of signalling could enhance immunosuppression in some scenarios. Subsequently TGFß inhibition was shown to synergise well with anti-PD1 treatment, with this observed across multiple mouse models of cancer (Mariathasan et al., 2018; Principe et al., 2019; Tauriello et al., 2018).

1.5 Neutrophils

1.5.1 Granulocytes

Granulocytes are members of the innate immune system that are responsible for the initial response to injury and are named due to the presence of granules within their cytoplasm. The granulocyte family is composed of mast cells, basophils and eosinophils, which are derived from GATA1 positive granulocyte-monocyte precursors, and neutrophils, which are derived from GATA1 negative granulocyte-monocyte precursors (Drissen et al., 2016). These cells develop in

the bone marrow in a process known as granulopoiesis before egressing into the blood and eliciting their response at distant tissue.

Mast cells are generally only found in their mature state within the tissue, often at mucosal and epithelial barriers. At these sites, they are able to respond rapidly to antigens for instance by recognising pathogen-associated molecular patterns or, most commonly, through the adaptive immune arm, via crosslinking of FcεRI, which binds IgE antibodies. Upon activation they degranulate, releasing their contents, which enhances the recruitment of T cells as well as increasing vascular permeability and mucous production, although they are predominantly known for their role in allergy causing bronchial constriction (Galli et al., 2020; Krystel-Whittemore et al., 2016). The role of mast cells in pancreatic cancer is unclear. The overexpression of Myc in pancreatic beta cells was shown to induce tumour formation in a mast cell dependent manner (Soucek et al., 2007); however, more recently in the dual recombinase KPF model mast cell depletion did not affect tumour development (Schonhuber et al., 2014).

Similarly to mast cells, basophils are granulocytes that express FcεRI with the capacity to release mediators such as histamine, granzyme B, TNFα, IL-6 and IL4, although they comprise less than 1% of human leukocytes (Marone et al., 2020). Basophils are reported to circulate in the blood and enter tissues upon detection of inflammatory stimuli, although it has been shown that murine basophils are present in the lung in steady state and may differ in their function with the capacity to stimulate alternately activated alveolar macrophages (Cohen et al., 2018). It was shown that higher numbers of IL-4 secreting basophils in the tumour draining lymph nodes of PDAC patients associated with poor prognosis with implantation of orthotopic tumours derived from $KP^{fl/fl}C$ cell lines in basophil deficient mice failing to grow (De Monte et al., 2016).

Eosinophils are found in a low numbers in the circulation but are more numerous in tissue, with these numbers fluctuating depending on inflammatory stimulus. Eosinophils release their granules which contain cytokines such as IL-10, IL-13, IL-4, TNF and IFNγ, as well as eosinophil peroxidase and eosinophil cationic protein (Weller and Spencer, 2017). Eosinophils have been shown to have a mixed role in cancer with evidence supporting both a promoting and restraining

function. Interestingly, it has been shown that inflammatory activated eosinophils can promote CD8+ T cell influx in a solid tumour model while enhancing classical macrophage activation (Carretero et al., 2015).

1.5.2 The normal function of neutrophils

Neutrophils are an essential component of the innate immune system that respond rapidly to tissue damage with the aim of suppressing infection. Deficiencies or aberration of neutrophil function results in increased susceptibility to, and recurrence of bacterial and fungal infections (Lekstrom-Himes and Gallin, 2000). One of the major functions of the bone marrow (BM) is myelopoiesis with haematopoietic stem cells (HSC) retained in a niche supported by osteoblasts and endothelial cells. A neutrophil unipotent progenitor was identified in both the mouse and human BM (Zhu et al., 2018) and neutrophils develop from progenitor cells through to eventual mature cells, which egress from the BM (Grieshaber-Bouyer et al., 2021). The differentiation of HSCs into neutrophils is controlled by transcription factors such as CCAAT enhancer binding protein (C/EBP)-α (Zhang et al., 1997) C/EBPϵ (Yamanaka et al., 1997) and PU.1 (Satake et al., 2012), with the deletion of any of these resulting in a lack of mature neutrophils. These transcription factors control differentiation of the HSCs through myeloblast, promyelocyte, myelocyte and band cell stages before eventual development of polymorphonuclear granulocytes or neutrophils (Evrard et al., 2018). Egress from the BM is controlled by the differential expression of two chemokines receptors CXCR4 and CXCR2. Chemokine CXCL12, produced by reticular cells in the niche (Sugiyama et al., 2006), binds CXCR4 and retains stem cells within the BM, with deletion of either the receptor (Eash et al., 2009) or chemokine (Nagasawa et al., 1998) culminating in abrogated myelopoiesis and reduced egress of mature neutrophils. Within this niche endothelial cell production of stem cell factor (SCF), which binds c-KIT, is required to maintain the HSC pool (Ding et al., 2012). CXCL12 production in the BM niche (Semerad et al., 2005) and CXCR4 expression on neutrophils (Kim et al., 2006) was shown to be down regulated upon G-CSF (granulocyte colony-stimulating factor) stimulation, which can occur in stress conditions, including being released by PDAC cells (Pickup et al., 2017). Neutrophils isolated from human blood show high expression of CXCR2 and are chemoattracted through this receptor by CXCL1 and CXCL2 (Martin et al., 2003). Injection of G-CSF causes an increase in

blood levels of CXCL1, through thrombopoietin, subsequently promoting neutrophil mobilization from the BM (Kohler et al., 2011). Therefore, through CXCR2 signalling and the decrease in CXCR4 signalling mature neutrophils can egress from the BM into the blood.

Once circulating in the blood, neutrophils are required to cross the vascular walls in order to access sites of damage or infection. Selectin binding between neutrophils and endothelial cells causes a 'rolling' phenotype, which allows a slowing of neutrophil movement in the blood in order to enhance transmigration across the endothelial walls by sensing further adherence molecules. Inflammatory stimulation of endothelial cells, through IL1 or tumour necrosis factor (TNF) (Bevilacqua et al., 1989), increases the expression of E selectin. L-selectin (CD62L) on neutrophils was revealed to facilitate 'rolling' through binding to E-selectin (CD62E) on endothelial cells (Abbassi et al., 1993), with inhibition of CD62L reducing leukocyte rolling (Ley et al., 1991).

Firm adhesion is then initiated through integrins $\alpha_1\beta_2$ (CD49a/CD18), $\alpha_L\beta_2$ (CD11a/CD18) and $\alpha_M\beta_2$ (CD11b/CD18) on neutrophils binding to intracellular adhesion molecules (ICAMs) on the endothelial cells. Neutrophils lacking, or with inhibited CD11b/CD18, exhibit reduced transmigration (Phillipson et al., 2006; Sumagin et al., 2010), with CD11a/CD18 also demonstrated to be important in transvasation (Hyun et al., 2019). The stimulation of endothelial cells by TNFα (Sumagin and Sarelius, 2006) or IFNγ (Sumagin et al., 2014) culminates in an upregulation of ICAM-1, with ICAM-1 and CD11a/CD18 co-located in ring structures during the transmigration of neutrophils (Shaw et al., 2004). Chemokine activation of G-protein coupled receptors such as CXCR2 by CXCL1 promotes the arrest of neutrophils (Block et al., 2016) to further encourage neutrophil transvasation. CXCR2-deficient mice showed total ablation of neutrophil invasion into tissue, with inhibition of CXCL1 or CXCL2 partially re-capitulating this finding (Girbl et al., 2018).

Upon reaching the site of damage, neutrophils begin their task of dealing with the infection. They do this through multiple mechanisms. They are potent producers of further chemoattractants, such as CXCL1 and CXCL12, to recruit inflammatory cells. They also secrete cytokines to stimulate immune cells. Two neutrophil populations with opposing capacity to activate macrophages have

been described, with IL-10 or IL-12-producing neutrophils able to alternately activate or classically activate macrophage populations, respectively (Tsuda et al., 2004). Further, neutrophils contain multiple granules, which they acquire in stepwise fashion during their development (Bainton et al., 1971; Xie et al., 2020). Primary granules (azurophilic), acquired at the promyelocytes stages, are the first obtained and contain proteins such as peroxidase, serine proteases, cathepsin G, defensins, neutrophil elastase and myeloperoxidases. Secondary granules (specific), containing lactoferrin, follow at the myelocytes stage, with tertiary (gelatinase) granules, which contain matrix metalloproteinases (MMPs), forming at late neutrophil stages (Cowland and Borregaard, 2016). Following neutrophil activation, the granules are secreted in reverse order, highlighting the potency of more mature neutrophils. Neutrophils are also able to extrude their cytoplasmic DNA and mitochondrial DNA (Lood et al., 2016) in a process known as NETosis, which acts as a neutrophil extracellular trap (NET) to bind and coat infectious organisms to mark them for degradation (Brinkmann et al., 2004).

Neutrophils are generally thought to have a short circulating half-life, although there have been variations reported as to the length of this. One study, utilising heavy water tracing, highlighted a half-life of around 5.4 days (Pillay et al., 2010), however, subsequent studies, using stable isotopes, have determined it to be around 16 hours (Lahoz-Beneytez et al., 2016). Stimulation of cultured neutrophils with IL-1ß, TNF-α, IFNγ, GM-CSF or G-CSF significantly extended their survival (Colotta et al., 1992), with tumour infiltrating neutrophils also highlighted to survival longer than their splenic equivalents (Sawanobori et al., 2008).

Evidence of neutrophil reverse trans-endothelial migration has also been shown (Woodfin et al., 2011), with movement from damaged tissue back into the blood stream observed, and thought to be caused by increased vascular leakiness (Owen-Woods et al., 2020) or downregulation of junctional adhesion molecule C (Woodfin et al., 2011). Further, there is evidence of these neutrophils reaching secondary organs and eliciting damage at those sites (Owen-Woods et al., 2020).

1.5.3 Neutrophil Maturity

Increasing evidence has elucidated that neutrophils are a heterogeneous population. Single cell sequencing has highlighted that blood borne and splenic neutrophils could be split into three distinct populations, with elevated BM derived immature neutrophils populations found in the blood during infection (Xie et al., 2020). There is evidence that sterile inflammation also promoted an influx of more immature neutrophils into both the inflamed tissue and the blood (Grieshaber-Bouyer et al., 2021).

There is evidence that chronic diseases, such as cancer, result in the increased release of immature neutrophils that are distinct from their mature counterparts (**Figure 4**). In a recent study, CyTOF was used to distinguish between markers expressed on proliferating and non-proliferating haematopoietic cells extracted from the BM. Proliferating neutrophils were shown to have increased expression of c-Kit and CXCR4, but decreased expression of CXCR2, CD62L and Ly6G. Furthermore, this study showed that $CD11b^{+}Gr\text{-}1^{+}$ neutrophils could be split into three populations, pre-neutrophils, immature neutrophils and mature neutrophils with distinct transcriptional profiles. Pre-neutrophils were defined by $cKit^{hi}CXCR4^{hi}$ expression, whereas, immature neutrophils were $cKit^{lo}CXCR4^{lo}Ly6g^{lo/hi}CXCR2^{lo}$, and mature neutrophils exhibited $Ly6G^{hi}CXCR2^{hi}$ expression and were CD101 positive. Development through pre-neutrophil, immature and mature neutrophil stages was accompanied with a decrease in cell cycle and transcription/translation regulation alongside an increase in chemotaxis and response to microbial stimuli pathways denoting their reduced granule production but increased effector function (Evrard et al., 2018). In orthotopic PDAC transplant experiments, it was shown that mice with high tumour burden presented with more intra-tumoural and circulating immature neutrophils when compared to mice with low tumour burden, indicative of systemic effects influencing egress of less mature neutrophils from the BM (Evrard et al., 2018; Pickup et al., 2017). Further, increased neutrophil progenitor cells were found out with the BM in a subcutaneous melanoma model, with a tumour promoting function and expression of PD-L1 (Zhu et al., 2018). Interestingly, further functional changes in neutrophils have also been affected by maturity. For instance, NETosis is a function reserved for mature neutrophils,

as immature neutrophils isolated from acute myeloid leukaemia patients were unable to do so under stimulation (Lukasova et al., 2013).

Previous studies have also delineated markers on neutrophils that are indicative of increased effector function. For example ICAM-1 expression on neutrophils highlighted a population with increased reactive oxygen species generation and phagocytic activity (Woodfin et al., 2016). A $CD62L^{lo}$ population, shown to increase in proportion following endotoxin exposure, had an altered proteome compared to both circulating mature and immature neutrophils, although more closely resembling the mature neutrophils (Tak et al., 2017). These $CD62L^{lo}$ neutrophils were able to inhibit T cell proliferation by release of H_2O_2 into the T-cell-neutrophil immune synapse (Pillay et al., 2012). A $cKIT^{+}$ population of neutrophils was also shown to expand with tumour growth in a mouse model of breast cancer, with loss of this population upon tumour resection (Coffelt et al., 2015). This population also exhibited a role in metastasis (Kuonen et al., 2012), whilst displaying an altered metabolism, which allowed them to maintain T cell immune suppression through reactive oxygen species (Rice et al., 2018). Expression of cKIT was predominantly found on pre-neutrophils (Evrard et al., 2018). Another marker thought to denote neutrophil maturity, although its full function has not yet been elucidated, is Ly6G. Monoclonal antibody blockade of Ly6G reduced neutrophil recruitment in an integrin $ß_2$ mediated manner (Wang et al., 2012), however, a subsequent report contradicted these findings, with neutrophil recruitment unchanged upon identical treatment (Yipp and Kubes, 2013). Intriguingly, expression of Ly6G was shown to denote neutrophil maturity in a study of *Streptococcus pneumonia* infection, with the pathogen cleared by mature $Ly6G^{hi}$ neutrophils, whilst, $Ly6G^{int}$ splenic resident neutrophils proliferate to expand the mature neutrophil pool (Deniset et al., 2017). These studies collectively emphasise that neutrophils do not exist as a simple homogenous population. Delineation of neutrophils with an increased effector function is possible by examination of their surface marker expression and understanding the impact of this on disease states is key for elucidating the full role of neutrophils.

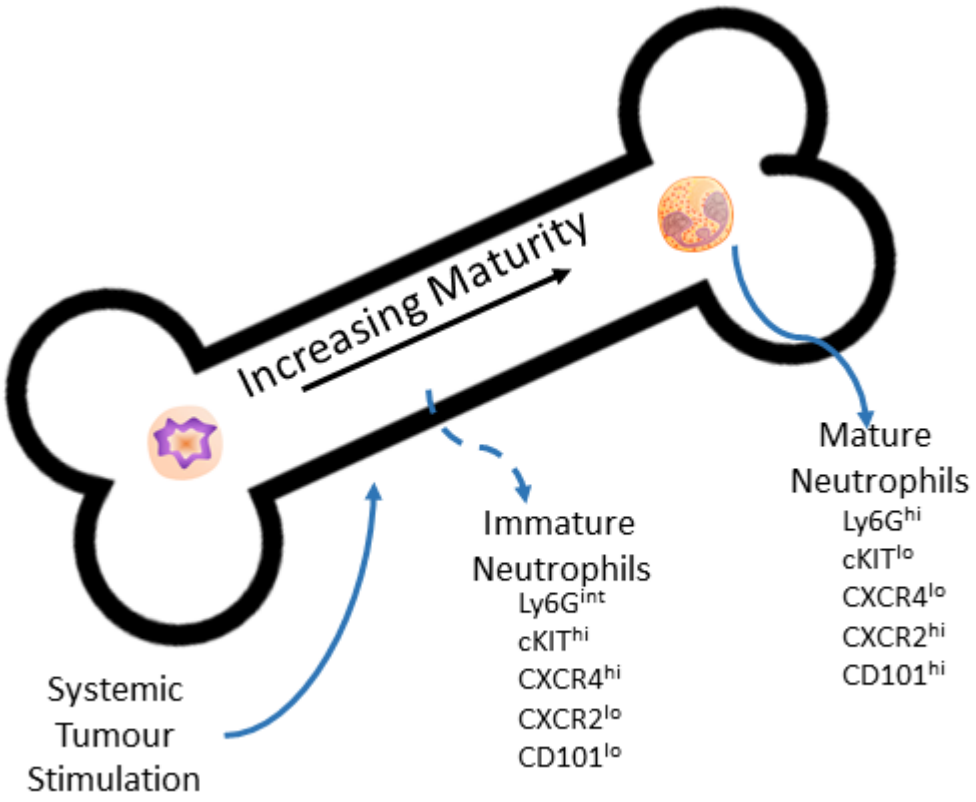

Figure 4 The systemic effects of cancer promotes the egress of immature neutrophils Schematic outline of the neutrophil maturation in the blood. Systemic stimulation caused by tumour presence increases the egress of immature neutrophils into the periphery. Markers shown which are proposed to distinguish between mature and immature neutrophils.

1.5.4 Neutrophils in Cancer

Transcriptionally, tumour associated neutrophils (TANs) have been found to be distinct from their naïve counterparts, with a reduction in peroxidase gene expression and granule proteins. However, they exhibit increased antigen presenting gene expression and inflammatory response genes such as TNFα and IL-1β. They also display elevated chemokine expression with T cell chemoattractants, CCL17, CXCL9, CXCL10 and CXCL16, neutrophil chemoattractants, CXCL1, CXCL2 and CCL3, B cell chemoattractant, CXCL13, and macrophage chemoattractants, CCL2, CXCL10 and CCL7, all being elevated (Fridlender et al., 2012), indicative of tumour site education or priming of neutrophil function. Further confirmation of tumour site education of neutrophils was demonstrated in tumour transplant models. Neutrophils were extracted from both early and late stage tumours with early stage TANs presenting with more H_2O_2, nitric oxide and TNFα, thereby having elevated

cytotoxic function. Depletion of neutrophils resulted in reduced tumour growth, but only when depleted from late stage tumours, denoting a switch from anti-tumorigenic to pro-tumorigenic TANs through tumour education (Mishalian et al., 2013).

It has been demonstrated that neutrophils also have an important role in metastasis of multiple cancer types. Circulating cancer cells have been shown to cluster with pro-tumorigenic neutrophils in the blood, with those cancer cells exhibiting greater expression of cell cycle progression genes and able to better form metastasis than those clustered without neutrophils (Szczerba et al., 2019). Neutrophils have been shown to be able to suppress natural killer cells (Spiegel et al., 2016), as well as T cells (Pillay et al., 2012; Zea et al., 2005) thereby suppressing immune mediated clearance of metastasis. Alongside this, contralateral subcutaneous injection of a tumour cell line, which induces blood neutrophilia, increased the metastatic capacity of a generally lowly metastatic cell line injected in the adjacent flank, with splenectomy or neutrophil depletion reducing the metastatic burden (Spiegel et al., 2016). Further, in breast cancer, a cascade involving γδ T cells and neutrophils was shown to promote metastasis. The production of IL-1ß was found to stimulate IL-17 production from γδ T cells, resulting in a systemic increase in G-CSF and elevated neutrophil numbers. The neutrophils were then polarized to a CD8 T cell suppressive state thereby facilitating metastasis. Depletion of γδ T cells, IL-17, G-CSF or neutrophils works to abrogate this metastatic cascade (Coffelt et al., 2015). Elevated levels of the $cKIT^+$ pro-metastatic neutrophils were also shown (Coffelt et al., 2015; Kuonen et al., 2012). IL-1ß was also demonstrated to activate endothelial cells promoting cancer cell transvasation (Spiegel et al., 2016). Within a metastatic model of colorectal cancer, neutrophils were also demonstrated to be key players in metastasis. Neutrophils were recruited to both the primary and metastatic site, and depletion of $Ly6G^+$ neutrophils or disruption of their chemotaxis through small molecule inhibition of CXCR2, culminated in a significantly reduced metastatic burden. The authors also found elevated *Tgfb2* expression at metastatic sites, therefore inhibition of Alk5, TGFß ligand trapping, or deletion of *Alk5* on neutrophils resulted in reduced metastasis with decreased neutrophil infiltration (Jackstadt et al., 2019).

PDAC cells were shown to express neutrophil chemoattractants CXCL1, CXCL2, CXCL5, CXCL8 alongside G-CSF, which is known to stimulate neutrophil egress from the BM (Ijichi et al., 2011; Nywening et al., 2018; Pickup et al., 2017; Steele et al., 2016). $CXCR2^+$ neutrophils are also elevated in the circulating blood of PDAC patients, with higher levels indicative of worse prognosis (Nywening et al., 2018). Patients presenting with a high neutrophil to lymphocyte ratio, both pre-operatively and in the metastatic disease setting, generally have worse outcome (Nywening et al., 2018; Piciucchi et al., 2017). In the metastatic KPC mouse model of human PDAC depletion of $Ly6G^+$ neutrophils, CXCR2 blockade or *Cxcr2* deletion resulted in reduced metastasis. Interestingly CXCR2 inhibition in combination with gemcitabine extended survival in these pre-clinical models. However, CXCR2 inhibition synergised most effectively with anti-PD1, due to enhanced T cell infiltration in CXCR2 inhibitor treated mice, with the combination significantly prolonging survival (Steele et al., 2016). A subpopulation of P2RX1 positive neutrophils was also shown to exist in PDAC liver metastasis. They were associated with immunosuppression through expression of PD-L1 and elevated expression of pro-tumoural neutrophil markers (Wang et al., 2021). Collectively, neutrophils are presented as bad actors in PDAC with their most prominent feature in enhancing metastasis.

Contrastingly, a few publications have presented an anti-metastatic function of neutrophils. Elevated neutrophil numbers were shown in the lung 7 days post orthotopic implantation of 4T1 breast cancer cells, with depletion of neutrophils following implantation culminating in increased lung metastasis. Further, 4T1 tumour educated neutrophils were able to inhibit lung metastasis in comparison to G-CSF stimulated neutrophils, in a tail vein injection metastatic model (Granot et al., 2011). Although this intriguingly pointed to an anti-metastatic function of neutrophils, tumours did still spontaneously metastasise to the lung in the presence of neutrophils. It is perhaps more likely that, as is shown by *Mishalian et al*, early neutrophils are anti-tumourigenic with prolonged exposure to tumour priming them to adopt a pro-tumourigenic role (Mishalian et al., 2013). Therefore, early intervention as shown in the above study is more likely to deplete the pro-tumourigenic neutrophils.

TGFß signalling has also been implicated to have a polarizing role on neutrophil function in cancer. Mice bearing transplanted lung cancer-derived tumours were treated with an ALK4/ALK5 inhibitor (SM16), resulting in elevated tumour neutrophil numbers which correlated with increased *Cxcl2*, *Cxcl5*, *Ccl1* and C*xcl1* expression in tumours, however, systemic neutrophils numbers were unchanged. The treatment culminated in a reduced tumour growth, which was lost upon neutrophil-specific depletion. Isolated neutrophils from the SM16-treated tumours were more cytotoxic in co-culture in comparison to their untreated counterparts. Expression of arginase, shown to suppress T cells (Zea et al., 2005), was decreased in SM16-treated neutrophils, whereas TNFα and ICAM-1 were elevated, with the later proven to be increased at the cell surface. The authors conclude that neutrophils can exists as either tumour promoting or tumour suppressive, with TGFß signalling dictating fate (Fridlender et al., 2009).

1.6 Mouse models of PDAC

With pancreatic cancer being a uniformly lethal disease, effective models of the disease are required to understand progression and to develop effective therapeutic strategies. The understanding of the genetics of human disease has contributed to the development of mouse models, with models developed that can recapitulate the genetic permutations observed in patients, as well as the histopathology and even the metastatic nature of PDAC.

1.6.1 KPC model

The 'gold standard' model used to study PDAC is the KPC model. This model was reported in 2005 by the Tuveson lab and targets conditional oncogenic LSL-$Kras^{G12D}$ and $Trp53^{LSL\text{-}R172H/+}$ alleles specifically to cells of the pancreatic lineage through pancreatic and duodenal homeobox 1 (Pdx1)-driven CRE expression (Hingorani et al., 2005). *Pdx1* is expressed from embryonic day 8.5 in mice and is essential for the development of the pancreas (Gu et al., 2003). CRE recombinase specifically excises *LoxP* sites in the genome, therefore, with Lox-STOP-Lox (LSL) sites preceding the point mutated *Kras* and *Trp53* genes in their endogenous loci expression was restricted to only CRE recombinase expressing cells. Within all other non-CRE recombinase expressing tissues heterozygous *Kras* and *Trp53* expression was sufficient for their normal function. Within 1 year all

Pdx1-Cre; LSL-Kras$^{G12D/+}$*; LSL-Trp53*$^{R172H/+}$ (KPC) mice succumbed to invasive and metastatic PDAC with a median survival of 5 months. Interestingly, loss of heterozygosity of *Trp*53 was required for conversion of PanIN lesions to PDAC, with other major tumour suppressors remaining intact. Metastasis, as is also seen in the human disease, was found in both the liver and lungs. Histopathological analysis highlighted that KPC tumours could present with well or poorly differentiated tumours, further representative of human disease. Thus, this model effectively recapitulated the biology of human PDAC.

Additionally, the KPC model is refractory to many of the frontline therapies used to treat human PDAC. For instance, xenograft or orthotopic transplantation models using PDAC cells lines have reduced growth upon gemcitabine treatment. However, the tumours from the autochthonous KPC mice were largely unaffected, mimicking the limited efficacy of gemcitabine in human patients (Burris et al., 1997; Olive et al., 2009). However, gemcitabine treatment of smaller mouse PDAC can provide therapeutic benefit, indicating the benefits of early disease diagnosis (Gopinathan et al., 2015).

Prior to publication of the KPC mouse the Tuveson and DePinho labs both published a model with pancreas specific expression of *Kras*^{G12D} driven by *Pdx1-Cre* or a knock in *Ptf1a-Cre* (Ptf1a$^{+/Cre}$) allele (KC). Both *Pdx1* and *Ptf1a* are required for the development of the pancreas, with deletion of either resulting in failure to develop acinar cells and therefore the mice do not develop a pancreas, although islets still develop in *Ptf1a* null mice (Jonsson et al., 1994; Krapp et al., 1998). *Pdx1* is expressed from embryonic day 8.5 (E8.5) in the posterior foregut and also the developing pancreatic buds and therefore expression can be found in the duodenum, stomach, bile duct and pancreatic tissue. *Ptf1a* expression is observed from E9.5 in the pancreas, but can also be detected in neural precursors (Burlison et al., 2008). These models displayed only pre-invasive neoplastic lesions with infrequent progression to frank PDAC. The models also effectively recapitulated the PanIN progression of human disease with higher grade PanINs observed more frequently as the mice age (Aguirre et al., 2003; Hingorani et al., 2003). Targeting of oncogenic *Kras* to the acinar cells in the adult pancreas, through *Mist1* and *Elastase* driven tamoxifen inducible CRE-recombinase, has also been shown to driven PanIN development

but not invasive carcinoma in the absence of other mutations or inflammation (Habbe et al., 2008). Subsequently, a mouse model able to revert oncogenic *Kras* activation through a tetracycline-mediated on/off system was developed. Upon exposure to doxycycline, oncogenic *Kras* was 'switched-on' with PanIN lesions developing, however, upon doxycycline withdrawal, therefore 'switching-off' oncogenic *Kras*, these lesions resolve even in a $Trp53^{+/-}$ model. This study, highlighted that continued activation of oncogenic *Kras* is required throughout disease progression (Collins et al., 2012).

Deletion, specifically within the adult pancreas has also been modelled, with a similar progression of disease noted. A Pdx1 driven tamoxifen inducible Cre-recombinase allele was generated to facilitate lineage tracing of duct or islet cell progenitors (Gu et al., 2002). CRE recombinase bound to a modified oestrogen receptor (ERT) (Indra et al., 1999) facilitates sequestering of the recombinase to the cytoplasm, therefore, distant from its site of action (Danielian et al., 1998). ERT is exquisitely sensitive to tamoxifen but not natural oestrogen receptor ligands and upon tamoxifen stimulation the recombinase complex traffics to the nucleus and thereby recombines *LoxP* regions. Induction of $Kras^{G12D}$ within the adult pancreas produced PanINs similar to those in the non-inducible KC mouse (Jean-Paul et al., 2008).

1.6.2 Modelling deletion of other tumour suppressors in PDAC

With *CDKN2A* being silenced or mutated frequently in human PDAC (Aguirre et al., 2017; Bailey et al., 2016), mouse modelling was conducted to determine how deletion of this gene effects pancreatic cancer progression. *Aguirre et al*, showed that deletion of both *CDKN2A* protein products $p16^{INK4A}$ and $p19^{ARF}$, via the CRE recombinase driven excision of lox flanked exon 2 and 3, alongside oncogenic *Kras* resulted in accelerated PanIN progression and development of PDAC. The pancreas specific deletion of *Cdkn2a* alone had no effect on pancreatic development, nor did it give rise to any neoplasms. These tumours presented with a well differentiated morphology with concomitant sarcomatoid regions (Aguirre et al., 2003).

1.6.3 TGFβ signalling deficient models

With the TGF-ß signalling pathway frequently altered in human PDAC, mouse modelling of disruption of the signalling pathway has also been examined. In back to back publications in 2006 deletion of *Smad4* or *TGFBR2* was shown to accelerate development of PDAC in the presence of oncogenic *Kras*. *Bardeesy et al*, showed that homozygous deletion of *Smad4*, via *Pdx1-Cre* or *Ptf1a-Cre* driven excision of lox flanked exons 8 and 9, had no effect on normal pancreatic development. However, when deletion was driven alongside $Kras^{G12D/+}$ (KSC) mice rapidly developed PDAC with a survival range between 8 and 24 weeks of age (Bardeesy et al., 2006). *Ijichi et al.*, showed a similarly rapidly accelerated tumourigenesis with a median survival of 59 days in a *Ptf1a-Cre;* $Kras^{G12D/+}$*;* $Tgfbr2^{lox/lox}$ (KTC) mouse model (Ijichi et al., 2006). Although both models disrupted the TGF-ß signalling pathway and emphasised its importance as a potent tumour suppressor with a quicker progression of disease in comparison to the KPC model, the disease progression differed. In the KSC mouse there was evidence of IPMN development alongside PanINs and subsequent progression to PDAC, whereas, the KTC showed progression through PanIN stages only, suggesting that abrogating the TGF-ß signalling pathway on its own will differ from the disruption of both the BMP and TGF-ß signalling pathways, which occurs in *Smad4* knockouts.

Although at end-point tumours are grossly and histologically similar to the PDACs noted in the KPC model, there is less metastasis in the KSC and KTC model. This may be due to the large burden of the primary tumour resulting in clinical end-points before metastatic seeding can take hold, and in fact, the longest-lived KTC do present with liver metastasis.

Interestingly, in a model of oncogenic *Kras*, under the control of the *Elastase* promoter, crossed with mice with whole body haploinsufficiency of *Alk5*, only 50% of mice presented with pancreatic lesions while 100% of the *Alk5* wild-type mice develop PanINs. The authors, however, show that lesions in the haploinsufficient model are larger, although less abundant (Adrian et al., 2009). Subsequent follow up in this model confirmed these findings with the authors further elucidating that heterozygous deletion of *Alk5* within the epithelial cells accelerated transformation with increased fibroblast infiltration and

desmoplasia (Principe et al., 2016). A *Pdx1-Cre; LSL-Kras^{G12D}; Alk5$^{fl/fl}$* model resulted in pancreatic tumour formation, however, this was accompanied by both squamous stomach and skin tumours, complicating the ability to study pancreatic cancer (Acosta et al., 2013). The KSC model also developed stomach tumours (Bardeesy et al., 2006). Collectively, these studies highlight the discrepancy between epithelial specific and stroma TGFß signalling, while providing further proof that TGFß signalling is a potent tumour suppressor during disease initiation.

Together these mouse models highlight that oncogenic KRAS is required but insufficient to drive PDAC on its own, with additional mutations in tumour suppressor genes necessary for disease progression. This corresponds effectively with human data, in which oncogenic KRAS is present in 95% of cases but additional mutations in tumour suppressor genes occur frequently. Loss of the three major tumour suppressor genes, *Cdkn2a*, *Trp53* and S*mad4*, accelerated PDAC progression in mouse models when compared to oncogenic KRAS on its own and faithfully recapitulate the human disease.

1.6.4 The KPF mouse model

More recently, the Saur lab developed a dual recombinase mouse model of PDAC. They employed *Pdx1* promoter driven expression of Flippase (*Pdx1-Flp*) recombinase, which is able to recombine *Frt* sites within the genome. To drive PDAC development they designed an allele of oncogenic *Kras* gene preceded by an FRT-STOP-FRT site (*Kras$^{FSF-G12D/+}$*) and crossed this model with mice bearing a heterozygous deleted *Trp53* gene, via the flanking of exon the gene with *FRT* sites. They showed that similar to the KC model the KF (*Pdx1-Flp; Kras$^{FSF-G12D/+}$*) mice develop pre-neoplastic PanINs and eventual frank PDAC over a similar time-period with a median survival of 401 days. The addition of the heterozygous deletion of *Trp53* in the KPF model (*Pdx1-Flp; Kras$^{FSF-G12D/+}$; Tp53$^{Frt/+}$)* accelerates disease progression with a median survival of 183 days, again broadly similar to the KPC mouse. Histopathological analysis shows that tumours and pre-neoplastic lesions are similar in both the Flippase and CRE recombinase driven models. Further, the KPF model develops metastasis to similar sites and at a similar frequency to the gold standard KPC mouse model (Schonhuber et al., 2014).

The advantage of using *Pdx1-Flp* was the capacity develop a dual recombinase mouse model via concomitant expression of CRE recombinase. The Saur lab employed a tamoxifen inducible CRE recombinase in the *Rosa26* locus preceded by a FSF site (FSF-Cre^{ERT2}), therefore, targeting expression of Cre^{ERT2} to only the *Pdx1-Flp* expressing cells. Alternatively, they could express *Cre* under the control of a different promoter; in this study, they used *Cpa* promoter, expressed in mast cells. The expression of the CRE-recombinase allows for the recombination of *LoxP* sites and therefore, with different promoters to drive CRE expression, genes can be controlled spatially. When employing a tamoxifen inducible CRE recombinase the timing of gene alteration can also be controlled, ultimately allowing for the spatial and or temporal control of gene expression within PDAC (Schonhuber et al., 2014).

Subsequently the KPF model has been used to examine fibroblasts specific ablation of genes in the developing PDAC. For instance, *Chen et al*, utilised an *Acta2a* driven Cre recombinase to excise the *Collagen I* gene from αSMA^{+} fibroblasts, thereby spatially controlling specific genetic permutations (Chen et al., 2021). Further, tracing of fibroblast populations within PDAC was possible in the KPF model. Tamoxifen inducible Cre recombinase was expressed from the Gli1 or Hoxb6 locus, alongside a conditional LSL-fluorescent protein in the *Rosa26* locus. Upon tamoxifen treatment, the fluorescent protein was expressed and therefore the $Gli1^{+}$ or $Hoxb6^{+}$ fibroblast populations could be tracked at different stages of PDAC tumorigenesis (Garcia et al., 2020).

Aims of Thesis

I aim to develop a new model of TGFβ signalling deficient driven PDAC that better recapitulates the progression of human disease, using a dual recombines mouse model.

I aim to assess the biology of this model in comparison to standard genetically engineered mouse model of PDAC to elucidate new potential therapeutic targets. Further, I aim to understand the ‘doubled-edged sword’ function of TGFβ signalling as both a tumour suppressor and tumour promoter at different stages in carcinogenesis.

To determine the importance of TGFβ signalling and ligand production in a restricted and pan-fibroblast population of CAFs within the dual recombinase mouse model of PDAC.

To provide insight into the predicted suppressive function of TGFβ signalling on the neutrophil population in a dual recombinase mouse model of PDAC.

Chapter 2 Materials and Methods

2.1 Animal Work

The completion of all animal experiments was conducted under the guidance of the UK Home Office regulations. Work was carried out under Project licence PP8411096 (March 2020-onwards) and 70/8375 (pre March 2020), and approved by the University of Glasgow Animal Welfare and Ethical Review Board. The mice, during mating and weaning, were housed in individually ventilated cages. They were provided, ad libitum, with irradiated diet and water in sterilised pouches. Mouse handling was conducted in laminar flow changing stations. Experiment mice were house in conventional caging. Environmental and behavioural enrichment were provided with tissue, fun tunnels, and nesting material. Mice of both sexes were used in all experiments.

2.2 Genetically engineered mice

2.2.1 Genotyping

Genotyping was performed after weaning with excess tissue from ear notching sent to Transnetyx (Cordova, TN, USA) for DNA genotyping. Transnetyx utilise real time-PCR to detect specific allelic alterations.

2.2.2 Clinical End-points

Mice were monitored at least twice weekly and sacrificed upon observation of the stated symptoms.

- Abdominal distension
- Cachexia like loss of body conditioning
- Reduced mobility and/or hunching
- Jaundice
- Paling of footpads
- Diarrhoea
- Slowed or accelerated respiration

Mice older than 1 year of age were also monitored thrice weekly and monitored for appearance and motility. Mice were sacrificed before 18 months of age.

When sacrificing mice two schedule 1 methods were used: predominantly cervical dislocation of the neck followed by exsanguination of the femoral artery, or exposure to rising concentration of carbon dioxide followed by cervical dislocation.

2.2.3 Post mortem dissection

After euthanasia, mice were prepped for dissection with abdominal application of 70% ethanol. The peritoneum was opened and the organs inspected with abnormalities noted. Organs were removed with spleen, liver, lung and piece of PDAC or pancreas fixed in 10% neutral buffered formalin. A chunk of the tumour was cut into smaller pieces with half fresh frozen and half stored in RNAlater (ThermoFisher, #AM7021). A portion of tail was also fresh frozen. Blood sampling through cardiac puncture was taken prior to dissection from relevant mice, with blood transferred to heparin-coated tubes. Blood was processed by the ProCyte Haematology Analyser (IDEXX) to determine cellular populations or was utilised for downstream flow cytometry processes.

2.2.4 The KPF model of spontaneous PDAC

The KPF (*Pdx1-Flp; FSF-Kras$^{G12D/+}$; Trp53$^{frt/+}$*) mouse describe by *Schonhuber et al.* was maintained in house (Schonhuber et al., 2014). They were bred on a mixed background. The KF (*Pdx1-Flp; FSF-Kras$^{G12D/+}$*) and KPF mice were used in ageing cohorts, with KF and *Pdx1-Flp* expressing mice used in time-point studies.

2.2.4.1 Genetic Alleles

The following alleles were crossed into the KPF mice; *Alk5* (Larsson et al., 2001), *Tgfb1 (Azhar et al., 2009)*, *Gli1-Cre^{ERT} (Ahn and Joyner, 2004)*, *Col1a2-Cre^{ER} (Zheng et al., 2002a)* and *Ly6G-Cre (Hasenberg et al., 2015)*.

2.2.4.2 Cohorts

Breeding of appropriate genotypes of these mice generated the cohorts shown in Table 1

Table 1 Genetics of mouse models generated

Tumour Initiation	Abbreviations
Pdx1-Flp; FSF-Kras$^{G12D/+}$; FSF-Cre^{ER}; Alk5$^{fl/fl}$	*KAF*
Pdx1-Flp; FSF-Kras$^{G12D/+}$; FSF-Cre^{ER}; Tgfb1$^{fl/fl}$	*KTF*
Pdx1-Flp; FSF-Kras$^{G12D/+}$; FSF-Cre^{ER}	*KF*
Established Tumour	
Pdx1-Flp; FSF-Kras$^{G12D/+}$;Trp53$^{frt/+}$; FSF-Cre^{ER}	*KPF*
Pdx1-Flp; FSF-Kras$^{G12D/+}$;Trp53$^{frt/+}$; FSF-Cre^{ER}; Alk5$^{fl/fl}$	*KPF; Alk5$^{fl/fl}$*
Pdx1-Flp; FSF-Kras$^{G12D/+}$;Trp53$^{frt/+}$; FSF-Cre^{ER}; Tgfb1$^{fl/fl}$	*KPF; Tgfb1$^{fl/fl}$*
Fibroblast specific targeted deletion in established models	
Pdx1-Flp; FSF-Kras$^{G12D/+}$;Trp53$^{frt/+}$; Gli-Cre^{ERT}	*KPF^{G}*
Pdx1-Flp; FSF-Kras$^{G12D/+}$;Trp53$^{frt/+}$; Gli-Cre^{ERT}; Alk5$^{fl/+}$	*KPF^{G}; Alk5$^{fl/+}$*
Pdx1-Flp; FSF-Kras$^{G12D/+}$;Trp53$^{frt/+}$; Gli-Cre^{ERT}; Alk5$^{fl/fl}$	*KPF^{G}; Alk5$^{fl/fl}$*
Pdx1-Flp; FSF-Kras$^{G12D/+}$;Trp53$^{frt/+}$; Gli-Cre^{ERT}; Tgfb1$^{fl/fl}$	*KPF^{G}; Tgfb1$^{fl/fl}$*
Pdx1-Flp; FSF-Kras$^{G12D/+}$;Trp53$^{frt/+}$; Col1a2-Cre^{ER}	*KPF^{C}*
Pdx1-Flp; FSF-Kras$^{G12D/+}$;Trp53$^{frt/+}$; Col1a2-Cre^{ER}; Alk5$^{fl/+}$	*KPF^{C}; Alk5$^{fl/+}$*
Pdx1-Flp; FSF-Kras$^{G12D/+}$;Trp53$^{frt/+}$; Col1a2-Cre^{ER}; Alk5$^{fl/fl}$	*KPF^{C}; Alk5$^{fl/fl}$*
Pdx1-Flp; FSF-Kras$^{G12D/+}$;Trp53$^{frt/+}$; Col1a2-Cre^{ER}; Tgfb1$^{fl/+}$	*KPF^{C}; Tgfb1$^{fl/+}$*
Pdx1-Flp; FSF-Kras$^{G12D/+}$;Trp53$^{frt/+}$; Col1a2-Cre^{ER}; Tgfb1$^{fl/fl}$	*KPF^{C}; Tgfb1$^{fl/fl}$*
Fibroblast specific targeted deletion in pre-neoplastic tissue	
Pdx1-Flp; FSF-Kras$^{G12D/+}$; Gli-Cre^{ERT}	*KF^{G}*
Pdx1-Flp; FSF-Kras$^{G12D/+}$; Gli-Cre^{ERT}; Alk5$^{fl/fl}$	*KF^{G}; Alk5$^{fl/fl}$*
Pdx1-Flp; FSF-Kras$^{G12D/+}$; Gli-Cre^{ERT}; Tgfb1$^{fl/fl}$	*KF^{G}; Tgfb1$^{fl/fl}$*
Pdx1-Flp; FSF-Kras$^{G12D/+}$; Col1a2-Cre^{ER}	*KF^{C}*
Pdx1-Flp; FSF-Kras$^{G12D/+}$; Col1a2-Cre^{ER}; Alk5$^{fl/fl}$	*KF^{C}; Alk5$^{fl/fl}$*
Pdx1-Flp; FSF-Kras$^{G12D/+}$; Col1a2-Cre^{ER}; Tgfb1$^{fl/fl}$	*KF^{C}; Tgfb1$^{fl/fl}$*
Neutrophil specific targeted deletion	
Pdx1-Flp; FSF-Kras$^{G12D/+}$;Trp53$^{frt/+}$; Ly6G-Cre	*KPF^{L}*
Pdx1-Flp; FSF-Kras$^{G12D/+}$;Trp53$^{frt/+}$; Ly6G-Cre; Alk5$^{fl/+}$	*KPF^{L}; Alk5$^{fl/+}$*
Pdx1-Flp; FSF-Kras$^{G12D/+}$;Trp53$^{frt/+}$; Ly6G-Cre; Alk5$^{fl/fl}$	*KPF^{L}; Alk5$^{fl/fl}$*
Pdx1-Flp; Ly6G-Cre	
Pdx1-Flp; Ly6G-Cre; Alk5$^{fl/+}$	
Pdx1-Flp; Ly6G-Cre; Alk5$^{fl/fl}$	

2.2.4.3 Established Tumour Experiments

KPF mice of the relevant genetics were palpated weekly and upon detection of a palpable tumour, an ultrasound was conducted with the VisualSonics Vevo 3100

Preclinical Imaging System (FujiFilm) to confirm tumour presence. Mice were subsequently induced over 3 or 4 days with intraperitoneal injection depending on the model. These mice were monitored at least 3 times a week, with an ultrasound conducted weekly until clinical end-points were reached.

2.2.4.4 Time-point Cohorts

Mice of the relevant genetics were aged to appropriate time-point (generally 42 days or 70 days). Mice were either euthanized and harvested at this stage or recombination was induced by tamoxifen induction. Following induction mice were monitored thrice weekly, undergoing routine palpation or ultrasound depending on the genetics and/or tumour detection. At clinical end-points or at time-points mice were euthanized and harvested. Time-point experiment layouts are shown in the relevant figures.

2.2.4.5 Tamoxifen induction of gene deletion

Tamoxifen (Merck Life Science UK Ltd, T5648) was prepared by dissolving 1g into 10ml of 100% ethanol creating a 100mg/ml solution. Once fully dissolved this was diluted in either sunflower oil (Sigma, #S5007) or corn oil (Sigma, #C8267) to generate a 10mg/ml stock.

Mice were either administered tamoxifen, via intraperitoneal injection, at defined time-points or upon confirmation of tumour presence but only once mice were at least 20 grams in weight. Models with epithelial-targeted gene deletion were administered tamoxifen in corn oil over three days with 2mg administered at each injection. Mice expressing *Gli1-Cre*^{ERT} or *Col1a2-Cre*^{ER} were administered tamoxifen in sunflower oil over 4 days with 3mg injected on day 1 and 2mg injected on the subsequent days. Dosage regimens are also specified in the relevant figures for each model.

2.2.5 Imaging

2.2.5.1 Ultrasound

Using the Visualsonics Vevo 3100 imaging system (FujiFilms) mice were subjected to ultrasound pre-induction either to confirm normal non-transformed pancreas,

or to confirm tumour presence post palpable detection of PDAC. Follow up scans were performed weekly to measure tumour growth. In general, the protocol outline by, *Goetze et al* (Goetze et al., 2018) was used. In brief, mice were prepared with removal of abdominal fur with depilatory cream. Mice were anaesthetised in 0.2L/min medical air with 2% isoflurane in the induction chamber. Once under sedation the mice were transferred onto a heated table in supine position. Mice were maintained under sedation throughout the procedure through delivery of anaesthesia via a nose cone. The fore and hind paws of the mouse were adhered to the table at probes allowing ECG and respiration monitoring. Ultrasound gel was applied to the abdominal region and the transducer (MX550D, 40MHz, Axial resolution 40μm). The transducer was placed on the mouse abdomen under firm pressure and mice scanned from upper abdominal region to lower region on both the right and left side, with images saved. Upon detection of PDAC a three-dimensional scan was conducted. The transducer was moved to the centre of the tumour and an integrated motor assembly scanned between two user-defined points (top and bottom of tumour mass) taking multiple sequential images which generates a 3-dimensional image of the region. Mice were then carefully removed from the table and allowed to recover, scans took <10 minutes to complete.

Ultrasound images were analysed with VevoLab software (Version 3.1.1 VisualSonics). Three-dimensional images were generated using 3D mode. Using the 3D mode, borders were drawn around the tumour across multiple non-sequential frames within the three-dimensional construct. The software was able to determine the tumour border for the intermittent frames automatically based on user-defined regions; however, all automatically determined borders were checked and corrected by myself. An area of total tumour volume was the output from this analysis.

2.2.5.2 Xenogen *in vivo* imaging system (IVIS)

The liver, pancreas, spleen and mammary fat pad were dissected and placed on a petri dish. The Xenogen *in vivo* imaging system (PerkinElmer) was used to measure tissue fluorescence. Tissues were placed inside the machine and excited at 465nm and 535nm, for GFP and Tomato, respectively. Background fluorescence was controlled for by mammary fat tissue. Tissue taken from a

control mouse lacking the reporter construct was also used in all instances of imaging.

2.3 Histology

2.3.1 Tissue fixation

Formalin fixed samples were transferred to 70% ethanol after >48hour fixation period and paraffin embedded by the CRUK Beatson histology department.

2.3.2 Immunohistochemical staining

Immunohistochemical (IHC) staining was conducted either by me or by the CRUK Beatson Histology department utilising standard histological techniques. 4μM tissue sections were cut from formalin fixed paraffin embedded tissue and mounted onto slides (blank slides).

Slides were dewaxed with 3x5 minute washes in Xylene, followed by tissue rehydration with 2x3 minute washes in 100% alcohol followed by a 3 minute wash in 70% alcohol and then washed in water. Antigen retrieval was performed with 10mM sodium citrate buffer pH6 with slides submerged in buffer and heated, in a pressure cooker in the microwave for 10 minutes at pressure. Slides were subsequently cooled for 30 minutes at room temperature and washed in 0.05% Tris-buffered saline with 0.05% Tween (TBS-T).

Endogenous peroxidases were blocked through a 15-minute incubation with 3% hydrogen peroxide followed by 3x3 minutes wash in TBS-T. Incubation for 1 hour at room temperature with 5% normal serum (goat/rabbit) was performed to block tissue from non-specific antibody binding.

Incubation with primary antibody diluted in 5% normal serum was performed overnight at 4ºC in a humidified container. Slides were washed 3x3 minutes in TBS-T. Appropriate biotinylated secondary antibody from the Vectastain kit (VECTASTAIN® Elite ABC-HRP Kit, Peroxidase (Rabbit IgG) PK-6101, or Mouse IgG, PK-6102) was used diluted in 5% normal serum. Slides were incubated for 1 hour at room temperature with anti-rabbit/mouse biotinylated secondary antibody, depending on host species of primary antibody (1 drop secondary antibody into

10ml 5% serum). Slides were washed for 3x3 minutes in TBS-T before incubation with avidin/biotin complex (A and B reagents from the Vectastain kit), which was prepared 30 minutes before hand in TBS-T, for 1 hour at room temperature. Slides were washed for 3x3 minutes in TBS-T and positive staining visualised with 3,3-diaminobenzidine (DAB) (Dako K3468), formulated with 1 drop of chromogen to 2mls of substrate. Slides were then washed in water to terminate the reaction. Leica ST5020 performed counterstaining, with Haematoxylin, before dehydrating and applying Dibutylphthalate Polystyrene Xylene (DPX) mounting medium and a coverslip. Alternately, coverslips were mounted using the Leica CV5030.

There were some variations to the protocol for particular stains. F4/80 was antigen retrieved through proteinase K. Anti-Hamster biotinylated secondary (Invitrogen A18893) at 1:500 diluted in 5% rabbit serum was used in podoplanin staining. A list of antibodies used for IHC is shown in table 2. Sirius red staining was performed on dewaxed and rehydrated tissue sections, which were incubated for 2 hours in picrosirius red solution, formulated with 0.1% Direct red 80 in distilled water and 0.1% Fast Green in distilled water, diluted 1:9 with aqueous picric acid. Slides were washed in distilled water and then dehydrated and mounted.

Table 2 Antibodies used for IHC slide staining

Protein	Clone	Concentration	Supplier
αSMA	1A4	1/25000	Sigma-Aldrich (a2547)
Ck19	EPNCIR127B	1/1000	Abcam (ab133496)
Cleaved Caspase 3	Asp175	1/500	Cell Signaling (#9661)
CD3	SP7	1/100	Abcam (ab16669)
CD8	4SM15	1/500	eBioscience (14-08-8-82)
Ccng1	Polyclonal	1:1000	ThermoFisher (PA5-92375)
E-cadherin	36/E-cadherin	1/300	BD biosciences (610181)
F4/80	CI:A3-1	1/200	Abcam (ab6640)
Ki67	MIB-1	1/100	Dako (M7240)
Ly6G	1A8	1/60,000	BioXcell (BE0075-1)
MPO	A0398	1/200	Dako (A0398)
Podoplanin	RTD4E10	1/1000	Abcam (ab11936)
pSMAD3	EP823Y	1/40	Abcam (ab52903)
p21	HUGO291	1/150	Abcam (ab107099)
Vimentin	D21H3	1/100	Cell Signalling (#5741)

2.3.3 Scoring IHC

IHC slides were visualised using the Olympus BX53 and images taken using Olympus SC100 camera with cellsans standard software. Field of view counts (CD3, CD8, MPO) were performed over 30 fields of view using the 40x objective. PanIN images were analysed using ImageJ (version 1.52) with positive and negatively stained cells counted in epithelial cells only using the Point Tool module (Ki67, p21, cleaved caspase 3, pSMAD3).

Slides were digitally scanned using the Aperio AT2 slide scanner. The digital scans were analysed using Indica Labs HALO software (version 3.1). Different algorithms were used to analyse individual stains. For instance, diffuse stained slides such as F4/80, podoplanin, αSMA and Sirius red were analysed used the Area Quantification algorithm (version 2.17). Nuclear and cytoplasmic staining was quantified using the Cytonuclear algorithm (version 2.09). Annotations layers were drawn on the slide images to define regions of interest to be analysed, for instance *bona fide* tumour regions or PanIN regions.

2.3.3.1 Islet cell area and transformed area analysis

H&E stained slides of pancreatic tissue were digitalized. Using HALO software an annotation layer was drawn around the outer edges of the pancreas to define total pancreatic tissue area. Subsequent annotations were drawn around islet cell regions or transformed tissue regions specifically to define total islet area or totally transformed area. A percentage of islet area or transformed tissue area was calculated from these two measurements (**Figure 5**).

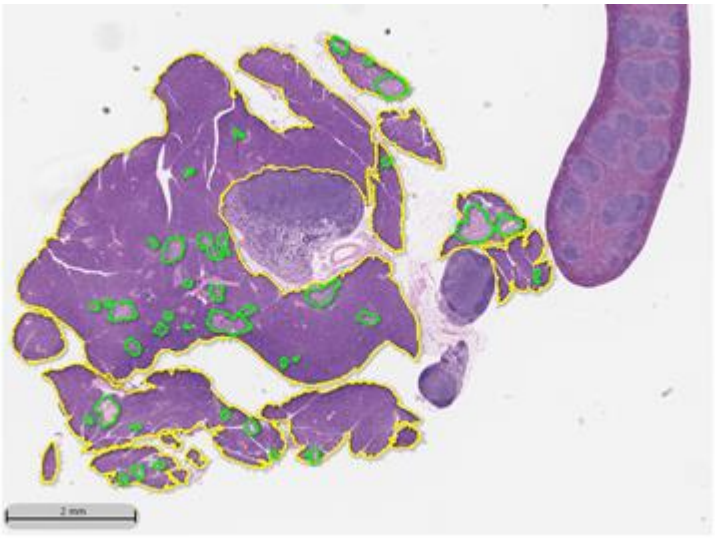

Figure 5 HALO software analysis of the proportion of islet area or transformed tissue area in the pancreas
Using HALO software annotation layers were drawn around digitalised H&E stained tissue sections. The total pancreas area is outlined by a yellow annotation layer with transformed pancreatic tissue in green, with non-pancreatic tissue not annotated.

2.3.3.2 Area quantification analysis

Positive staining was defined based on the intensity of DAB (or picrosirius red stain), and the percentage of area positive staining was calculated for these stains. When histoscore (HS) was used, I defined thresholds for low, moderate and strong intensity of staining. HS was calculated via the following calculation (1x % area of low positive staining) + (2x % area of moderate positive staining) + (3x % area of strong positive staining).

2.3.3.3 Cytonuclear quantification

Cell count was defined based on haematoxylin intensity. Positive staining was defined by the intensity of either nuclear or cytoplasmic DAB. The percentage of positively stained cells was calculated by division of total positive cell numbers over total cell number.

2.3.3.4 Metastasis scoring

A single H&E stained slide, per mouse, of liver or lungs sections was viewed under the microscope. Presence of microscopic lesions of pancreatic origin with greater than 10 cells were counted as metastasis. The presence and number of metastases at each site was noted.

2.3.4 Immunofluorescence staining

Blank slides were dewaxed, rehydrated, antigen retrieved and blocked as specified in the above IHC technique section. Slides were incubated overnight at 4ºC in a humidified container with primary antibodies αSMA, pSMAD3 and podoplanin at 1:10,000, 1:100 and 1:1000 respectively, diluted in 5% normal goat serum (Dako X0907). Slides were subsequently washed for 3x3 minutes in TBS-T. Slides were incubated for 1 hour at room temperature with fluorescent protein conjugated secondary antibodies at 1:500 dilution in 5% normal goat serum (**Table 2**). Slides were washed for 3x3 minutes in TBS-T. A single drop of DAPI mounting media (Abcam ab104139) was applied to the tissue before a coverslip was placed onto the slide. Coverslips were sealed (Biotium #23005) and stored at 4ºC in the dark until being imaged.

Table 3 Fluorescent protein conjugated secondary antibodies

Secondary	Species	Fluorescent protein	Supplier
Anti-Hamster	Goat	AF488	Abcam (ab173003)
Anti-Mouse	Goat	AF647	Abcam (ab150115)
Anti-Rabbit	Goat	AF594	Abcam (ab150088)

2.3.4.1 Immunofluorescence imaging and analysis

Stained slides were imaged on the Nikon A1R Z600 using NIS Elements AR (version 4.5) software. Lasers at 404nm, 488nm, 594nm and 647nm excited DAPI, AF488, AF594 and AF647 proteins respectively, with emission collected in filters 450/50, 525/50, 595/50 and 700/75, for each fluorophore respectively. Single stained slides were used as controls in each experiment. I defined positive staining as any staining detected above background as defined from the single stained tissue sections. Laser power was limited to prevent saturation. Images were taken at 40x magnification. Images were analysed on ImageJ. Nuclear pSMAD3 positive and negative fibroblasts were counted across 5 40x images using the Point Tool module and the percentage of positive fibroblasts were calculated from the total counts. Fibroblasts were defined as both αSMA and podoplanin positive.

2.3.5 RNAscope

RNAscope for mouse *Alk5* (RNAscope LS 2.5 Probe-Mm-Tgfbr1, #406208) was performed using manufacturer's instructions and performed on the Leica Bond RX autostainer.

2.4 Flow cytometry

Flow cytometry was used to analyse the expression of proteins on individual cell populations. The BD LSRFortessa Cell Analyzer was used with the following lasers 355nm, 405nm, 488nm, 561nm and 641nm. BD FACSDiva Software was used during acquisition and FlowJo version 10.8 was used to analyse data.

Fluorescence-activated cell sorting (FACS) was performed with assistance from University of Glasgow flow cytometry technicians. The BD FACSAria Fusion flow cytometer was used.

2.4.1 Cell isolation

Blood was sampled via cardiac puncture and stored in EDTA coated tubes until processing. The spleen, liver, lungs, and PDAC/pancreas were dissected and stored in PBS until processing.

Red blood cell lysis of blood was performed using RBC lysis buffer (eBioscience 00-4333-57). 50µl of blood per 1ml of RBC lysis buffer for 10 minutes was found to be optimal (data not shown). The reaction was stopped with volume-to-volume (v/v) dilution with RPMI supplemented with 10% foetal bovine serum (FBS, Gibco #10270106) and 2mM EDTA (RPMI-FBS/EDTA). Cells were pelleted by centrifugation at 400 relative centrifugal force (RCF) for 5 minutes at 4^{o}C. Pellets were re-suspended in PBS supplemented with 1% weight-to-volume bovine serum albumin (BSA: Sigma, #A7906) and 0.05% sodium azide (Thistle Scientific Ltd #40-2000-01), termed PBA. Cells were then passed through a 70µm nylon mesh.

The spleen was mechanically dissociated through a 70µm nylon mesh into RBC lysis buffer for 10 minutes at room temperature. The reaction was terminated

through addition of v/v RPMI-FBS/EDTA and cells pelleted through centrifugation at 400 RCF. Cells were then re-suspended in PBA.

The lungs were cut into small pieces and digested in RPMI supplemented with 5% v/v FBS and 2mM EDTA for 30 minutes at 37ºC with continuous agitation. Cells were the passed through a 70µm nylon mesh filter and centrifuged at 400 RCF for 5 minutes. Cells were then re-suspended in PBA.

From the liver 0.5 grams of tissue was processed. The liver was finely minced and dissociated with incubation in RMPI-FBS/EDTA supplemented with 1.2mg/ml Collagenase D (Roche, #70505525) and 1mg/ml DNase I (Roche, #104716728001), for 30 minutes at 37ºC with continuous agitation. Cells were passed through a 70µm nylon mesh filter and pelleted via centrifugation at 400 RCP for 5 minutes. Pellets were re-suspended in PBA.

Tumour or pancreas was finely minced in ice cold RPMI. Chopped tissue was transferred to a gentleMACs C tube (Miltenyi Biotec, #130-093-237) with 2.35ml of RPMI supplemented with 100µl Enzyme D, 50µl Enzyme R and 12.5µl Enzyme A (Miltenyi Biotec, Tumour dissociation kit, Mouse, # 130-096-730). Tissue was dissociated with a gentleMACs Dissociator (Miltenyi Biotec), using the 37C_m_TDK_2 program setting, for tough tissue, for 42 minutes. Dissociated tissue was filtered through a 70µm nylon filter before centrifuging at 400 RCF for 5 minutes. Cells were re-suspended in RBC lysis buffer for 10 minutes with the reaction terminated with v/v PBA. Cells were pelleted by centrifugation at 400 RCF and then re-suspended in PBA.

2.4.2 Staining protocol

For staining, cells from each sample were loaded into individual wells of a 96 well v-bottom plate (Greiner Bio-One Ltd, #651180). The plate was centrifuged at 400 RCF for 5 minutes with the supernatant discarded. A volume of 50µl of Live/Dead marker zombie yellow (Biolegend, #423103), suspended at 1µl per 1ml PBS, was added to the well and the plate incubated for 15 minutes in the dark at 4ºC. All subsequent incubations were performed in the dark at 4ºC. Cells were then pelleted by centrifugation at 400 RCF, supernatants discarded, and cells re-suspended in PBA (washed in PBA). Cells were then incubated with anti-CD16/32

(Biolegend, #101320), to block Fc binding for 15 minutes. Cells were then washed in PBA, before incubation for 30 minutes with 50µl of antibody mix prepared in Brilliant Stain Buffer (BD, #563794).The antibodies used can be found in **Table 4**. For each staining panel fluorescence minus one (FMO) controls were used, in which the sample was stained for all fluorophores except one to determine the cut-off point between background and positive staining. Cells were then washed three times in PBA, before fixing (Invitrogen, IC fixation buffer, #00-8222-49). Cells were washed and stored in 175µl PBA for analysis. Compensation samples for each fluorophore were prepared with UltraComp eBeads (ThermoFisher, #01-2222-42) stained with a single fluorescently conjugated antibody.

Table 4 Antibodies used for Neutrophil Flow Cytometry

Antigen	Clone	Conjugated fluorophore	Dilution	Supplier
Ter119	TER119	FITC	1/200	Biolegend (#116206)
Siglec-F	E50-2440	BB515	1/200	BD (#564514)
Nkp46	29A1.4	FITC	1/200	Biolegend (#137606)
CD115 (CSF1R)	AFS98	AF488	1/200	Biolegend (#135512)
CD3	145-2C11	FITC	1/200	Biolegend (#100306)
CD19	6D5	FITC	1/200	Biolegend (#115506)
CD45	30-F11	BV650	1/200	Biolegend (#103151)
CD11b	M1/70	BV605	1/400	Biolegend (#101257)
Ly6G	1A8	APC	1/400	Biolegend (#127614)
ICAM-1	YN1/1.7.4	PerCP-Cy5.5	1/200	Biolegend (#116124)
CD62L	MEL-14	BUV395	1/200	BD (#740218)
CD101	Moushi101	PE-Cy7	1/200	ThermoFisher (#25-1011-82)
c-KIT	2B8	APC-Cy7	1/100	Biolegend (#105826)
CXCR4	L276F12	BV421	1/100	Biolegend (#146511)
CXCR2	SA045E1	PE	1/100	Biolegend (#149610)

2.5 Cell culture

2.5.1 Murine pancreatic cancer cell lines

2.5.1.1 Cell line preparation and maintenance

Tumours were dissected and a 50µg piece minced in Dulbecco's modified eagle medium (DMEM) (ThermoFisher, #21969035) supplemented with 10% FBS, 1% Penicillin/Streptomycin (ThermoFisher, #15140-122) and 2mM L-glutamine (ThermoFisher, #25030-024) (culture medium) in a laminar flow hood. The cell suspension was transferred to a T25 cell culture flask with 5ml culture medium supplemented with an additional 0.5ml FBS (20% total supplement). Cell lines were stored in humidified incubators maintained at 37°C with 5% CO_2 concentration. The media was changed twice weekly until cells were close to confluence. Upon confirmation that cells were confluent, they were passaged. Media was aspirated, cells washed with 5ml of PBS, and 10% trypsin (Gibco, #15090-046) applied for 5-10 minutes at 37°C. Cells were then washed off the surface with culture media and split into flasks at 1:10 dilution for further passage, or as required for further experiments. Established cell lines were maintained in T75 flasks in 15ml of culture media. Cells lines were initially passaged five times to favour ductal cells (Hingorani et al., 2005).

2.5.1.2 Freezing down cell lines

Following detachment via trypsin, cells were washed and suspended in freezing media (90% FBS: 10% DMSO). 1ml aliquots of suspended cells were transferred to Cryovials and slowly frozen down to -80°C. To re-establish cell lines the frozen cryovials were defrosted quickly at 37°C and re-suspended in culture media supplemented with an additional 10% FBS.

2.5.1.3 Protein cell lysate preparation

Media was removed and the cells washed twice with PBS. On ice, 250ul of RIPA lysis buffer was added to the cells and allowed to incubate for 10 minutes. Cells were scraped into the buffer and transferred into an Eppendorf tube. The protein was centrifuged for 15 minutes at 12,000 RPM at 4°C. The supernatant was collected and stored at -20°C for future use. RIPA buffer was formulated

with 50mM Tris (pH 7.4), 150mM NaCl, 1% Triton-X-100, 0.5% Deoxycholate and 0.1% SDS in distilled water to make a 500ml solution. When required for lysis, 2ml of this buffer was supplemented with 25µl 100mM Phenylmethylsulfonyl fluoride (PMSF), 2µl aprotinin, 2µl 0.5M NaF and 2µl 100mM Na_3VO_4 and used immediately. Protein lysate was also prepared from fresh frozen tumour samples through similar methods, although supplemented T-PER Tissue Protein Extraction Reagent (ThermoFisher, #78510) was used instead of RIPA buffer.

2.5.1.4 Clonogenic Assay

After cells had been trypsinised, a proportion was collected and counted using the CellDrop cell counter (DeNovix). Cells were stained for Trypan blue 0.4% (ThermoFisher, # T10282) at 1:1 volume after passage through a 21-gauge needle. A single cell suspension was generated to accommodate a seeding density of 400 cells per well in 3ml of culture media in 6-well plates. After 24, hours media was aspirated and cells were incubated with nutlin3a (Merck, #N6287) diluted in DMSO and culture media at various concentrations (range 0.1µM – 10µM). DMSO only treated cells were used as controls. After 24 hours nutlin3a supplemented media was aspirated and cells washed gently with PBS before incubation for 5 days with 3ml of culture media. After 5 days, media was aspirated and cells washed gently with PBS. Cells were then fixed with 50% methanol for 10 minutes. Plates were then washed and allowed to dry overnight. Plates were incubated for 5-10 minutes with Crystal violet, with a thorough wash completed subsequently. Plates were left to dry overnight before scanning to digitalise the images. Digital images were scoring through manual counting with the imageJ Point Tool module counting all purple spots as individual colonies.

2.6 Western Blot

Protein concentration was determined use a Bicinchoninic acid (BCA) assay (ThermoFisher, Pierce BCA Protein Assay Kit, #23227). Protein samples were thawed on ice and diluted with RIPA buffer. Into a 96 well plate, 10µl of protein was added per well. Standards of known concentration of BSA were loaded (80, 100, 200, 400, 1000, 2000 µg/ml) and RIPA buffer was loaded in triplicate as blank control. The developing solution was mixed at 50:1 ratio of Reagent A to Reagent B and 200µl was added to each well. The plate was incubated in the

dark at 37ºC for 30 minutes. The absorbance was measured at 562nm and the protein concentration was calculated by plotting a standard curve of the absorbance of blank corrected BSA standards of known concentrations. From the standard curve, the concentration of protein was determined and used to standardize loading.

Protein samples were prepared with running buffer (ThermoFisher, #NP0007), Sample reducing agent (ThermoFisher, #NP0004) and RIPA buffer before being heat blocked for 5 minutes at 95ºC. Proteins were then loaded on a 4-12% bis-tris gel (ThermoFisher, #NP0323) submerged in MOPS SDS buffer (ThermoFisher, #NP0050) and run for 1 hour at 200 volts. The protein was then transferred onto a polyvinylidene fluoride (PVDF: GE Healthcare Life Sciences, #10600032) membrane with this membrane blocked for 30 minutes at room temperature in 5% BSA. The membrane was then incubated overnight at 4ºC with primary antibody (Mouse mAb p53, Cell Signalling, #2524 or Ccng1, Invitrogen, #PA5-36050) at 1:1000 dilution in 5% BSA. The membrane was washed for 3x5 minutes in TBT-T and then incubated for 1 hour with secondary antibody (Anti-Mouse HRP linked, Cell signaling, #7076 or Anti-rabbit-HRP linked, Cell signaling, #7074) at 1:10,000 dilution in 5% BSA. The membrane was then washed before incubation with enhanced chemiluminescent (ECL) horseradish peroxidase substrate (ThermoFisher, #34579) prepared by mixing equal concentrations of Stable Peroxide Solution and Luminol/Enhancer Solution. Staining was then visualised with the ChemiDoc (BioRad) system. Membranes were then stripped of antibodies with Reblot Plus Strong Antibody Stripping Solution (Millipore, #2504), before staining for loading control ß-Actin (Sigma, #25441, 1:10,000 dilution), blotted as described above.

2.7 RNA processing

RNA was extracted either from RNAlater (Sigma, #R0901) preserved tumour pieces or from sorted cells. When extracting from the tumour the RNAlater preserved pieces were defrosted on ice with a single 2mm chunk of tissue removed for dissociation. Dissociation was performed in tubes containing ceramic beads (Hard Tissue homogenizing CK28, Precellys, #P000911-LYSK0-A) with 350µl of RLT buffer from the RNeasy Mini Kit (Qiagen, # 74104). The Precellys Tissue Homogeniser (Bertin Technologies) was used to dissociate tissue

at 4ºC. When working with cells they were lysed in RLT buffer by passing through a 0.9mm syringe five times. V/V mixing of dissociated tissue with 70% ethanol was conducted. Subsequently this was transferred to an RNeasy spin column and centrifuged for 15s at 10,000 RPM with the flow through discarded. 700µl of Buffer RW1 was added to the RNeasy spin column before centrifugation for 15s at 10,000 RPM, discarding the flow through. 500µl of Buffer RPE was added to the spin column before centrifugation for 15s at 10,000 RPM, with this step repeated once more with a 2 minute long spin in the centrifuge with flow through discarded. RNeasy spin columns were then centrifuged for 1 minutes at 10,000 RPM. 21µl of RNase free water was added to the RNeasy spin column, which was centrifuged for 1 minute at 10,000 RPM, with the elute collected. DNA contamination was removed using TURBO DNA-free kit (ThermoFisher, #AM1907). DNase Buffer and TURBO DNase was added to the RNA sample and incubated at 37ºC for 30 minutes. DNase inactivating reagent was added and incubated for 5 minutes. Samples were centrifuged at 10,000 RPM for 1 and half minutes with the supernatant retained. Samples were stored at -80ºC.

RNA quality and quantity was determined using the NanoDrop Spectrophotometer (ThermoFisher). A measurement of A260/A280 determines contamination and a ratio of around 2.0 was desired.

2.7.1 RTqPCR

From the purified RNA, 500ng was taken to perform RTqPCR. The QuantiTect Reverse Transcription (RT) Kit (Qiagen, #205311) was used. The RT mix was formulated with 1µl quantiscript RT (qRT), 4µl qRT buffer and 1µl qRT primer mix. The RNA sample was incubated with 2µl of gDNA wipeout buffer on heat block at 45ºC for 2 minutes. RT mix was then added to sample and incubated at 25ºC for 3 minutes, before incubation for 10 minutes at 45ºC followed by a 5 minutes incubation at 85ºC, generating complementary DNA (cDNA). Samples were then placed immediately onto ice. A no-RT (NRT) sample was also produced.

A qPCR mix was formulated with 5µl Sybr green, 0.5µl forward primer (0.5µM), 0.5µl reverse primer (0.5µM) and 1µl of cDNA sample or NRT sample or 1µl of RNAase free water. Samples were denatured at 95ºC before cycling through the

following steps 40 times; 94°C for 10s, 60°C for 30s, 72°C for 30s and collection of Sybr green output.

Relative gene expression was calculated using the $2^{-\Delta\Delta Cq}$ method:

Cq values are average of technical replicates from each sample.
ΔCq = Cq (gene of interest) – Cq (housekeeping gene)
ΔΔCq = ΔCq (sample of interest) – ΔCq (control sample).
Fold gene expression = $2^{-\Delta\Delta Cq}$

Table 5 Primers used for RTqPCR

Primer Target	Forward	Reverse
Alk5	GAAAAGCAGTCAGCTGGCCTT	ATCCAGACCCTGATGTTGTCAT
B-actin	GTG ACG TTG ACA TCC GTA AAA	GCC GGA CTC ATC GTA CTC C

2.8 RNA sequencing

All RNA sequencing data was generated by the CRUK Beaton Institute Molecular Technology Services. Before RNAseq was performed, the quality of the RNA was determined. The Agilent 2200 Tapestation with RNA Screentape (Agilent, ThermoFisher) was used, with an RNA Integrity Number (RIN) value of ≥ 7.5 required to proceed with the sample for RNAseq.

Following the manufactures instructions in the TruSeq Stranded mRNA library RNA Sample Preparation Guide (Illumina, #20020594) RNAseq libraries were generated using Illumina TruSeq RNA LT sample preparation kit. Initially, a PolyA selection was performed on 100ng of RNA, and then a heat fragmentation step was performed to generate insert size between 120-200 bp. cDNA strands were synthesised from the RNA using SuperScript III Reverse Transcriptase (Invitrogen, 18080-044) with random primers. The libraries were then subjected to 13 cycles of PCR. The Qubit v2.0 HS DNA assay (Invitrogen, Q32854) was used to quantify the RNAseq libraries. Libraries were sequenced (36-bp paired-end) using the NextSeq500 sequencer (Illumina).

All raw data was analysed by a trained bioinformatician, with adaptor trimmed sequences aligned to mouse genome build GRCm38.98.

2.9 Statistical analysis

All statistical analysis was performed using Graphpad Prism version 7.04, with details of the statistical analysis used in appropriate figure legends.

Chapter 3 A Novel Model of TGFβ signalling deficient driven PDAC

3.1 Introduction

According to multiple human PDAC datasets, mutations of the TGFß signalling pathway occur in ~47% of cases (Aguirre et al., 2017; Bailey et al., 2016). The most prevalent mutation occurs in *SMAD4* with aberrations in *TGFBR2* and *ALK5* also occurring frequently in a non-concomitant manner. Subsequently mouse modelling of pancreas specific deletion of *Smad4* or *Tgfbr2*, in combination with oncogenic $Kras^{G12D}$, resulted in PDAC development with a reduced survival compared to $Kras^{G12D}$ expression alone (Bardeesy et al., 2006; Ijichi et al., 2006), highlighting TGFß signalling as a potent tumour suppressor in disease initiation.

Although these models convincingly portray TGFß signalling as a tumour suppressor, they do not fully recapitulate the stepwise acquisitions of mutations as in human disease (Feldmann et al., 2007). Further, deletion of *Alk5* or *Smad4* alongside $Kras^{G12D}$, driven by Pdx-1, has the propensity to cause squamous stomach tumours, and skin tumours in mice (Acosta et al., 2013; Bardeesy et al., 2006), which complicate their use for investigating pancreatic cancer. However, through the utilisation of a dual recombinase (DR) mouse model expressing pancreas specific Flippase and a tamoxifen inducible Cre recombinase deletion of genes can be conducted in a spatially and temporally distinct manner (Schonhuber et al., 2014). This allows for the investigation of disruption of the TGFß signalling pathway in adult pancreas, generating a model of PDAC that recapitulates the stepwise acquisition of mutations observed in human disease.

3.2 Experimental Aims

Through the utilisation of the DR mouse model, my aims were to investigate the deletion of the TGFß receptor *Alk5* or the receptor ligand *Tgfb1* in a temporal manner in pancreatic cells co-expressing oncogenic $Kras^{G12D}$. The capacity to delete genes in a sequential manner will better recapitulate human disease where mutations beyond oncogenic *Kras* are acquired in a stepwise fashion as the disease progresses. Therefore, building upon evidence in previous publications in which embryonic deletion of TGFß signalling in oncogenic *Kras*

expressing cells accelerates carcinogenesis, I hypothesise that deletion of *Alk5* in *Kras*^{G12D} expressing cells in the adult pancreatic tissue will drive PDAC formation. I also wanted to investigate the early source of TGFß ligand, through the deletion of *Tgfb1* in oncogene-transformed cells, in order to determine if autocrine signalling was essential for maintaining TGFß induced growth arrest in PanINs or if loss of ligand from tumour cells could affect the surrounding microenvironment and thus influence tumour development or progression.

3.3 Results

3.3.1 Utilising the DR mouse to control pancreatic gene expression in a spatial and temporal manner

Utilisation of the *Pdx1-Flp; FSF-Kras^{G12D}; Trp53$^{Frt/+}$* (KPF) mouse model (**Figure. 6A**) crossed with mice expressing an FRT-Stop-FRT(FSF)-Cre^{ER} allele, generated a mouse model in which I was able to delete lox flanked genes in a cell and time specific manner by the administration of tamoxifen. In this model, tamoxifen inducible Cre-recombinase expression was restricted to Pdx1 expressing cells, which are expressing Flippase, therefore allowing for pancreatic specific gene deletion (**Figure. 6B**). This enables specific examination of the function of TGFß signalling at various time points via crossing this model with mice bearing either *Alk5* or *Tgfb1* floxed genes. The *Alk5* gene has *lox* sites before and after exon 3 (Larsson et al., 2001) and *Tgfb1* has a *lox* flanked exon 6 (Azhar et al., 2009), therefore neither generates a functional protein upon CRE recombination (**Figure. 6C**). Conditional deletion of the *Alk5* and *Tgfb1* genes is required as whole body deletion of either is lethal (Larsson et al., 2001; Shull et al., 1992), but over and above conventional deletion, the DR model allows additional temporal control of deletion.

This model expresses an enhanced green florescent protein (EGFP)/Tomato switch construct (**Figure. 7A**) in the *Rosa26* locus. An *frt* flanked stop site prevents expression in cells negative for flippase, however, in flippase recombined cells EGFP is expressed. Upon CRE recombination the *lox* flanked EGFP is cleaved and tomato is expressed in its place. This construct allowed visualisation of GFP in the normal pancreas of mice with the reporter construct but not in mice lacking the construct (**Figure. 7B Left Panel**) with tissue autofluorescence controlled for using mammary fat pad tissue. GFP expression was specific to the pancreas and was not detected in the spleen or liver, as would be expected with PDX1 driven flippase. Upon tamoxifen induction, RFP expression can be detected specifically in the pancreas and only in models which have the construct (**Figure. 7B Right Panel**). This confirms pancreas specific expression of both flippase and a tamoxifen inducible CRE recombinase that is functional in recombining *lox* flanked sites.

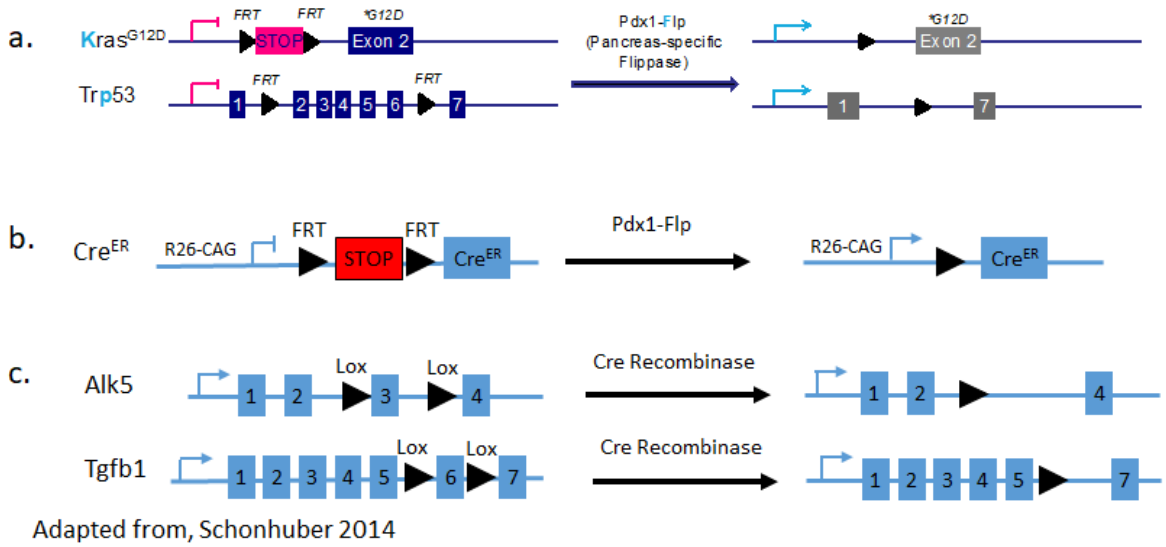

Figure 6 A mouse model of spatial and temporal gene deletion of *Alk5* or *Tgfb1*
A. Schematic of the KPF mouse model genetics. Pdx-1 driven expression of *Flippase* recombines at FRT sites culminating in pancreatic specific expression of $Kras^{G12D}$ and heterozygous deletion of *Trp53*.
B. A schematic of the tamoxifen inducible CRE recombinase under the control of the CAG promoter in the Rosa26 locus. Only in cells expressing *Flippase* will the FRT flanked STOP site be excised, thereby allowing expression of Cre^{ER}.
C. Schematic of the endogenous *Alk5* gene, with lox flanked exon 3, or the endogenous *Tgfb1* gene, with lox flanked exon 6. Upon *Cre-recombinase* expression the lox flanked exons are excised and the protein is no longer expressed

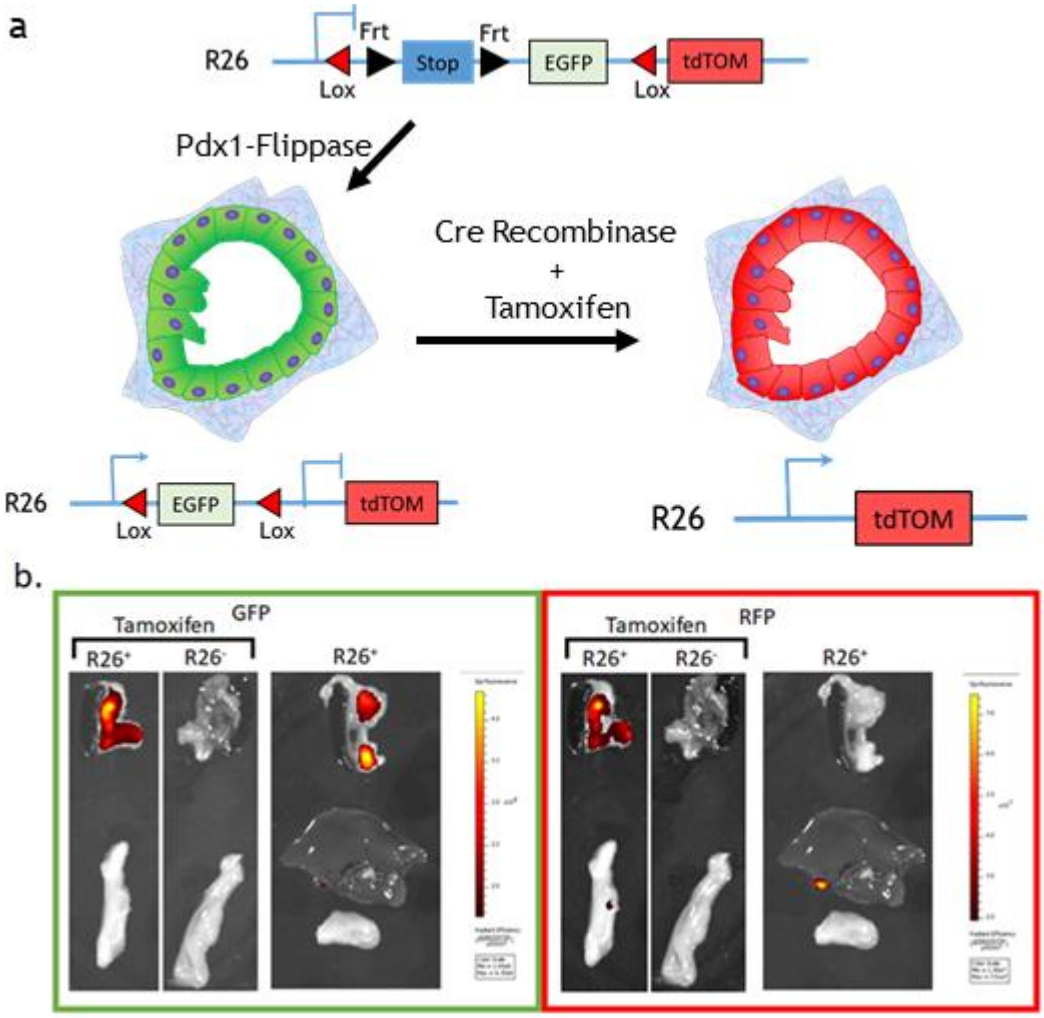

Figure 7 Pancreatic specific expression of Flippase and Cre-recombinase
A. Schematic of the EGFP/Tomato switch construct within the Rosa26 locus (top). Flippase recombination of the FRT sites allowed expression of GFP. Upon tamoxifen administration and expression of *Cre-recombinase*, lox sites were recombined, excising the GFP portion and driving expression of Tomato.
B. Representative images of dissected pancreas, spleen, liver and mammary fat tissue imaged on the Xenogen in vivo imaging system (IVIS) to detect fluorescence. GFP expression was detected specifically in the pancreas but only in mice expressing the reporter allele ($R26^-$ are reporter negative mice) (Left Panel). Upon tamoxifen induced CRE recombination RFP expression was detected, again only in the pancreas and in mice which express the reporter allele. When tamoxifen was not administered, RFP expression was not observed in the pancreas of mice that have the reporter (Right Panel)

3.3.2 Pancreas specific deletion of Alk5 or Tgfb1 does not affect pancreatic homeostasis

With confirmation of pancreas specific Flippase and CRE recombinase expression, I sought to interrogate the function of TGFß signalling in the adult pancreas. Therefore, via intraperitoneal tamoxifen administration, *Tgfb1* or *Alk5* were deleted from the pancreas in 6 week old *Pdx1-Flp; Kras^{WT}; Trp53^{WT}* mice (**Figure. 8A**). These mice were sampled three weeks post induction and pancreata were formalin fixed and embedded in paraffin. Slides were examined through haematoxylin and eosin (H&E) staining. After three-week, the deletion of either *Alk5* or *Tgfb1,* targeted to the pancreas did not result in any alteration to pancreatic histology (**Figure. 8B**). Pancreata presented with normal acinar and ductal composition, although islet area was reduced with *Alk5* deletion (**Figure. 8C**).

Therefore, examination of islet cell composition was undertaken to detect whether deletion of *Alk5* influenced specific islet cell populations. Islets are composed of five distinct cell types; α-, ß-, γ-, δ and ε-cells which produce glucagon, insulin, pancreatic polypeptide, somatostatin and ghrelin respectively. Therefore, I stained tissue sections for synaptophysin, a pan islet marker, insulin, glucagon, ghrelin and somatostatin (**Figure. 9**) and analysed, using HALO software, the proportion of positive cells across the pancreas (**Figure. 10**). The proportion of α, ß and δ cells in the pancreas was unchanged upon deletion of *Alk5* or *Tgfb1,* denoted by glucagon, insulin and somatostatin positive staining, respectively. As expected, the majority of the islet stained positive for insulin, with ß cells composing up to 80% of the islet mass, while α and δ cells are located around the periphery of the mouse islets and make up 15-20% and 5-10% of the cells, respectively. Conspicuously the presence of ε cells was very uncommon in the adult pancreas, as was to be expected (Wierup et al., 2002), nevertheless, ghrelin expression was similar across the three genotypes, ultimately suggesting that *Alk5* and *Tgfb1* appear to be dispensable for adult pancreas homeostasis in the steady state.

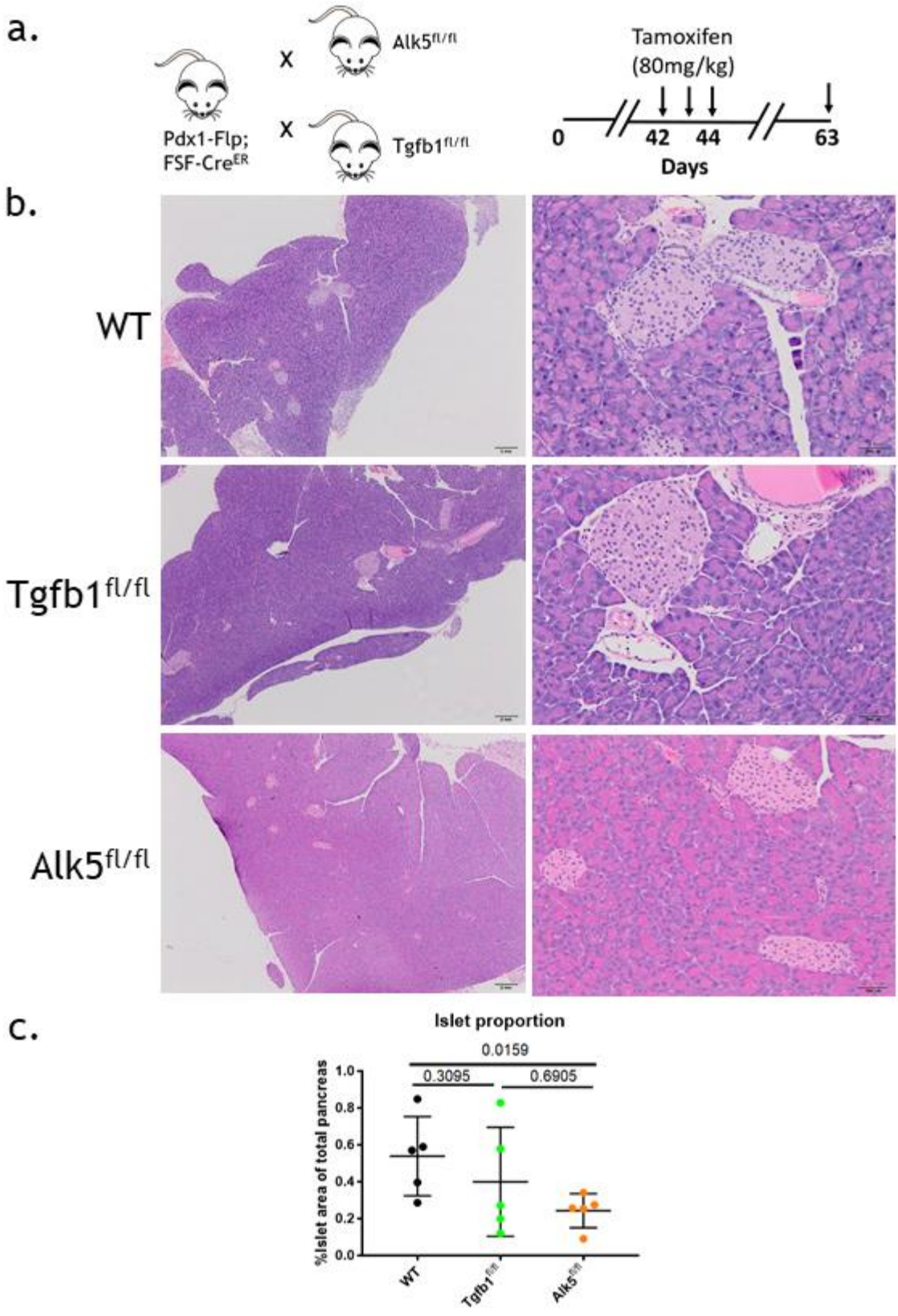

Figure 8 Adult pancreas homeostasis is unaffected by deletion of *Alk5* or *Tgfb1*
A. *Pdx-1-Flippase; Kras^{WT}; p53^{WT}* mice were crossed to either *FSF-Cre^{ER} Alk5$^{fl/lf}$* or *FSF-Cre^{ER} Tgfb1$^{fl/fl}$* mice. Mice were induced via intraperitoneal injection of tamoxifen for three consecutive days. Mice were sampled three weeks post induction.
B. Representative images of H&E stained sections from the sampled pancreata. The pancreas presents with normal acinar, islet and ductal morphology when *Alk5* or *Tgfb1* are deleted. (Scale bar left = 2mm, scale bar right = 500µm)

C. Quantification of islet area as a proportion of total pancreas area showing that deletion of *Alk5* resulted in reduced islet area compared to WT mice, (n=5 per genotype, Mann Whitney p-value as indicated).

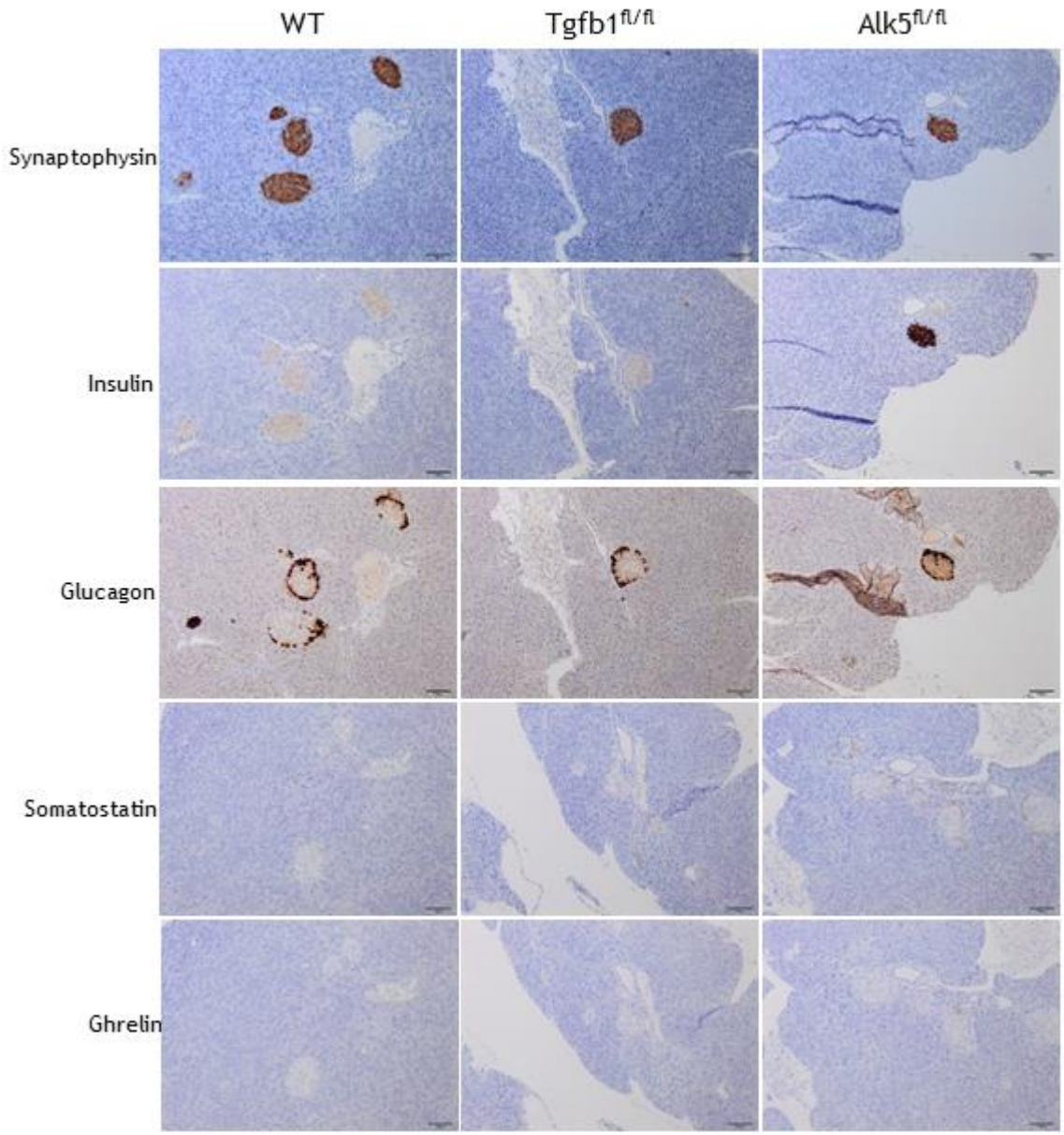

Figure 9 Islet cell composition is unchanged by *Alk5* or *Tgfb1* deletion
Representative images of IHC stained sections of pancreata from *Pdx1-Flp; FSF-Cre^{ERT}* (WT), *Pdx1-Flp; FSF-Cre^{ERT}; Tgfb1$^{fl/fl}$* (Tgfb1$^{fl/fl}$) or *Pdx1-Flp; FSF-Cre^{ERT}; Alk5$^{fl/fl}$* (Alk5$^{fl/fl}$) mice, stained for the islet cell markers synaptophysin, insulin, glucagon, somatostatin and ghrelin. Synaptophysin is a pan-Iset markers, β cells stain positive for insulin, α cells stain positive for glucagon, δ cells stain positive for somatostatin and ϵ cells stain positive for ghrelin. (Scale bars = 1mm)

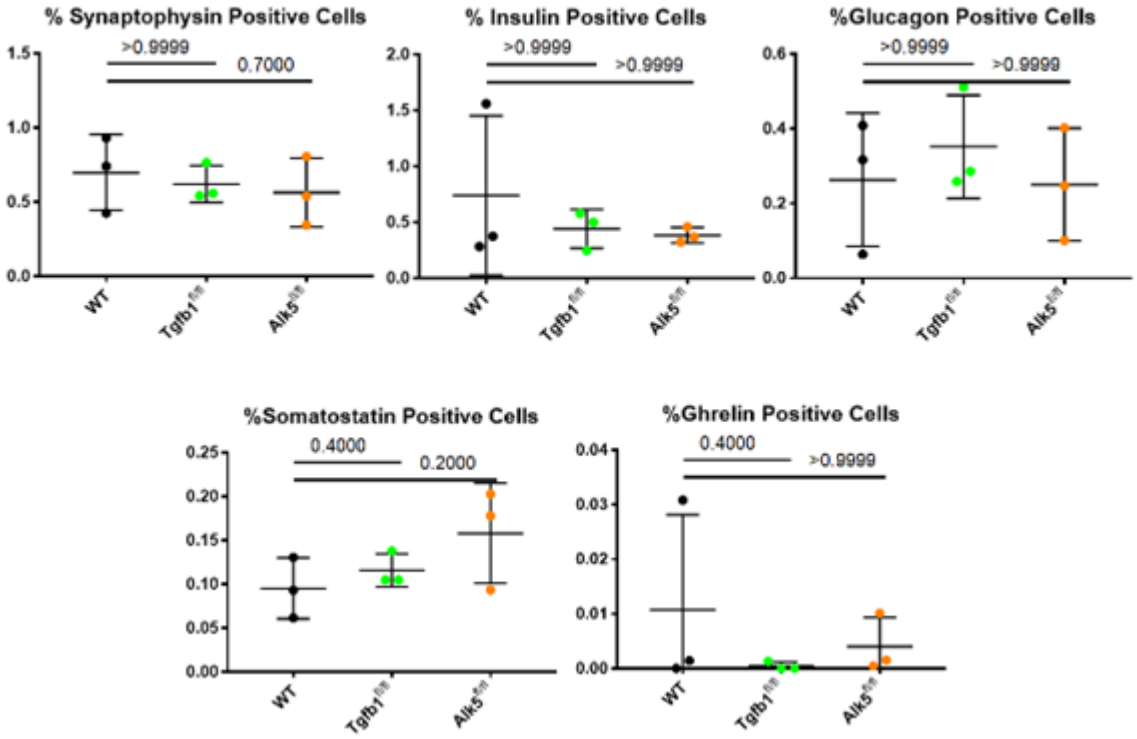

Figure 10 Quantification of islet cell composition
Quantification of the denoted IHC stained tissue sections using HALO software. The percentage of positive cells as a proportion of the total cells in the pancreas, in the indicated genotypes, of the pancreatic islet cell markers is shown. *Pdx1-Flp; FSF-CreERT* (WT), *Pdx1-Flp; FSF-Cre^{ERT}; Tgfb1$^{fl/fl}$* (Tgfb1$^{fl/fl}$) or *Pdx1-Flp; FSF-Cre^{ERT}; Alk5$^{fl/fl}$* (Alk5$^{fl/fl}$) (n= 3, Mann-Whitney p values indicted).

3.3.3 Deletion of *Alk5* but not *Tgfb1* in *Kras^{G12D}* expressing pancreatic cells drives tissue transformation

Following on from findings that deletion of *Alk5* or *Tgfb1* in the normal pancreas did not affect organ homeostasis, I investigated how deletion of these genes would influence oncogenic Kras^{G12D} driven tumour initiation. This was interrogated by crossing the KF (*Pdx1-Flp; FSF-Kras$^{G12D/+}$*) mouse model bearing tamoxifen inducible CRE recombinase with mice carrying either *Alk5$^{fl/fl}$* (KAF) or *Tgfb1$^{fl/fl}$* (KTF) alleles. The KF model presents with PanINs at 6 weeks of age, similar to the KC model, with more advanced PanINs present at 10 weeks (**Figure.11**). The expression of oncogenic *Kras* is sufficient to drive PanIN development with progression to PDAC occurring over long latency, unless accelerated with additional mutation of tumour suppressors (Schonhuber et al., 2014).

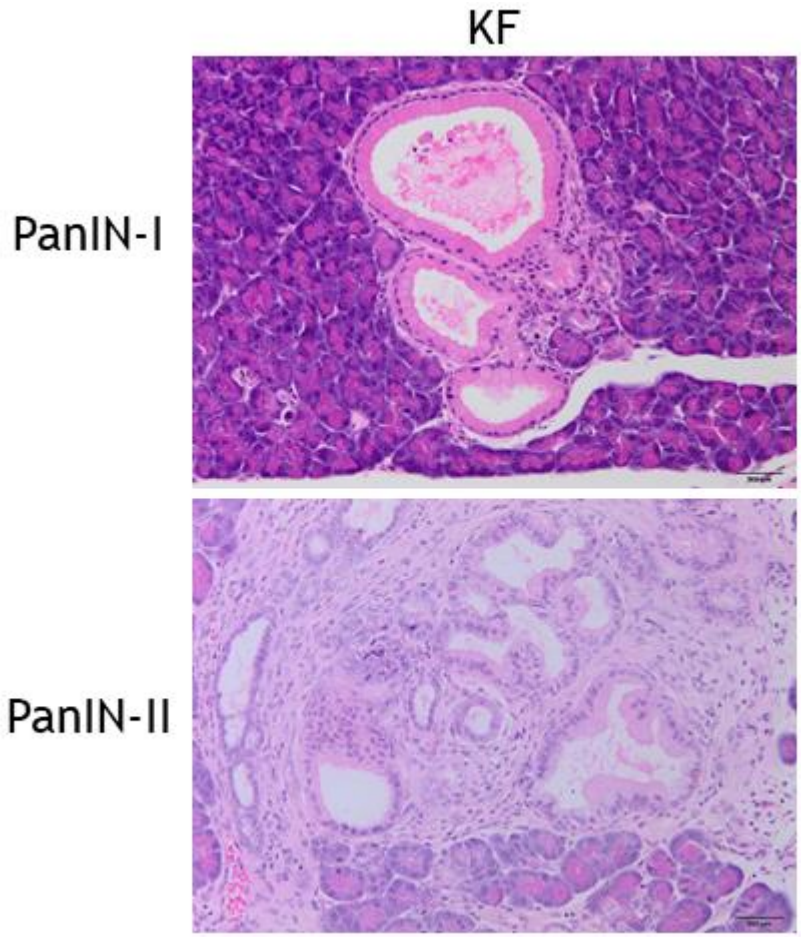

Figure 11 Pdx1-Flp activation of oncogenic *Kras^{G12D}* drives PanIN development
Representative images of H&E stained tissue sections for the stated genotypes at 6week and 10week of age. PanINs were detectable in the KF and KC model as early as 6 weeks, with examples of progressed PanIN-II lesions shown at 10weeks of age. (Scale bar = 500μm).

Therefore, 6-week-old KF mice were induced with tamoxifen, whereby deletion of either *Alk5* or *Tgfb1* occurred in *Kras^{G12D}* co-expressing cells, and sampled 1 week or 3 weeks post induction (**Figure. 12**). In the KF mice, low grade PanINs and pancreatic transformation was observed in the pancreas. The deletion of *Alk5* in the Kras^{G12D} positive cells culminated in increased pancreatic transformation with elevated PanIN burden (**Figure. 12**). This can be evidenced as early as 1-week post induction with further progression noted in the 3-week post-induction time point. Quantification of this was performed by measurement of transformed area as a proportion of the total pancreas area from a single H&E slide analysed through HALO (**Figure 13**). These data demonstrated that TGFβ signalling represses PanIN progression in early disease and that reduced responsiveness to ligand, via receptor deletion, resulted in accelerated pancreas transformation. However, I was unable to visualise PanINs in the majority of KF mice with deletion of *Tgfb1*. Although this could suggest that autocrine TGFβ1 is required for the maintenance of PanIN lesions, I noted that penetrance within the Pdx1-flippase model was incomplete. For instance, 66% of KPC mice reach clinical end-points due to PDAC related phenotypes with practically no mice surviving over 1 year of age. In comparison 52% of the KPF mice in my colonies survived beyond 1 year without developing PDAC, with only 40% presenting with PDAC related phenotypes. Although this reduces the pool of tumour bearing mice for analysis, the KPC model frequently presents with papilloma and can develop off target phenotypes such as lymphomas, which are not prevalent in the KPF model. This did, however, create more difficulty in studying the initiating events in pancreatic tumorigenesis. Therefore, solid conclusions could not be drawn in the KTF model with a sample size of only 3 mice. Due to less than 50% of KPF mice undergoing pancreatic transformation additional numbers are required to match those of the KF and KAF cohorts to mitigate against analysis skewed towards the subset of mice which would not go on to develop PanIN lesions. Further, even with the greater sample number in the KAF and KF cohorts it is clear two populations exist, those with and those without PanINs, it would be important to add additional numbers to those cohorts to bolster those presenting with PanIN lesions and allow firmer conclusions about any accelerated phenotype noted.

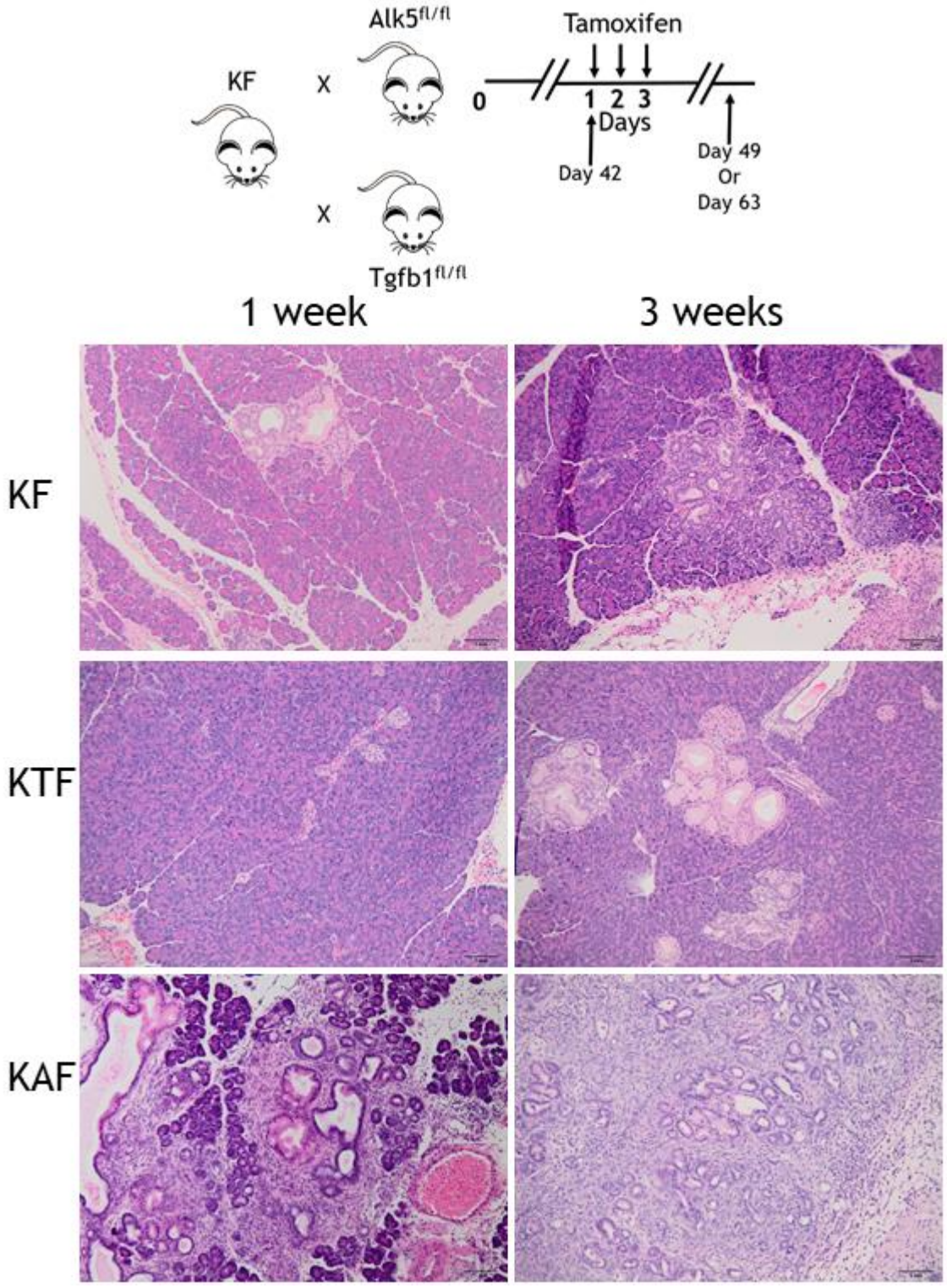

Figure 12 KAF mice display increased pancreatic transformation compared to KF mice
The pancreas was harvested from KF, KTF and KAF mice 1 or 3 weeks post tamoxifen induction, administered at 6 weeks of age. Representative images of H&E stained tissue sections for the stated genotypes at each time point are shown. The KAF mice present with a greater burden of pancreatic transformation compared to the KF controls. NB, the representative image for KTF mice harvested 1 week after induction does not show PanINs as no PanINs were detected in any of these mice sampled at this timepoint. (Scale bars = 1mm).

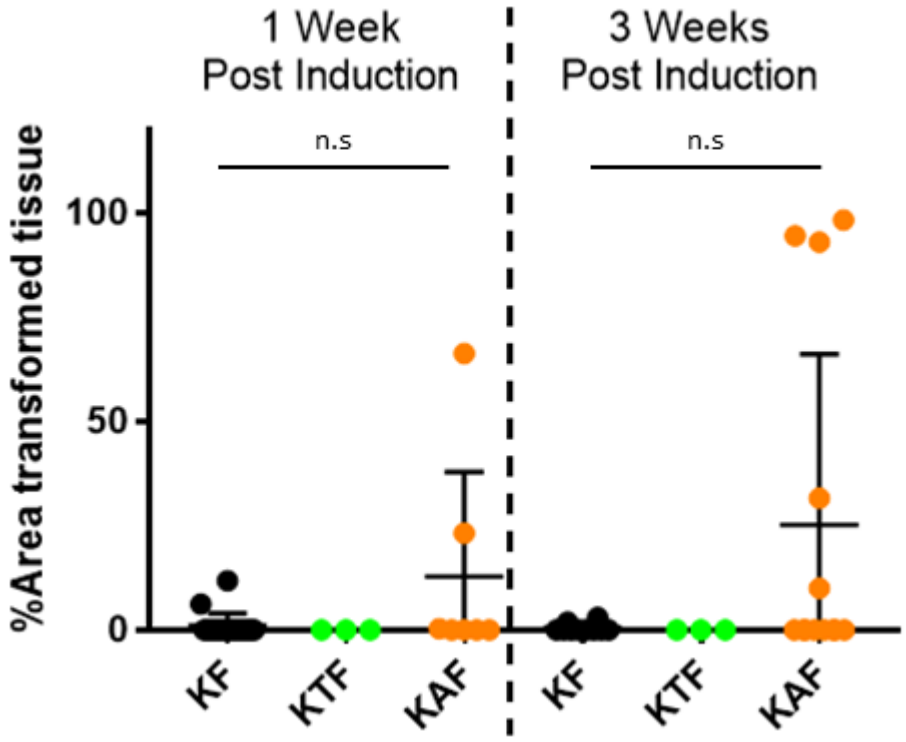

Figure 13 The KAF mice have an increased proportion of pancreatic transformation compared to KF mice
HALO software was used to analyse H&E strained tissue sections to determine the proportion of transformed pancreatic tissue at either the 1 week or 3 week post induction time-points in the KF, KTF and KAF mouse models. The KAF mice presented with increased pancreatic tissue transformation compared to the KF mice. (n=18, 3, 7, respectively) (n= 10, 3, 13, respectively) (Mann Whitney test used, n.s = not significant).

Due to the incomplete penetrance of PanIN development, I cannot conclude that deletion of *Tgfb1* within neoplastic cells effects the progression of the lesions from these data. I observed some low-grade PanIN lesions in 1/3 KTF mice 3 weeks post induction but in 0/3 one week post induction. This does suggest that deletion of *Tgfb1* does not completely eradicate PanIN development. However, increased numbers would help to determine whether the penetrance of PanINs is significantly reduced, or not, in this model. This incomplete penetrance is seen across models, even in the accelerated KAF model, with a proportion of time-point mice failing to exhibit PanIN lesions when their presence would have been expected (4/7 have no PanIN burden 1week post induction).

With incomplete penetrance noted previously at the 6-week time point, I repeated the experiment with the administration of tamoxifen at 10 weeks of age. I hypothesised this would provide insight into whether the KF model

presented with a slower progression of PanIN development, with 6-week inductions occurring too early, or if indeed it was incomplete penetrance of disease. However, I observed broadly similar results to those within the 6-week model (**Figure 14**) with the KAF mice presenting with increased pancreatic transformation in comparison to both the KF and KTF mice. Quantification of the area transformed, highlighted the progressive transformation of the total pancreas area upon *Alk5* deletion with no normal acinar structure retained 3 weeks post induction (**Figure 15**). However, incomplete penetrance was still noted, precluding any more conclusive results from the *Tgfb1* deletion model.

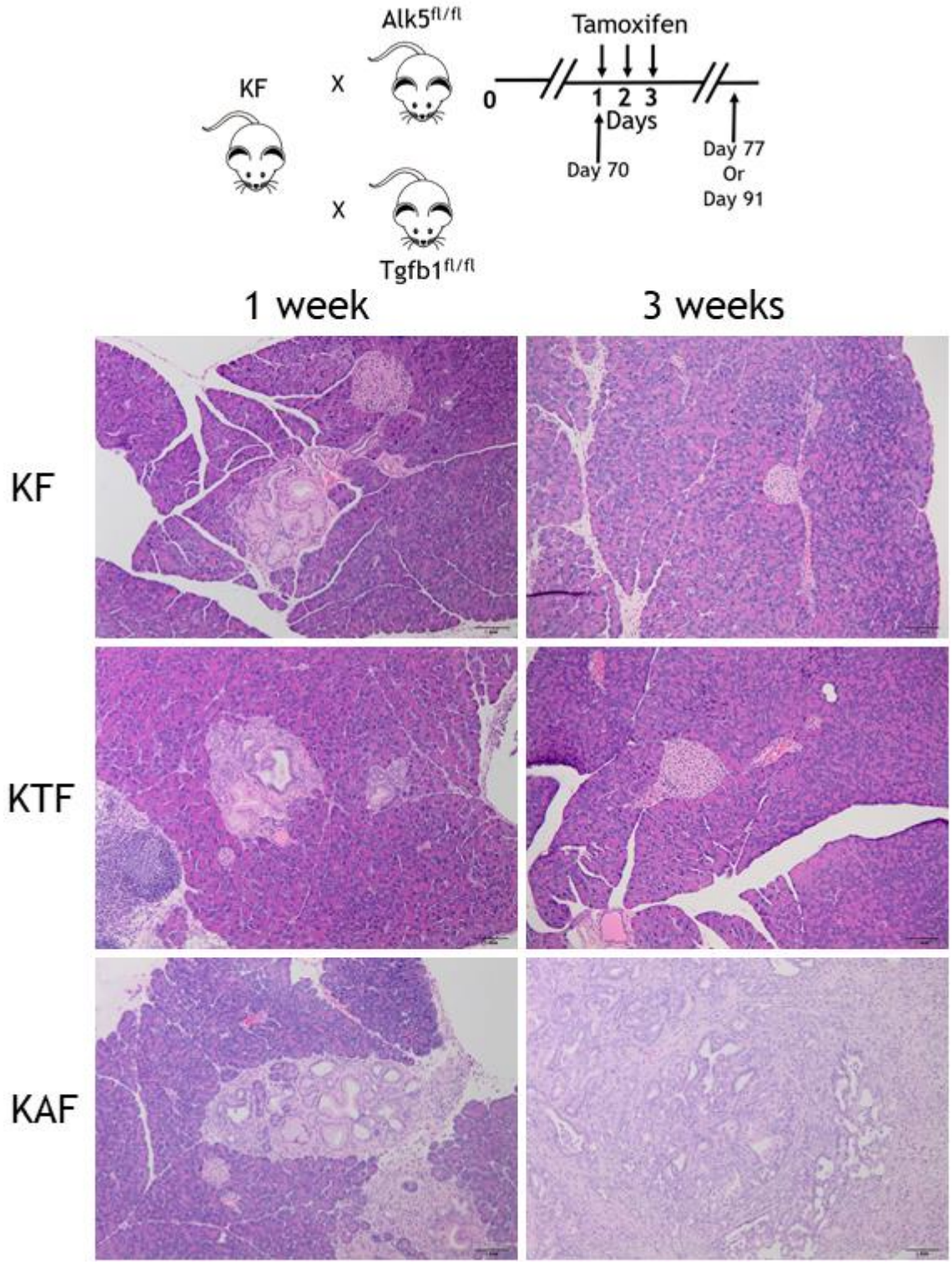

Figure 14 The KAF mice display increased pancreatic transformation compared to the KF mice when induced at 10 weeks of age
The pancreas was sample from KF, KTF and KAF mice 1 or 3 weeks post tamoxifen induction, administered at 10 weeks of age. Representative images of H&E stained tissue sections for the stated genotypes at each time point is shown. NB, the representative image for KF and KTF mice harvested 3 weeks after induction does not show PanINs as no PanINs were detected in any of these mice sampled at this timepoint. (Scale bars = 1mm).

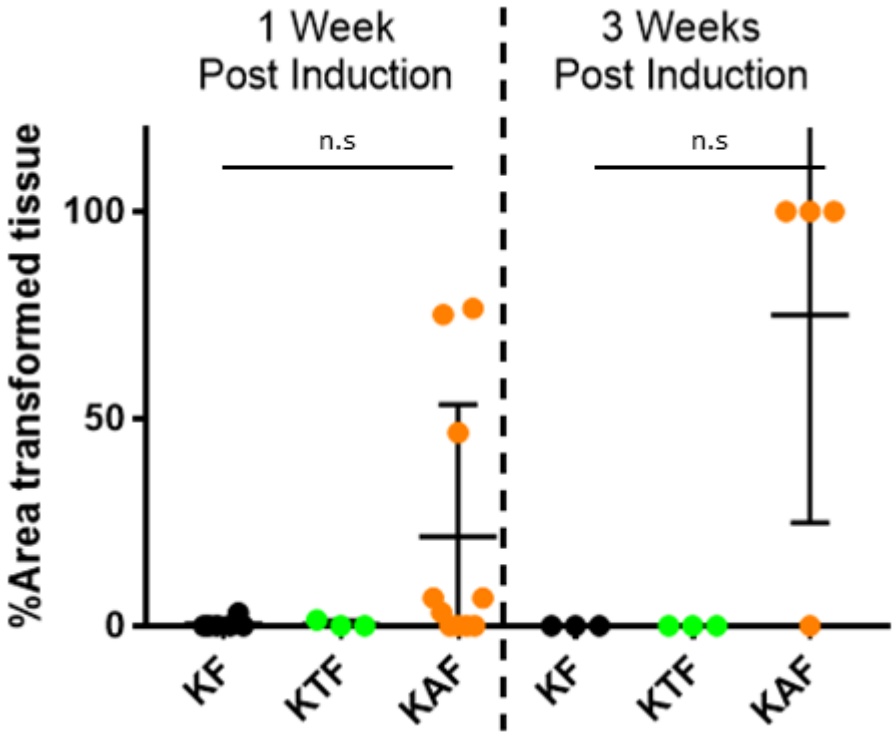

Figure 15 KAF mice presented with an increased area of pancreatic transformation compared to KF mice when induced at 10 weeks of age
HALO software was used to analyse the proportion of transformed pancreatic tissue at either the 1 week or 3 week post induction time-points in the KF, KTF and KAF mouse models. The KAF mice presented with increased pancreatic tissue transformation compared to the KF mice. (n= 6, 3, 11, respectively) (n= 3, 3, 4, respectively) (Mann Whitney test used, scale bars represent standard deviation, n.s = not significant).

3.3.4 The KAF model presents with decreased epithelial TGFβ signalling and increased proliferation

In order to interrogate the mechanism for the increased initiation in the KAF mice, I performed IHC analysis on sections from KF and KAF models, with the KTF model excluded due to low PanIN penetrance in these mice.

I hypothesised that deletion of *Alk5* would result in a decrease in downstream TGFβ signalling, which was specifically interrogated via pSMAD3 expression in PanIN regions. It was noted that pSMAD3 staining was high in the KF model representing active TGFβ signalling. In the KAF model, the proportion of pSMAD3 positive cells in *bona fide* PanINs was slightly, but, significantly reduced, suggesting knockout of TGFβ signalling at least in some of the PanIN epithelial cells (**Figure 16**). However, this antibody has the potential to bind other phosphorylated SMADs such as pSMAD1, and therefore could also be capturing activation of other TGFβ signalling family members. Therefore, I conducted a stain with a pSMAD2 antibody, which shows greater specificity to its target, and similar findings were observed with reduced epithelial nuclear pSMAD2 but not total ablation (data not shown).

Interestingly pSMAD3 levels appear elevated in PanIN adjacent tissue undergoing ADM/acinar atrophy in the KAF model, making quantification challenging. This high level of pSMAD3 in this tissue could either point to a stress response, due to increased transformation resulting in acinar atrophy in surrounding areas, to incomplete recombination of the *Alk5* gene, to activation by via other TGFβ superfamily receptors, or intriguingly to enhanced ligand production by the receptor deficient transformed cells. Therefore, I investigated whether the pSMAD3 positive areas carry oncogenic KRAS via staining for phosphorylated ERK, a downstream indicator of activated KRAS signalling. I also stained for CRE recombinase to define if cells had the potential to recombine lox flanked genes and performing *Alk5* RNAscope to confirm gene deletion. This approached allowed me to elucidate if these were 'bystander' lesions that were driven by the *Alk5* deleted epithelium and did not carry genetic mutations or if they are $KRAS^{G12D}$ positive cells which had failed to recombine lox sites in the *Alk5* gene.

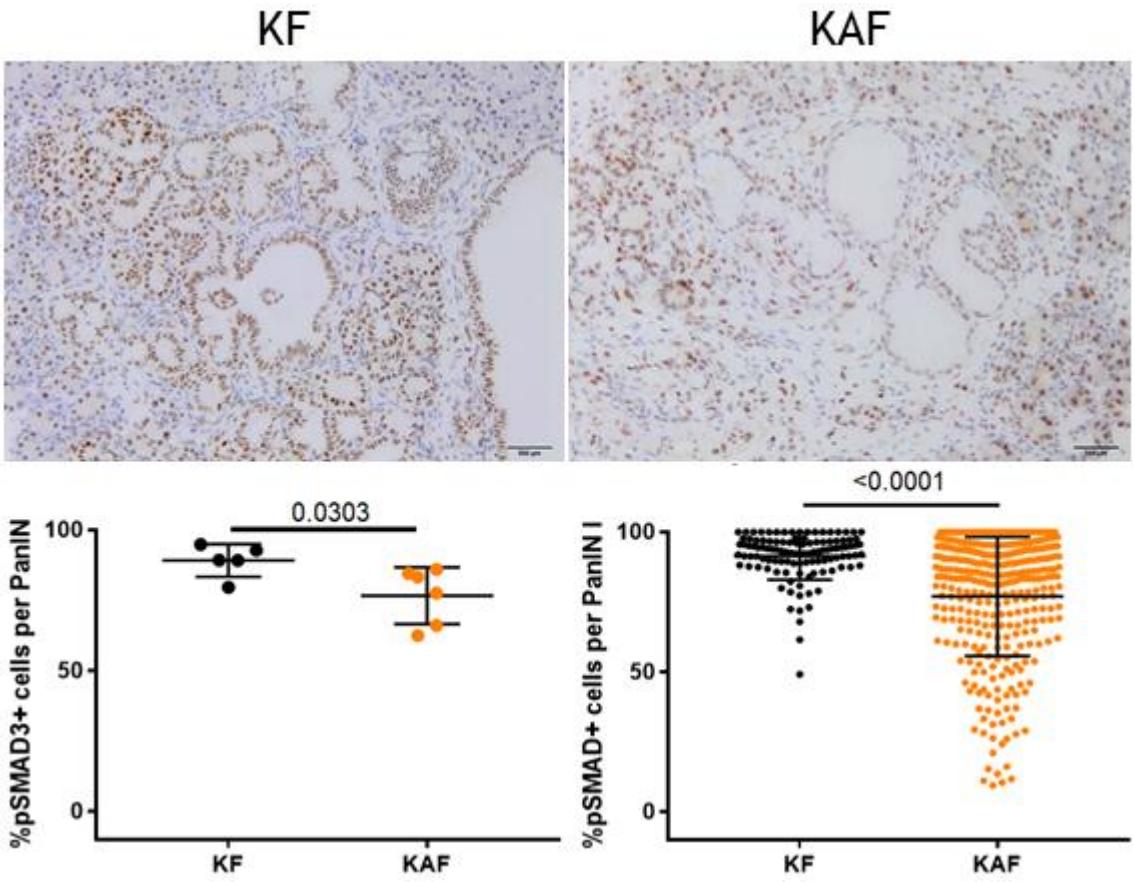

Figure 16 The KAF model had reduced PanIN epithelial pSMAD3^{+} cells compared to KF PanINs
Representative images of pSMAD3 IHC stained tissue sections for the stated genotypes (Scale bars = 500μm). Quantification of the proportion of pSMAD3^{+} cells within PanINs across a single slide per mouse is shown, left, with the proportion of pSMAD3^{+} epithelial cells across all counted PanINs shown, right. The KAF model displays reduced pSMAD3^{+} cells within PanINs compared to the KF model (n=5, 6 respectively). (Mann-Whitney P-values indicated).

The *Alk5* RNA scope was inconclusive in confirming the epithelial deletion of the receptor in the KAF model. This was due to lack of detection of *Alk5* within any of the tissue stained even in the KF model. As shown in **Figure 17**, very few cells stained positive for *Alk5* transcripts, with those that were positive existing exclusively within the stroma of the developing PanIN. This perhaps indicated low levels of *Alk5* RNA, below detection levels, within the pancreas, or poor RNA quality within the tissue, as opposed to cells ubiquitously lacking ALK5 expression.

The expression of pERK was clearly visualised across all epithelial cells of the PanIN but was not seen in the adjacent normal acinar tissue (**Figure 18**). This was indicative of active KRAS and would suggest that RAS signalling was

activated in all PanIN as well as surrounding ADM lesions of the KAF model. However, pancreatic inflammation itself is known to trigger expression of KRAS and activation of its effectors (Assi et al., 2021) so these data were still inconclusive.

When staining for Cre recombinase we noted positive staining within the nuclei in transformed epithelium but not in normal ducts, and importantly not in surrounding ADM/atrophied acinar tissue (**Figure 19**). The nuclear positive staining indicated active CRE in the correct site to recombine *loxP* sites. Therefore, due to the phenotype combined with expression of epithelial CRE recombinase, pERK and decreased pSMAD3 activation in the *bond fide* PanINs, we can conclude that *Alk5* was deleted within some, but not all, of the *Kras* transformed cells in the KAF model. However, this was sufficient to drive increased pancreatic transformation.

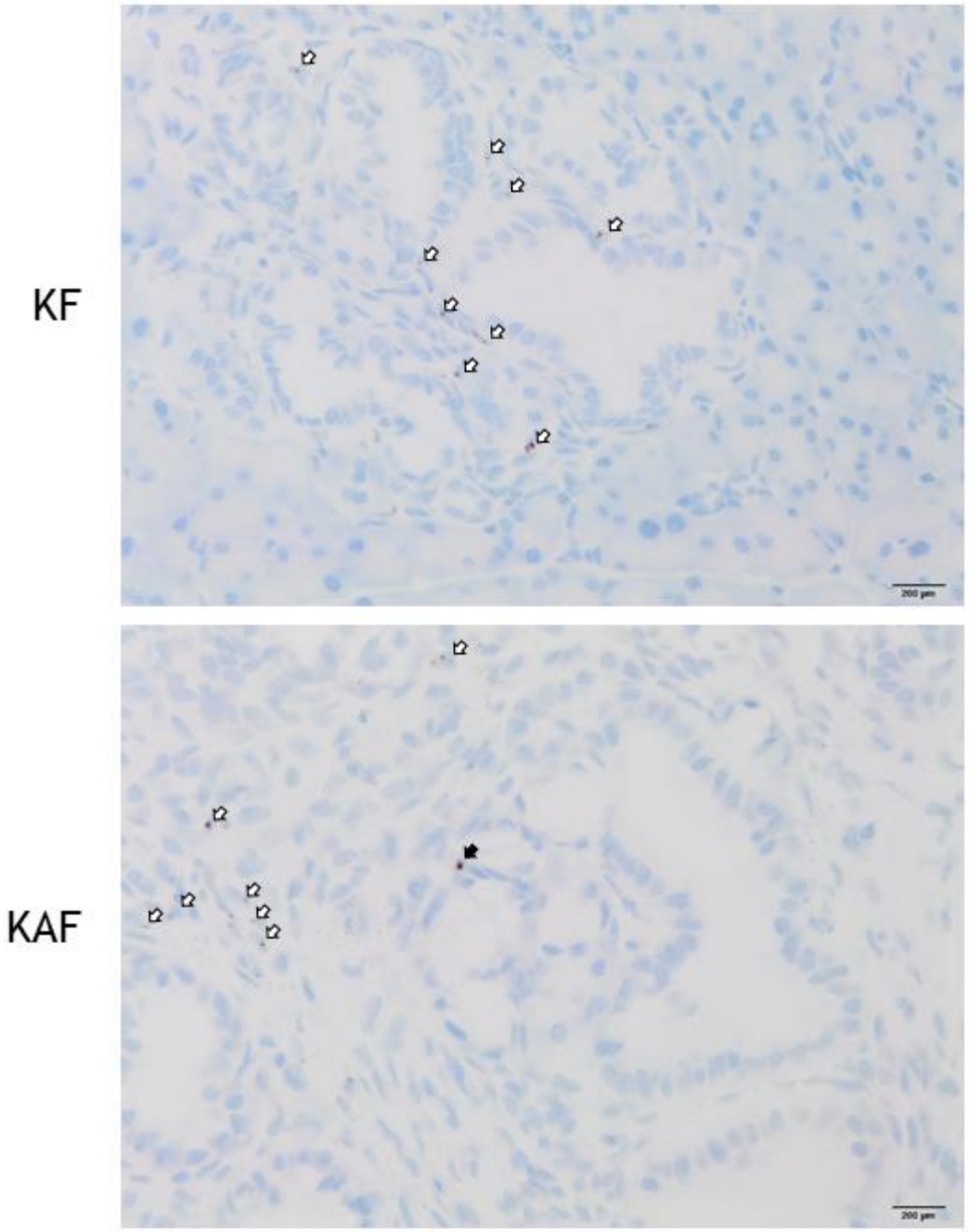

Figure 17 *Alk5* expression detected in the stroma but not the epithelium of PanINs
Representation images of PanIN lesion from sections stained for *Alk5* via RNAscope. Stromal positive staining was noted in both KF and KAF lesion, however, no appreciable epithelial expression of *Alk5* was detected. White arrow heads indicated positive staining in stromal areas, with black arrow heads denoting any epithelial specific positive staining. (Scale bars = 200μm).

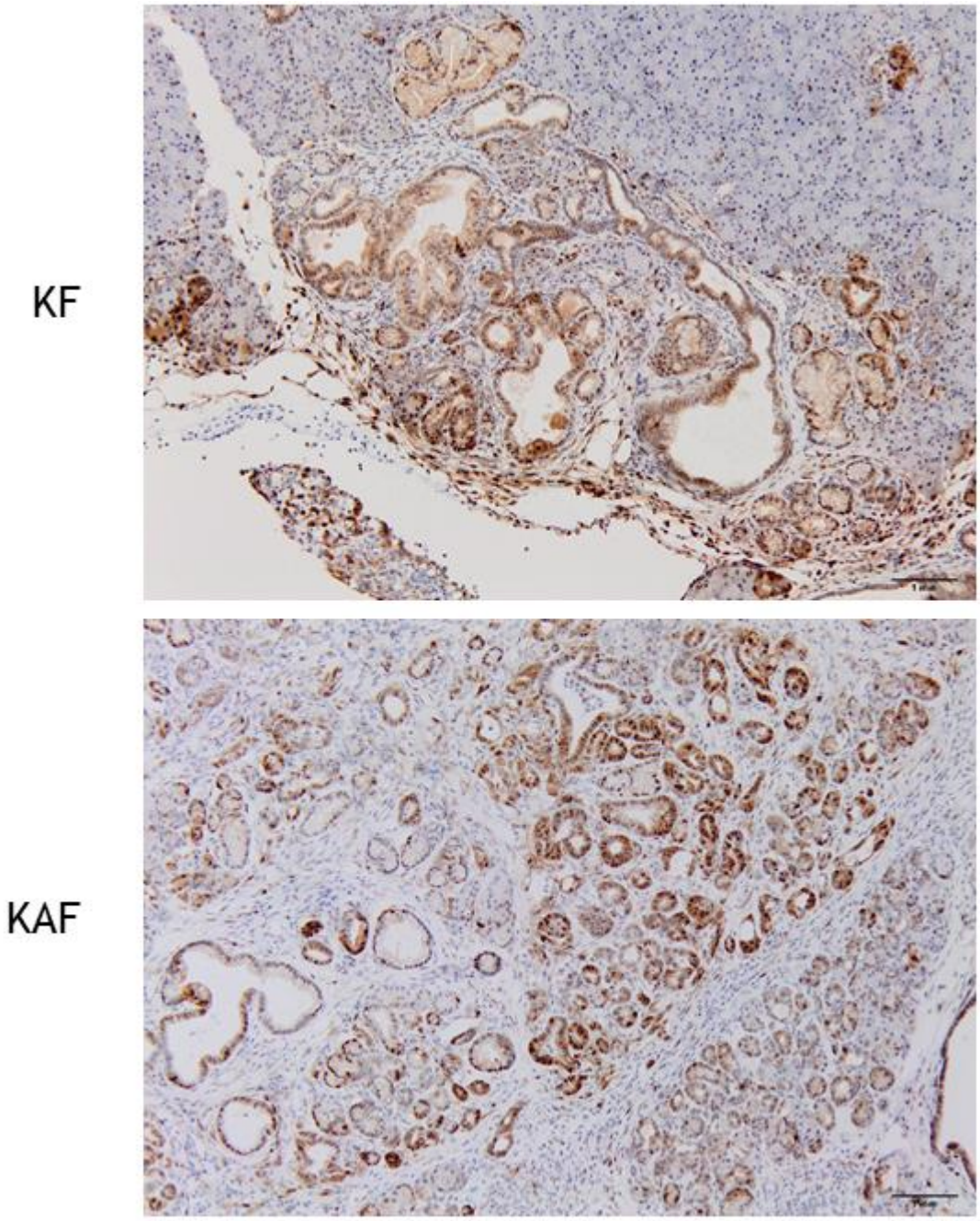

Figure 18 pERK is ubiquitously detected in PanIN lesions and surrounding ADM in both KF and KAF mice regardless of model
Representative images of pERK IHC stained PanIN tissue sections for the stated genotypes. High levels of pERK were noted in areas of ADM and PanIN lesion in both genotypes, with no pERK stain in the adjacent healthy acinar tissue noted. (Scale Bars = 1mm).

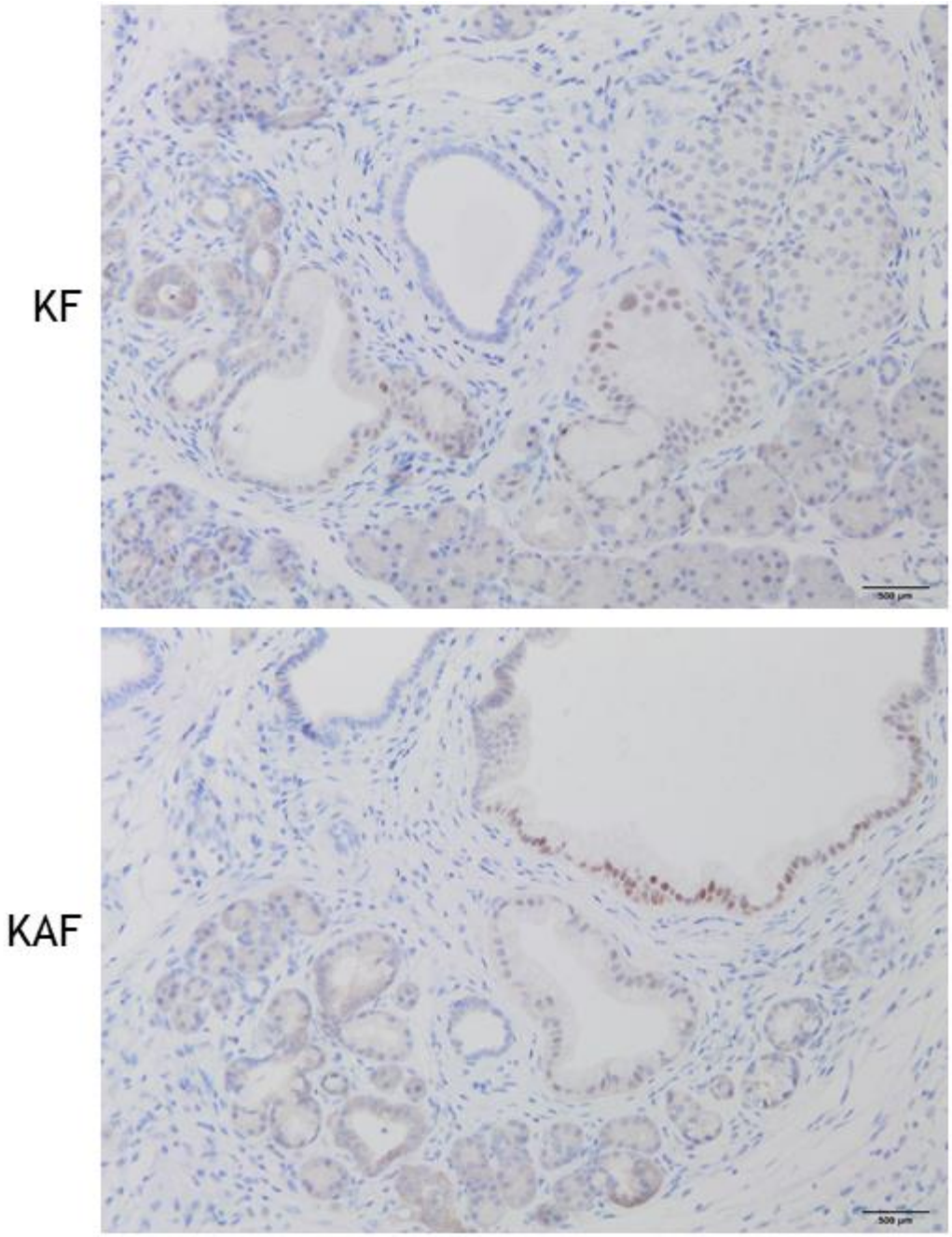

Figure 19 CRE recombinase was detected in the PanIN epithelium only
Representative images of IHC for CRE Recombinase on PanIN tissue sections for the stated genotypes. Positive CRE Recombinase staining was noted in nuclear regions of PanIN epithelium only. Both stromal cells and normal ducts were negative. There was no difference between KF and KAF mice in terms of CRE recombinase expression. (Scale bars = 500μm).

Given the role of TGFß as a potent tumour suppressor, I also wanted to assess the proliferative status of lesions in the models. Alongside the loss of downstream TGFß signalling the KAF model showed more epithelial proliferation within the PanIN regions, measured by increased Ki67 positive staining when compared to the KF model (**Figure 20**). This confirmed that deletion of *Alk5* in the KAF model removed the TGFß induced growth arrest on $Kras^{G12D}$ transformed cells, highlighting further that TGFß signalling is a potent tumour suppressor in disease initiation.

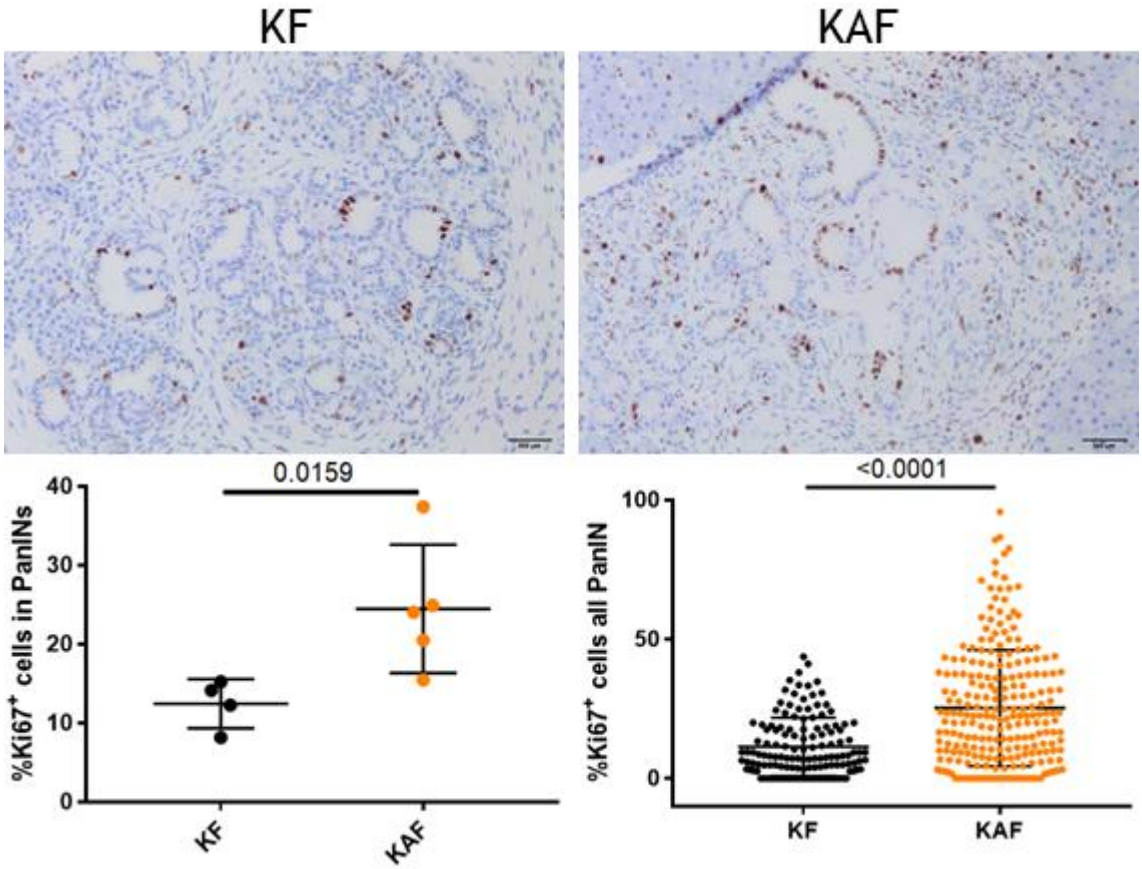

Figure 20 PanINs in KAF mice have increased epithelial proliferation compared to PanINs in KF mice
Representative images of Ki67 IHC stained tissue sections for the stated genotypes (Scale bars = 500µm). Quantification of the proportion of $Ki67^+$ PanIN cells per mouse counted is shown, left, with the proportion of $Ki67^+$ cells across all counted PanINs shown, right. The KAF model presents with an increased proportion of highly proliferation PanINs compared to the KF model (n=4, 5, respectively) (Mann Whitney P values indicated).

3.3.5 Deletion of *Alk5* but not *Tgfb1* in *Kras^{G12D}* expressing models reduces survival

Continuing from the findings in the KAF model, that deletion of *Alk5* following Kras^{G12D} expression increased pancreatic transformation, the next aim was interrogate this in an ageing model. Six-week-old KF, KTF or KAF mice were induced with tamoxifen over three days and aged until clinical end-points or the end of the experiment, age 450days, was reached (**Figure 21**).

Before beginning induction all mice were screened by high resolution ultrasound to confirm they had no early detectable pancreatic tumours. They were subsequently followed up post induction upon detection of palpable tumours with weekly ultrasound scans. Representative images can be seen in **Figure 22** with normal pancreas (**Left**) and PDAC outlined in blue (**Middle & Right**). The software allows for the construction of 3D images of the PDAC and therefore we were able to calculate the volume of the tumour and plot its development over time. The KAF model shows continuous growth of the primary PDAC until clinical end-points are reached (**Figure 23**).

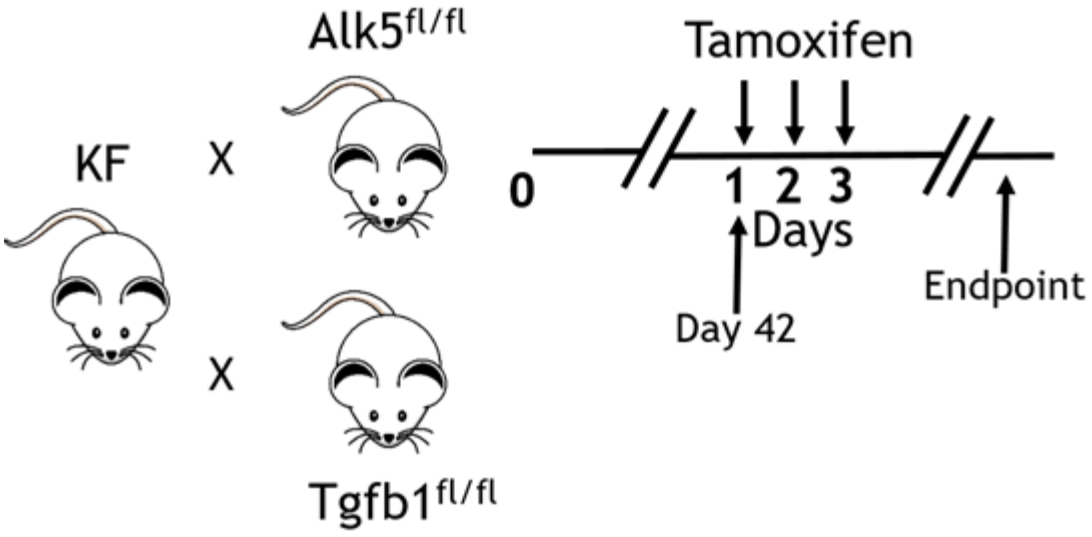

Figure 21 KF, KAF and KTF mice were induced at 6weeks of age with tamoxifen
The KF, KTF and KAF models were induced at 6 weeks of age following ultrasound confirmation of normal pancreatic appearance. Tamoxifen was administered over 3 days. Mice were palpated weekly and subjected to ultrasound upon detection of a palpable tumour. Mice were aged until clinical end-points were reached.

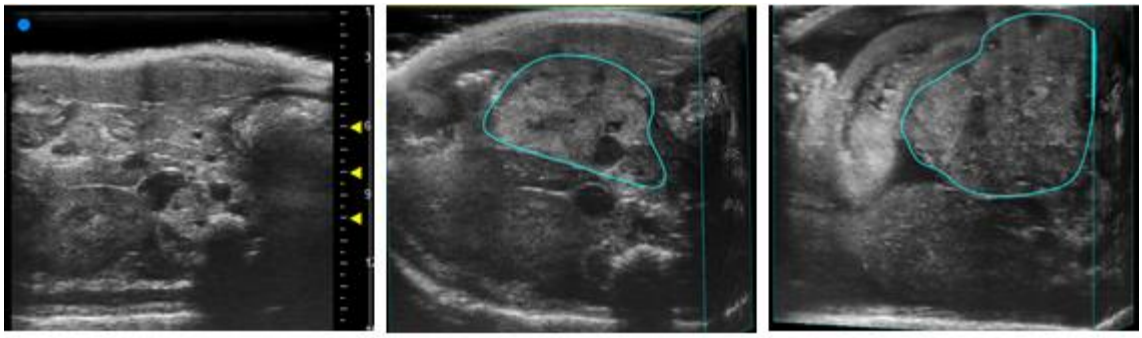

Figure 22 Representative images of ultrasound analysis of normal and tumour pancreas
Ultrasound was used to screen KF, KTF and KAF mice prior to induction to confirm normal pancreatic morphology, left. Upon detection of a palpable tumour ultrasound was used to generate a 3D measurement of the tumour (middle). Weekly US was used to track the growth of tumours over time, with a representative end-point tumour with ascites, shown right.

Survival analysis shows a dramatically reduced survival in a proportion of KAF, but not KTF mice, compared to the KF control mice (**Figure 23**). There was notable lack of penetrance in these long-term cohorts, as can be seen with the KAF mice surviving beyond 1 year of age post induction (7/11), meaning that acceleration was not significant. Therefore, I also conducted a survival study with induction occurring at 10 weeks of age, to test, as mentioned previously, whether the KF model presented with a higher burden of PanINs at this later time-point and would therefore have more Flp recombine cells, and thus more recombined Cre^{ER} and higher levels of recombination post tamoxifen induction. This induction regime again showed a reduced long-term survival of the KAF but not the KTF mice compared to the KF mice, with growth of primary pancreatic tumours observed via US (**Figure 24**). However, as observed in the inductions commencing at 6weeks of age, not all KAF mice presented with pancreatic tumours with 52% (12/23) surviving over 1 year post induction.

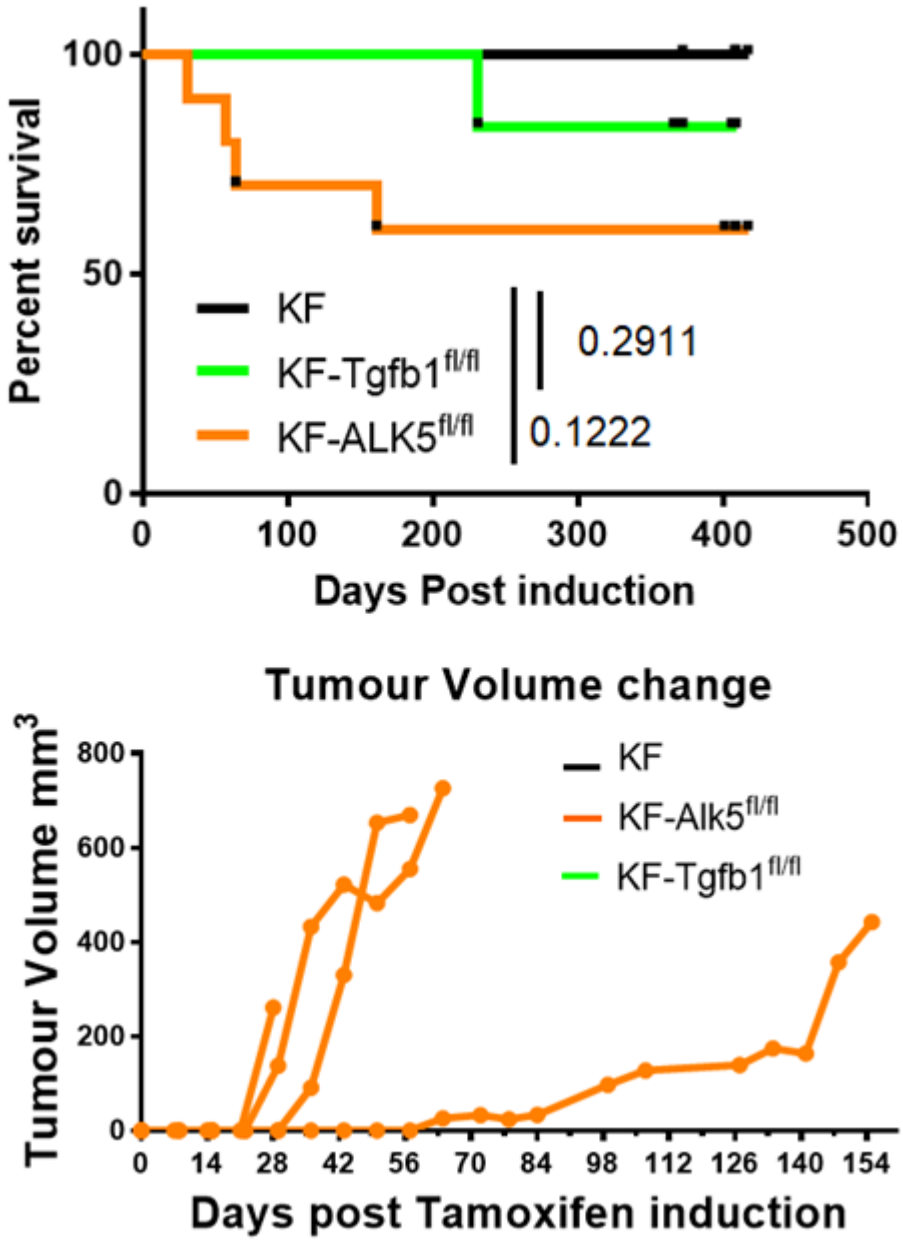

Figure 23 The KAF model shows reduced survival in ageing cohorts when induced at 6 weeks of age compared to both the KF and KTF models
Kaplan-Meier survival analysis of the KF, KTF and KAF mice induced at 6 weeks of age. The KAF model present with a non-significant reduction in survival in comparison to the KF and KTF models, with development of PDAC. The KF and KTF models did not present with any palpable tumours. (n=5, 5, 11, respectively). Tumour growth, measured from 3D US scans, is shown in the bottom graph, with only the KAF mice presenting with primary PDAC. (n=4)

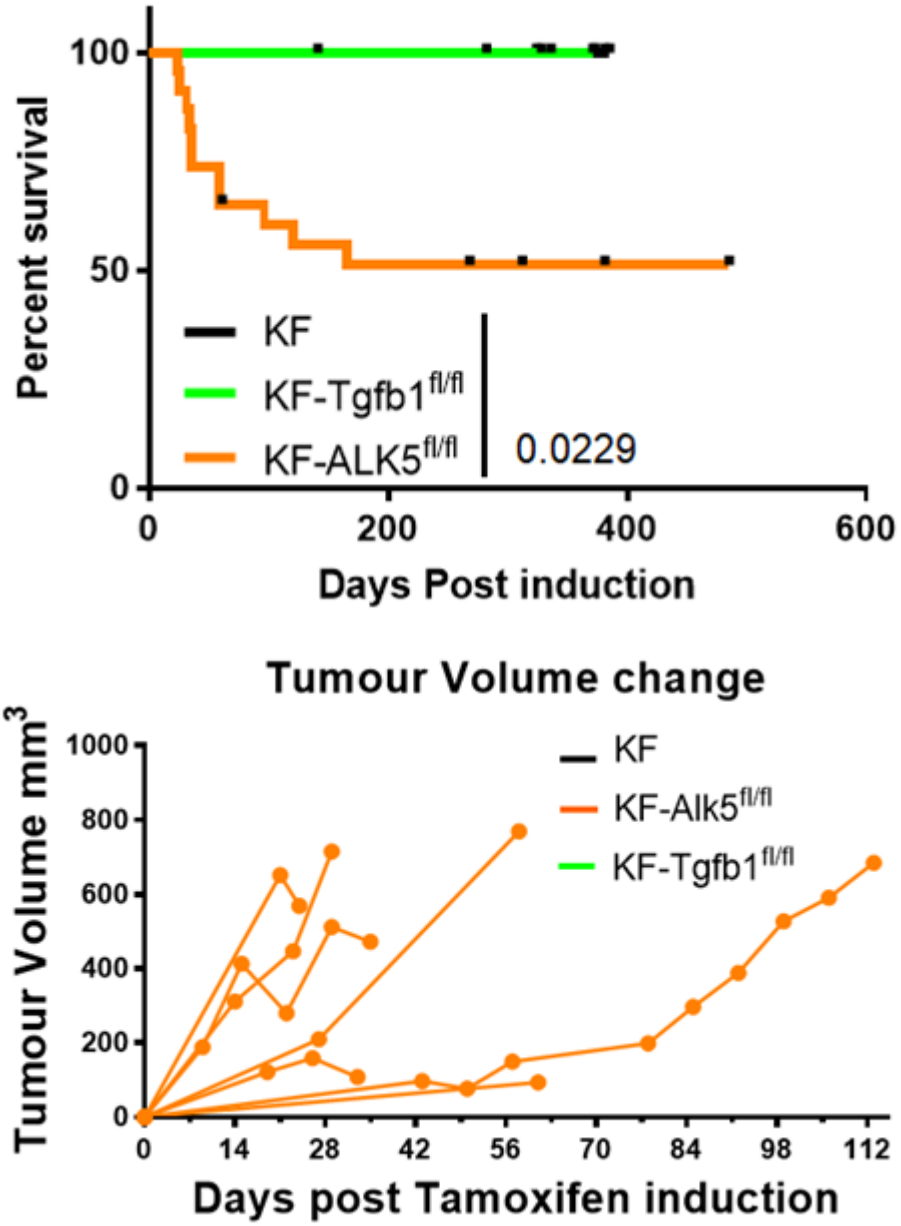

Figure 24 The KAF model shows reduced survival in ageing cohorts when induced at 10 weeks of age compared to both the KF and KTF models
Kaplan-Meier survival analysis of the KF, KTF and KAF mice induced at 10 weeks of age. The KAF model present with a significant reduction in survival in comparison to the KF and KTF models, with development of PDAC. The KF and KTF models did not present with any palpable tumours. (n=8, 8, 23 respectively). Tumour growth, measured from 3D US scans, is shown in the bottom graph, with only the KAF mice presenting with primary PDAC (n=7)

I next characterised the tumours developing in the KAF model. Representative images of H&E staining show almost total loss of normal acinar tissue within the pancreas of the KAF mice sampled at clinical end-points, with tissue almost completely replaced by PDAC. This contrasts with the KF, KTF and KAF mice, euthanized at timed end-points (>450 days without clinical signs), which present with normal pancreatic architecture (**Figure 25**). Due to the lack of penetrance in the KF and KTF mice, I was unable to conclude whether deletion of TGFß1 had any impact on tumour initiation and or progression. Although the KTF mice presented with no PanINs and did not exhibit an altered survival, I could not determine if this effect was mediated via reduced TGFß1 ligand or from lack of penetrance in general.

The KAF tumours also have significant stromal infiltration denoted by high levels of the pan-fibroblast marker podoplanin, as well as significant macrophage infiltration and large quantities of collage deposition, all hallmarks of PDAC TME, and similar to that observed in tumours from the KPF mouse model. However, differences in the TME composition in end-point tumours were observed between the models. For instance, collagen deposition was elevated in the KAF tumours with a greater proportion of the tumour area staining positive for Sirius red, although this did not reach significance (**Figure 26**). Fibroblasts are major producers of the ECM (Tian et al., 2019), therefore I investigated whether the abundance of these cells was elevated in the KAF tumours. However, fibroblasts populations appeared unchanged, with the area of both podoplanin and αSMA positive staining similar across the tumours of the two genotypes (**Figure 27**). There was a slight, but significant increase in T cells infiltration, with more $CD3^+$ cells in intra-tumoural areas in KAF tumours compared to KPF tumours. However, there was no elevation in the cytotoxic T cell population, denoted by CD8 expression (**Figure 28**). Macrophages were also more abundant in the KAF tumours, with the percentage area of F4/80 positive staining elevated, although this did not reach significance (**Figure 29**). TGFß signalling was still active across the pancreas, with downstream $pSMAD3^+$ staining unchanged between the KPF and KAF mice (**Figure 30**), with proliferation and cell death, measured by Ki67 and cleaved caspase 3 staining (**Figure 31**) respectively, also unchanged. Collectively, these data suggest that KPF and KAF tumours are broadly similar at

end-point, although alterations in the collagen deposition and immune infiltrate were detected.

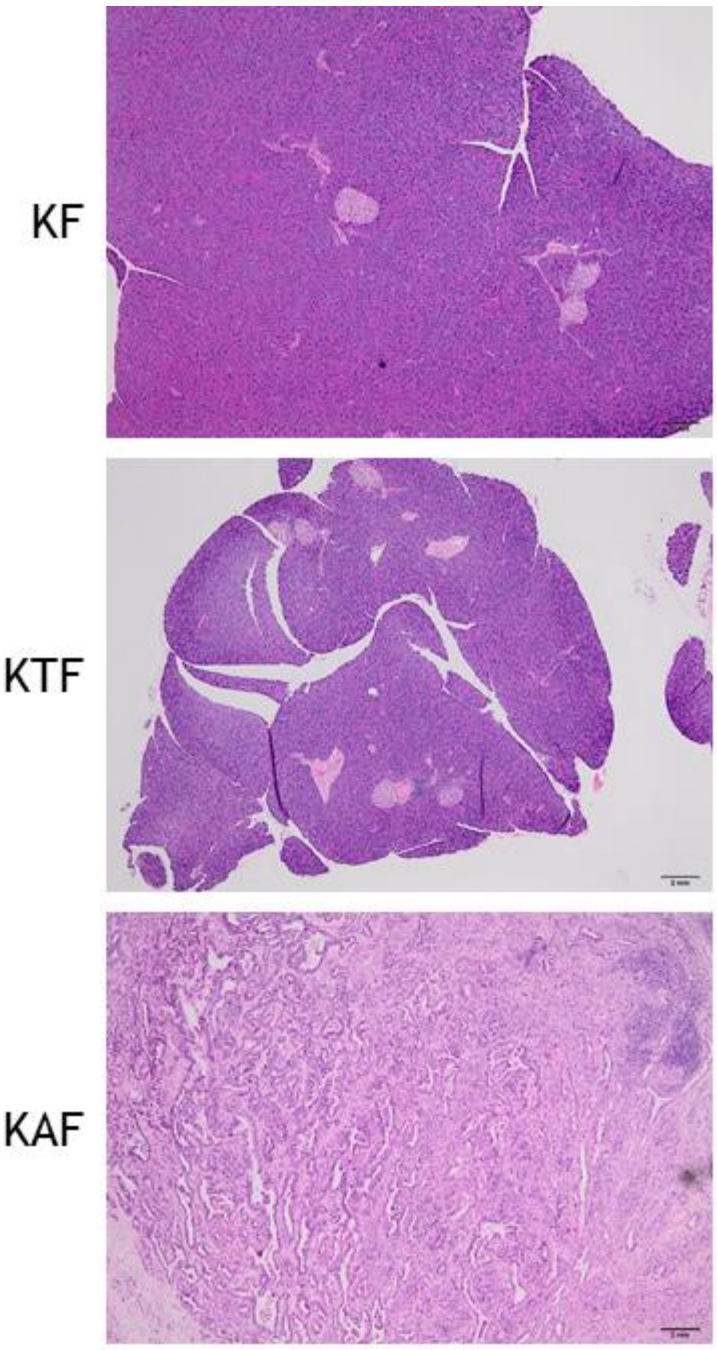

Figure 25 KAF mice present with PDAC at clinical end-point
Representative images of H&E stained tissue sections for the stated genotypes at end-point (timed end-point for KF and KTF, clinical for KAF). The KF and KTF model present with grossly normal pancreas when sampled at 450days of age. The KAF mice, sampled with pancreatic tumours, present with tumours recapitulating all the histological features of PDAC. (Scale bars = 2mm).

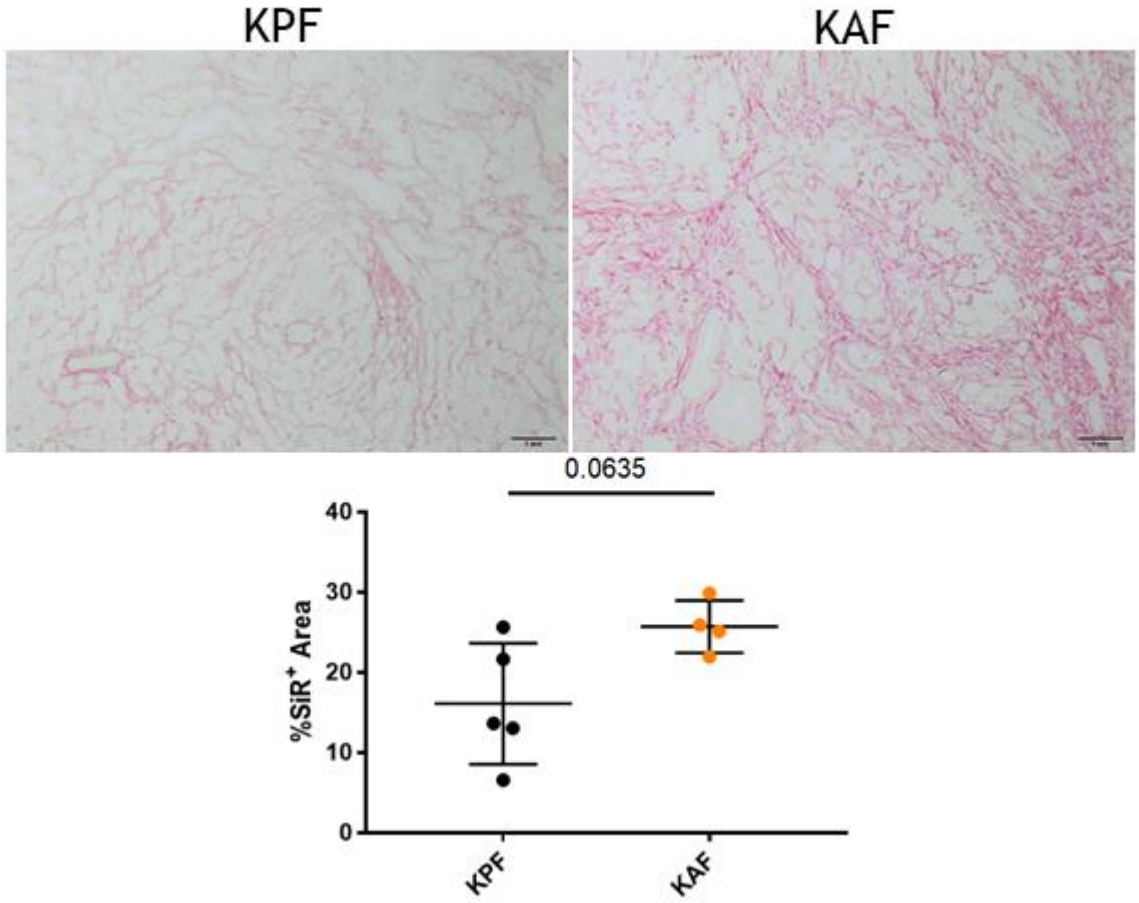

Figure 26 Increased collagen deposition was observed in the KAF end-point tumours compared to KPF tumours
Representative images of Sirius Red stained tissue from KPF and KAF end-point tumours (Scale bars = 1mm). HALO software quantification of the positive area of Sirius Red within *bona fide* tumour regions is shown. (n= 5, 4, respectively) (Mann Whitney P values indicted).

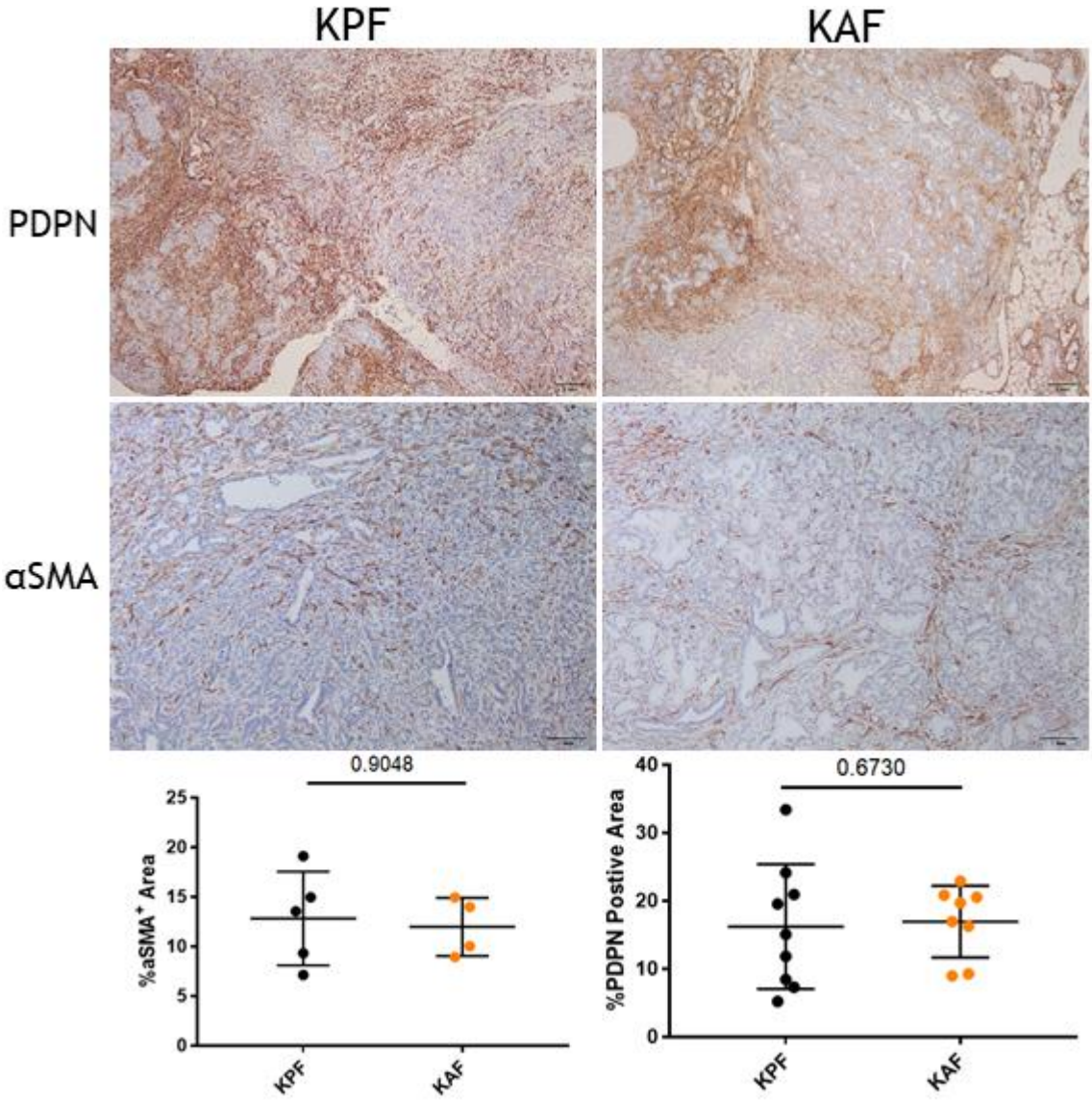

Figure 27 There was no difference in fibroblast accumulation between KAF and KPF tumours

Representative images of podoplanin (PDPN) (top) (Scale bars = 2mm) and αSMA (Bottom) (Scale bars = 1mm) IHC stained tissue from KPF and KAF end-point tumours. HALO software quantification of the positive area of podoplanin staining (n= 9, 8, respectively) or αSMA staining (n=5, 4, respectively) within *bona fide* tumour regions is shown. (Mann Whitney P values indicted).

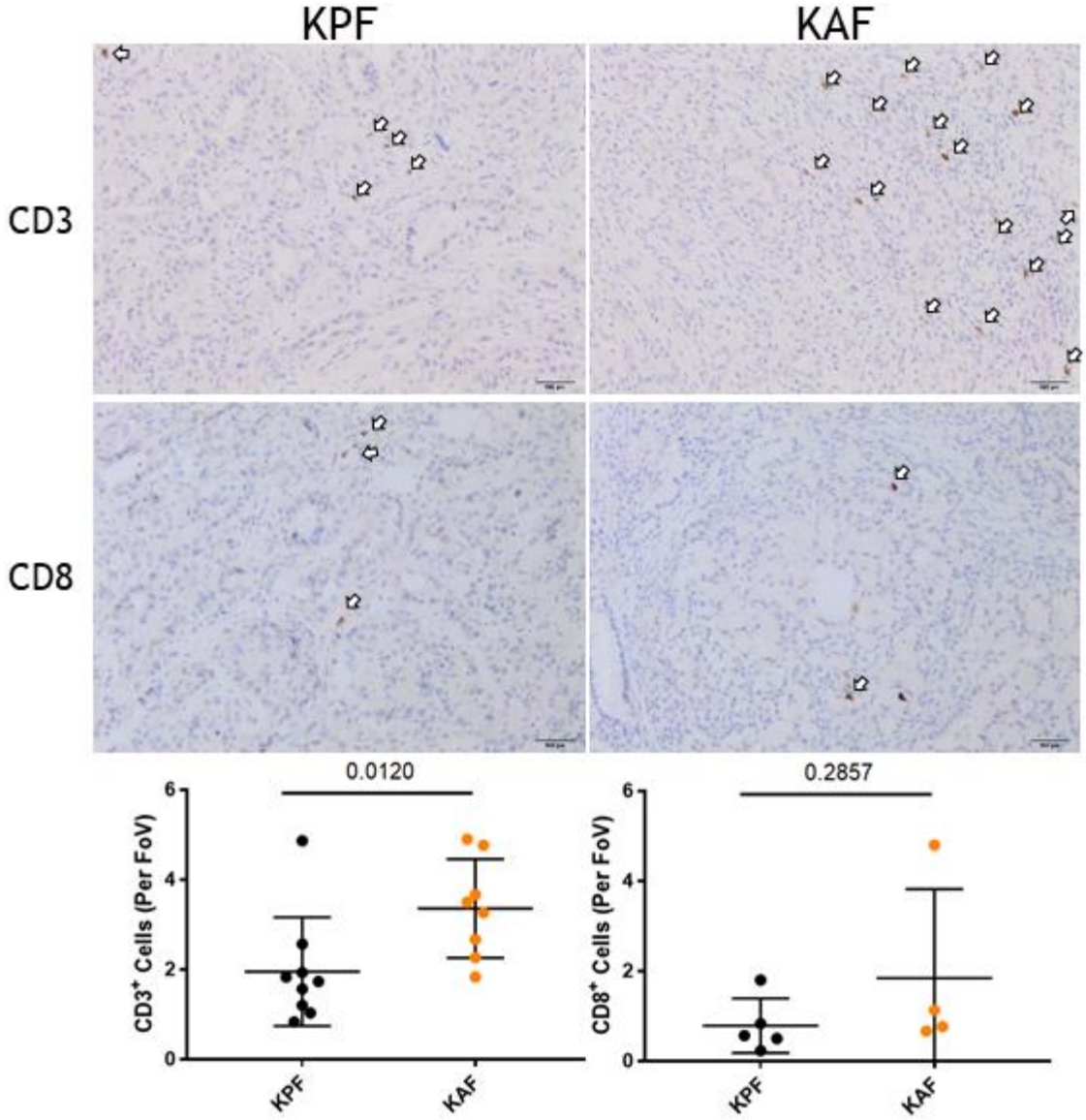

Figure 28 CD3⁺ but not CD8⁺ T cell infiltration was increased in KAF tumours compared to KPF Tumours

Representative images of CD3 (top) and CD8 (Bottom) IHC stained tissue from KPF and KAF end-point tumours (Scale bars = 500μm). Positive cells were counted across 30x fields of view for each tumour and the average count per field of view (Per FoV) is shown in the graphs. (CD3, n= 9, 8, respectively) (CD8, n=5, 4, respectively) (Mann Whitney P values indicted).

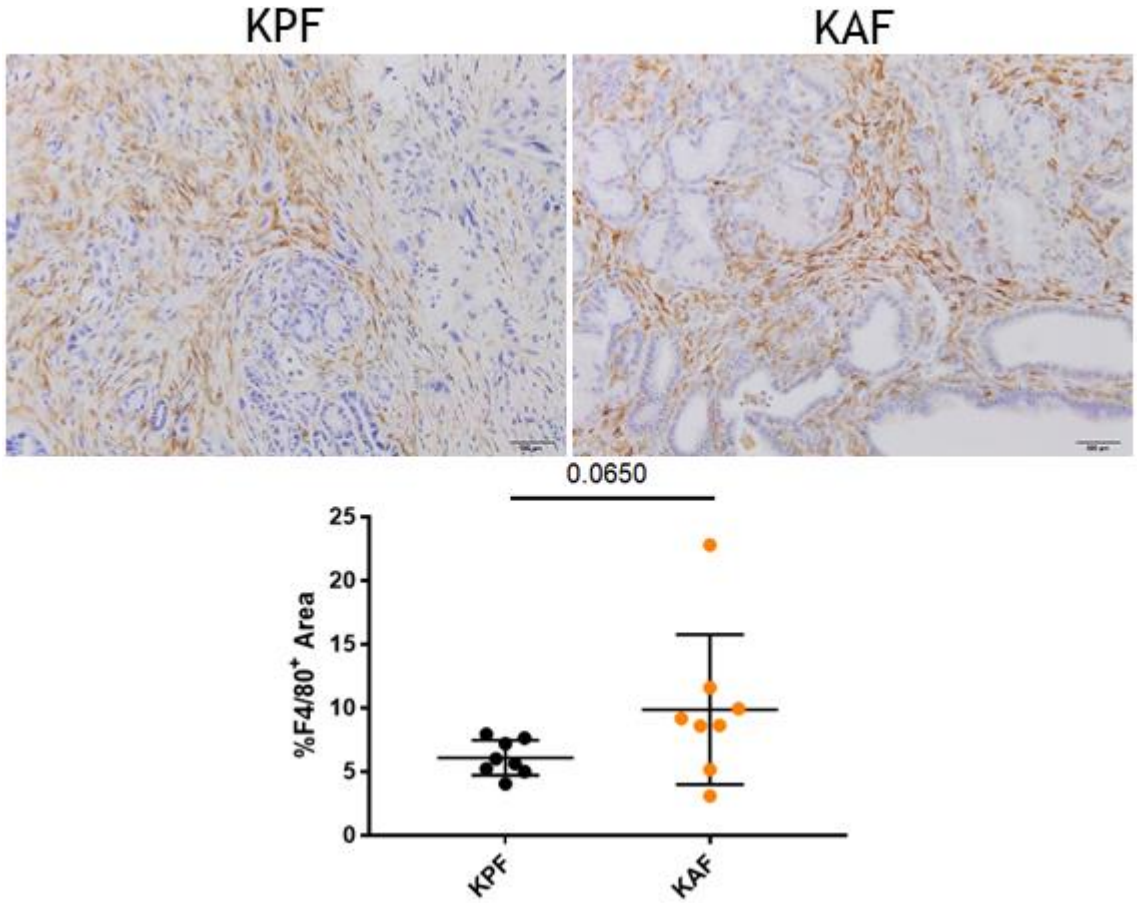

Figure 29 Macrophage infiltration was increased in KAF tumours compared to KPF tumours Representative images of F4/80 IHC stained tissue from KPF and KAF end-point tumours (Scale bars = 500μm). HALO software quantification of the positive area of F4/80 staining within *bona fide* tumour regions is shown. (n= 8) (Mann Whitney P value indicted).

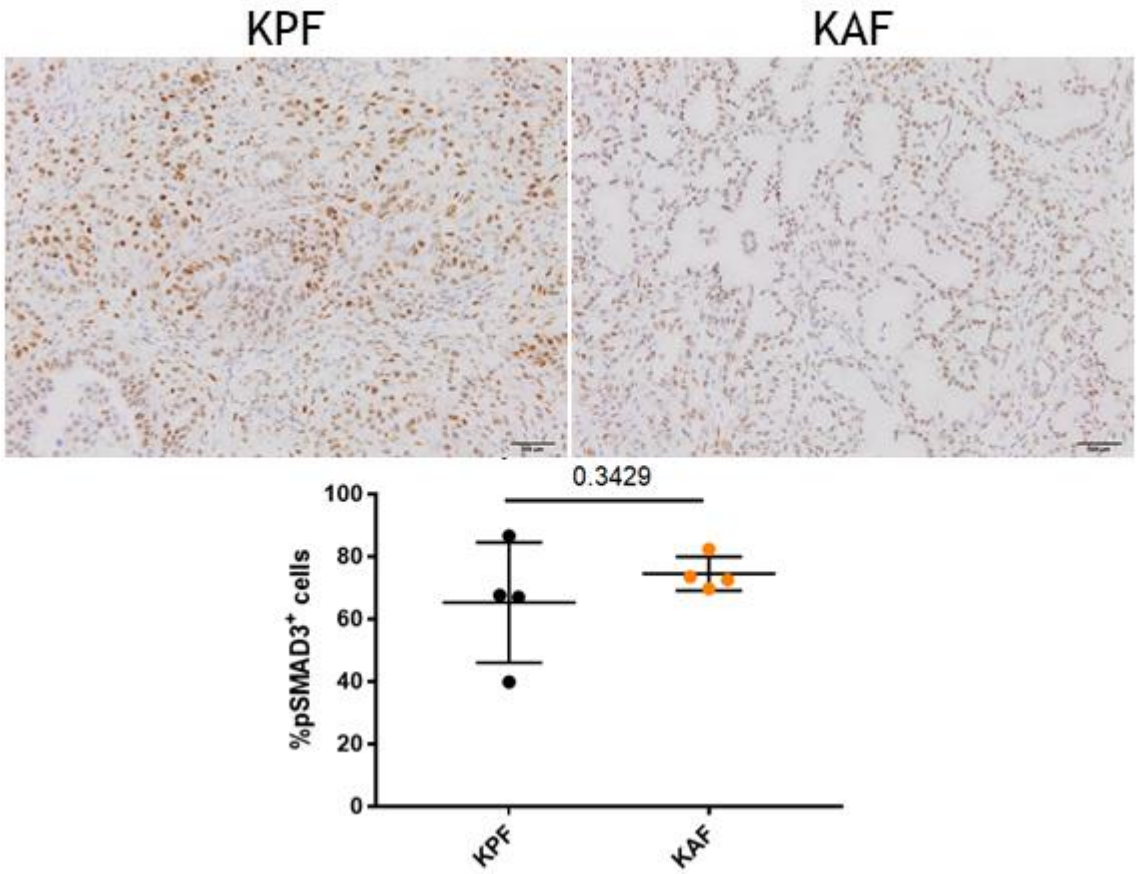

Figure 30 pSMAD3^{+} cells are unchanged in the KAF tumours compared to KPF tumours
Representative images of pSMAD3 IHC stained tissue from KPF and KAF end-point tumours (Scale bar = 500μm). HALO software quantification of the proportion of pSMAD3+ cells within *bona fide* tumour regions is shown. (n= 4) (Mann Whitney P value indicted).

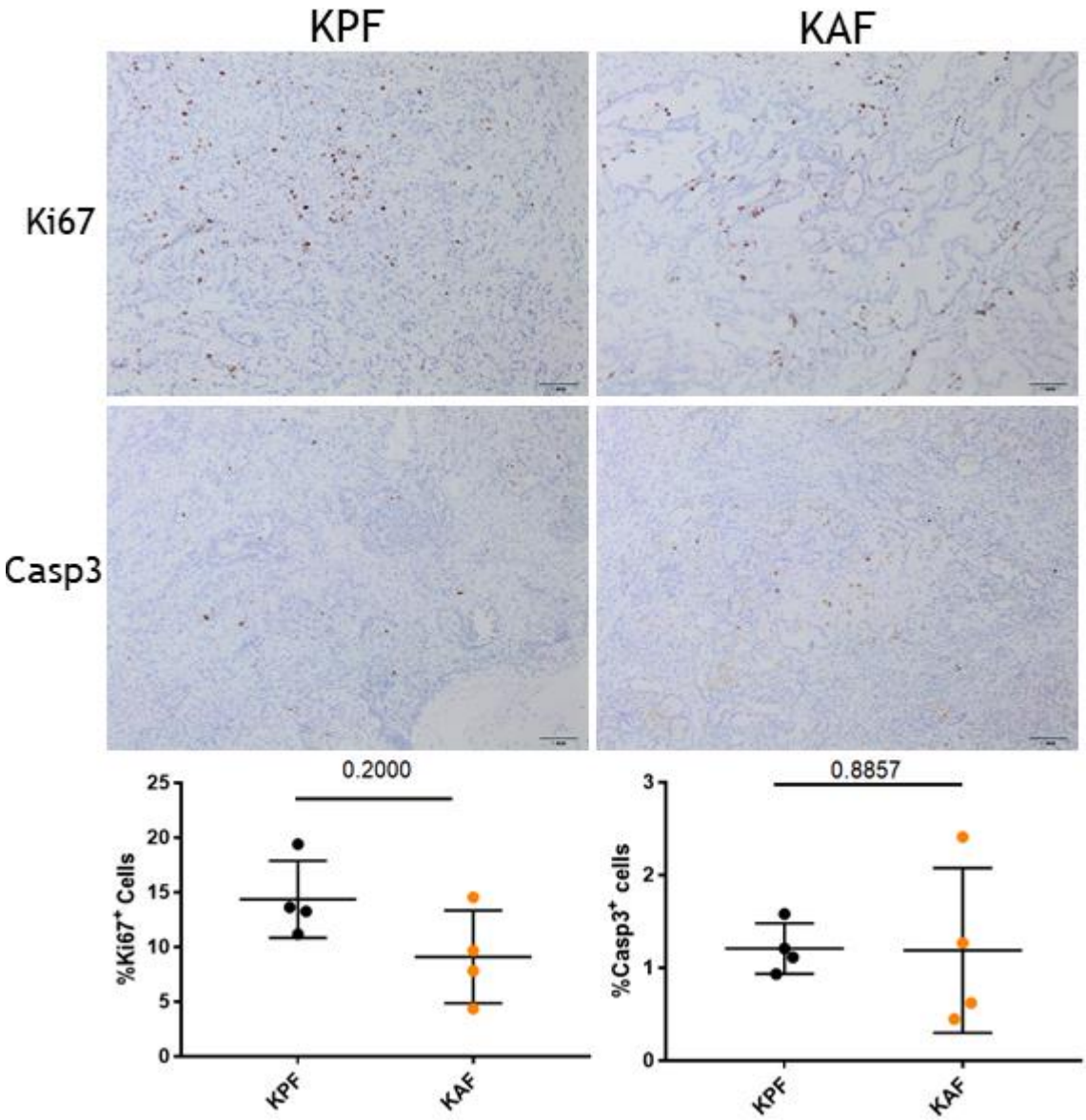

Figure 31 Proliferation and cell death were unchanged between KAF and KPF end-point tumours
Representative images of Ki67 (top) and Cleaved Caspase 3 (Casp3) (Bottom) IHC stained tissue from KPF and KAF end-point tumours (Scale bars = 1mm). HALO software quantification of the proportion of $Ki67^+$ or $Casp3^+$ cells within *bona fide* tumour regions is shown.(n= 4) (Mann Whitney P value indicted).

The KAF mice tend to reach end-point due to large primary tumour burden; however, we sought to investigate if there was any metastatic burden. At dissection, no macroscopic metastases were observed in tumour bearing KAF model nor, unsurprisingly, in the KF or KTF mice. Assessment of micro-metastasis to the liver and lungs was conducted via examination of a single H&E stained slide of each tissue type per mouse. No metastases were observed in any of the models at either the 6-week or the 10-week induction time points.

Tumour growth in this model is very rapid, and metastasis may not occur due to the speed of primary tumour growth, however, metastases have been observed in other models with similar latency. It may be that p53 mutation is required to drive metastasis, as previously observed in our lab, or it is possible that *Alk5* deletion can affect metastasis due to the known role of TGFβ signalling in EMT.

3.4 Discussion

The TGFß signalling pathway is a frequently mutated and dysregulated pathway in PDAC (Bailey et al., 2016). Mouse modelling of pancreas specific *Smad4* (KSC) or *Tgfbr2* (KTC) deletion was shown to enhance tumorigenesis in oncogenic Kras tumour models (Bardeesy et al., 2006; Ijichi et al., 2006). I have corroborated these findings in a next generation mouse model of PDAC. Importantly, the temporal and spatial control of gene deletion within this model provides a system more closely representing the progression of disease in patients. The acquisition of mutations is known to occur in a stepwise fashion following the oncogenic transformation by KRAS (Feldmann et al., 2007). The KAF model described here replicates this effectively through the tamoxifen-controlled deletion of *Alk5*, with tamoxifen administered at defined stages. For instance, the deletion in early $Kras^{G12D}$ transformed PanIN lesions culminates in accelerated tumorigenesis and overt transformation of almost the total pancreas three weeks post induction. Although similar findings are apparent in the KSC and KTC mouse models, the embryonic nature of activation of $Kras^{G12D}$ alongside TGFß signalling abrogation, means mice are essentially borne with widely transformed tissue, contrasting with the KAF model, which develops PDAC solely within the adult pancreas environment. The KAF tumours have a comparable TME to that observed within the KPF model, with significant infiltration of fibroblasts and macrophages and deposition of an abundance of collagen. Furthermore, this model was superior for examination of pancreatic tumour development than the *Pdx1-Cre; LSL-*$Kras^{G12D}$*;* $Alk5^{fl/fl}$ model, which presented with, and succumbed to, stomach tumours and skin carcinomas with incidental pancreatic transformation (Acosta et al., 2013).

I have demonstrated that downstream TGFß signalling was decreased in the epithelium of PanIN lesions in the KAF model, with CRE also expressed in PanIN epithelium. TGFß signalling was shown to induce senescence in oncogene transformed pancreatic cells, however, *Alk5* deletion in those cells abrogated the senescence phenotype and elevated proliferation (Acosta et al., 2013). The decreased epithelial pSMAD3 staining in the KAF mice was accompanied with an elevated PanIN proliferation when compared to the KF model. This could indicate that PanIN epithelial cells have overcome oncogene-induced senescence

upon deletion of *Alk5* and therefore explain the increased transformation observed.

It was also possible that deletion of *Alk5* increased the initiation of PanIN lesions, alongside the elevated proliferation of existing lesions. There was an abundance of ADM/acinar atrophy induced in the KAF model with high pERK staining noted, indicative of active RAS signalling. Adjacent to the pSMAD3 low PanIN regions, pSMAD3 levels appeared high in these regions, indicative that *Alk5* was not deleted in those cells. Unfortunately, the failure of *Alk5* RNAscope to define epithelial loss of the receptor rendered it impossible to identify if the adjacent regions had recombined *Alk5* or were induced as 'bystander' lesions. Interestingly, expression of a constitutively active Alk5 receptor was shown to drive ADM in a mouse model expressing pancreas specific $Kras^{G12D}$ (Chuvin et al., 2017). A further study revealed that, pancreas specific *Tgfbr2* deletion in a $Kras^{G12D}$ driven pancreatic cancer model led to elevated stromal TGFß1 levels (Principe et al., 2016). With active TGFß signalling shown to regulate the expression of TGFß ligands, it is tempting to speculate that in the KAF model, loss of the ALK5 receptor leads to elevated TGFß ligand production that can act in a paracrine manner on the cells surrounding the PanINs and explain the increased activation of pSMAD3 in these regions.

It was notable that pSMAD3 was only reduced and not completely abrogated upon *Alk5* deletion in the adult pancreas, whereas in mice with embryonic deletion of *Tgfbr2,* the downstream signalling components are completely ablated in PanIN lesions (Principe et al., 2016). However, there was rapid progression and development of PDAC in the KAF mice suggesting that depletion in a small number of cells is sufficient to drive disease progression, more closely resembling the progression in humans.

This model does have the caveat of reduced penetrance, with the failure to develop tumours in 60% of KPF mice with the correct genetics, differing from the KPC model (33%). Although the reduced presentation of off-target effects in the KPF negate the increased number of mice required, it becomes more problematic when attempting to examine disease initiation. As a result, in this work, conclusions could not be drawn on the KTF model. With TGFß signalling shown to be a potent tumour suppressor (Bardeesy et al., 2006; Ijichi et al.,

2006) it was not unexpected that we observed such a strong phenotype in the KAF model, however, a more nuanced effect would be expected to be observed in the KTF model. With deletion of 1 of 3 TGFß ligands, TGFß1, I was aware that there may be some redundancy in the model. However, with TGFß1 existing as the predominant ligand and with TGFß signalling conventionally shown to be a potent activator of CAFs (Biffi et al., 2019), I hypothesised that the stromal infiltrate could be altered in the early lesions. With fibroblasts in close proximity to cancer cells suspected to develop a 'myCAF' phenotype (Ohlund et al., 2017), within the simpler PanIN setting, where cancer cells form a larger proportion of the lesion, we would expect most CAFs to develop as 'myCAFs' or as a pre-cursor population (Dominguez et al., 2020). Therefore, loss of TGFß1 ligand in a cell, which is a major constitutive part of this lesion, would be predicted to have a notable effect. The inability of the KTF model to develop PanINs was an interesting observation; however, at the moment this cannot be attributed to *Tgfb1* deletion due to the lack of penetrance in the *Pdx1-Flp* model. Analysis of 6 or 10 week old KPF *Tgfb1*$^{fl/fl}$ mice (and KPF controls) shortly following induction might partially mitigate this problem and allow more robust testing of this hypothesis.

It would also be of interest to investigate the early TME of the KAF PanIN lesions. The end-point KAF tumours appear to have elevated collagen deposition compared to the KPF tumours, although this does not reach significance. Collagen is a major component of the ECM in PDAC and fibroblasts are major producers (Tian et al., 2019), particularly the 'myCAFs' which are driven by TGFß signalling (Biffi et al., 2019). However, in the KAF tumours fibroblast populations are unaltered in comparison to the KPF, with pan-fibroblasts markers podoplanin and 'myCAF' marker αSMA staining a similar proportion of the tumour. *Principe et al*, using an elastase-cre driven Kras^{G12D} mouse model, showed that epithelial *Tgfbr2* deletion resulted in elevated collagen deposition alongside an increased abundance of αSMA positive cells (Principe et al., 2016). Although the KAF model also presents with increased collagen, the αSMA abundance was unchanged. However, I compared the end-point tumours to the KPF model, whereas the previous study compared to pancreas expressing *Kras*^{G12D} only. More importantly, by end-point, many alterations have occurred and stromal signalling that can drive tumour initiation may no longer be

apparent. In support of my observation of increased collagen in the KAF tumours, a stiffer matrix has also been highlighted in *SMAD4* deficient patient PDAC samples, as well as in the KTC mouse model, driven through a mechanosignalling feedback loop with STAT3 activation (Laklai et al., 2016). Fibroblasts stimulated with TGFß1 also show increased production of ECM molecules (Schneider et al., 2001; Shek et al., 2002) and with *Tgfb2* deficient PDAC model shown to have elevated stromal TGFß1 (Principe et al., 2016), this may explain the findings in the KAF model with elevated collagen, but no change in fibroblast accumulation.

The increased CD3 T cell infiltrate in the KAF model is also interesting to note, particularly given that the cytotoxic T cell population of $CD8^+$ cells is not changed. This would indicate that the increased T cells are $CD4^+$, which have a helper function more than direct cytotoxicity. It would perhaps be expected that increased stromal collagen would impede T cell infiltration, however, a KPPF (*Pdx1-Flp; FSF-Kras^{G12D}; Trp53$^{frt/frt}$*) model with αSMA specific deletion of collagen I, and consequently decreased stromal collagen content, had reduced CD3 T cell infiltration, with the authors suggesting that stromal collagen and T cell infiltration may negatively correlate (Chen et al., 2021). The model used by *Principe et al*, presented with a decrease in CD8 T cell infiltration when epithelial *Tgfbr2* was deleted, whereas the $CD4^+FoxP3^+$ T regulatory cell population was elevated (Principe et al., 2016). This population was immunosuppressive and generally predicted to be worse for survival, although whether this is true in pancreatic cancer is potentially dependent on disease stage (Zhang et al., 2020). Therefore, potentially this sub-population of $CD4^+$ T cells could be increased in the KAF tumour, although further study is required to confirm this hypothesis. Further, it has been suggested that TGFß signalling negatively regulates PD-L1 expression on cancer cells, therefore, elevated PD-L1 may be expressed on the KAF tumour epithelium (Principe et al., 2019) and therefore the increase T cell infiltrate is being suppressed. Additionally, the increased macrophage infiltration within the KAF tumour may promote immunosuppression, with macrophage depletion through CSF1R inhibition enhancing $CD8^+$ T cell infiltration and decreased T regulatory cell populations in KPC tumours (Candido et al., 2018).

Collectively I have demonstrated that *Alk5* deletion targeted specifically to the $Kras^{G12D}$ expression cells within the pancreas is sufficient to drive pancreatic tumorigenesis in the adult pancreas. This model demonstrates a progression model that better recapitulates the human disease and may provide a very useful model, representing a significant subset of patients, in which to perform pre-clinical therapeutic experiments.

Chapter 4 Investigating the biology of TGFβ signalling-deficient PDAC

4.1 Introduction

With the inactivation of TGFß signalling prevalent in more than 50% human PDAC, through mutation of *SMAD4, ALK5* or *TGFBR2*, the generation of a novel mouse model that better recapitulates this subset of patients is required (Bailey et al., 2016). Pdx1-CRE driven *Alk5* deletion alongside oncogenic *Kras* expression in mouse models drives pancreatic transformation, however, mice develop squamous skin and stomach tumours (Acosta et al., 2013; Morton, Unpublished), limiting their use for studying PDAC. Therefore, new models are needed, particularly to enable preclinical testing. Patient tumours can be rapidly sequenced, and transcriptomes generated, which allows stratification of patients into treatment groups where they are predicted to respond best, for instance, in large-scale trials such as Precision-Panc (Dreyer et al., 2020a; Dreyer et al., 2020b). With the increasing focus on stratified approaches to treat PDAC, expanding our pool of models that mimic patient genetics is required to provide proof of concept for specific targeted therapies. Understanding of these models is also required as we still lack enough understanding to allow us to identify effective treatment options. New targets and novel therapeutic strategies that have undergone rigorous preclinical studies are needed to tackle this disease.

4.2 Experimental Aims

After successfully developing the KAF model of PDAC, driven by the stepwise acquisition of oncogenic $Kras^{G12D}$ followed by deletion of *Alk5*, I sought to interrogate differences in the TGFß signalling deficient driven tumour compared to the standard KPF (*Pdx1-Flp;* $Kras^{FSF\text{-}G12D/+}$*;* $Trp53^{fl/+}$) model. RNA sequencing data generated from end-point tumours of the KAF and KPF mice were compared, with the aim of discovering therapeutic vulnerabilities in *Alk5* deficient tumours as well as highlighting divergent features of either tumour type.

4.3 Results

4.3.1 Generation of RNA sequencing data comparing KAF and KPF end-point tumours

I extracted RNA from the end-point tumours of the previously described KPF mouse model and the novel KAF model. The KAF mouse was induced with tamoxifen over 3 days at 10 weeks of age and allowed to progress to clinical end-points. For comparison, I used tumour tissue from end-point KPF mice. These mice were control mice for a separate study and had been routinely palpated until a tumour was detected and confirmed by ultrasound, before being induced with tamoxifen for 3 days and aged until clinical end-points (**Figure 32**). Importantly, in these mice tamoxifen treatment was used as sham induction rather than inducing any recombination. Information regarding the mice utilised for RNA sequencing is listed in **Figure 33**. There are some difference to note between the two cohorts. For instance, the KAF mice analysed have median survival of 105 days at clinical end-point, compared to 149 days in the KPF mice. Further, the KAF were sampled significantly longer after induction than the KPF mice (median 35 compared to 6 days in the KPF model). The nature of the KAF model, which requires tamoxifen induction to drive tumour progression explains the longer survival post induction, with the accelerated progression of the tumour following deletion of *Alk5* explaining the lower average age at clinical end-point. Although the KPF is an imperfect control for comparing the role *Alk5* plays in specifically driving an alternate tumour development, as it introduces the variable of *Trp53* deletion, tumours did not develop in most KF mice, at least in the time-frame permitted by our project licence. Further, any tumours that develop in this model would likely accumulate many additional unknown mutations introducing significant heterogeneity in terms of gene expression and making data analysis more challenging. I also considered that comparison of end-point tumour with end-point tumour would provide greater insight into potential targets for stratified therapy then comparison with normal or PanIN bearing tissue from the same mice.

As a first step, principal component analysis (PCA) was performed to detect if samples cluster in a cohort specific manner. PCA simplifies the data and accounts for variation over lower PC dimensions, in this case with two

dimensions, PC1 and PC2. I noted from the data that PC2 accounts for most of the variation between cohorts. From this PCA it is evident that KAF tumours samples cluster distinctly from the KPF clustering, indicative with this simplified analysis that tumours driven by TGFß signalling deficiency exhibit a distinct transcriptomic landscape (**Figure 34**).

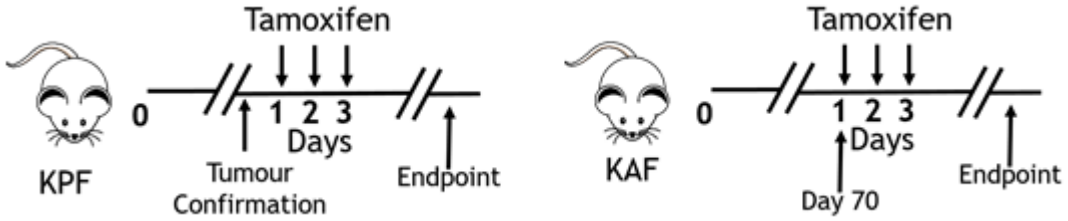

Figure 32 RNA was extracted from the KPF and KAF mice
Upon detection of a palpable tumour and confirmation via ultrasound, the KPF mouse was induced for 3 days with tamoxifen before sampling at clinical end-points. At 10weeks of age the KAF model was induced for 3 days with tamoxifen and aged until clinical end-point was reached and the tumour was sampled.

Condition	Genotype	Gender	Clinical Information	Age (days)	Survival post Induction (days)
KPF	Pdx1^{flp}; FSF-Kras$^{G12D/+}$; Trp53$^{fl/+}$; FSF-Cre^{ERT}	Male	PDAC, Liver Met	241	14
KPF	Pdx1^{flp}; FSF-Kras$^{G12D/+}$; Trp53$^{fl/+}$; FSF-Cre^{ERT}	Male	PDAC, Damaged Lungs, No macroscopic mets	122	10
KPF	Pdx1^{flp}; FSF-Kras$^{G12D/+}$; Trp53$^{fl/+}$; FSF-Cre^{ERT}	Male	PDAC, No macroscopic mets	149	6
KPF	Pdx1^{flp}; FSF-Kras$^{G12D/+}$; Trp53$^{fl/+}$; FSF-Cre^{ERT}	Male	PDAC, with stomach attachment, No macroscopic mets	144	2
KPF	Pdx1^{flp}; FSF-Kras$^{G12D/+}$; Trp53$^{fl/+}$; FSF-Cre^{ERT}	Female	PDAC, damaged lungs, No macroscopic mets	127	6
KAF	Pdx1^{flp}; FSF-Kras$^{G12D/+}$; Trp53$^{+/+}$; FSF-Cre^{ERT}; Alk5$^{fl/fl}$	Male	PDAC, enlarged Bile duct, No macroscopic mets	106	35
KAF	Pdx1^{flp}; FSF-Kras$^{G12D/+}$; Trp53$^{+/+}$; FSF-Cre^{ERT}; Alk5$^{fl/fl}$	Female	PDAC, Ascites, No macroscopic mets	105	64
KAF	Pdx1^{flp}; FSF-Kras$^{G12D/+}$; Trp53$^{+/+}$; FSF-Cre^{ERT}; Alk5$^{fl/fl}$	Female	PDAC, Blocked Bile Duct, Jaundice, No macroscopic mets	105	35
KAF	Pdx1^{flp}; FSF-Kras$^{G12D/+}$; Trp53$^{+/+}$; FSF-Cre^{ERT}; Alk5$^{fl/fl}$	Male	PDAC, No macroscopic mets	92	24
KAF	Pdx1^{flp}; FSF-Kras$^{G12D/+}$; Trp53$^{+/+}$; FSF-Cre^{ERT}; Alk5$^{fl/fl}$	Male	PDAC, clear ascites, No macroscopic mets	134	58

Figure 33 Cohort information for RNA sequencing samples
The above mice were sampled at clinical end-point and RNA prepared for sequencing. 5 KPF tumours were used as the control to compare against 5 KAF tumours. The median age at end-point for the KPF mice = 149 days and for KAF mice = 105 days. The median time post tamoxifen induction in the KPF mice = 6 days and KAF= 35 days.

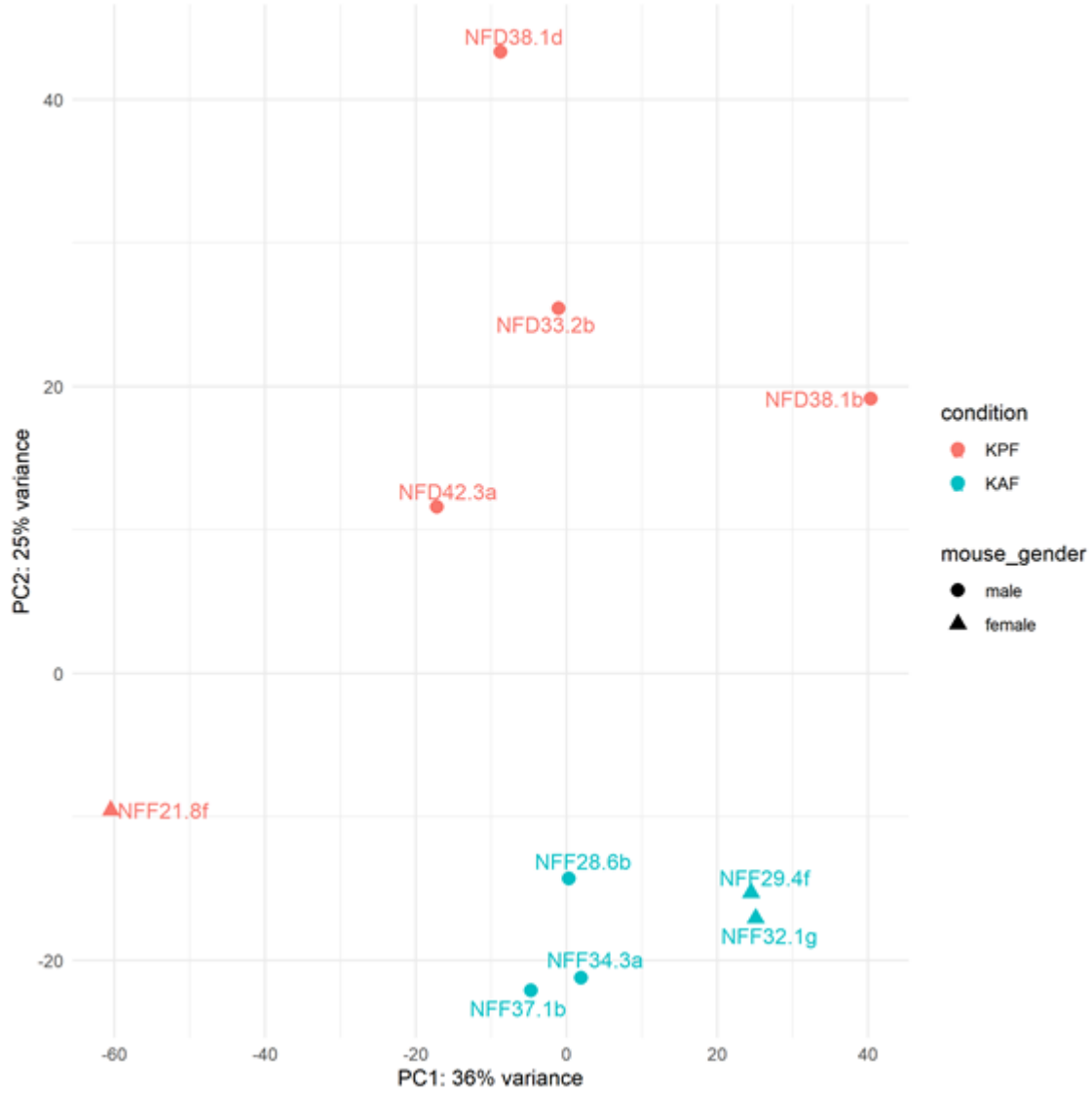

Figure 34 KAF samples cluster distinctly from KPF samples in a PCA
A PCA was conducted on the RNA sequencing data highlighting that KAF and KPF tumour samples cluster exclusively. Significant variation between the two conditions can be noted only in PC2.

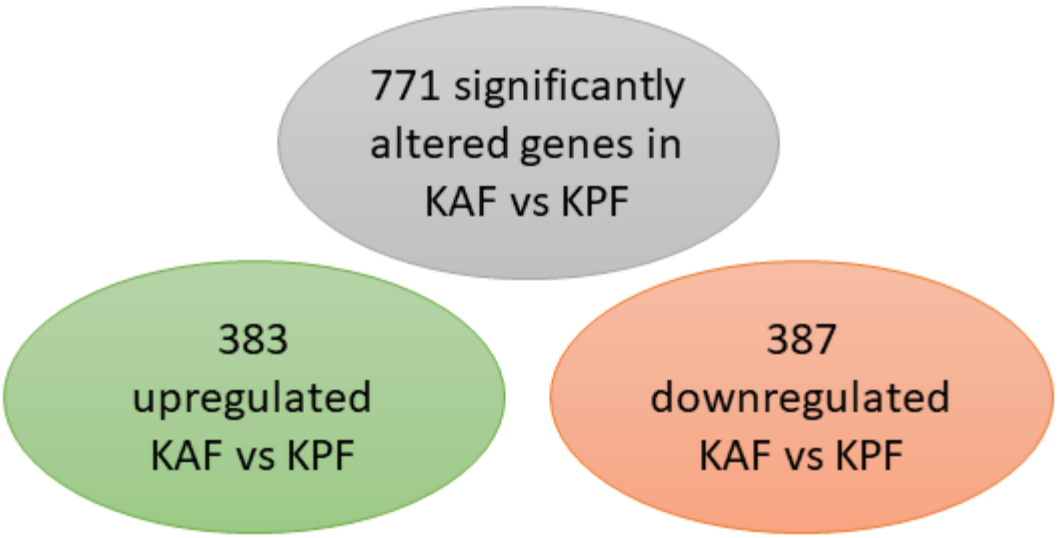

Figure 35 Significantly altered genes in KAF vs KPF tumours
From analysis of the RNAseq data, 771 genes were significantly altered in the KAF tumours compared to the KPF tumours at transcriptional level, 383 genes were upregulated and 387 genes were downregulated. Genes with a P-adjusted value of ≤ 0.05.

Following from the highlighted variation between KAF and KPF tumour by PCA, I investigated the specific transcriptional changes. I observed that 771 genes were significantly altered, with 383 of these upregulated and 387 downregulated in the KAF tumours compared to KPF tumours (**Figure 35**). This indicates a large proportion of change between the samples, highlighting that *Alk5* deletion driven tumours progress differently from those in the KPF model. Included in **Figure 36** and **Figure 37** are the lists of the top 25 upregulated or downregulated genes respectively.

Further the transcriptional subtype of the KAF tumours in comparison to the KPF tumours was investigated by detecting enrichment of genes in gene-sets associated with the ADEX, Immunogenic, Pancreatic progenitor and Squamous subtypes defined by *Bailey et al (Bailey et al., 2016)*. From this enrichment analysis it was apparent that the ADEX subtype was enriched in the KAF tumours in comparison to the KPF tumours (**Figure 38**), with this subtype defined by expression of genes associated with pancreatic differentiation.

Subsequently, gene set enrichment analysis (GSEA) was used to investigate specific pathways that were altered in KAF tumours compared with the KPF

tumours. Utilising the Hallmark gene set definitions, which group genes with similar biological processes, I highlighted that there were 5 pathways significantly enriched in the KAF tumours and 9 significantly enriched in the KPF tumours (**Figure 39**). In agreement with the models used, it was notable that P53 pathway signalling was enriched in the KAF, which were proficient for *Trp53*, as opposed to the KPF model. However, the TGFß signalling hallmark was not significantly enriched in the KPF, as might be expected due to the deletion of *Alk5* in the KAF model (**Figure 40**). I observed that the majority of genes in the TGFß signalling hallmark definition were enriched in the KPF model (33/51) however, none of these reached significance as denoted by the dashed line. Of course, these samples were taken from bulk tumours and the presence of TGFß signalling within the stroma could potentially override any loss of signalling in the epithelial cells only. Further, alternative TGFß family pathways are unaffected by the deletion of *Alk5* and those members are included in the TGFß hallmark gene set, as well as downstream signalling components. However, together these data highlight that the KAF tumours and KPF tumours were transcriptionally distinct, with specifically altered signalling pathways.

mgi_symbol	mgi_description	MeanExpr_KPF	MeanExpr_KAF	log2FoldChange
Zfp750	zinc finger protein 750	5.1	587.5	5.60
Inka2	inka box actin regulator 2	33.0	576.1	3.75
Rps27l	ribosomal protein S27-like	1845.3	3793.7	1.03
Chit1	chitinase 1 (chitotriosidase)	9.3	344.9	4.32
Ccng1	cyclin G1	3646.3	12194.9	1.70
Fam174b	family with sequence similarity 174, member B	186.5	2042.2	3.09
Zmat3	zinc finger matrin type 3	1927.0	5740.0	1.53
Cep126	centrosomal protein 126	38.0	117.4	1.58
Psrc1	proline/serine-rich coiled-coil 1	244.9	2481.9	2.89
Slc2a2	solute carrier family 2 (facilitated glucose transporter), member 2	16.4	1231.7	3.39
Ghrl	ghrelin	8.4	189.7	3.29
Fbxw9	F-box and WD-40 domain protein 9	1180.9	3036.6	1.31
Clps	colipase, pancreatic	6.1	501.9	3.06
Kazn	kazrin, periplakin interacting protein	1152.0	2629.5	1.16
Trim7	tripartite motif-containing 7	106.1	372.6	1.69
Sytl1	synaptotagmin-like 1	214.0	1459.0	2.36
Amd2	S-adenosylmethionine decarboxylase 2	9.4	412.1	3.01
Cela2a	chymotrypsin-like elastase family, member 2A	1.4	79.2	3.37
Pm20d1	peptidase M20 domain containing 1	47.9	473.8	2.61
Cpa1	carboxypeptidase A1, pancreatic	22.2	1648.2	2.68
Prox1	prospero homeobox 1	63.1	384.3	2.24
Amy2a3	amylase 2a3	18.4	3754.9	1.97
Try4	trypsin 4	0.0	54.3	2.99
Eda2r	ectodysplasin A2 receptor	272.4	1247.5	1.96
Zfp809	zinc finger protein 809	901.4	1704.8	0.90

Figure 36 Top 25 upregulated genes in KAF compared to KPF tumours
The top 25 genes significantly upregulated in KAF tumours compared with KPF tumours ranked by P-adjusted value. Significant genes have a p-adjusted value of ≤ 0.05.

mgi_symbol	mgi_description	MeanExpr_KPF	MeanExpr_KAF	log2FoldChange
Eif5al3-ps	eukaryotic translation initiation factor 5A-like 3, pseudogene	468.4	2.6	-6.14
Klhl1	kelch-like 1	557.6	1.5	-4.30
Pde4dip	phosphodiesterase 4D interacting protein (myomegalin)	3835.1	1487.5	-1.34
Acan	aggrecan	6012.0	34.1	-3.68
Zic3	zinc finger protein of the cerebellum 3	981.0	6.8	-3.31
Rnf125	ring finger protein 125	582.1	200.1	-1.48
Sema4f	sema domain, immunoglobulin domain (Ig), TM domain, and short cytoplasmic domain	689.0	25.3	-3.35
Dynap	dynactin associated protein	93.3	3.4	-3.30
Bpifb1	BPI fold containing family B, member 1	227.8	6.6	-3.23
Tubb4a	tubulin, beta 4A class IVA	607.5	156.8	-1.81
Ndst3	N-deacetylase/N-sulfotransferase (heparan glucosaminyl) 3	251.5	13.6	-3.01
Vegfa	vascular endothelial growth factor A	15827.3	3504.6	-1.97
Foxg1	forkhead box G1	797.1	4.6	-2.27
Gm6685	predicted pseudogene 6685	51.2	0.3	-3.90
Chrna1	cholinergic receptor, nicotinic, alpha polypeptide 1 (muscle)	212.1	6.7	-2.98
Gm11839	predicted gene 11839	90.1	2.0	-3.08
Klrc1	killer cell lectin-like receptor subfamily C, member 1	348.3	9.0	-2.90
Hmga2	high mobility group AT-hook 2	6186.8	410.1	-2.80
Smtnl2	smoothelin-like 2	541.0	128.0	-1.87
Gabre	gamma-aminobutyric acid (GABA) A receptor, subunit epsilon	1310.3	239.3	-2.12
Kcnt1	potassium channel, subfamily T, member 1	158.5	6.1	-2.89
Fgf18	fibroblast growth factor 18	151.6	17.8	-2.44
Mcpt8	mast cell protease 8	1477.7	27.3	-2.54
Sftpc	surfactant associated protein C	706.7	1.1	-1.31
Add2	adducin 2 (beta)	4869.1	288.0	-2.65

Figure 37 Top 25 downregulated genes in KAF tumours compared with KPF tumours
The top 25 genes significantly downregulated in KAF tumours compared with KPF tumours ranked by P-adjusted value. Significant genes have a p-adjusted value of ≤ 0.05.

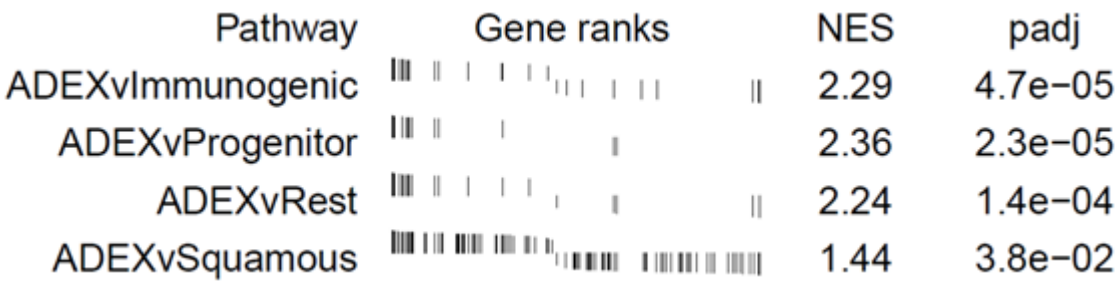

Figure 38 ADEX subtype was enriched in the KAF tumours compared to KPF tumours
GSEA was performed utilising gene sets defining the ADEX, Immunogenic, Pancreatic Progenitor (Progenitor) and Squamous pancreatic tumour subtypes defined by *Bailey et al (Bailey et al., 2016).* ADEX-associated gene expression was significantly enriched over the Immunogenic, Progenitor, Squamous and Rest (combination of all non-ADEX definitions) in the KAF tumours compared to the KPF tumours. Normalised enrichment score (NES) of a negative value highlight enrichment in the KPF, while positive values indicate enrichment in the KAF samples.

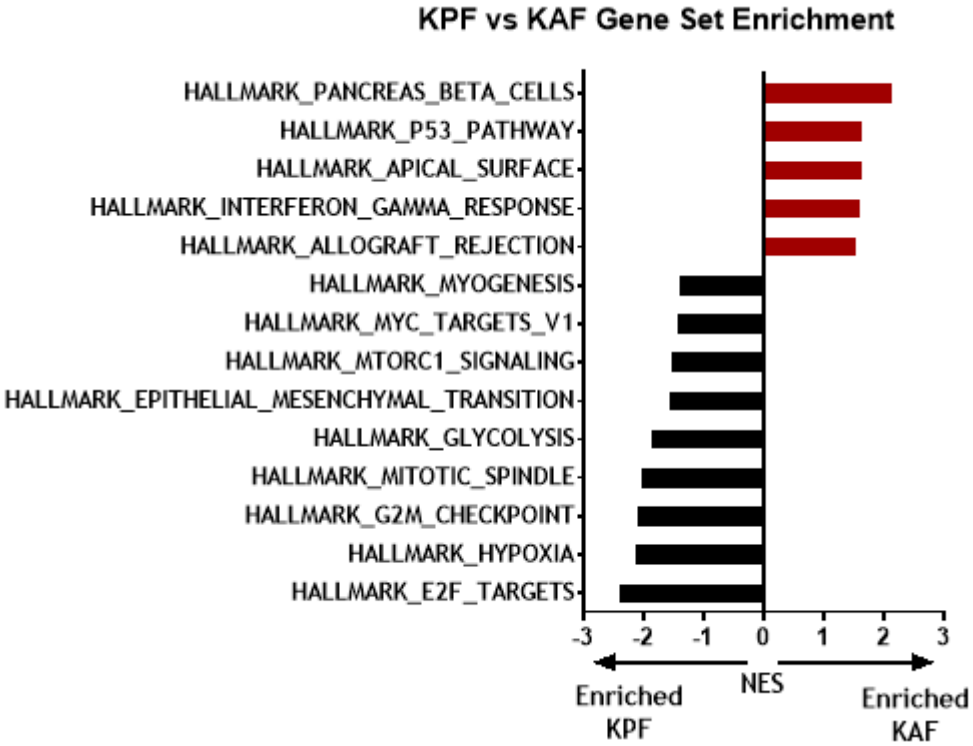

Figure 39 GSEA on RNAseq data from KAF vs KPF tumours
A GSEA was performed utilising the hallmark gene set definitions highlighting pathways significantly altered in KAF vs KPF tumours. Pathways enriched in the KAF tumours are shown in maroon bars and those enriched in the KPF tumours are shown in black bars. Hallmark gene sets shown are significantly altered with a P-adjusted value of ≤ 0.05. Normalised enrichment score (NES) of a negative value highlight enrichment in the KPF, while positive values indicate enrichment in the KAF samples.

Hallmark Gene Set	NES	P-adjusted Value
TGF_BETA_SIGNALING	-1.14	0.3814

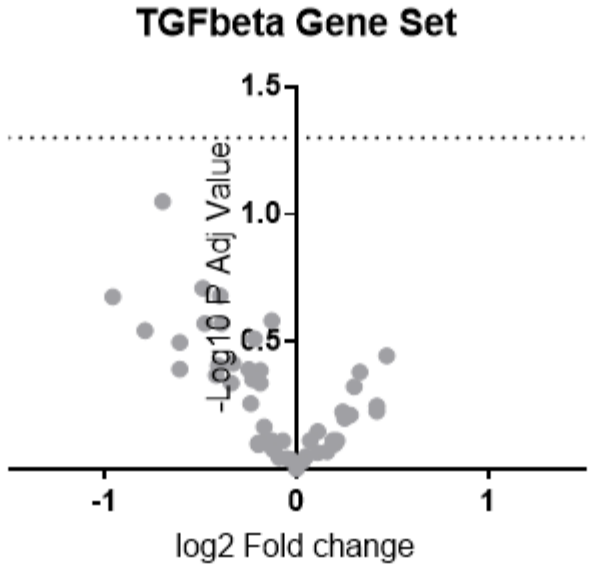

Figure 40 TGFβ signalling pathway was not significantly enriched in the KPF model
The TGFβ hallmark gene set was not significantly enriched in the *Alk5* proficient KPF tumours compared to the KAF tumours. A volcano plot of the genes in the TGFβ hallmark plotting the Log2 Gene fold change against –Log10 P adjusted Value with negative values representing enrichment in the KPF tumours and positive values indicating enrichment in the KAF tumours. Of the 51 genes in the hallmark, 33 were enriched in the KPF tumours, although none reached significance. The dashed line denotes significant gene changes with a P adjusted value ≤ 0.05.

4.3.2 Interrogating GSEA alteration in pancreas beta cells in the KAF model

With the GSEA highlighting that the hallmark of pancreatic beta cells was the top significantly enriched pathway, I sought to interrogate this in tumours. A volcano plot of the hallmark pancreatic beta cell gene set indicates that the majority of genes were enriched within the KAF tumours, five of which reach significance (**Figure 41**). Therefore, I investigated the expression of islet cell specific makers; synaptophysin (pan-islet), glucagon (α-cells), insulin (ß-cells), somatostatin (δ-cells) and ghrelin (ϵ-cells) (**Figure 42**). The pan-islet maker, synaptophysin, had significantly elevated expression in the KAF model, with markers of ß, δ and ϵ cells, also significantly elevated.

Hallmark Gene Set	NES	P-adjusted Value
PANCREAS_BETA_CELLS	2.12	0.0002

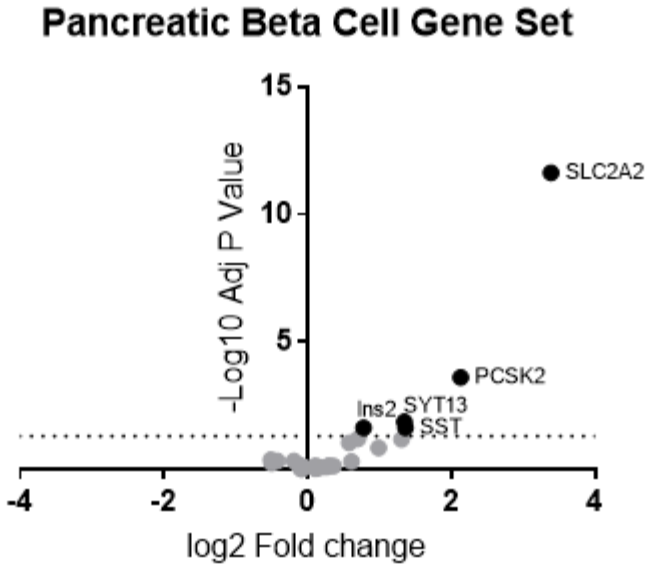

Figure 41 Pancreas Beta Cell hallmark genes were enriched in KAF tumours
The Pancreas beta cell hallmark gene set was enriched in the KAF tumours in comparison to the KPF tumours. A volcano plot of the genes in the pancreas beta cell hallmark plotting the Log2 fold change against –Log10 P adjusted Value with negative values indicating enrichment in the KPF tumours and positive values indicating enrichment in the KAF tumours. Of the 28 genes, 18 are enriched in KAF tumours with five being significantly enriched. The dashed line denotes significant gene changes with a P adjusted value ≤ 0.05.

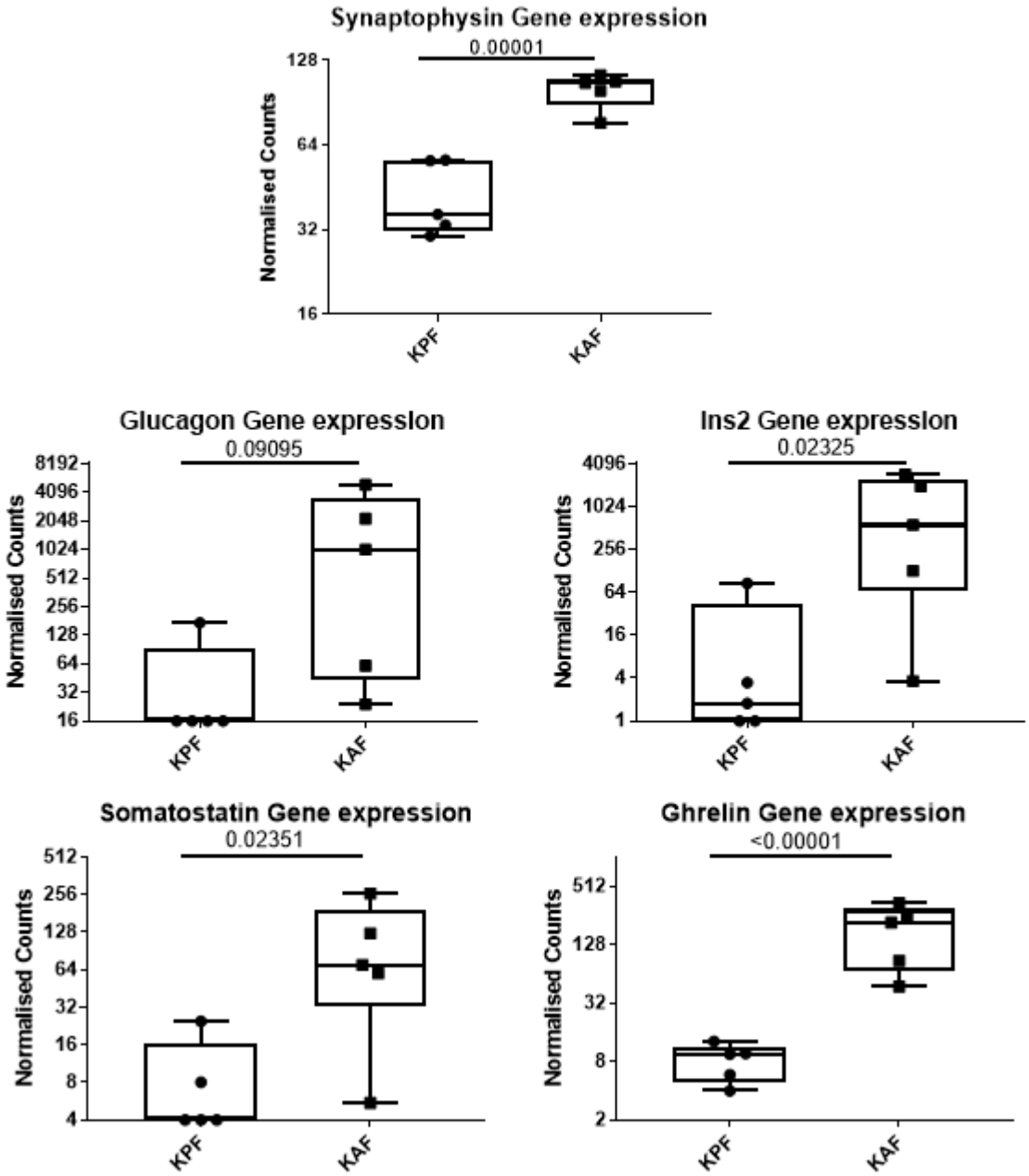

Figure 42 Increased islet cell marker expression in KAF vs KPF tumours
The expression of the pan-islet marker Synaptophysin is significantly increased in KAF vs KPF tumours. The islet cell markers Ins2 (Insulin), Somatostatin and ghrelin, representing β, δ and ϵ cell respectively are also significantly enriched in KAF tumours. P-adjusted values are indicated.

To further investigate these observations, I stained end-point tumours tissue for the same islet cell specific markers. This was to determine if the elevated expressed translated to protein level increases, as well as to interrogate the cellular location of the markers. With pancreatic neuroendocrine tumours (PNETs), for example insulinomas, developing from cells of the endocrine lineage and expressing endocrine markers (Wiedenmann et al., 1986), it was important to investigate the source of the tumours cells in the KAF model.

From the representative images of tumours immunohistochemically stained for the islet cell specific markers it was apparent that both complete islets and diffuse tumour infiltrated islet cell regions were evident (**Figure 43**). Insulin, as expected, and as shown previously in the wild type pancreas, was detected in the majority of islet cells, with glucagon and somatostatin at the periphery of the islets. Ghrelin, as observed in the wild type, was detected in very few of the islet cells, but interestingly, there were positive cells within the tumour epithelium. Notably, none of the islet cell stains were significantly increased as a percentage of total cells within the tumours areas in the end-point tumours from KAF mice compared to the KPF model (**Figure 44**). The epithelial staining of ghrelin was perhaps not surprising, given that it is a component of the apical surface hallmark gene set, which was also enriched in the KAF model (**Figure 45**). However, it is intriguing that expression was observed in tumour epithelium but not in normal acinar or duct cells, raising questions as to the function of this protein in disease states.

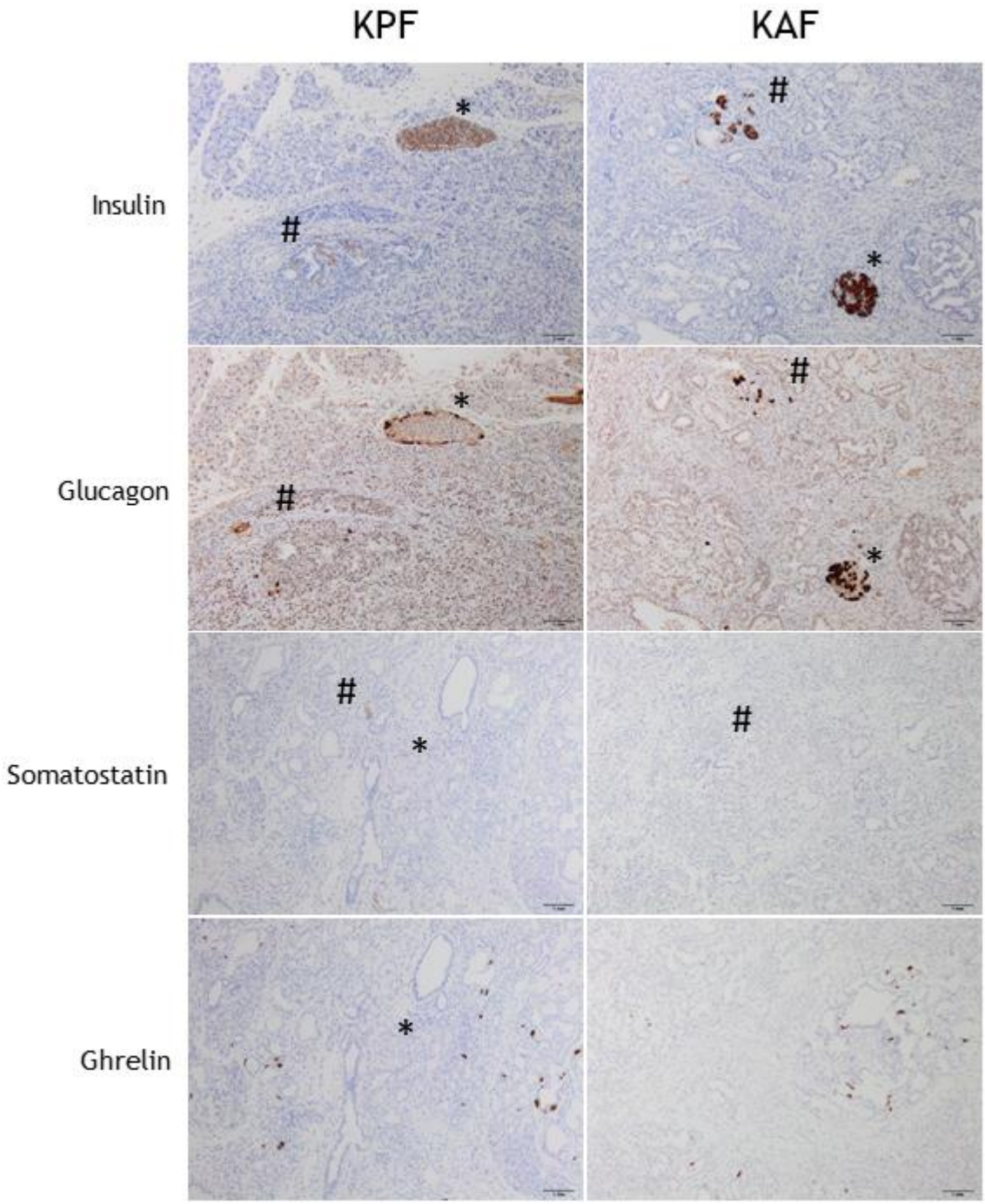

Figure 43 Representative images of islet cell maker staining in end-point KPF and KAF tumours
Representative images of KPF and KAF end-point tumours stained by IHC for the α, β, δ and ϵ markers glucagon, insulin, somatostatin and ghrelin respectively. Asterisks (*) indicates an intact islet region and the hash (#) indicates a tumour disrupted islet cell region. (Scale bars = 1mm).

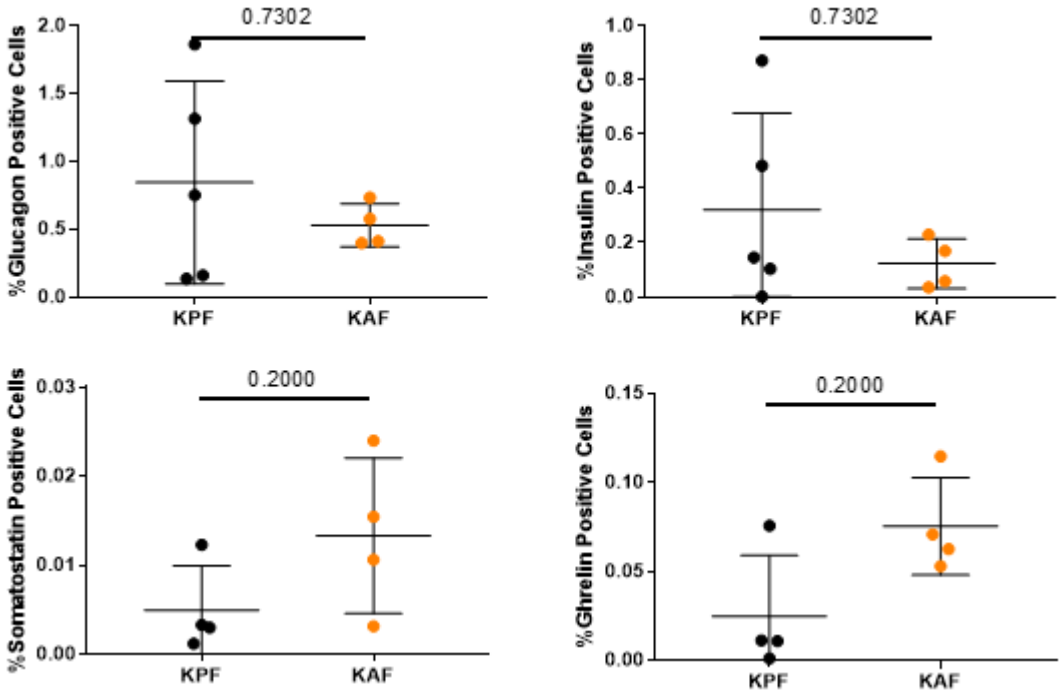

Figure 44 Quantification of the islet cell marker staining in KPF and KAF end-point tumours
HALO quantification for the percentage of positive cells for each marker across the tumour region in the KPF and KAF models, showing that there was no significant increase in staining for any islet marker in the KAF tumours compared to the KPF tumours. (n=5, 4, respectively, Mann-Whitney P values shown).

Hallmark Gene Set	NES	P-adjusted Value
APICAL_SURFACE	1.62	0.0466

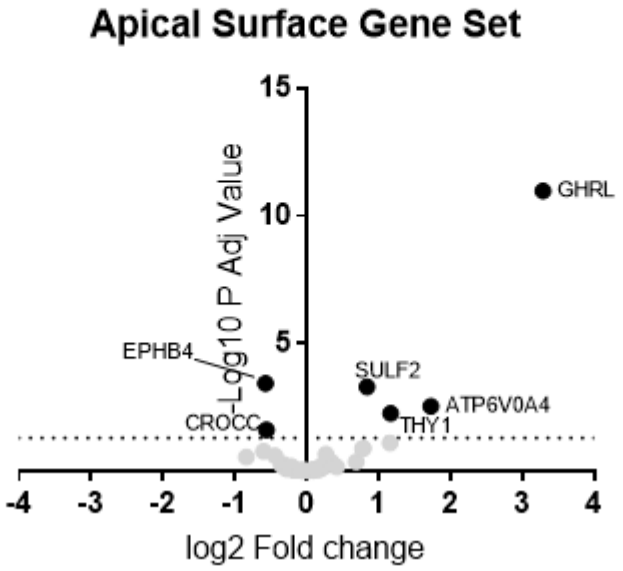

Figure 45 The apical surface hallmark gene set was enriched in KAF tumours compared to KPF tumours

The apical surface hallmark gene set was enriched in the KAF tumours in comparison to the KPF tumours. A volcano plot of the genes in the apical surface hallmark plotting the Log2 fold change against –Log10 P adjusted Value with negative values indicating enrichment in the KPF tumours and positive values indicating enrichment in the KAF tumours. Of the 38 genes, 19 are enriched in KAF tumours with four being significantly enriched, and 2 significantly enriched in KPF tumours. The dashed line denotes significant gene changes with a P adjusted value ≤ 0.05.

Synaptophysin proportion was, however, significantly increased in the KAF tumours, with staining in the islets and diffuse tumour invaded islet regions (**Figure 46**). This could in part explain the elevated pancreas beta cell signal observed as there was an overall elevated islet area in the KAF pancreata, although not necessarily driven by expansion of any one islet cell subtype. Although synaptophysin was significantly increased, the staining was found in expected cellular locations, in islet regions, so is unlikely to represent any change in tumour cell differentiation status. This staining pattern also contrasts with staining in tumours developing from the endocrine lineage, which show a diffuse and pan tumour expression of synaptophysin, or other islet cell marker, depending on the cell of origin (Wiedenmann et al., 1986).

Together these data demonstrate that enrichment of the pancreas beta cell hallmark in the KAF tumour can in part be explained by the elevated islet cell proportion in the end-point tumours. Further, it comprehensively eliminates the potential of development of tumours derived from the endocrine lineage due to the restricted pattern of staining for the various markers expressed by endocrine cells. However, the GSEA was also driven, in part, by the elevated expression of SLC2A2 (Glut2), a low affinity glucose transporter perhaps indicating metabolic alterations, which we did not investigate here.

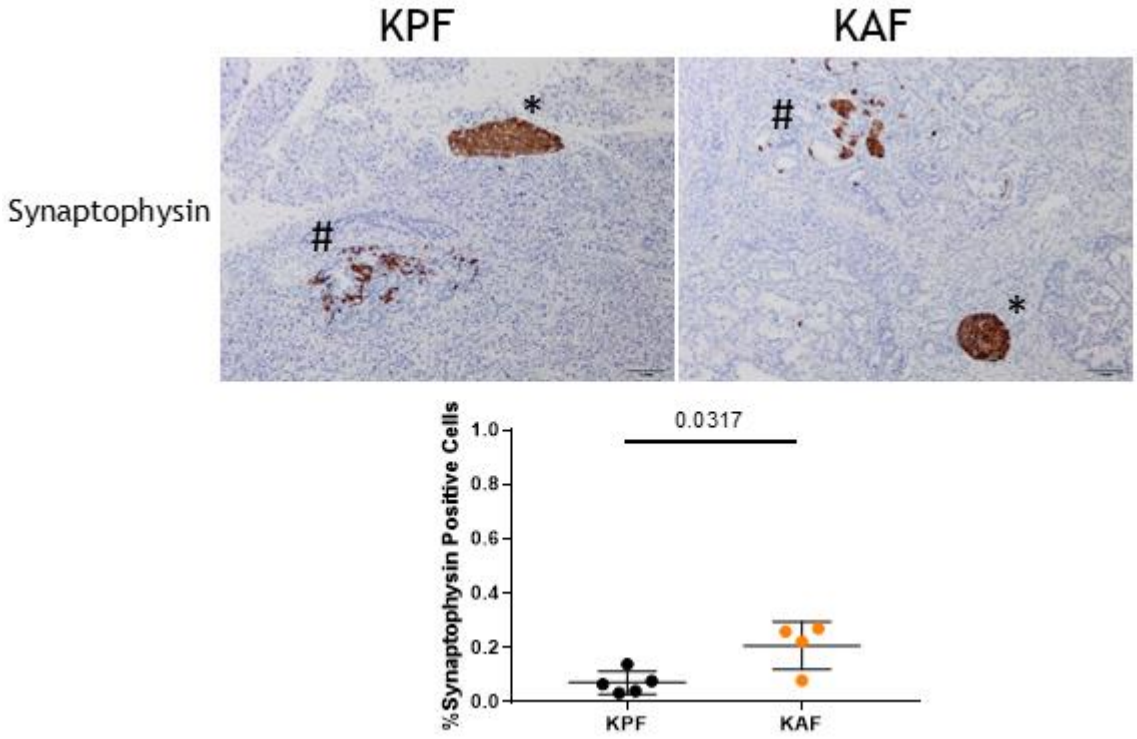

Figure 46 The percentage of synaptophysin cells was significantly increased in KAF tumours compared to KPF tumours
Top panels: Representative images of immunohistochemical staining for the pan-islet marker, synaptophysin (Scale bars = 1mm). Asterisks (*) indicates an intact islet region and the hash (#) indicates a tumour disrupted islet cell region. Lower panel: HALO quantification of the percentage of synaptophysin positive cells across the tumour region of the KPF and KAF models, showing that there was a significant increase in staining in KAF tumours compared to KPF tumours. (n= 5, 4, respectively, Mann-Whitney P values indicated).

4.3.3 Does the p53 pathway convey a targetable therapeutic vulnerability in the KAF mouse model?

With the enrichment of the p53 pathway gene set in the KAF tumours detected at RNA level, I sought to determine how the tumours are able to mitigate having functional p53 and whether activation of p53 can present as a therapeutic opportunity. To begin with, I examined patient data on cBioPortal with the aim of elucidating if the KAF model mimics the genetics of a subset of PDAC patients. From the TCGA pancreatic cancer data set, I queried the common mutations effecting the TGFβ signalling pathway, SMAD4, *TGFBR1* (*ALK5*) and *TGFBR2*, as well as *KRAS* and *TP53*. From this, I showed that, a subset of patients had mutations in *TGFBR1* and *KRAS* but not *TP53*, which the KAF mouse model replicates (4/175 patients, 2%). A mutual exclusivity analysis highlights that *TGFBR1* and *TP53* mutations had a tendency toward being mutually exclusive, again further justifying the KAF model as bearing a genetic resemblance to a subset of patients. The failure to reach significance was most likely accounted for by the low prevalence of *TGFBR1* mutations in the patient data set with only around 4% of patients carrying a *TGFBR1* alteration (7/175 patients) (**Figure 47**).

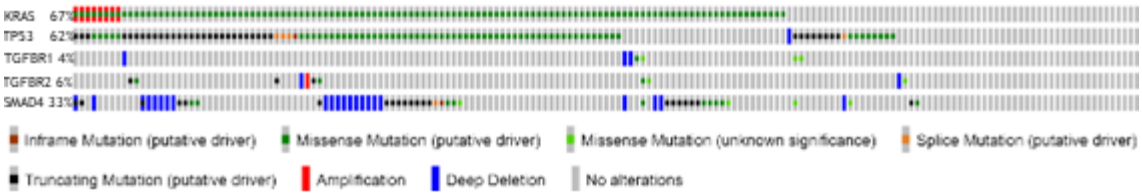

A	B	Neither	A Not B	B Not A	Both	Log2 Odds Ratio	p-Value	q-Value	Tendency
KRAS	TP53	40	27	18	90	2.889	<0.001	<0.001	Co-occurrence
KRAS	SMAD4	53	65	5	52	>3	<0.001	<0.001	Co-occurrence
TP53	SMAD4	50	68	17	40	0.791	0.075	0.249	Co-occurrence
KRAS	TGFBR2	56	108	2	9	1.222	0.23	0.423	Co-occurrence
TGFBR2	SMAD4	109	9	55	2	-1.183	0.243	0.423	Mutual exclusivity
TP53	TGFBR1	63	105	4	3	-1.152	0.254	0.423	Mutual exclusivity
TGFBR1	TGFBR2	158	6	10	1	1.397	0.37	0.514	Co-occurrence
TGFBR1	SMAD4	114	4	54	3	0.663	0.411	0.514	Co-occurrence
KRAS	TGFBR1	56	112	2	5	0.322	0.575	0.581	Co-occurrence
TP53	TGFBR2	63	101	4	7	0.126	0.581	0.581	Co-occurrence

Figure 47 A subset of patients had genetic mutations similar to the KAF mouse model
Utilising cBioPortal, I generated an OncoPrint image of the TCGA pancreatic cancer data set. I plotted the genes altered in the KAF model; *KRAS*, *TP53* and *TGFBR1*, as well as other key components of the TGFβ signalling pathway; *TGFBR2* and *SMAD4*. *TGFBR1* mutations are evident in 4% of cases (7/175 patients). A mutual exclusivity analysis highlights that *TGFBR1* and *TP53* have a tendency toward being mutually exclusive, with over half of the *TGFBR1* mutations occurring without a P53 alteration (4/7 patients).

I therefore examined the RNA data focussing on the hallmark P53 pathway gene set which was significantly enriched in the KAF samples. Of the 188 genes in the gene set, 114 were enriched in the KAF samples, 20 of which reached significance (**Figure 48**). This is indicative of active p53 signalling within the KAF tumours, however, some of the enriched genes are inhibitors of p53 signalling suggesting maintenance of the typically tight control on overt p53 activation. For instance, Cyclin G1 (Ccng1), a non-canonical member of the cyclin kinase family, was shown to be significantly enriched in the KAF tumours (**Figure 49**). CCNG1 has been shown to recruit protein phosphatase 2A (PP2A) to a complex with the well-known negative regulator of p53, mouse double minute 2 (MDM2), thereby facilitating the dephosphorylation and activation of MDM2 (**Figure 50**), also shown to be enriched in the KAF tumours (**Figure 49**).

Hallmark Gene Set	NES	P-adjusted Value
P53_PATHWAY	1.62	0.0033

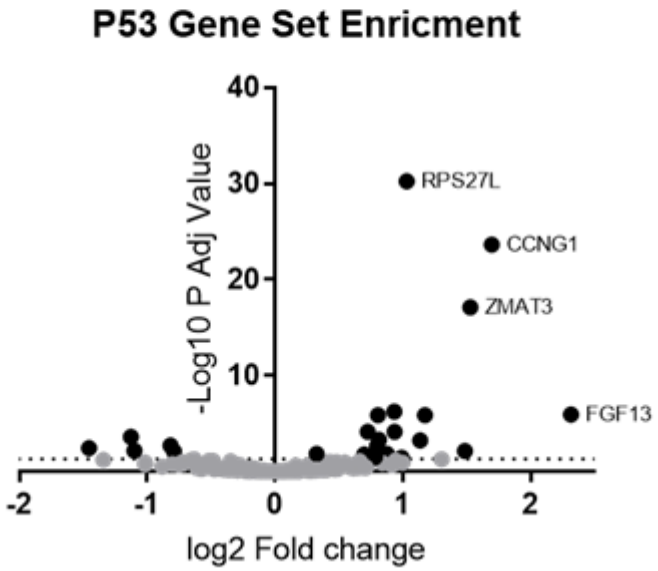

Figure 48 The p53 Pathway hallmark gene set was enriched in KAF vs KPF tumours
The p53 pathway hallmark gene set was enriched in KAF tumours in comparison to KPF tumours. Shown is a volcano plot of the genes in the p53 pathway hallmark plotting the Log2 fold change against –Log10 P adjusted value with negative values indicating enrichment in the KPF tumours and positive value indicating enrichment in the KAF tumours. Of the 188 genes, 114 are enriched in KAF tumours with 20 being significantly enriched. The dashed line denotes significant gene changes with a P adjusted value ≤ 0.05.

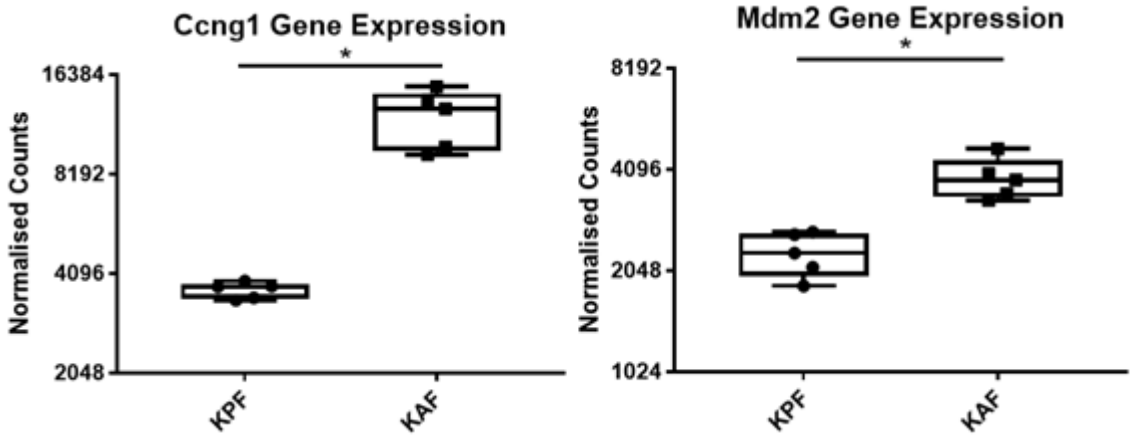

Figure 49 Expression of *Ccng1* and *Mdm2* was significantly increased in KAF vs KPF tumours
The expression of *Ccng1* and *Mdm2* was significantly enriched in KAF vs KPF tumours. P-adjusted values of <0.0001.

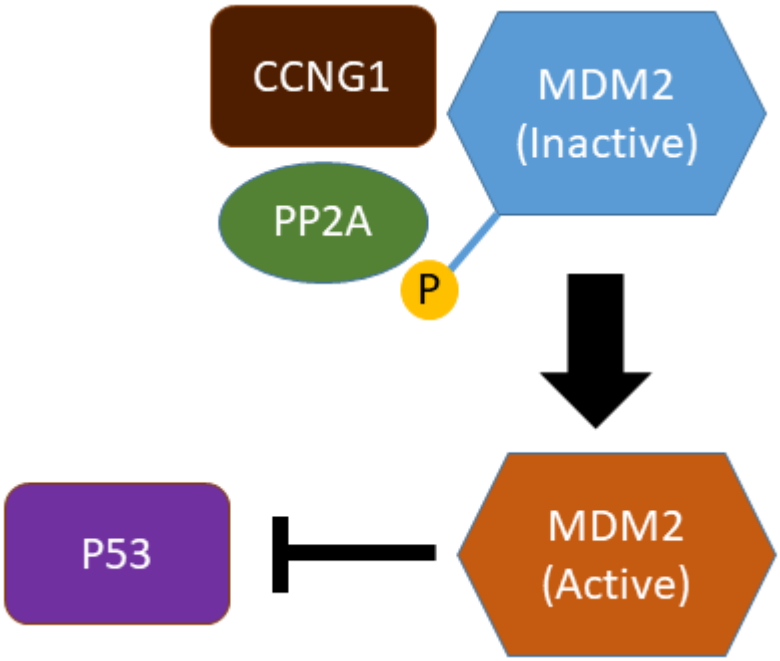

Figure 50 CCNG1 facilitates activation of P53 inhibitor MDM2
CCNG1 facilitates the recruitment of PP2A to a complex containing the p53 negative regulator MDM2. PP2A is able to de-phosphorylate and thereby activate MDM2. MDM2 then binds to and ubiquitinates p53 targeting it for proteosomal degradation.

Subsequently I stained end-point tumour tissue to detect CCNG1 protein expression. As noted in the representative images, staining is specifically located in the epithelial cells. In tumours of both genotypes, staining was heterogeneous and there were regions that expressed high or low levels of CCNG1, highlighted in the upper and lower images respectively. Quantification of the intensity of stains showed that there was no significant elevation in CCNG1 at the protein level in the KAF samples, in contrast with the RNAseq data (**Figure 51**).

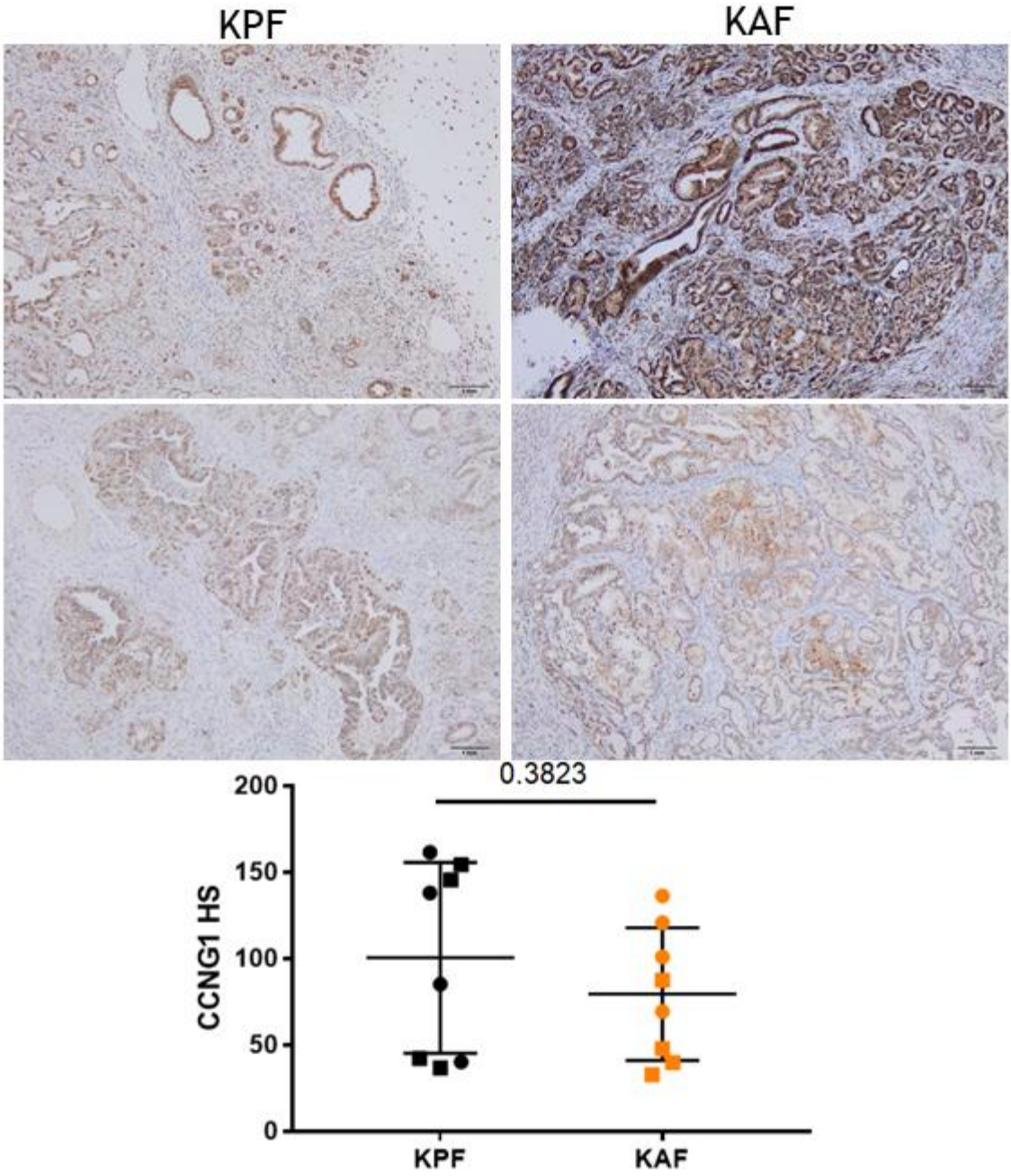

Figure 51 Staining for CCNG1 shows no change in protein levels between KAF and KPF tumours
Representative images of end-point tumour tissue IHC stained for CCNG1. The top images represent high levels of CCNG1 with the lower images representing low levels of CCNG1 (Scale bars = 1mm). Quantification of the staining intensity in tumours regions is shown in the graph, with circle markers indicating samples from the same tumours that were used for RNAseq. (n=8,8, respectively, Mann Whitney P values indicated).

Subsequently, I extracted protein from bulk tumours of the various genotypes and examined the levels of CCNG1 protein extracted by western blotting (**Figure 52**). There was no significant increase in CCNG1 levels detected in the KAF tumours compared to the KPF controls, again contrasting observations from the

transcriptional data. Further, *in vivo* deletion of *Alk5* or *Tgfb1* the cancer cells within established KPF tumours did not result in increased levels of Ccng1 protein.

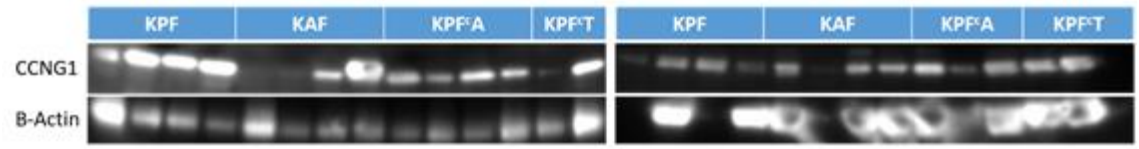

Figure 52 CCNG1 was not increased in tumour lysates from KAF tumours compared to KPF tumours
Protein lysate were prepared from tumours harvested from KPF, KAF, induced KPF; FSF-Cre^{ER}; *Alk5$^{fl/fl}$* (KPF^{C}A) and induced KPF; FSF-Cre^{ER}; *Tgfb1$^{fl/fl}$* (KPF^{C}T) mice at end-point. Western blots were performed on the protein lysates, which showed no consistent change in CCNG1 protein levels across any of the genotypes examined. (n= 8 (KPF), 8 (KAF), 7 (KPF^{C}A), 5 (KPF^{C}T), respectively).

There could be different reasons for the differences between the two genotypes in terms of differential gene expression but unchanged protein levels of CCNG1, including differences in post-translation modification or protein stability. Given that MDM2 gene expression was still increased in the KAF tumours, I wanted to investigate whether that could still indicated a therapeutic vulnerability. The cell lines were cultured and then treated with nutlin3a, an MDM2 inhibitor, for 24 hours and then cell lysates were prepared, and immunoblotting performed. Ccng1 protein abundance was unchanged following nutlin3a treatment. However, treatment caused an increase in p53 protein in 2/3 KAF cell lines but not in the KPF cell lines (**Figure 53**). This indicated that two of the KAF cell lines retained expression of p53, with p53 absent in the KPF lines as expected. Therefore, I performed a clonogenic assay, treating the cells with nutlin3a in order to examine sensitivity to p53 activation *in vitro*. Cells were plated and allowed to attach for 24 hours before treatment with increasing doses of nutlin3a for 24 hours, prior to washing and incubation in normal media for 5 days. At this time, cells were fixed and colonies counted after crystal violet staining. It was noted that treatment with nutlin3a was not sufficient to significantly reduce colony formation even at the highest concentrations in any of the cell lines treated (**Figure 54**). This indicated that removal of MDM2

suppression of p53 was not sufficient to induce cell death. However, stimulation with chemotherapeutic agents, which cause cell stress and drive increased p53, such a gemcitabine, oxaliplatin or radiation may synergise well with nutlin3a, as has been shown previously in p53 proficient PDAC cell lines (Candido et al., 2019).

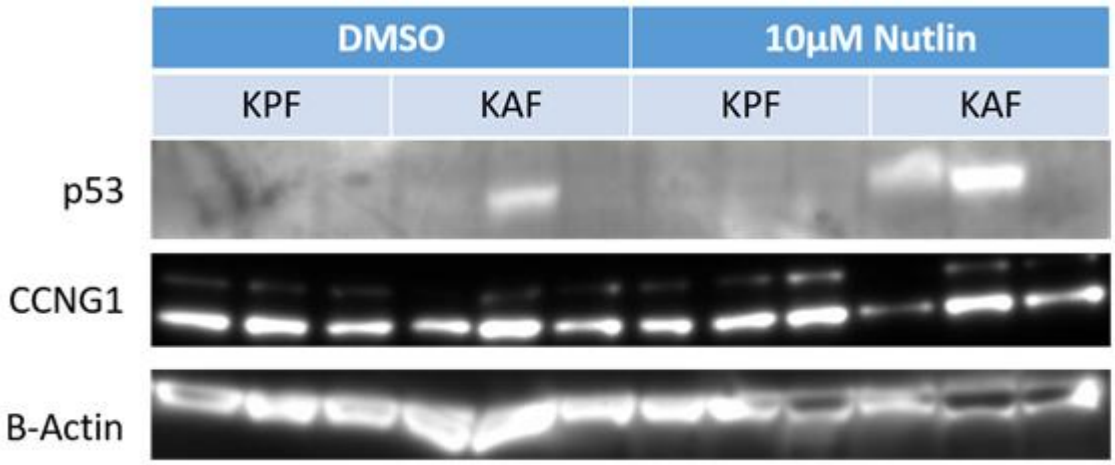

Figure 53 Nutlin3a treatment increases p53 expression in KAF but not KPF cells
KPF and KAF cell lines were treated with either DMSO or 10μM Nutlin3a for 24 hours, before protein was extracted and a western blot was performed. Nutlin3a increased p53 expression in 2/3 KAF cell lines but not in the KPF cell lines. Ccng1 expression was unchanged upon nutlin3a treatment, and was not different between KAF and KPF cells.

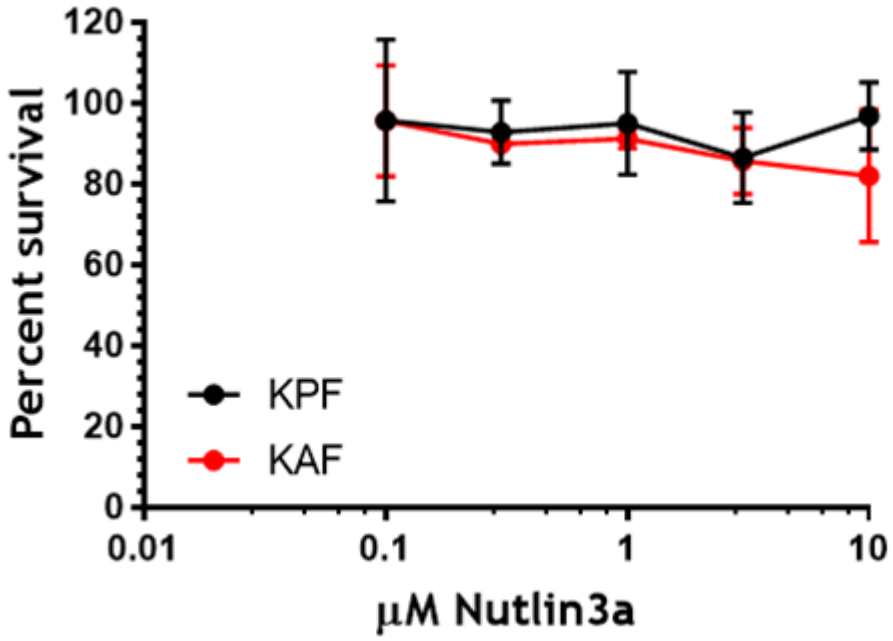

Figure 54 KAF and KPF cell lines were insensitive to Nutlin3a across a range of concentrations
KAF and KPF cell lines derived from end-point tumours were assayed to detect sensitivity to nutlin3a treatment. A clonogenic assay was performed, 400 cells per cell line were seeded and treated for 24 hours with a range (0.1 – 10µM) of nutlin3a concentrations, cells were then incubated for 5 days in full media before subsequent staining for crystal violet and positive colonies being counted. (2 technical replicates of 3 biological replicates, 2way ANOVA used).

4.3.4 Deletion of tumour epithelial *Alk5* within established KPF tumours does not affect survival but decreases metastasis.

With the hallmark for epithelial mesenchymal transition (EMT) enriched in GSEA on the KPF tumours, and the known role TGFβ signalling plays in driving EMT (Katsuno et al., 2019; Vincent et al., 2009), I sought to investigate how disruption of TGFβ signalling would impact established tumours. The volcano plot showing enrichment of the EMT hallmark gene set in KPF mice tumours is shown in **Figure 55**. The majority of genes in the EMT gene set were enriched in the KPF tumours (116/186) with 7 reaching significance. Notably, there were 9 genes significantly enriched in KAF tumours, indicating that some EMT related genes are expressed. Interestingly *Ctgf* was enriched in the KAF tumours, with this gene being induced by TGFβ signalling and involved in fibroblast mechnosignalling (Gao and Brigstock, 2005). Therefore, I sought to investigate the potential effect on metastasis. Since the KAF model does not develop metastasis, I utilised the KPF model with tamoxifen inducible deletion of expression of *Alk5* or *Tgfb1* specifically in transformed cells (**Figure 56**). The KPF model, as previously described, has the potential to develop both liver and lung metastases, as well as diaphragm metastases.

Hallmark Gene Set	NES	P-adjusted Value
EMT	-1.55	0.0087

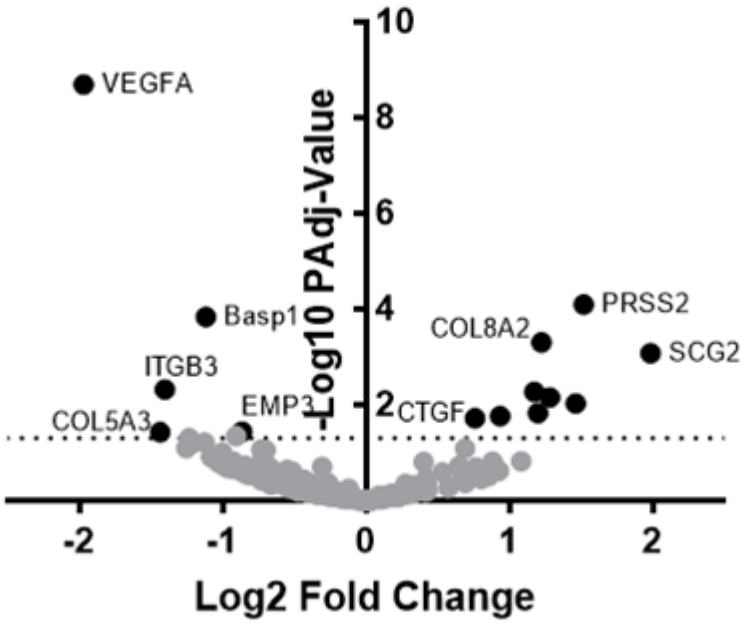

Figure 55 The EMT gene set was enriched in KAF tumours compared to KPF tumours
The EMT hallmark gene set was enriched in KPF tumours in comparison to KAF tumours. A volcano plot of the genes in the EMT hallmark gene set is shown plotting the Log2 fold change against –Log10 P adjusted Value with negative values indicating enrichment in the KPF tumours and positive values indicating enrichment in KAF tumours. Of the 200 genes, 70 were enriched in the KAF tumours with 9 being significantly enriched, 116 were enriched in the KPF tumours with 7 reaching significance. The dashed line denotes significant gene changes with a P adjusted value ≤ 0.05.

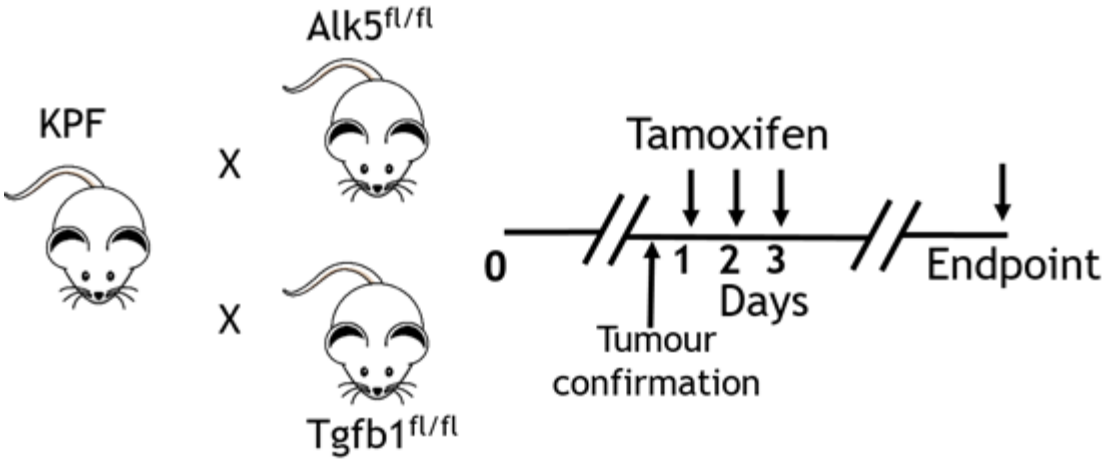

Figure 56 Mouse models of cancer cell specific deletion of *Alk5* or *Tgfb1* in established tumours
The KPF FSF-CRE^{ER} model was crossed to mice with *Alk5*$^{fl/fl}$ or *Tgfb1*$^{fl/fl}$ alleles. Upon detection of a palpable tumour and confirmation by ultrasound, mice were induced with tamoxifen over 3 days, with subsequent weekly follow up ultrasound until clinical end-points were reached.

I initially investigated the post-induction survival of the KPF, KPF; *Alk5*$^{fl/fl}$ or KPF; *Tgfb1*$^{fl/fl}$ models. Mice were palpated weekly until detection of PDAC, which was subsequently confirmed by ultrasound imaging. The mice were enrolled on 3-day long tamoxifen induction regime, with weekly ultrasound follow up to monitor any tumour volume changes. This allowed deletion of *Alk5* or *Tgfb1* specifically from the epithelial cells in established tumours. There were no significant changes in survival noted between the KPF, KPF; *Alk5*$^{fl/fl}$ and KPF; *Tgfb1*$^{fl/fl}$ models following induction, presenting with a median survival of 12, 15 and 11 days, respectively (**Figure 57**). These observations were interesting due to the contrasting effect of deletion of *Alk5* on initiation compared with tumour progression. These data would indicated that in established tumours, the TGFß signalling is no longer able to exert tumour suppressive activity, with deletion of *Alk5* no longer accelerating progression as was seen in when deletion occurred in pre-neoplastic lesions. The tumour epithelial deletion of *Tgfb1* having no impact on survival was perhaps less surprising due to other potential sources of the ligand. Although, due to the rapid progression to clinical endpoints from tumour detection and tamoxifen administration it is debatable whether I would be able to observe any acceleration following the deletion of *Alk5* or *Tgfb1*. From ultrasound imaging analysis it is clear that tumour growth was not accelerated when either *Alk5* or *Tgfb1* were deleted compared to the KPF controls (**Figure**

58). All tumours continued to grow at a similar rate following induction, as shown in the percentage tumour change (**Figure 58**) and although this suggests that deletion of either *Alk5* or *Tgfb1* does not accelerate tumour growth it is again possible that tumours, which are on average doubling in size between each scan, are at their maximum growth rate. Therefore, I can conclude that deletion of *Alk5* or *Tgfb1* within the epithelium of established tumours does not suppress PDAC growth and does not appear to accelerate disease although due to the rapid progression of the model this cannot be firmly established.

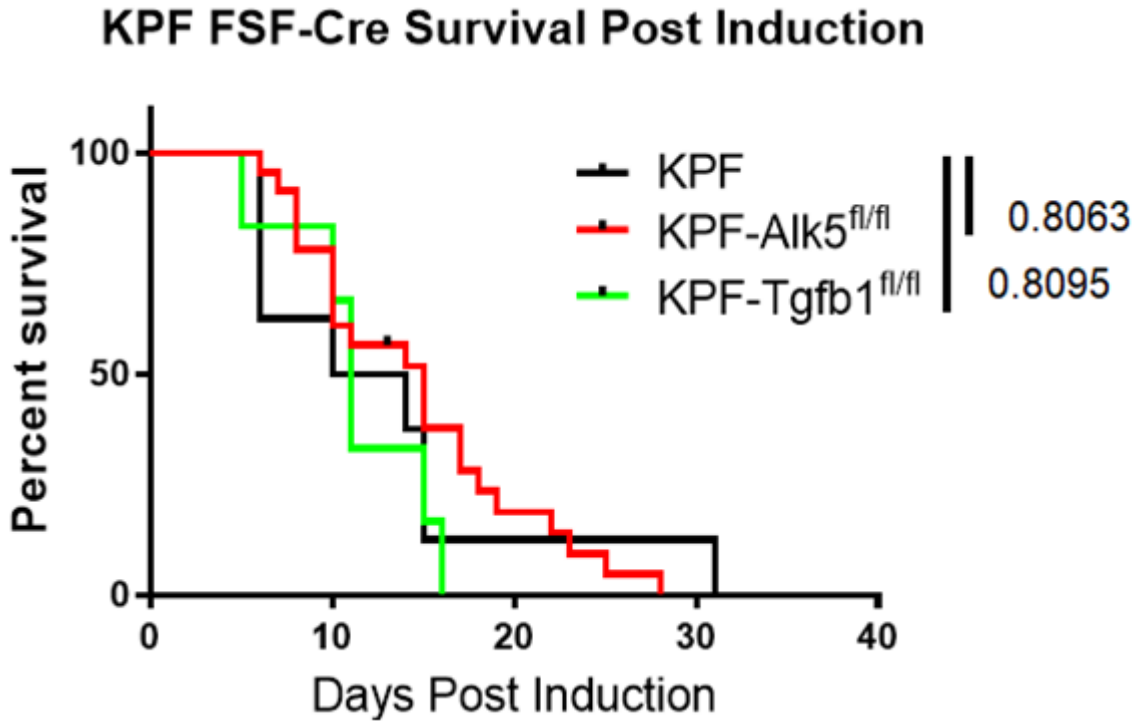

Figure 57 Deletion of *Alk5* or *Tgfb1* in the epithelium of established tumours does not alter survival
Kaplan-Meier survival analysis of the KPF, KPF; *Alk5*$^{fl/fl}$ and KPF; *Tgfb1*$^{fl/fl}$ mice post tamoxifen induction. There was no significant change in survival noted across any of the models. (Median survival, KPF= 12 days, KPF; *Alk5*$^{fl/fl}$= 15 days, KPF; *Tgfb1*$^{fl/fl}$= 11 days, n=8, 22, 6 respectively, Log-Rank P values indicated).

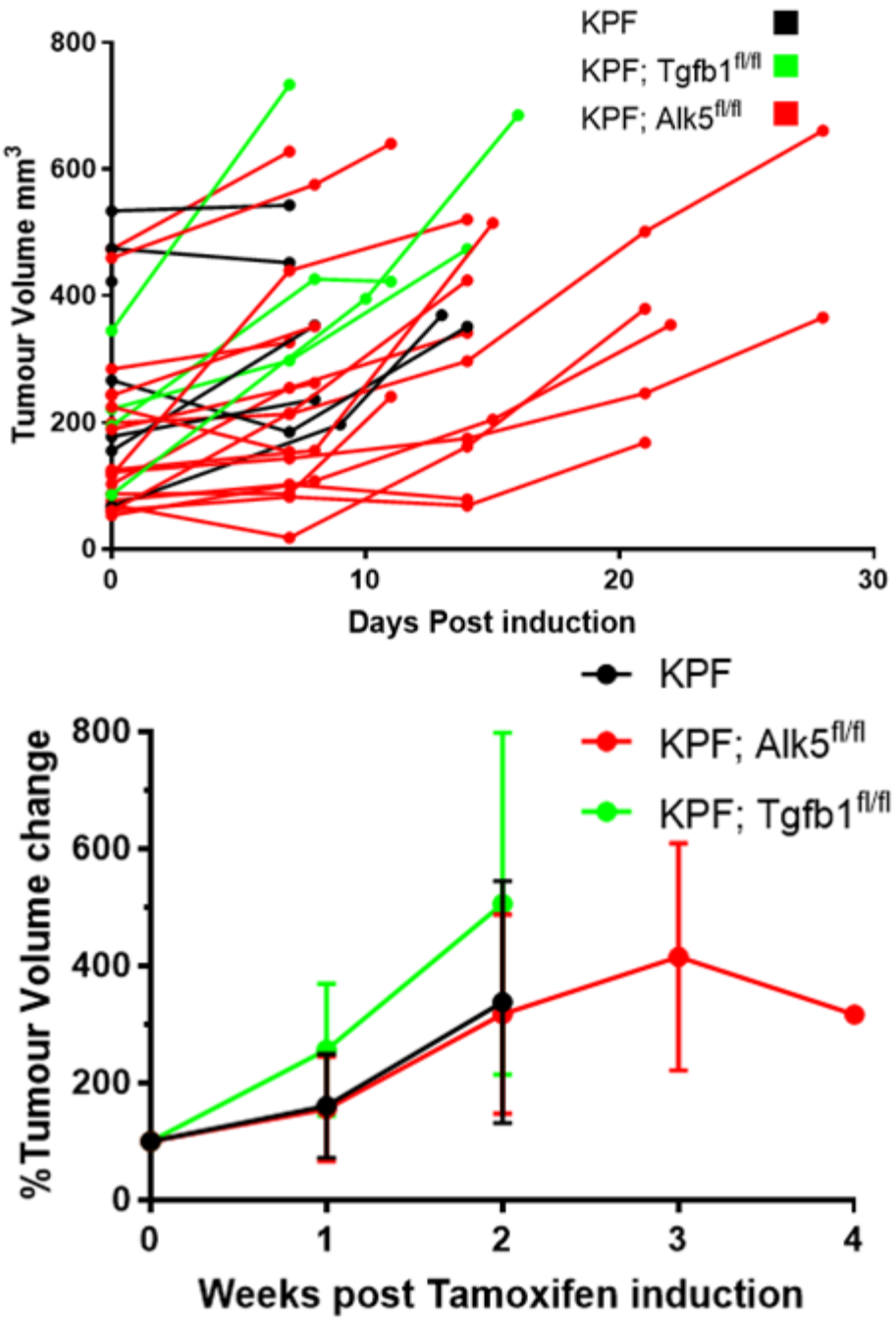

Figure 58 Tumour growth was unchanged in the KPF; *Alk5*$^{fl/fl}$ and KPF; *Tgfb1*$^{fl/fl}$ models when compared with the KPF model
Mice were imaged by ultrasound to confirm presence of PDAC prior to commencement of tamoxifen induction and were subsequently subjected to weekly ultrasound follow up. 3D measurement of tumours volumes was gathered pre-induction and at each subsequent follow up until clinical end-points were reached. The top graph shows the volume measurement of the pancreatic tumour (mm^3) in each mouse prior to induction and at each follow up. The bottom graph shows the median percentage change in tumour from the pre-induction volume for each cohort, with the standard deviation plotted. (n=7, 18, 4 respectively).

I subsequently performed a count of macro- and micro-metastatic lesions in mice sampled at clinical end-point due to PDAC related symptoms. The total percentage of mice presenting with metastases appears reduced in both the KPF; *Alk5*$^{fl/fl}$ and KPF; *Tgfb1*$^{fl/fl}$ model compared to the KPF control (**Figure 59**). Organs specific metastasis to the liver and lung was also reduced in these models. Further, concurrent metastasis to multiple sites was reduced in these models, although increased numbers are required as significance was not reached in any of the metastatic counts. It was also apparent that the KPF; *Alk5*$^{fl/fl}$ model had a greater reduction in incidence of metastasis than the KPF; *Tgfb1*$^{fl/fl}$ model. The reduction in metastasis does not translate to an increased survival in the mouse models as clinical end-points were reached due to the primary tumour burden. These data suggest that loss of TGFβ signalling or the capacity to produce TGFβ1 within the epithelial cells in established tumours reduces their metastatic capability, although not significantly.

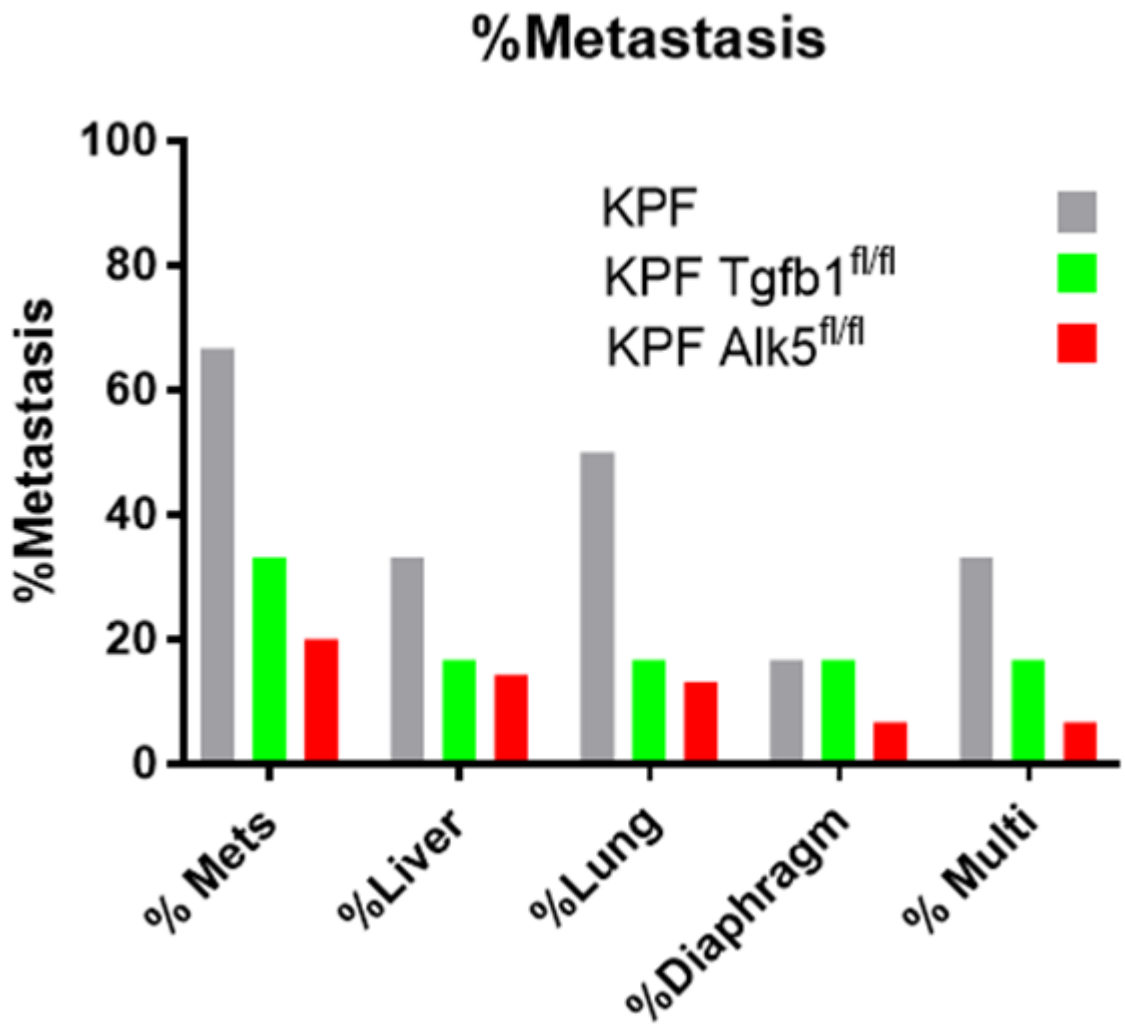

Figure 59 KPF; *Alk5*$^{fl/fl}$ and KPF; *Tgfb1*$^{fl/fl}$ mice present with reduced metastasis compared to KPF mice.
The percentage of mice presenting with macro- or micro-metastases to the various sites is shown. % Mets denotes the presence of any evidence of metastasis at any site, with % liver, % lung and % diaphragm reporting the presence of organ specific metastases. % Multi denotes mice presenting with concurrent metastases to multiple sites. (n= 6, 6, 15, respectively) (Fisher's exact Test used).

This apparent reduction in metastasis could be due, at least in part, to the decreased EMT capability of the *Alk5* deleted cells. I therefore, performed IHC of mesenchymal and epithelial markers in the end-point tumours in order to detect alterations in EMT in the KPF, KPF; *Alk5*$^{fl/fl}$ and KAF models. The KAF model was included due to the clear GSEA decrease in EMT noted in comparison to the KPF. Epithelial markers Ck19 (**Figure 60**) and E-cadherin (**Figure 61**) showed an epithelial restricted staining pattern. Ck19 staining was unchanged across the cohorts as quantified by HALO analysis in **Figure 64**. However, by HALO analysis the percentage of cells staining positive for E-cadherin was significantly reduced in the KAF model compared to both the KPF and KPF; *Alk5*$^{fl/fl}$ models. This was particularly interesting as E-cadherin positive cells were evident within the tumour epithelium in the KAF mice by visual examination. I noted that HALO analysis was incorrectly defining cells as negative in this model due to the cellular location of the staining. Representative images of E-cadherin staining, at increased magnification, are shown in **Figure 62** and demonstrate that KAF models present with a high level of strictly membranous E-cadherin, which was expected in purely epithelial cells. Loss of membranous E-cadherin and increased cytoplasmic E-cadherin is a key indicator of cells undergoing EMT (Hotz et al., 2007), which was noted in both the KPF and KPF; *Alk5*$^{fl/fl}$ model. This was in agreement with the RNAseq data shown, although surprisingly with the reduced metastasis in the KPF; *Alk5*$^{fl/fl}$ model observed, no change in E-cadherin localisation was noted. Mesenchymal marker vimentin was shown to stain the tumour stroma predominantly, most likely denoting CAFs in these regions (**Figure 63**). Quantification of vimentin showed no change across the models (**Figure 64**). Therefore, other mesenchymal markers should be utilised to determine if EMT is reduced within the *Alk5* deficient tumours.

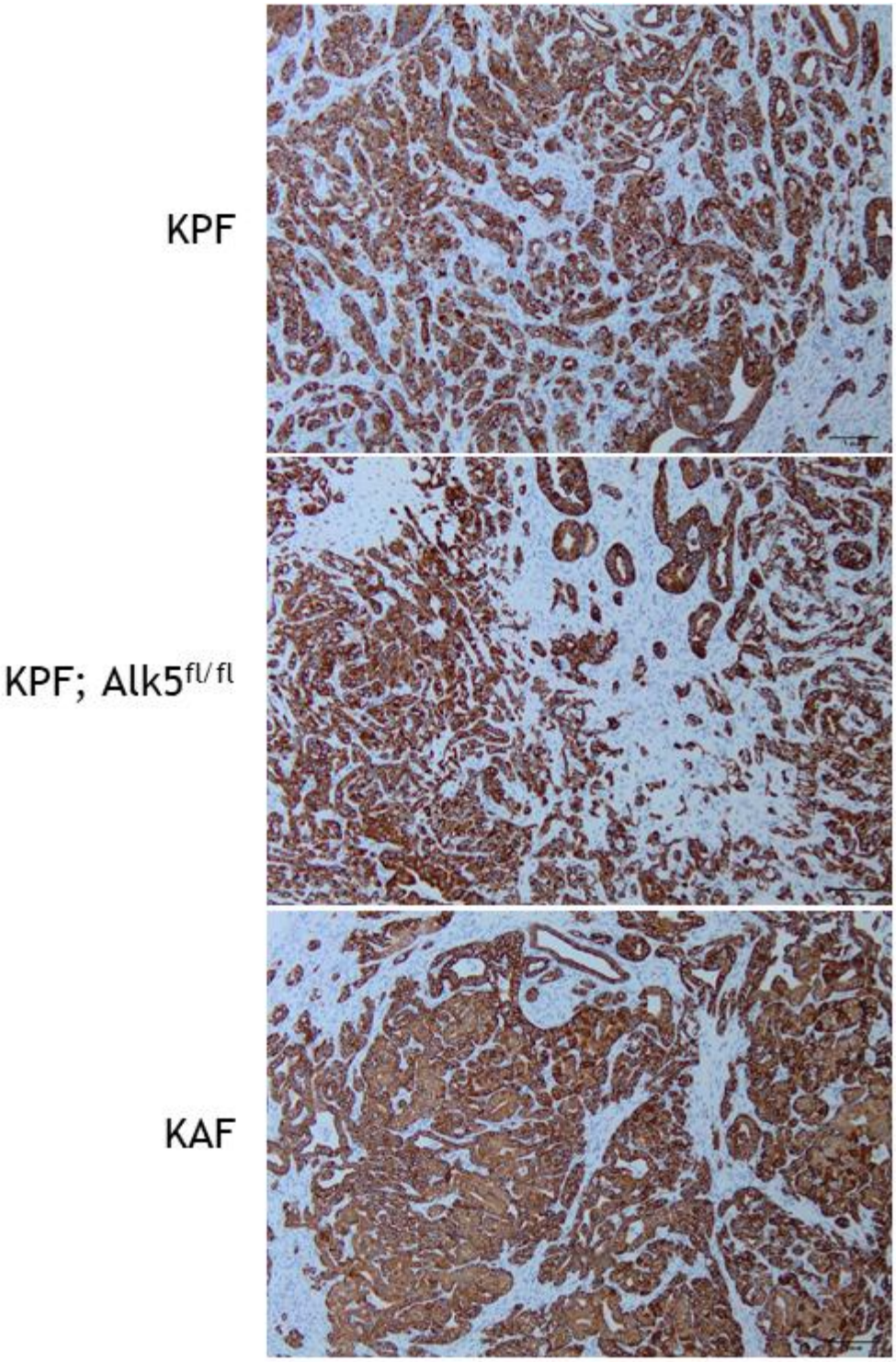

Figure 60 Representative images of Ck19 IHC staining in KPF, KPF; *Alk5*$^{fl/fl}$ and KAF end-point tumours
Representative images of Ck19 IHC stained sections from end-point tumours from KPF, KPF; *Alk5*$^{fl/fl}$ and KAF mice. Ck19 stains the epithelial cells specifically within the tumour. (Scale bars = 1mm).

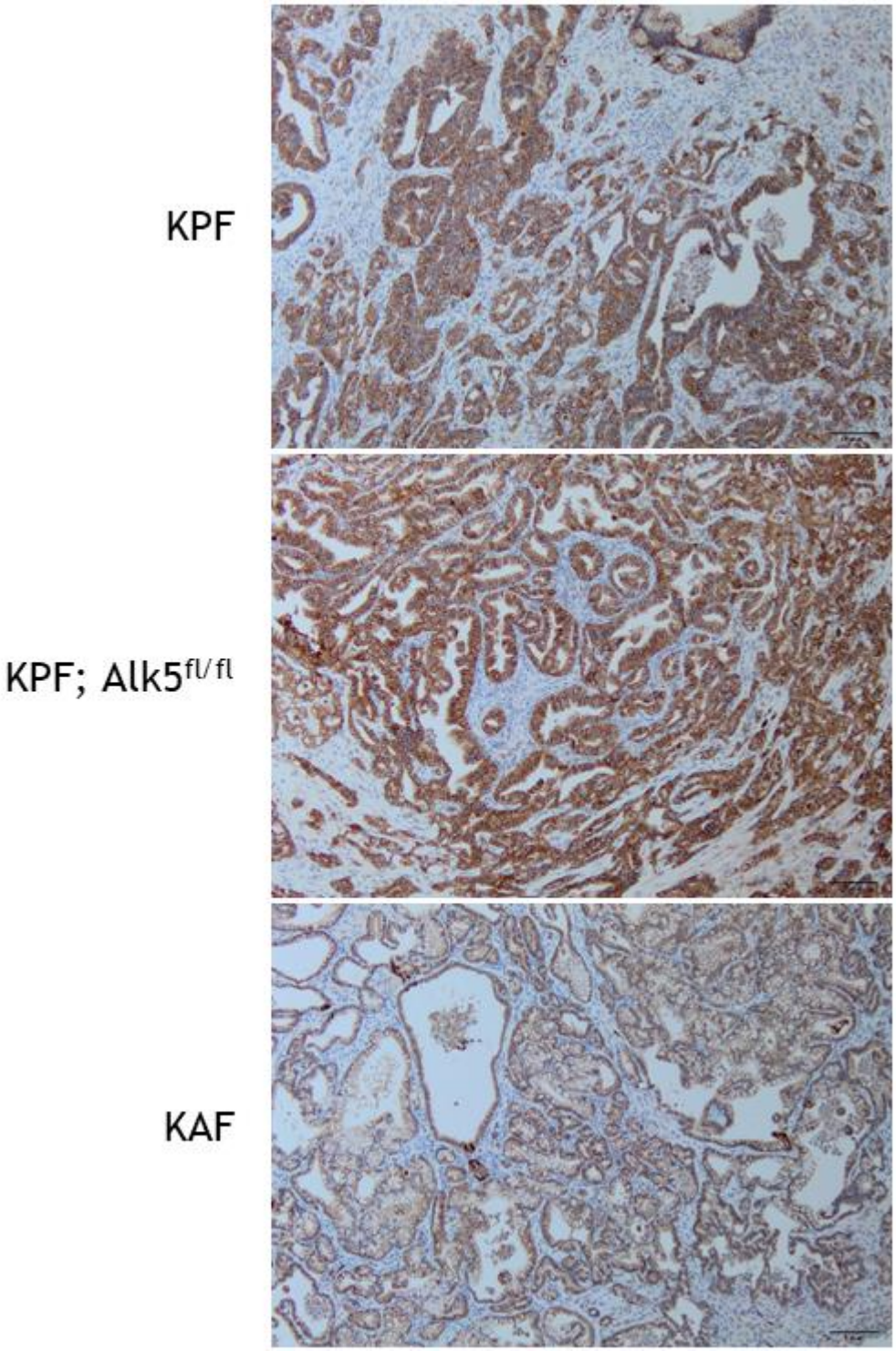

Figure 61 Representative images of E-cadherin IHC staining in KPF, KPF; *Alk5$^{fl/fl}$* and KAF end-point tumours
Representative images of E-cadherin IHC stained sections from end-point tumours from KPF, KPF; *Alk5$^{fl/fl}$* and KAF mice. E-cadherin stains the epithelial cells specifically within the tumour. (Scale bars = 1mm).

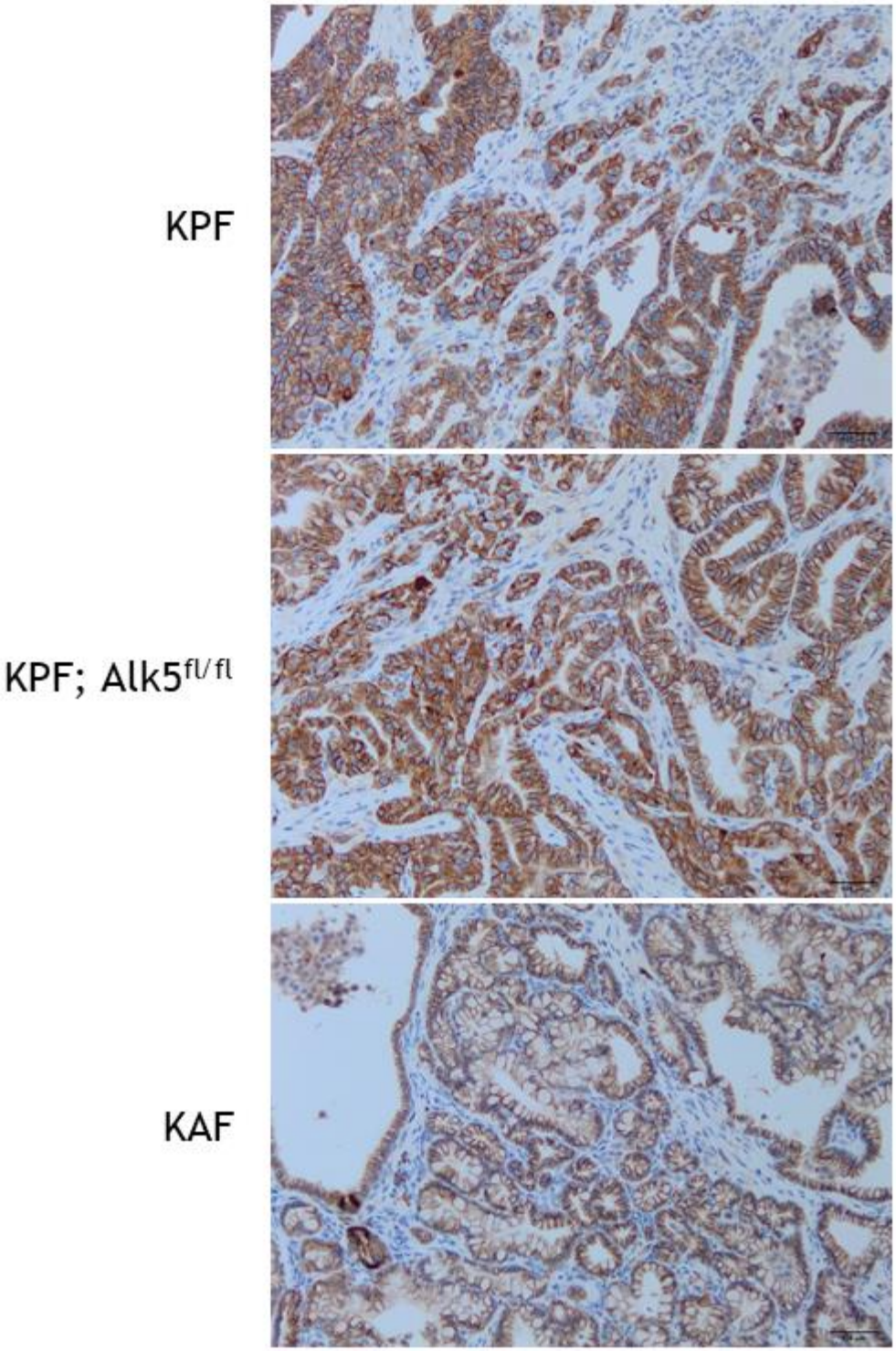

Figure 62 Representative images, at increased magnification, of E-cadherin IHC staining in KPF, KPF; *Alk5$^{fl/fl}$* and KAF end-point tumours
Representative images of E-cadherin IHC stained sections from end-point tumours from KPF, KPF; *Alk5$^{fl/fl}$* and KAF mice. E-cadherin stains the epithelial cells specifically within the tumour. Membranous staining denotes epithelial cells and cytoplasmic staining indicates cells undergoing EMT. KAF epithelial cells have little cytoplasmic positive staining, with a predominantly membranous stain compared to the KPF and KPF; *Alk5$^{fl/fl}$* tumours, which have more cytoplasmic E-cadherin positive staining. (Scale bars = 500μm).

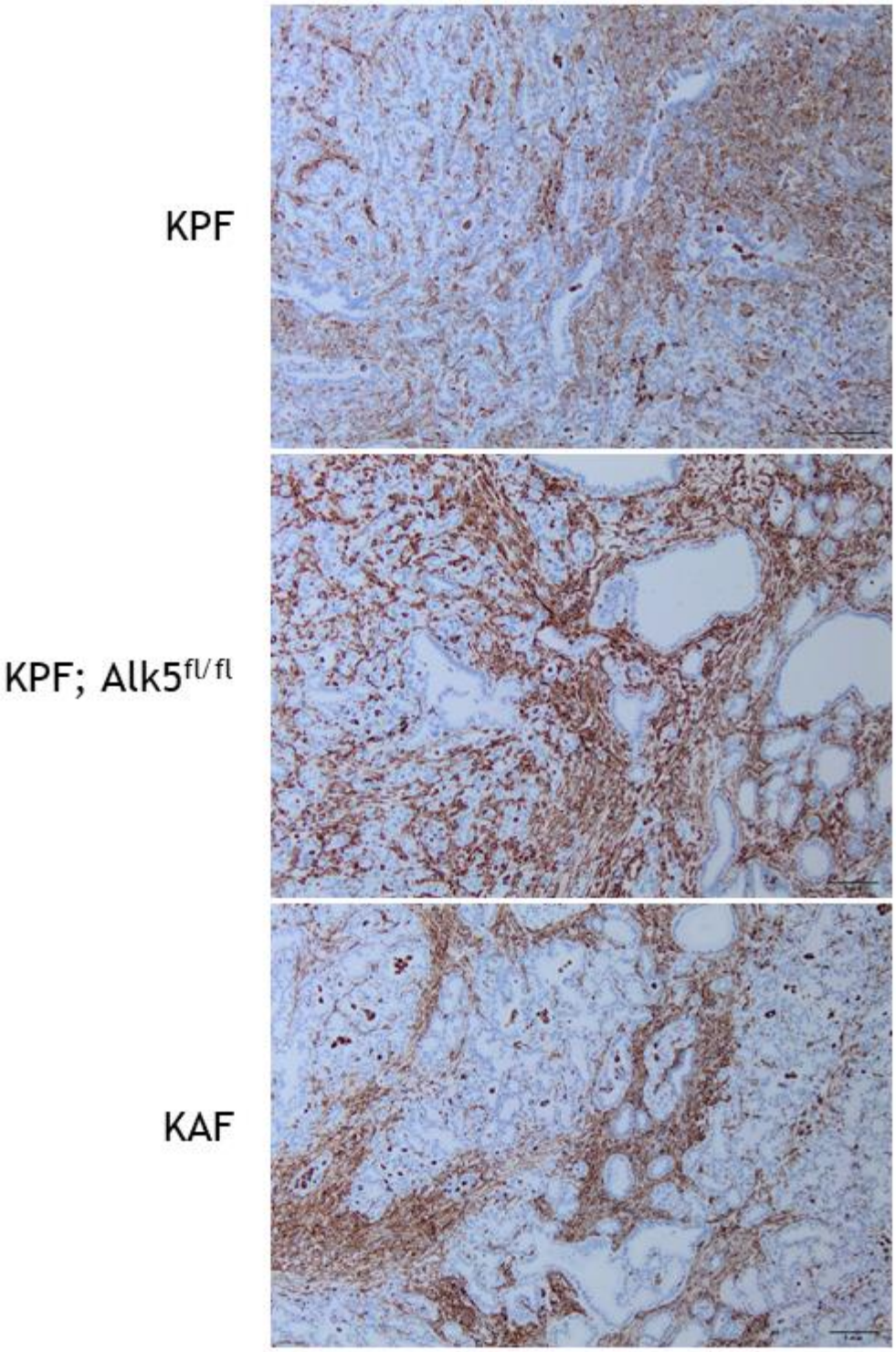

Figure 63 Representative images of vimentin IHC staining in KPF, KPF; *Alk5$^{fl/fl}$* and KAF end-point tumours
Representative images of Vimentin IHC stained sections from end-point tumours from KPF, KPF; *Alk5$^{fl/fl}$* and KAF mice. Vimentin is a marker of mesenchymal cells, however, it predominantly marks CAFs within PDAC, as can be seen across the mouse models. (Scale bars = 1mm).

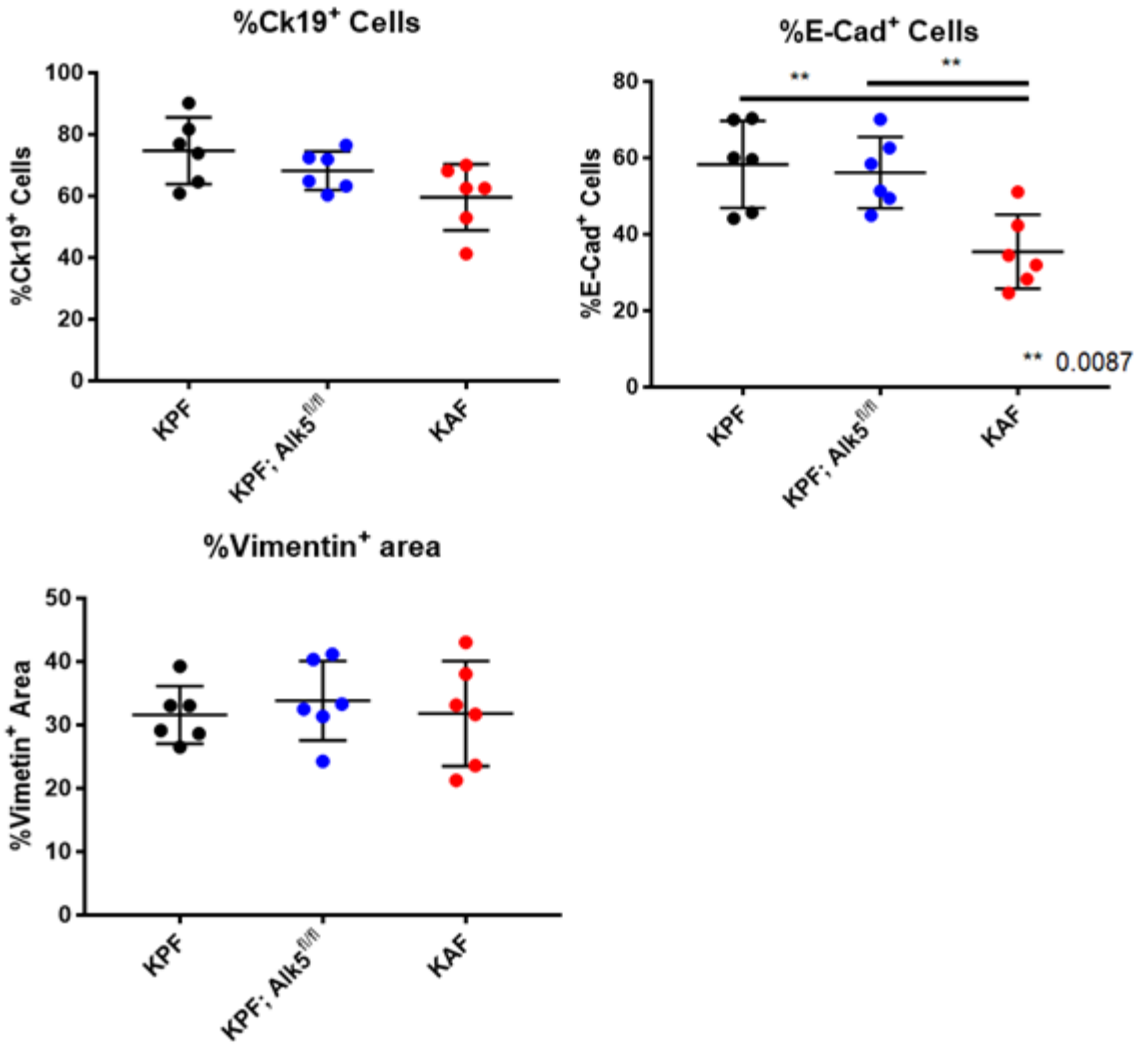

Figure 64 HALO quantification of the epithelial and mesenchymal markers
HALO software was used to determine the percentage of Ck19 or E-cadherin positive cells within *bona fide* tumour regions of the KPF, KPF; *Alk5*$^{fl/fl}$ and KAF mice. Ck19 proportions were unchanged, however, the proportion of E-cadherin positive cells was significantly decrease in the KAF tumours. The vimentin positive area within *bona fide* tumour regions was determined using HALO software, with no significant changes noted across the models. (n=6) (Mann Whitney P-values indicated).

4.4 Discussion

In this chapter, I have highlighted that the KPF and KAF end-point tumours are transcriptionally different. Most notably, the KAF tumours presented with enrichment for p53 pathway genes and the KPF tumours were enriched for EMT genes. Although, the KPF model is an imperfect control for detecting specific transcriptional changes attributable to *Alk5* loss, it does at least provide the basis for comparison to a tumour of known genetic lineage. The KF model can develop PDAC over a long latency; however, the accumulation of unknown genetic permutations during progression had the potential to induce more variability than a model with defined genetic deletion. Nevertheless, the comparison of KPF to KAF however, may have masked the some of the *Alk5* deletion specific changes.

The hallmark gene set of Pancreatic Beta Cells was enriched in the KAF tumours over the KPF tumours. I have shown that this increase was linked to the elevated islet area observed in KAF tumours, which was not caused by expansion of any particular islet cell lineage, as α, ß, δ and ϵ cells showed no significant change in their proportions across tumours. With pancreatic tumours of neuroendocrine lineage generally pan-positive for synaptophysin (Wiedenmann et al., 1986), I comprehensively ruled out KAF tumours originating from endocrine cells. Therefore, the KAF model develops PDAC with end-point tumours histologically similar to those from the KPF mouse model.

Although p53 pathway enrichment in the KAF model was unsurprising, given that the KPF model has a flipped *Trp53* allele and, is likely to have lost the second copy of *Trp53* as reported in the KPC model *(Hingorani et al., 2005)*, it presents a potential therapeutic vulnerability. For instance, it has been shown that restoration of wild-type *TP53* in human PDAC cell lines, increases sensitivity to nutlin3a treatment (Candido et al., 2019), an MDM2 inhibitor, which therefore allows P53 accumulation. Although, the KAF cell lines remained similarly resistant to nutlin3a as the KPF cells, even at high doses, it has previously been shown that nutlin3a synergises well with therapeutic agents such as cisplatin and gemcitabine, particularly in PDAC cells with wild type p53 reintroduced (Candido et al., 2019). Therefore, it would be of interest to examine the effects of combinations of these therapeutics on KAF cell lines and also *in vivo*, with the

KAF model representing a subset of around 2% of PDAC patients (significantly more if patients with mutations in TGFβ pathway genes and intact p53 are included).

CCNG1 has been shown to be a target gene of p53 and to interact with PP2A (Okamoto et al., 1996) with the effect of activating the p53 negative regulator, MDM2. Interestingly, p53 proficient cells overexpressing CCNG1 were reported to exhibit increased growth but were more sensitivity to cisplatin (Smith et al., 1997). A clinical trial of Rexin-G, a retroviral vector that is targeted to sites of collagen deposition and contains a dominant negative mutant version of CCNG1, was recently conducted in stage 4 advanced PDAC. Patients receiving a high dose had a median survival of 9.2 months, compared with 4.3 months at low dose (Chawla et al., 2019) and remarkably, of 15 patients, 12 patients had stable disease, 2 patients had a partial response and one patient remained in remission 12 years after treatment (Morse et al., 2021). I observed significantly elevated gene expression of *Ccng1* in the KAF tumours compared to KPF tumours, and although this did not translate to increased protein, it would be interesting to investigate whether this model would be more responsive to CCNG1 inhibition, particularly if this could be translated to the subset of patients with similar genetic permutations.

The reduction in EMT, noted in the KAF tumours compare to KPF tumours, was perhaps unsurprising given the established links between TGFβ signalling and EMT (Katsuno et al., 2019; Vincent et al., 2009), however, it does very nicely demonstrate that the tumour-suppressive and tumours-promoting TGFβ signalling outputs can be observed within the same model. The increased membranous expression of E-cadherin in the KAF tumours denoted a purely epithelial phenotype, whereas the increased in cytoplasmic E-cadherin, a marker of EMT (Hotz et al., 2007), was apparent in the KPF model. The KAF model was unable to form metastasis, which could be due to the short latency, however, deletion of *Alk5* in established KPF tumour models resulted in a reduction in metastasis, although non-significant. It has been suggested that metastasis is an early event in PDAC development, preceding frank tumour formation (Rhim et al., 2012). This would explain why complete ablation of metastasis was not observed in the KPF: $Alk5^{fl/fl}$ mice. The authors of that study also observed

reduced epithelial markers and elevated mesenchymal markers even within the PanIN lesions and blood borne metastatic cells. However, the KPF; *Alk5*$^{fl/fl}$ tumours present with a similar E-cadherin staining as the KPF tumours, and also, show no significant change in staining for the mesenchymal marker, vimentin. Although it has been reported that suppressing EMT in an autochthonous mouse model of PDAC, through genetic ablation of *Snai1* or *Twist* in epithelial cells , does not reduce metastasis (Zheng et al., 2015), the deletion of *Alk5* may have a more potent role on multiple EMT associated transcription factors, which could go beyond the deletion of just *Snai1* or *Twist*. It remains to be seen if this is the case in the KPF; *Alk5*$^{fl/fl}$ model, with staining for mesenchymal markers such as Snail, Twist, or ZEB1 and ZEB2 required to further investigate reduction in EMT.

EMT has also been shown to contribute to drug resistance, with human PDAC cell lines with reduced expression of EMT pathway genes shown to be sensitive to gemcitabine, fluorouracil and cisplatin (Arumugam et al., 2009). This was further confirmed in models with epithelial deletion of *Snai1* or *Twist,* with gemcitabine notably extending their survival compared with the KPC control mice (Zheng et al., 2015). This is an interesting are for follow up with the KAF model showing a reduction in EMT gene expression testing frontline conventional therapies will be important. However, analysis will be compounded by these tumours being proficient for p53, with human PDAC cells with wild-type p53 more sensitive to cisplatin (Candido et al., 2019). Collectively, increased EMT, CCNG1 and p53 proficiency have been shown to confer sensitivity to, cisplatin, in particular. Therefore, especially with the KAF model replicating the genetics of a subset of human PDAC cases, treatment of these mice with cisplatin would be useful to conduct.

The KAF tumours present with a more ductal morphology characterized by almost completely membranous staining of E-cadherin, alongside enrichment of the Apical Surface gene set and decreased EMT gene set compared to KPF tumours. Interestingly, these tumours also presented with increased collagen. This is perhaps reminiscent of a recent study where depletion of collagen I deposition by αSMA^{+} fibroblasts in a KP$^{Frt/Frt}$F mouse model resulted in a more undifferentiated tumour phenotype (Chen et al., 2021), suggesting that higher levels of stromal collagen can promote tumour differentiation. Depletion of

αSMA fibroblasts also resulted in similar more undifferentiated tumour phenotype (Oezdemir et al., 2014), however, alterations in the fibroblast populations were not observed in the KAF tumours. I also observed in the RNAseq data and GSEA that *Ctgf* was elevated in the KAF tumours. CTGF has been shown to be produced by both cancer cells (Iacobuzio-Donahue et al., 2002) and fibroblasts (Wenger et al., 1999), with TGFß signalling inducing its expression (Gao and Brigstock, 2005). Blockade of CTGF function through monoclonal antibody targeted therapy in the KPC model synergised well with gemcitabine to increase cell death and extend survival of tumour bearing KPC mice (Neesse et al., 2013), with this work translating to clinical trials that have shown moderate success (Picozzi et al., 2014). Whether the increased *Ctgf* levels in the KAF model originate from an increased activation of the stroma would be of interest, particularly if this increase translates to the subset of patients represented by this model.

The transcriptional stratification of the KAF tumour model also provided an interesting result with the ADEX subtype being significantly enriched over the other subtypes. Although *Bailey et al,* suggested their progenitor subtype (which overlaps with the classical subtype defined by *Collisson et al* and *Moffit et al*) was enriched for *Tgfbr2* mutations, indicative of disrupted response to TGFß signalling, this was not sufficient to skew the KAF tumours to a progenitor subtype. Enrichment for the ADEX subtype may indicate an increased expression of markers associated with differentiation, which was confirmed with the elevated expression of the pancreatic beta cell gene set. Patients stratified with an ADEX subtype of tumour have a similar survival to the Progenitor and Immunogenic subtype patients, and a better survival than Squamous subtype patients, although in the KAF model tumours have a rapid onset and survival is reduced. It would be of interest to note whether the KAF tumours are enriched in other published transcriptional subtype gene sets, for instance *Puleo et al,* showed that their ‘pure-classical’ subtype had a more well-differentiated phenotype, more reminiscent to what I note in the KAF tumours, with their ‘pure basal-like’ subtype being more poorly differentiated (Bailey et al., 2016; Collisson et al., 2011; Moffitt et al., 2015; Puleo et al., 2018).

Collectively, this chapter highlights the difference between TGFβ signalling deficient and proficient tumours. With the KAF tumours potentially representing a subset of patients, the therapeutic avenues discussed should be investigating within this model with the ultimate goal of translation to a stratified patient population, although more work is required to justify these targets in the KAF model.

Chapter 5 Role of TGFβ signalling in PDAC CAFs

5.1 Introduction

The TME of PDAC is characterized by a dense desmoplastic stroma, which results in an abundance of ECM deposition (Tian et al., 2019). CAFs play an important role in modulating cancer development with evidence supporting both a restraining and supportive effect on tumour growth (Lee et al., 2014; Oezdemir et al., 2014; Olive et al., 2009; Rhim et al., 2014). Additionally, this dense stromal network impedes therapeutic interventions and creates an immunosuppressive environment for cancer cells to thrive (Hutton et al., 2021; Hwang et al., 2008; Steele et al., 2021). TGFß signalling has been shown to drive fibroblast activation and promote the deposition of ECM components (Schneider et al., 2001; Shek et al., 2002). Intra-tumoural CAF heterogeneity has been recently documented, with three distinct subpopulations named 'myCAFs' (driven by TGFß signalling), 'iCAFs' and 'apCAFs' described (Biffi et al., 2019; Elyada et al., 2019; Ohlund et al., 2017). Gli1 and Hoxb6 have also been shown to mark distinct populations, with $Gli1^{+}$ fibroblasts rare in healthy pancreas but expanding during tumourigenesis (Garcia et al., 2020). I sought to investigate the importance of TGFß signalling in CAF subtypes in tumour initiation and progression using a next generation autochthonous model of PDAC.

5.2 Experimental Aims

Through the abrogation of TGFß signalling, driven by fibroblast specific deletion of *Alk5* or ligand *Tgfb1,* I investigated how this influenced survival and TME composition in the next generation DR model of PDAC. This allowed for the deletion of *Alk5* or *Tgfb1* within established tumours and at early initiating stages specifically targeted to the fibroblast populations via fibroblast promoter driven expression of tamoxifen inducible CRE-recombinase. I used two fibroblast specific promoters, *Gli1* and *Col1a2,* to drive expression of CRE-recombinase, which caused deletion in a restricted fibroblast population and pan-fibroblast population respectively.

5.3 Results

5.3.1 Utilising the next generation DR mouse model to investigate TGFβ signalling specifically in fibroblasts

To interrogate TGFß signalling specifically in fibroblasts I crossed the KPF mice with mice expressing the *Gli1-Cre^{ER}* allele (KPF^{G}) (**Figure 65**) (Ahn and Joyner, 2004). The *Gli1* promoter drives expression of tamoxifen inducible CRE-recombinase in cells that expressed Gli1 only. *Gli1* was expressed specifically in fibroblasts within PDAC with cancer cells producing SHH ligand (Bailey et al., 2008; Garcia et al., 2020). This model was also crossed with the *Alk5* floxed allele (Larsson et al., 2001) or the *Tgfb1* floxed allele (Azhar et al., 2009) discussed previously (**Figure 65**), thereby, permitting targeted deletion of these genes specifically in Gli1 positive fibroblast populations.

In order to confirm fibroblast specific expression of the CRE-recombinase I also crossed these mice with mice expressing the GFP/Tomato switch construct (as described in **Figure 7 (Chapter 3**). GFP was noted across the whole pancreas only in mice that had the construct (R26^{+}), but not in the pancreas of mice that did not express the construct (R26^{-}). Upon tamoxifen administration, GFP but very little tomato fluorescence was observed in the pancreas, due to the *Flippase* expression in pancreatic lineage cells only, which were the predominant population in the normal pancreas. There was no tomato fluorescence observed, which was expected as only fibroblasts expressed the CRE-recombinase required to excise GFP and allow tomato to be expressed, and in the normal pancreas, fibroblasts are a low abundance population, meaning we were unlikely to detect significant fluorescence by IVIS (**Figure 66**).

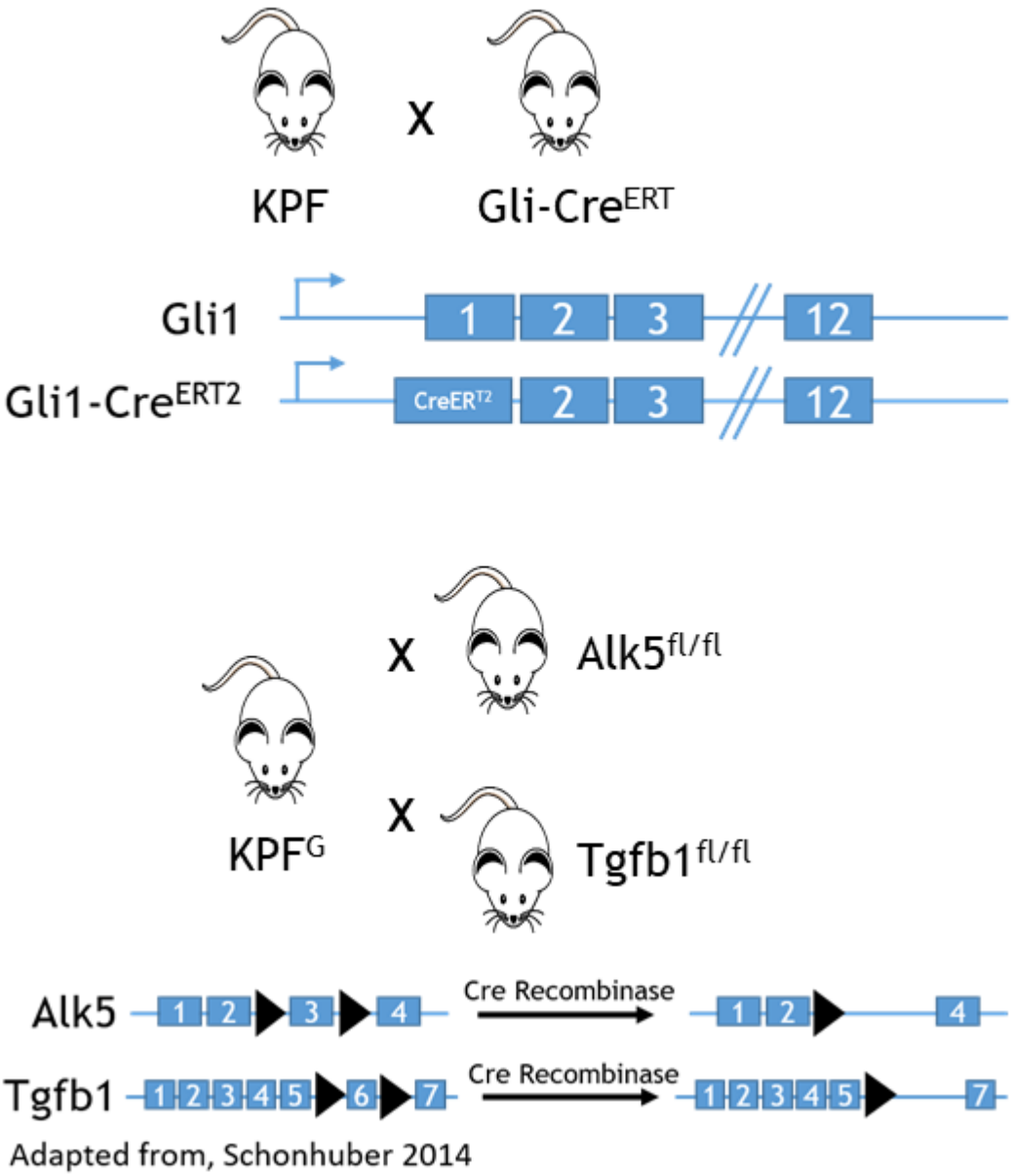

Figure 65 Fibroblast specific expression of CRE recombinase
The KPF mouse model was crossed to mice expressing the Gli1 driven tamoxifen inducible CRE recombinase allele. This allele replaces exon 1 of the endogenous *Gli1* gene with *CreER^{T2}* thereby driving expression of the CRE recombinase in Gli1 positive cells only. The KPF^{G} mice were then crossed with mice expressing either the *Alk5$^{fl/fl}$* or *Tgfb1$^{fl/fl}$* allele to drive deletion of these genes in Gli1 positive cells only.

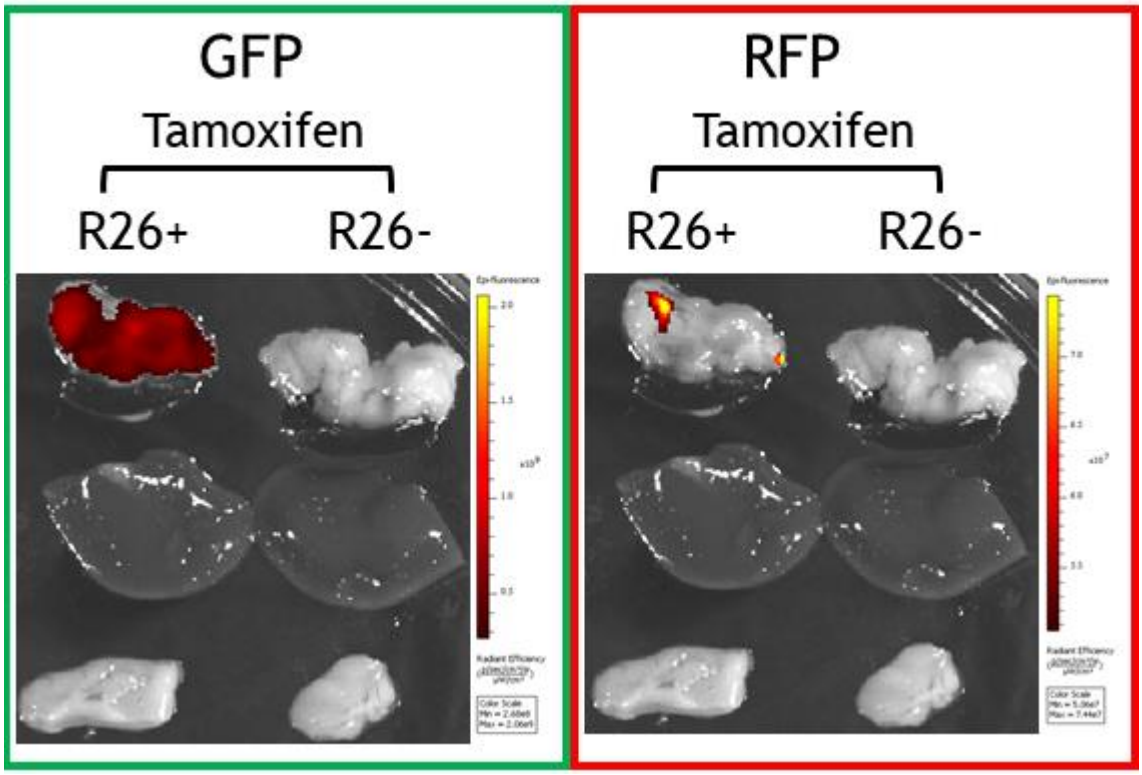

Figure 66 IVIS imaging of GFP and RFP in the pancreata of mice bearing the reporter
Representative images of the pancreas, spleen, liver and mammary fat pad imaged on the IVIS. GFP expression was detected only in the pancreas and restricted to the tissue that had the GFP/Tomato reporter construct (R26+) but not the tissue that was negative for this reporter construct (R26-). Fibroblast specific expression of RFP cannot be detected after tamoxifen administration due to the low proportion of affected cells.

Staining for GFP and RFP was also conducted on pancreatic tissue from the *Pdx1-Flp; Kras^{WT}; p53^{WT}* mouse model following a short-term induction. Mosaic expression of GFP was observed across acinar cells and islets (**Figure 67**), but no RFP expression was detected (**Figure 68**). This confirms appropriate expression of Pdx1-driven Flippase in the pancreatic tissue causing GFP expression. However, CRE-Recombinase was not expressed in the pancreatic tissue, as Gli1 expression was restricted to fibroblasts and therefore tomato positive cells were not detected in pancreatic lineage cells. However, tomato positive fibroblasts could not be visualised in the wild type pancreas either, even in perivascular regions where Gli1 positive fibroblasts have been proposed to be found in normal pancreatic tissue (Garcia et al., 2020). The lack of RFP staining is most likely due to the low prevalence of fibroblasts in normal pancreatic tissue (**Figure 68**).

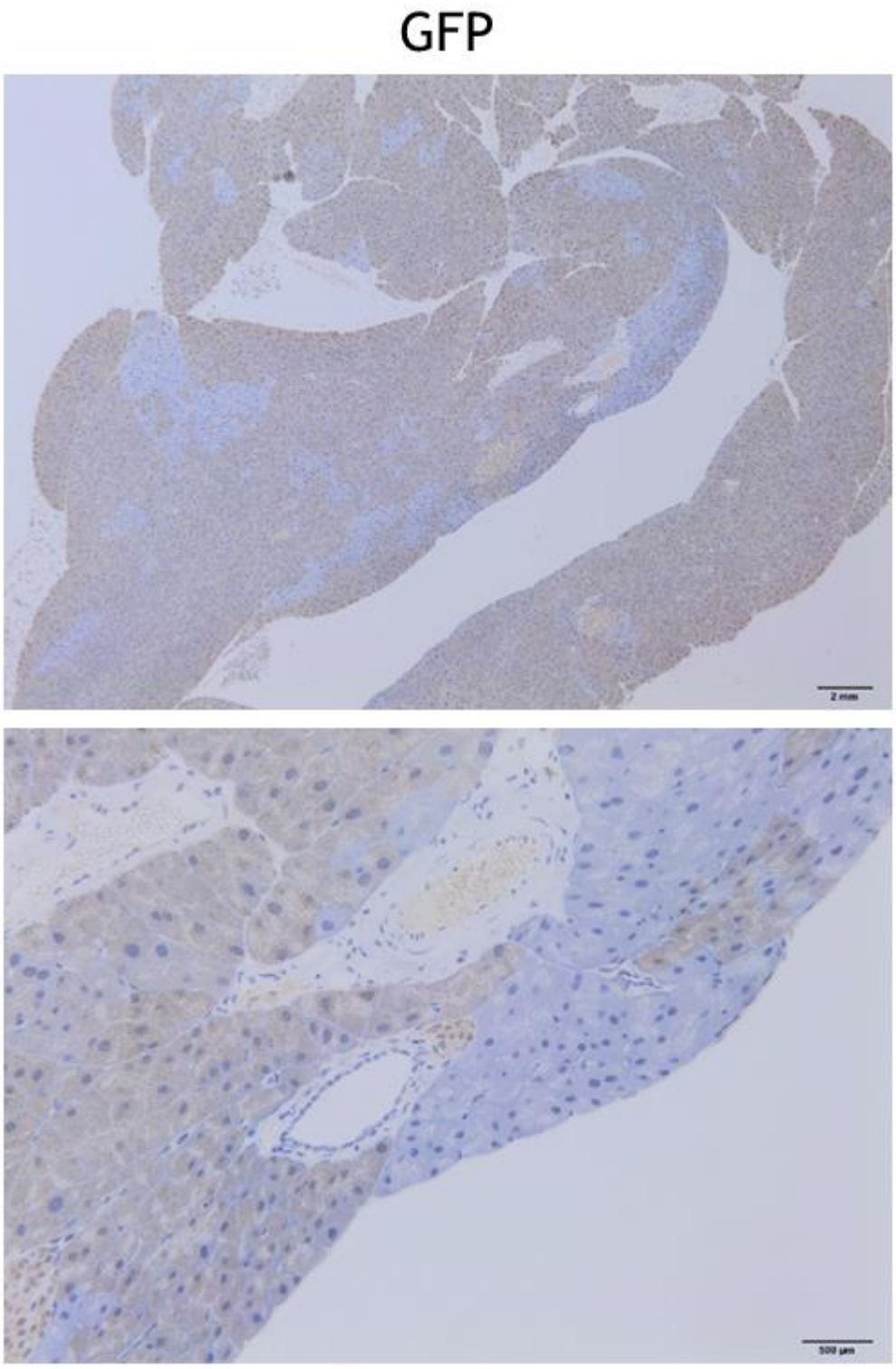

Figure 67 GFP expression was restricted to Flippase expressing pancreatic cells
Representative images of GFP IHC stained pancreata harvested from *Pdx1-Flp; Gli1-Cre^{ERT2}* mice 4 days post tamoxifen induction. GFP expression is restricted to the pancreatic lineage cells. (Top Scale bar = 2mm, Bottom scale bar = 500μm).

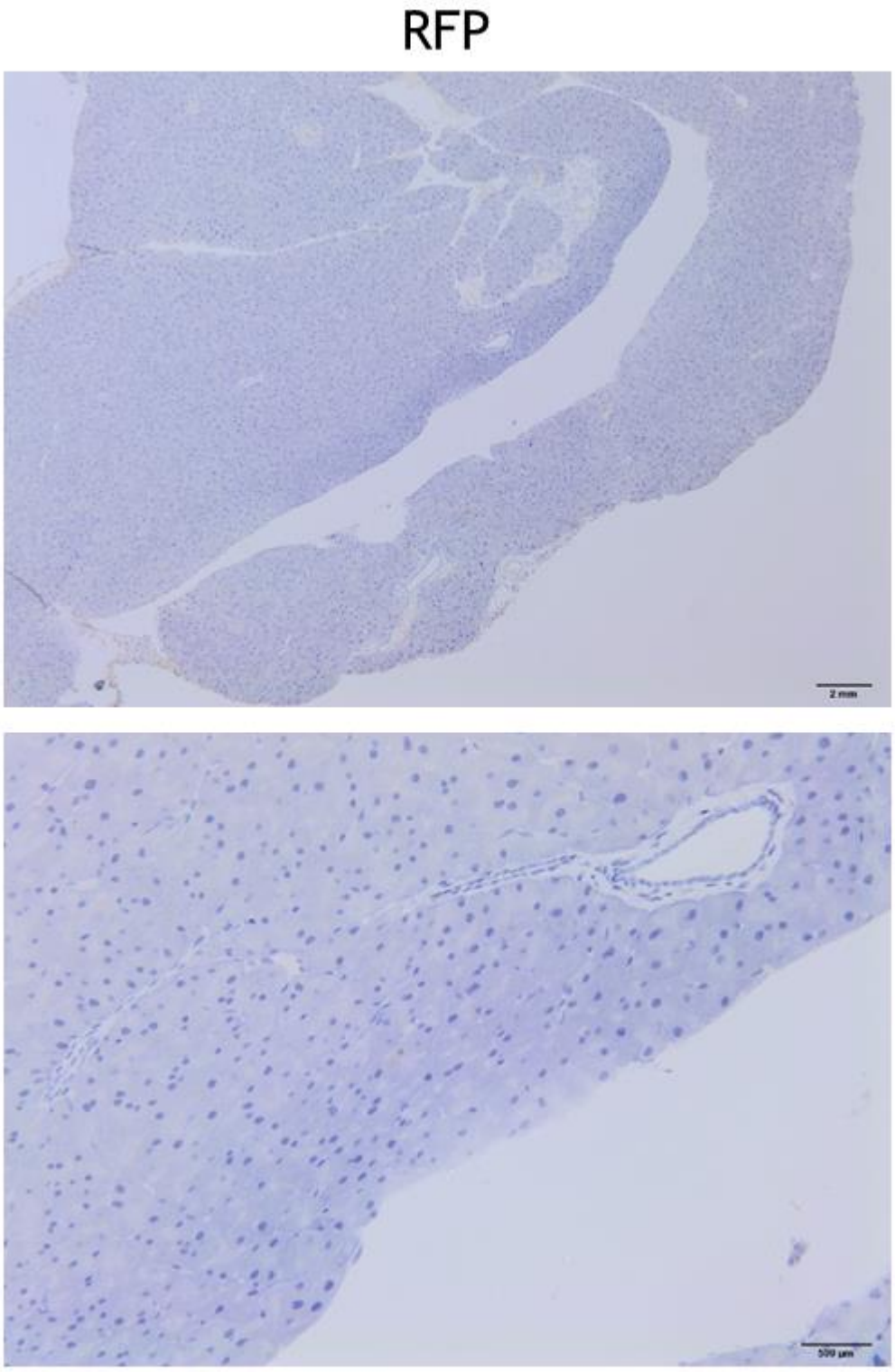

Figure 68 RFP expression is not detected in the pancreas
Representative images of RFP IHC stained pancreata harvested from the *Pdx1-Flp; Gli1-Cre^{ERT2}* model 4 days post tamoxifen induction. RFP was not visible across the pancreas. (Top Scale bar = 2mm, Bottom scale bar = 500µm).

Therefore, to visualise fibroblast specific RFP expression, I conducted staining in tumour tissue, which is infiltrated with abundant fibroblasts, from KPF^{G} mice with the GFP/tomato switch construct. It was apparent that in mice expressing the construct, GFP positive staining was visible in the transformed epithelial tissue but not in the stromal beds surrounding the tumour cells, further indicating tumour cells arise from the Pdx1 positive Flippase expressing cells and validating the specificity of the system (**Figure 69**). Tomato positive staining was found within the stromal tissue and only upon tamoxifen administration, indicative of fibroblast specific expression of the CRE-recombinase, which is controllable via tamoxifen (**Figure 70**).

Further confirmation of fibroblast specific expression of CRE-recombinase was shown via positive staining for CRE in a fibroblast specific pattern in the KPF^{G} model (**Figure 71**). Control tissue-expressing Pdx1 driven CRE-recombinase highlights an islet and tumour cell specific staining, as expected (Top left panel). Regardless of the *Tgfb1*/*Alk5* status in the KPF^{G} mice CRE expression was noted in the tumours, however, the staining appears to mark only a subset of the total fibroblasts, given the abundance of fibroblasts normally present in KPF tumours. This would be in agreement with recently published data indicating that $Gli1^{+}$ fibroblasts make up a subpopulation of 'myCAFs' in pancreatic cancer (Steele et al., 2021).

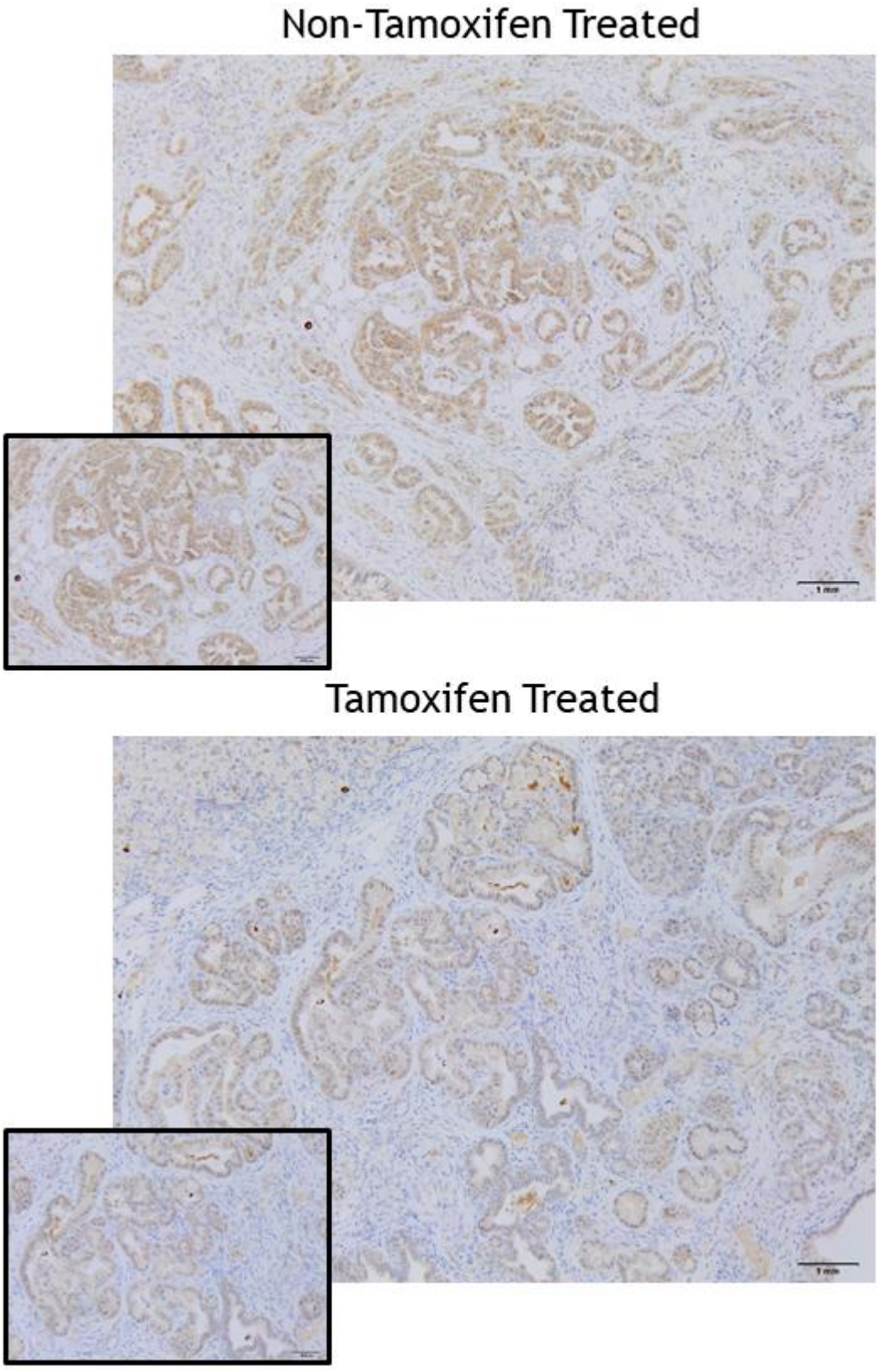

Figure 69 GFP expression is restricted to the epithelium in KPF^{G} mice
Representative images of GFP IHC stained KPF^{G} end-point tumour tissue. GFP staining was positive in the epithelial cells specifically and was found regardless of tamoxifen administration. (Scale bars = 1mm, inset scale bar = 500μm).

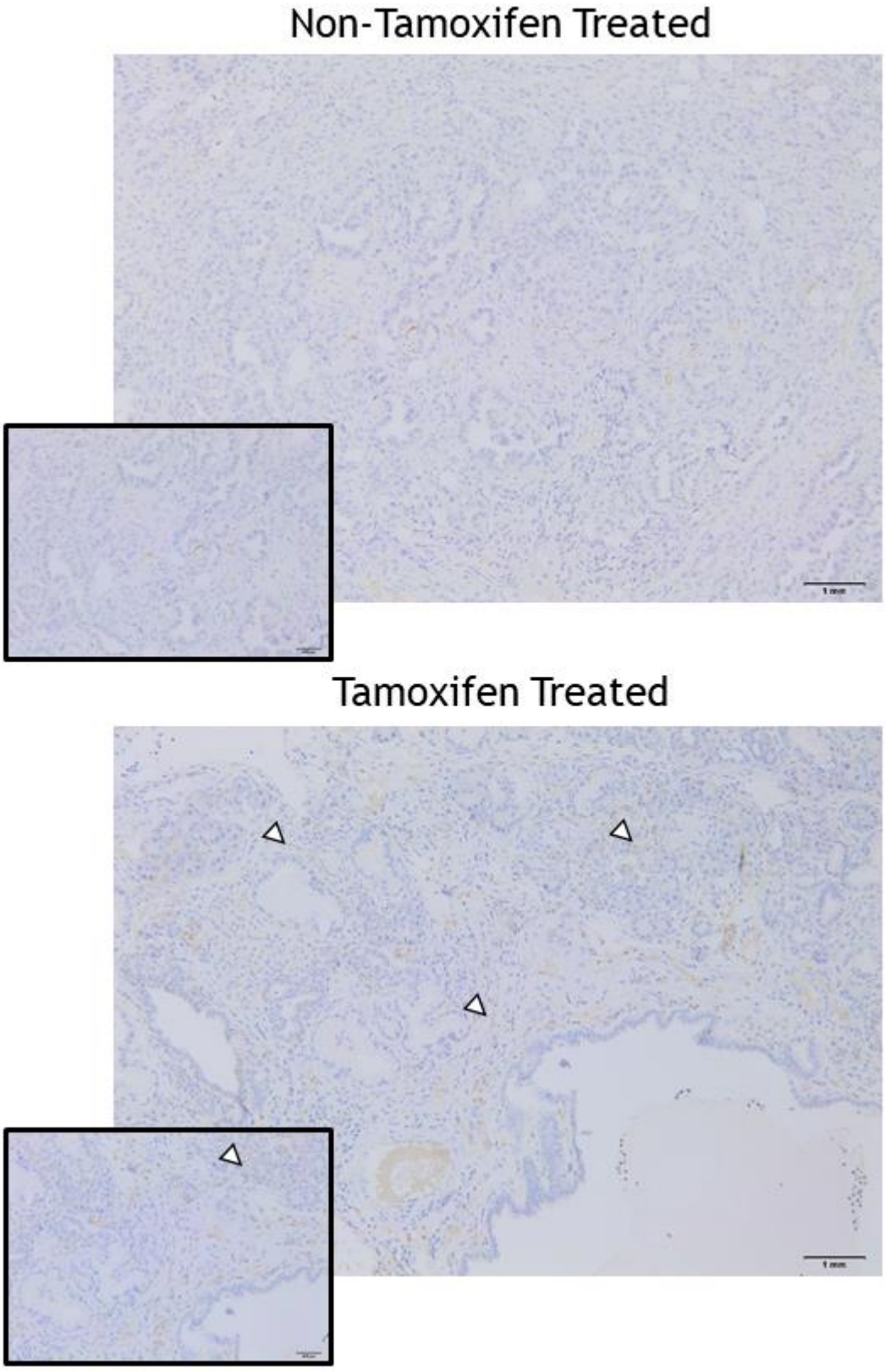

Figure 70 Tamoxifen administration drives RFP expression in CRE expressing fibroblasts
Representative images of RFP IHC stained KPF^{G} end-point tumour. RFP staining was weak but as indicated by the arrow-heads stained specifically in stromal areas and only in mice induced with tamoxifen. (Scale bars = 1mm, inset scale bar = 500µm).

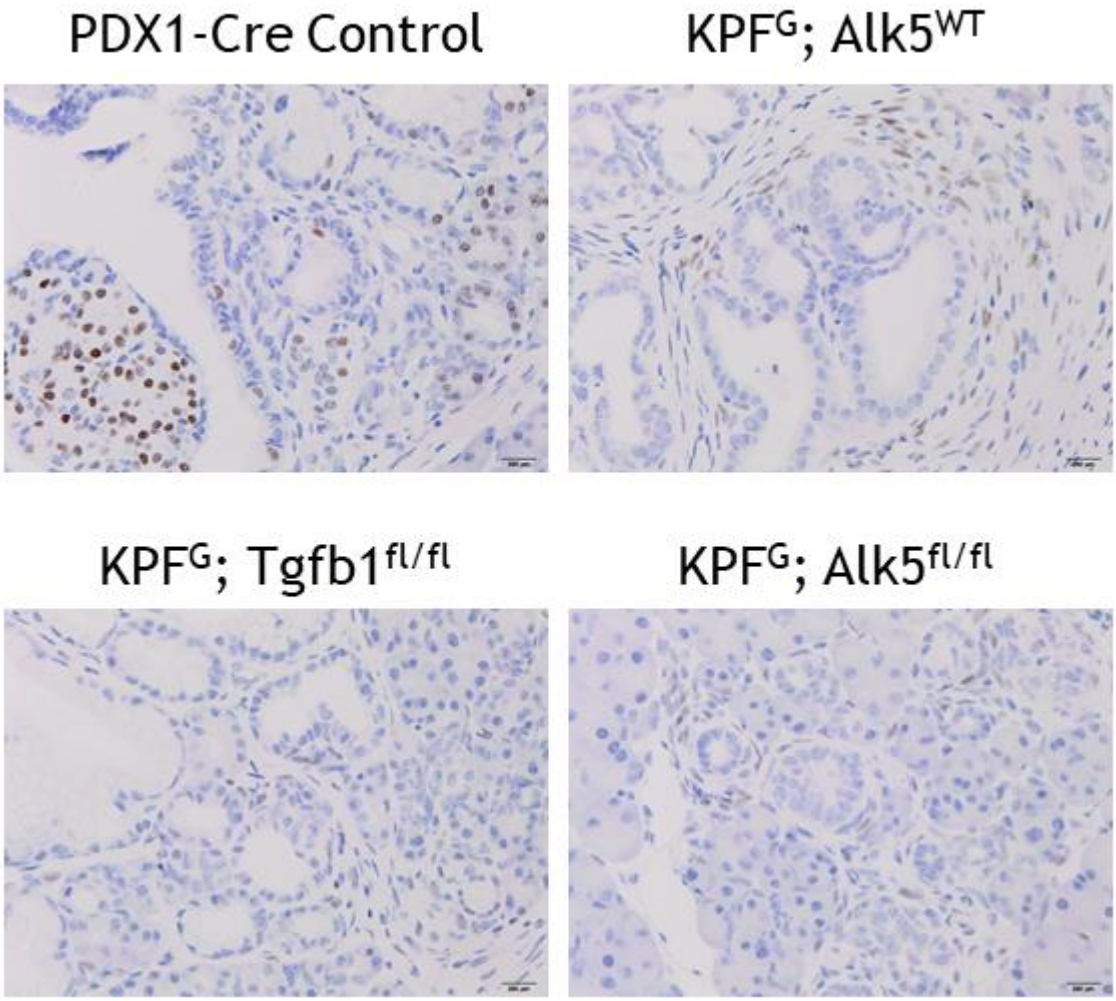

Figure 71 CRE recombinase is expressed specifically in fibroblasts in *Gli1-CreER* mouse models
Representative images of CRE-recombinase IHC stained tissue sections from KPF^{G} mice, which were induced with tamoxifen with tumours sampled at clinical end-point. The top left panel shows tissue from a *Pdx1-Cre; Kras$^{LSL-G12D/+}$; Alk5$^{fl/fl}$* mouse and demonstrates tumour cell and islet cell specific CRE-recombinase staining. KPF^{G} tissue was positive for CRE-recombinase in the stromal areas but not the epithelial areas of the PDAC and positive staining was independent of the floxed allele.(Scale bars = 200μm).

Combined, I have shown that Gli1 driven expression of CRE-recombinase permits specific targeting of a subset of the tumour infiltrating fibroblasts in the KPF^{G} model.

5.3.2 Gli1$^+$ fibroblast specific deletion of *Alk5* or *Tgfb1* in established tumours does not impact on survival in the KPF mouse model

Upon confirmation that CRE-recombinase was expressed in a fibroblast specific manner, I sought to investigate how the deletion of *Alk5* or *Tgfb1* would affect tumour maintenance in the KPF^G mice. I therefore palpated and confirmed the presence of PDAC in KPF^G mice before administration of tamoxifen. I subsequently followed tumour progression with weekly ultrasounds, until clinical end-points were reached. I observed no significant changes in tumour growth post tamoxifen induced deletion of either *Alk5* or *Tgfb1* compared with induced control mice (**Figure 72**). In agreement with the ultrasound data, the survival of the KPF mice was unchanged in both the *Alk5* heterozygous deleted and *Tgfb1 Gli1-cre* models in comparison to control induced KPF mice (**Figure 73**). However, the homozygous deletion of *Alk5* in Gli1$^+$ fibroblasts resulted in a slight reduction in survival, post tamoxifen induction, when compared to the KPF^G mice (median survival 16 vs 10 days).

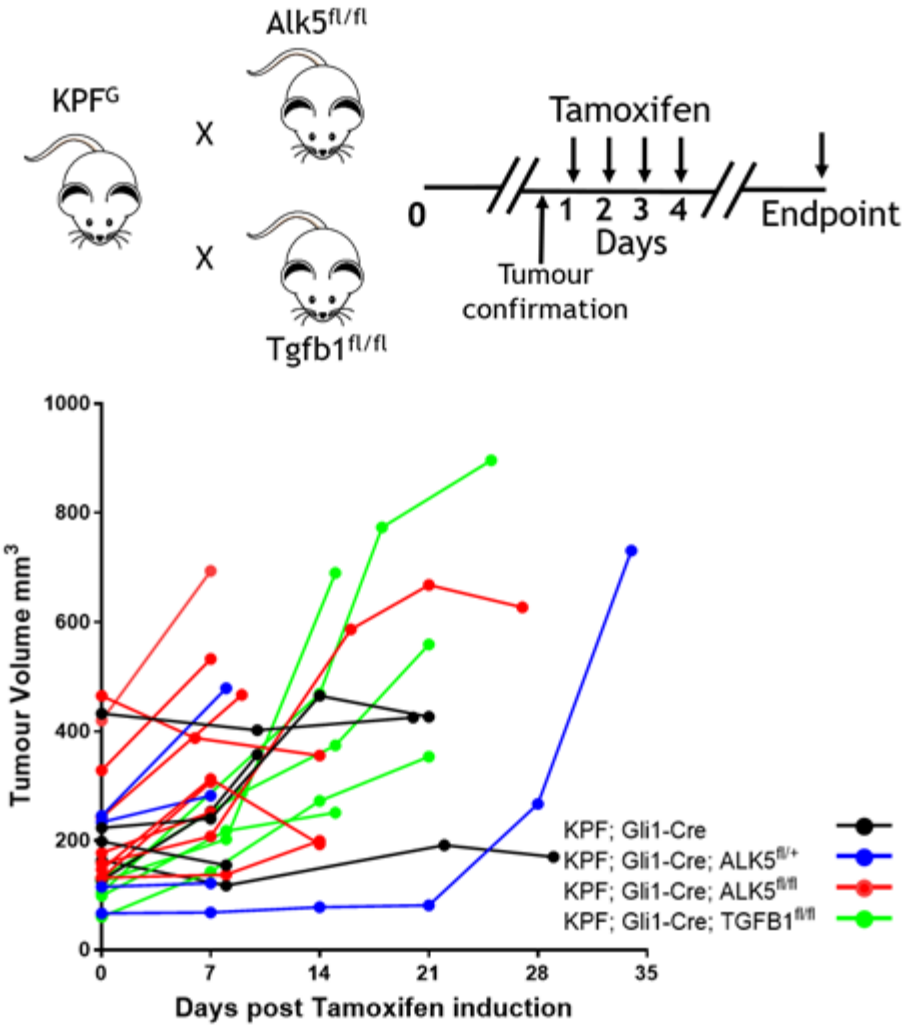

Figure 72 Deletion of *Alk5* or *Tgfb1* does not affect the growth of KPF^{G} tumours
Upon detection of palpable tumours in KPF^{G} mice, ultrasound was used to confirm and measure tumour volume before commencing tamoxifen induction. The top panel shows the treatment regimen the mice followed upon detection of a palpable tumour. An abdominal US was conducted weekly on tamoxifen induced mice and tumour volume was calculated to track tumour growth. Deletion of *Alk5* or *Tgfb1* in Gli1^{+} fibroblasts had no impact on tumour growth.

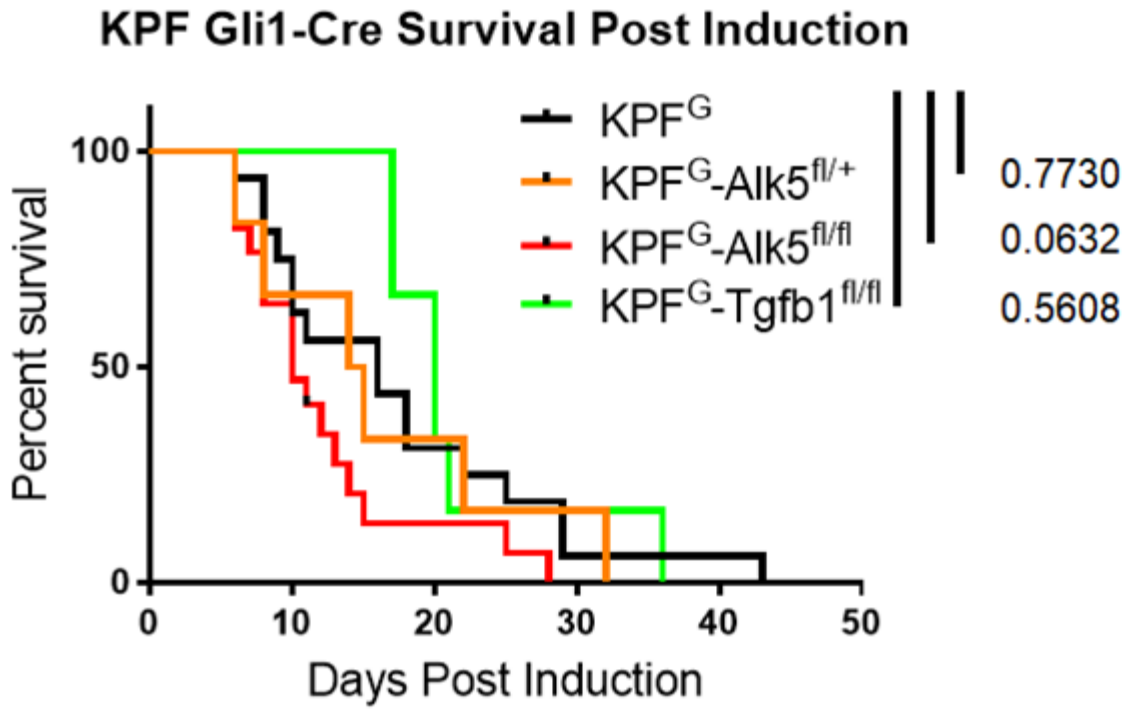

Figure 73 Gli1-cre^{ER} driven deletion of *Alk5* but not *Tgfb1* reduces survival of KPF mice
Kaplan-Meier survival analysis of KPF^{G}, KPF^{G}; *Alk5*$^{fl/+}$; KPF^{G}; *Alk5*$^{fl/fl}$ and KPF^{G}; *Tgfb1*$^{fl/fl}$ mice. Upon detection and confirmation via ultrasound of a palpable tumour, mice were induced with tamoxifen. Heterozygous deletion of *Alk5* or homozygous deletion of *Tgfb1* does not change the survival in comparison to the KPF^{G}, however, homozygous deletion of *Alk5* slightly reduces survival (N=6, 6, 16, 16, respectively, Median Survival= 15, 20, 16 and 10 days post induction respectively).

A proportion of the KPF mice presented with metastasis to the liver and the lungs at end-point, and with fibroblast depletion studies highlighting more invasive disease, we therefore sought to examine if perturbation of the Gli1^{+} fibroblast population would affect the metastatic burden in these models. Representative images of both liver and lung metastasis in the various models is shown in **Figure 74**. Metastasis was unchanged when *Alk5* was deleted in the Gli1^{+} population in comparison to the wild type (**Figure 75**). However, it was interesting to note that metastasis to the liver occurs more frequently when *Tgfb1* was deleted in the Gli1^{+} fibroblast population.

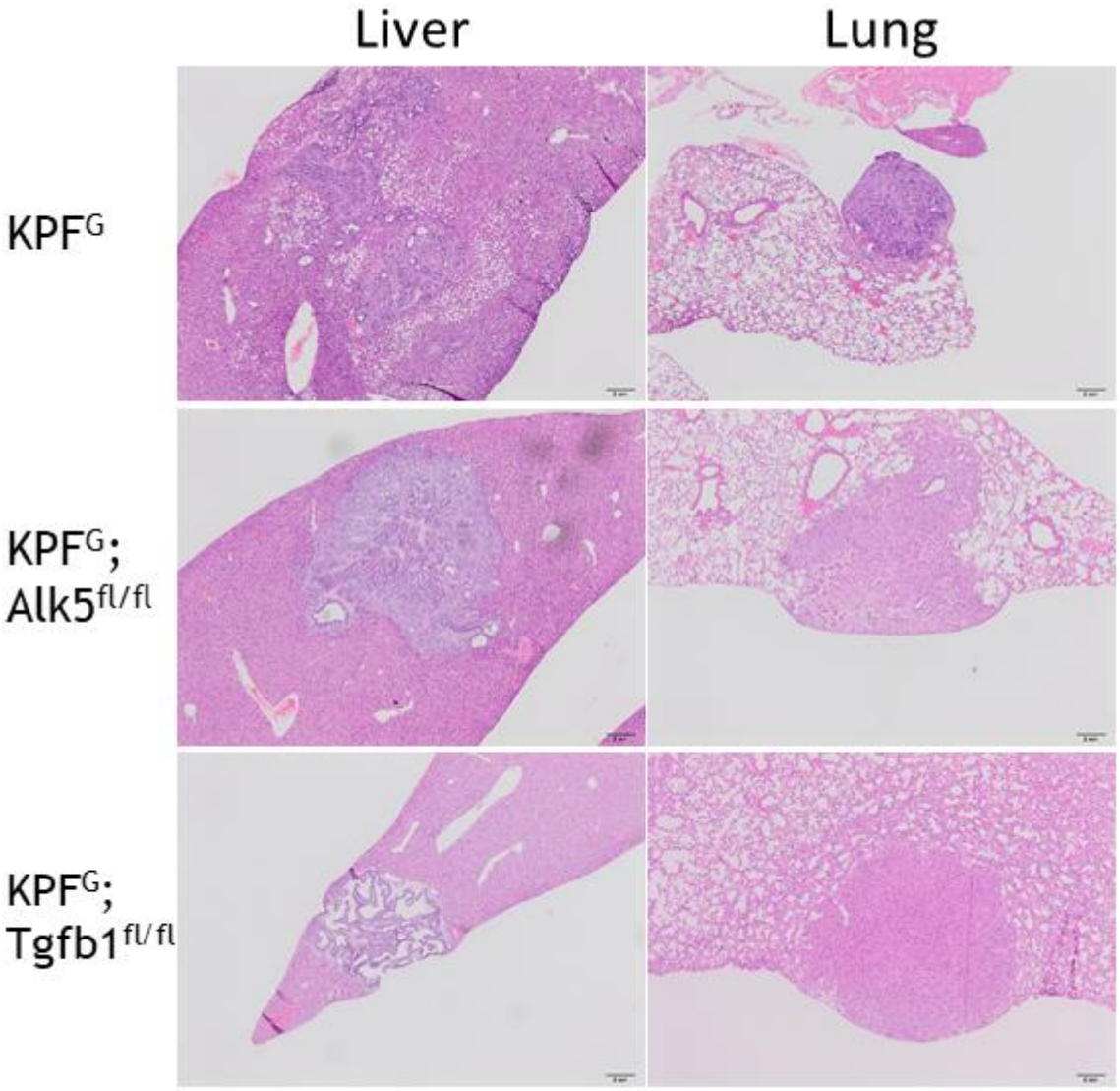

Figure 74 Representative images of H&E stained metastatic lesions in the KPF^{G} mice
Representative images of H&E stained metastatic lung and liver tissue sections from KPF^{G}, KPF^{G}; *Alk5$^{fl/fl}$* and KPF^{G}; *Tgfb1$^{fl/fl}$* mice which were induced following detection of a palpable tumour. Metastatic lesions were distinguishable from the normal tissue architecture due to their ductal morphology. (Scale bars = 2mm).

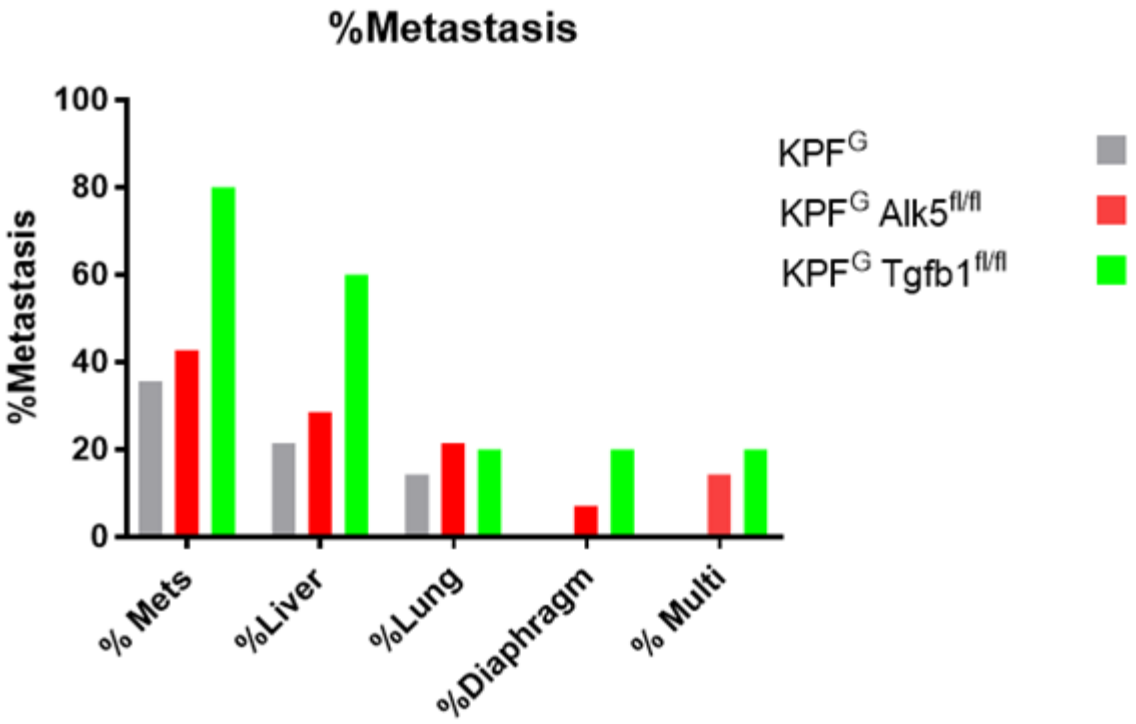

Figure 75 KPF^{G}, KPF^{G}; *Alk5$^{fl/fl}$* and KPF; *Tgfb1$^{fl/fl}$* mice had no significant change in metastasis

The percentage of mice presenting with macro- or micro-metastasis to the various sites is shown. % Mets denotes the presence of metastasis, with % liver, % lung and % diaphragm reporting the presence of organ specific metastasis. % Multi denotes mice presenting with concurrent metastasis to multiple sites. (n= 14, 14, 5, respectively) (Fisher's exact Test used).

5.3.3 Gli1^{+} fibroblast specific deletion of *Alk5* or *Tgfb1* in PanINs in the KF mouse model

Subsequently, I investigated if fibroblast specific deletion of *Alk5* or *Tgfb1* would influence pre-neoplastic lesion development. Therefore, KF^{G} mice were induced at 6 weeks of age and sampled 7 days post induction, with PanINs counted from H&E stained tissue sections (**Figure 76**). Quantification of the PanINs showed no change in the abundance of PanIN-1 or PanIN-3 lesions, however PanIN-2 lesions were significantly increased in the KF^{G}; *Tgfb1*$^{fl/fl}$ mice compared to the KF^{G} controls, and there was also a trend towards increased PanIN-1s in this model (**Figure 77**). Representative H&E images from time-point KF^{G} mice show that across the genotypes stromal composition remains largely similar, with no obvious alterations to the rest of the pancreas noted (**Figure 78**).

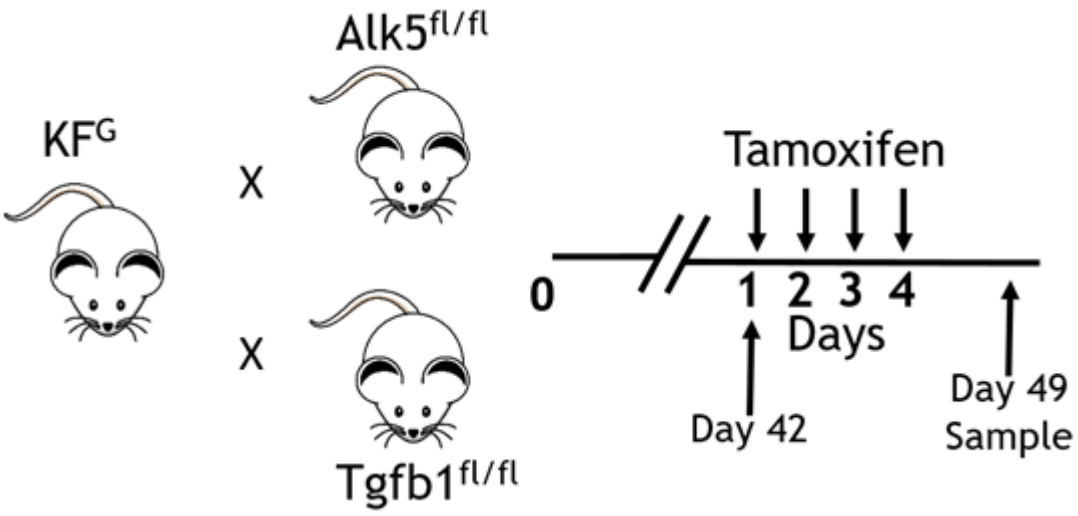

Figure 76 Short-term induction regime in KF^{G} mouse models
The KF^{G} mouse was crossed with mice expressing either *Alk5*$^{fl/fl}$ or *Tgfb1*$^{fl/fl}$ alleles and at 6 weeks of age tamoxifen was administered before sampling a week post-induction start date.

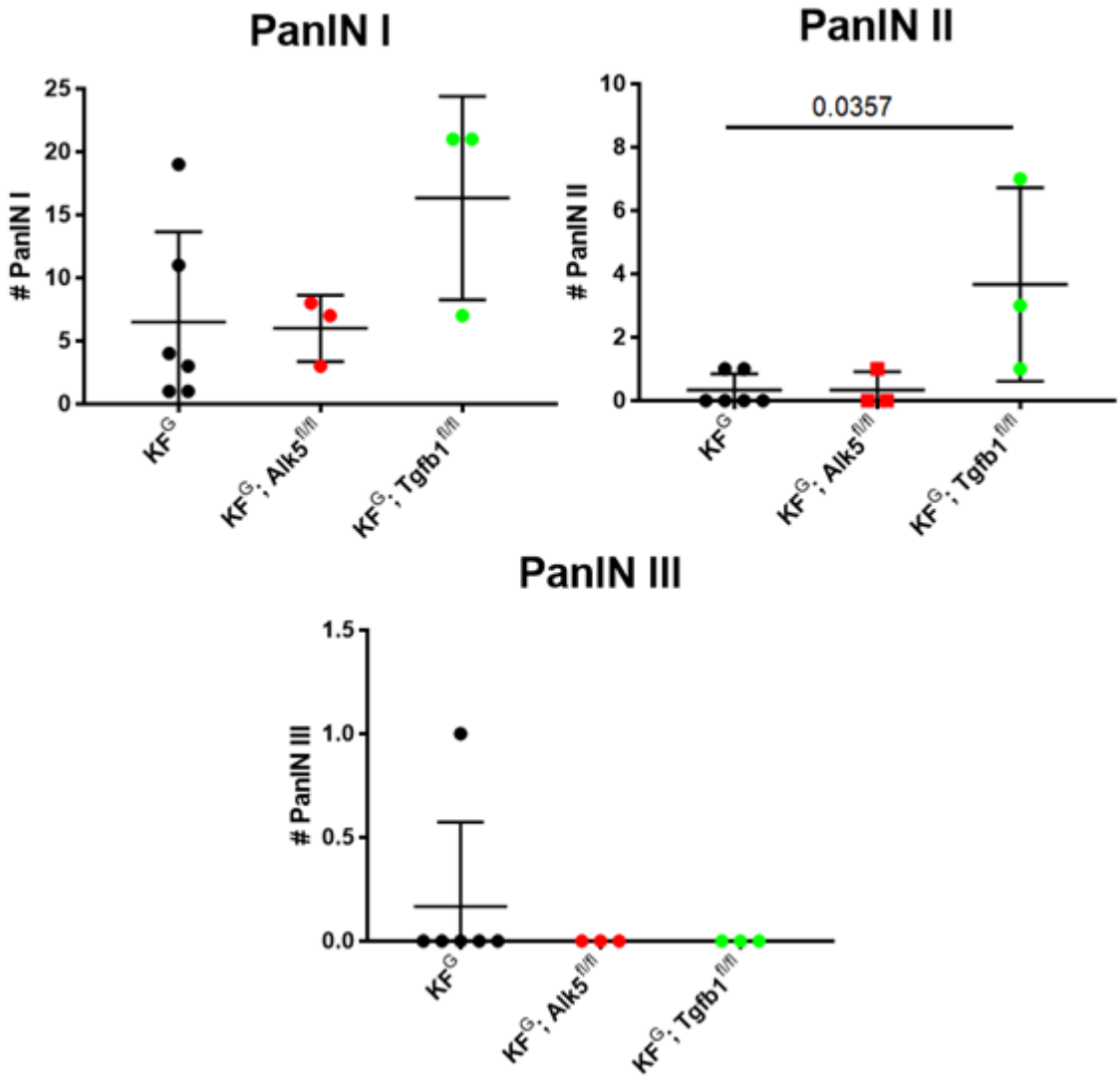

Figure 77 Gli1 driven deletion of *Tgfb1* but not *Alk5* increases PanIN-II burden compared to KF mice
Quantification of total number of PanINs counted in time point KF^{G}; KF^{G}; $Alk5^{fl/fl}$ or KF^{G}; $Tgfb1^{fl/fl}$ mice across one H&E stained pancreas tissue slide from an individual mouse with the total number of PanIN I, PanIN-II or PanIN-III counted across the whole tissue. (n= 6, 3, 3, respectively. Mann Whitney P values indicated).

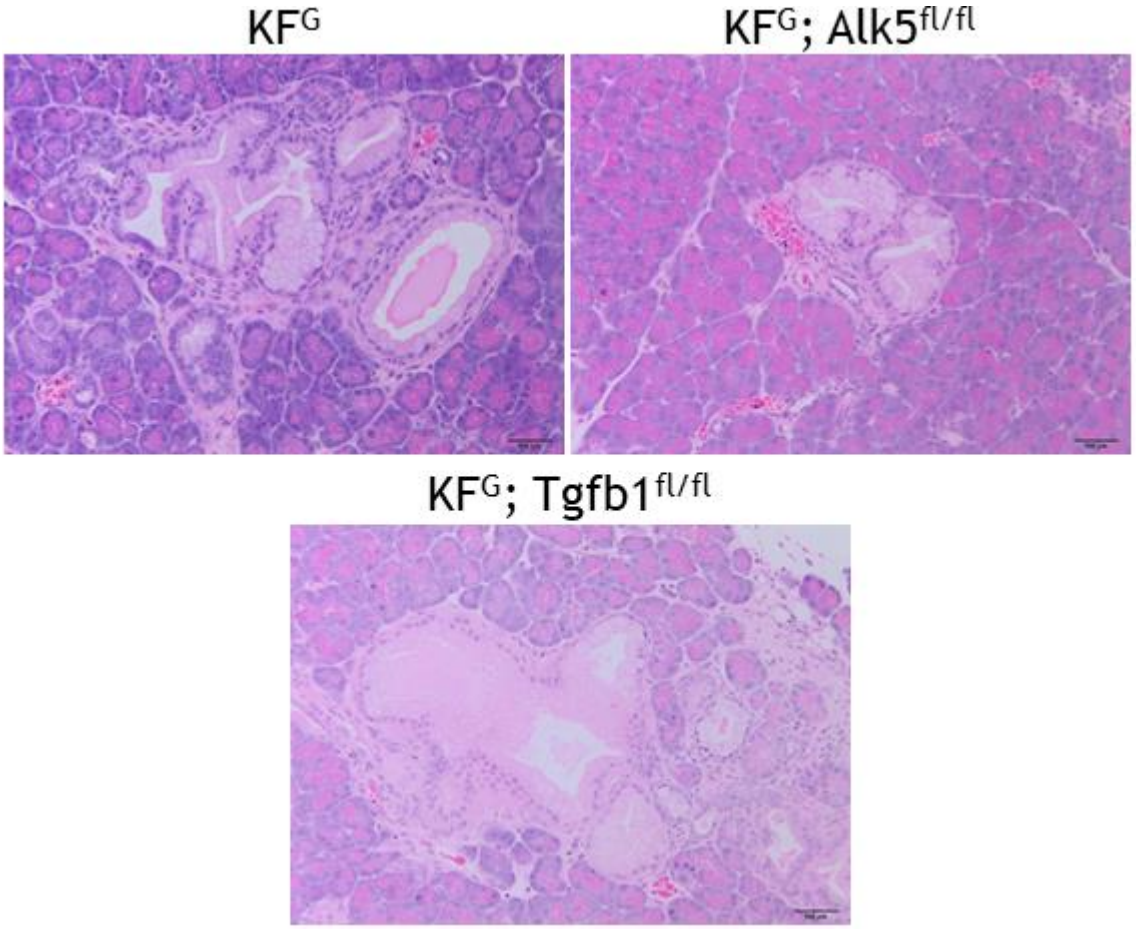

Figure 78 Representative images of H&E stained PanINs in KF^{G} models
Representative images of H&E stained tissue sections. Images of PanIN lesions across the various genotypes of the KF^{G} model sampled at 7 weeks of age, 1-week post tamoxifen induction, are shown. (Scale bars = 500μm).

Further, the proliferation of the PanINs was measured via IHC staining of Ki67. Representative images highlight that proliferative cells are present within the epithelial components of the PanIN regions, and the number of positive and negative cells in the epithelium were counted specifically to calculate the proportion of Ki67 positive cells per PanIN (**Figure 79**). Quantification is shown in the bottom graphs of **Figure 80** with the left graph showing the average proportion of Ki67 positive cells in PanINs across the whole tissue section per mouse. Through this analysis, there was no significant change in Ki67 PanIN staining proportion across the cohorts, although PanINs in KF; *Tgfb1*$^{fl/fl}$ mice had a slightly elevated Ki67 proportion compared to KF controls. The right hand graph shows the proportion of Ki67^{+} cells across all PanINs counted in all of the mice of each genotype. When analysed in this way there was a small but significant increase in the proportion Ki67^{+} cells when *Tgfb1* was deleted specifically from the Gli1^{+} fibroblasts.

Accompanying this proliferation count, I also performed a count of apoptosis within the PanIN cells specifically via staining for cleaved caspase 3. The representative images highlight that a very low proportion of the epithelial cells are undergoing apoptosis in these early PanIN lesions. This was further demonstrated by the quantification, highlighting a low percentage of PanIN cells positive for cleaved caspase 3, with a large proportion of PanINs having no positive staining. There was no significant differences in cleaved caspase 3 staining across the PanINs, counted either as an average per mouse or an average per PanINs, between the KF^{G} cohorts (**Figure 80**).

Next, I investigated the level of senescence in the PanIN lesions via staining for p21. With TGFß signalling shown to play a role in the senescence associated secretory phenotype, and to be a driver of senescence (Acosta et al., 2013), I investigated if loss of this signalling pathway or the ability to produce ligand in Gli1^{+} fibroblasts would affect the PanIN lesions. PanIN cells staining positive for p21 were counted as performed for the Ki67 staining, with the proportion of p21 positive cells elevated in the KF^{G}; Alk5$^{fl/fl}$ cohort, which was significant when counting across all PanINs. When averaged per mouse, p21 appears elevated in the KF^{G}; Alk5$^{fl/fl}$ PanINs in comparison to the KF^{G} and KF^{G}; Tgfb1$^{fl/fl}$ mice, although not significantly so (**Figure 81**). Although TGFß has been shown to drive

senescence, the lack of the ligand produced by Gli1$^+$ fibroblasts does not appear sufficient to cause a decrease in the senescence of the PanIN cells, suggesting that there still exists sufficient ligand in the early microenvironment from alternate sources or other mechanisms of senescence are sufficient to compensate. However, the lack of the Alk5 receptor on Gli1$^+$ fibroblasts does elevate senescence in the PanIN cells, perhaps indicating a feedback loop through Alk5 signalling on these fibroblasts, which can induce senescence via increased TGFβ1 production.

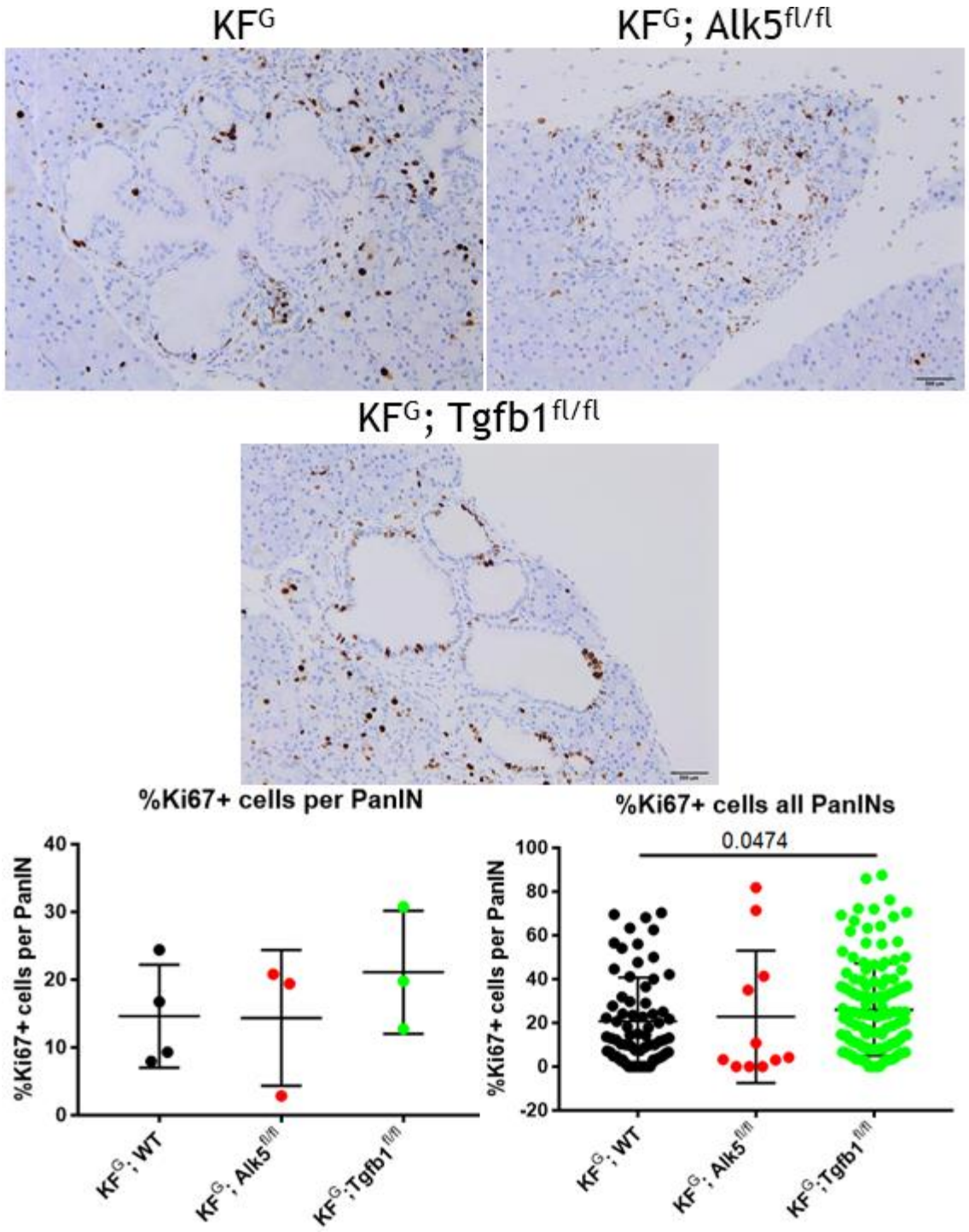

Figure 79 Ki67 staining on KF^G PanINs
Representative images of Ki67 IHC staining on PanIN bearing pancreatic tissue from time point KF^G, KF^G; *Alk5$^{fl/fl}$* and KF^G; *Tgfb1$^{fl/fl}$* mice (Scale bars = 500μm). Quantification of the % of Ki67$^+$ cells per PanIN counted across all PanINs present in the time points is shown in the right graph, with KF^G; *Tgfb1$^{fl/fl}$* PanINs having a significantly increased proportion of Ki67 per PanIN. The left graph shows the average proportion of Ki67$^+$ cells per PanIN per mouse. (n= 4, 3, 3, respectively). There was no significant change in the proportion of Ki67$^+$ cells when analysed across individual mice. (Mann Whitney test used, significant P values indicated).

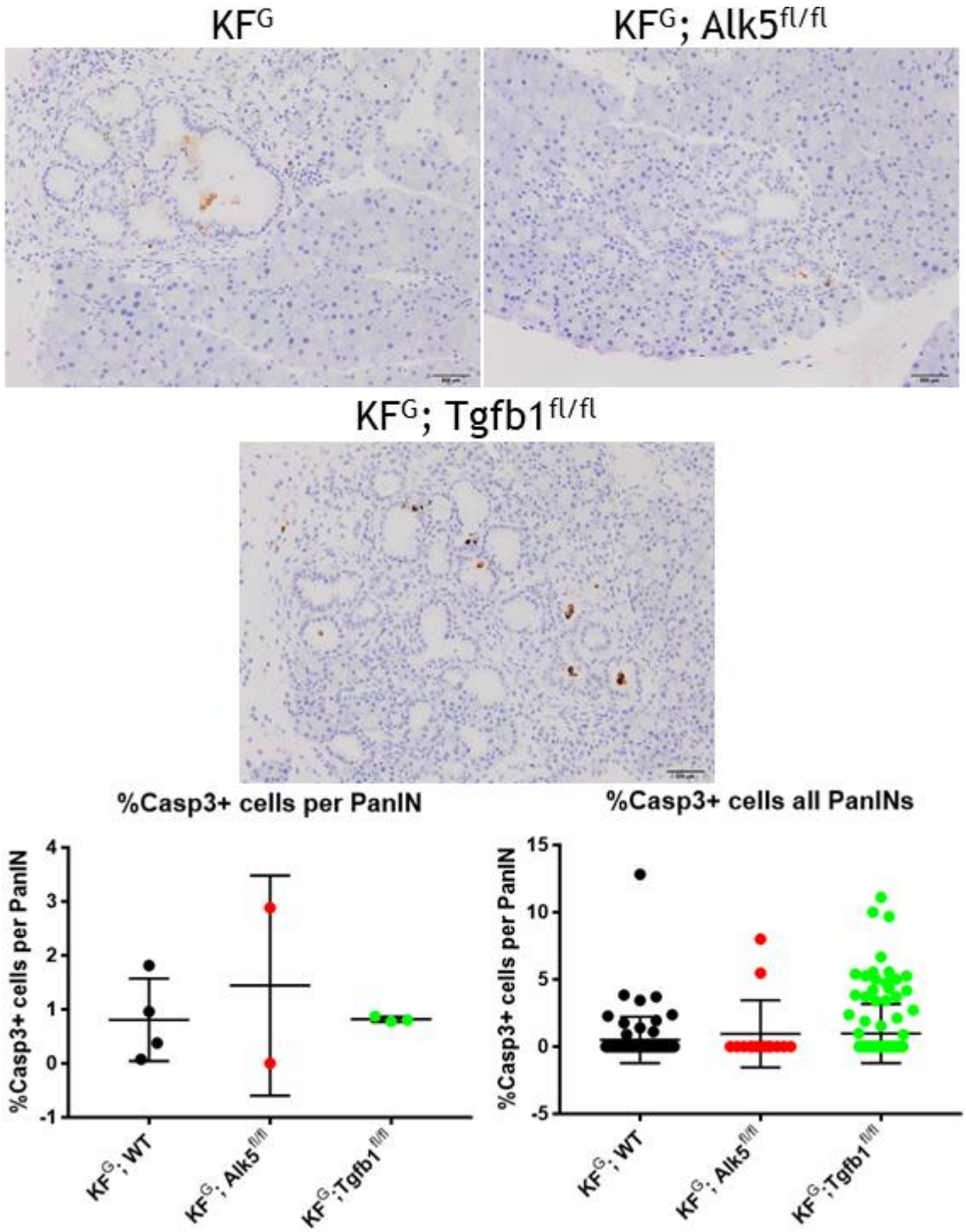

Figure 80 Cleaved caspase 3 staining on KF^G PanINs
Representative images of cleaved caspase 3 IHC staining in PanIN lesions in time point KF^G, KF^G; *Alk5*$^{fl/fl}$ and KF^G; *Tgfb1*$^{fl/fl}$ mice (Scale bars = 500μm). Quantification of the percentage of Casp3$^+$ cells per PanIN counted across all PanINs present in the mice is shown in the right graph. The left graph shows the average proportion of Casp3$^+$ cells in all PanINs per mouse (n= 4, 2, 3, respectively). There was no significant change in proportion of Casp3$^+$ cells when analysed across individual mice. (Mann Whitney test used, significant P-values indicated).

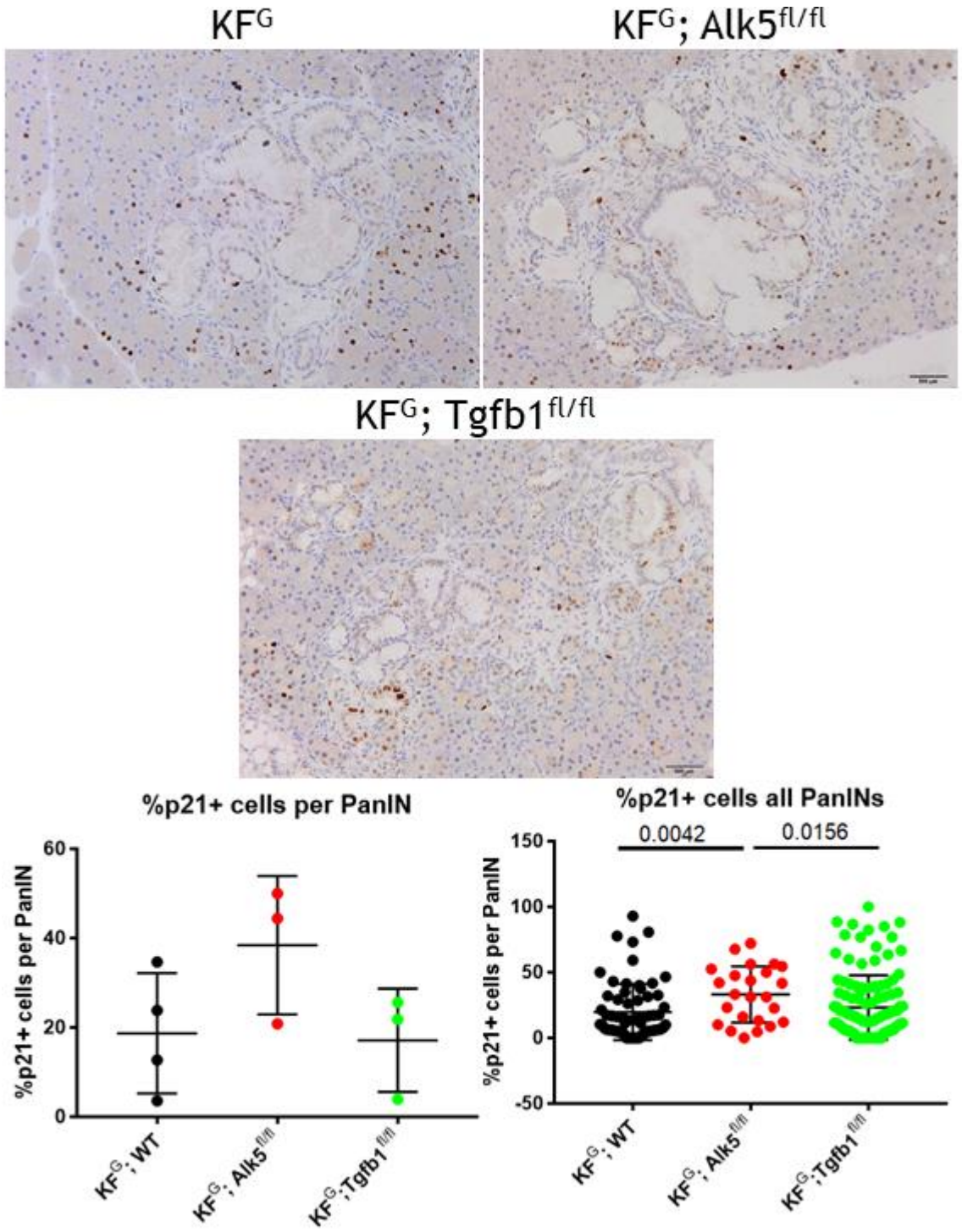

Figure 81 p21 staining on KF^{G} PanINs
Representative images of p21 staining in PanIN lesions in time point KF^{G}, KF^{G}; *Alk5$^{fl/fl}$* and KF^{G}; *Tgfb1$^{fl/fl}$* mice (Scale bars = 500µm). Quantification of the percentage of p21^{+} cells per PanIN counted across all PanINs present is shown in the right graph. There was a significantly increased proportion of PanINs with higher levels of staining of p21 in the KF^{G}; *Alk5$^{fl/fl}$* cohort. The left graph shows the average proportion of p21^{+} cells per PanIN per mouse (n= 4, 3, 3, respectively). There was no significant change in proportion of p21^{+} cells when analysed across individual mice. (Mann Whitney test used, significant P values indicated).

Although the number presented here are low, collectively, the KF; *Tgfb1*$^{fl/fl}$ model appears to present with an increased abundance of more advanced PanIN lesions, with an increased proportion of proliferating PanIN cells, perhaps indicating that TGFß1 ligand production by a subset of fibroblasts is important for controlling PanIN progression, or potentially that decreased ligand production could result in upregulated receptor expression in these CAFs, thus altering their tumour-promoting potential. Interestingly, the KF; *Alk5*$^{fl/fl}$ mice present with elevated PanIN cell cycle arrest, although no change in PanIN abundance was detected.

These data led me to investigate the microenvironment around the PanIN lesions in mice of the different genotypes. Infiltration of fibroblasts into the PanIN lesions of the KF^{G}; KF^{G}; *Alk5*$^{fl/fl}$, and KF^{G}; *Tgfb1*$^{fl/fl}$ was measured by staining for the pan-CAF marker, podoplanin, and quantifying the positive area in PanIN regions. Representative images of the podoplanin IHC stained sections are shown in **Figure 82**, with no change in fibroblasts abundance detected across the models. With the 'myCAF' subset of fibroblasts shown to be driven by TGFß signalling (Biffi et al., 2019), I also investigated the abundance of expression of the 'myCAF' marker, αSMA, in the PanIN regions. Within the PanINs, αSMA^{+} cells accumulate similarly to the podoplanin^{+} fibroblasts. There was also no change in the abundance of αSMA^{+} staining across the models (**Figure 83**), suggesting that fibroblast infiltration and identity (at least in terms of the 'myCAF/iCAF' ratio) was unchanged upon Gli1 driven deletion of either *Alk5* or *Tgfb1* within PanIN lesions.

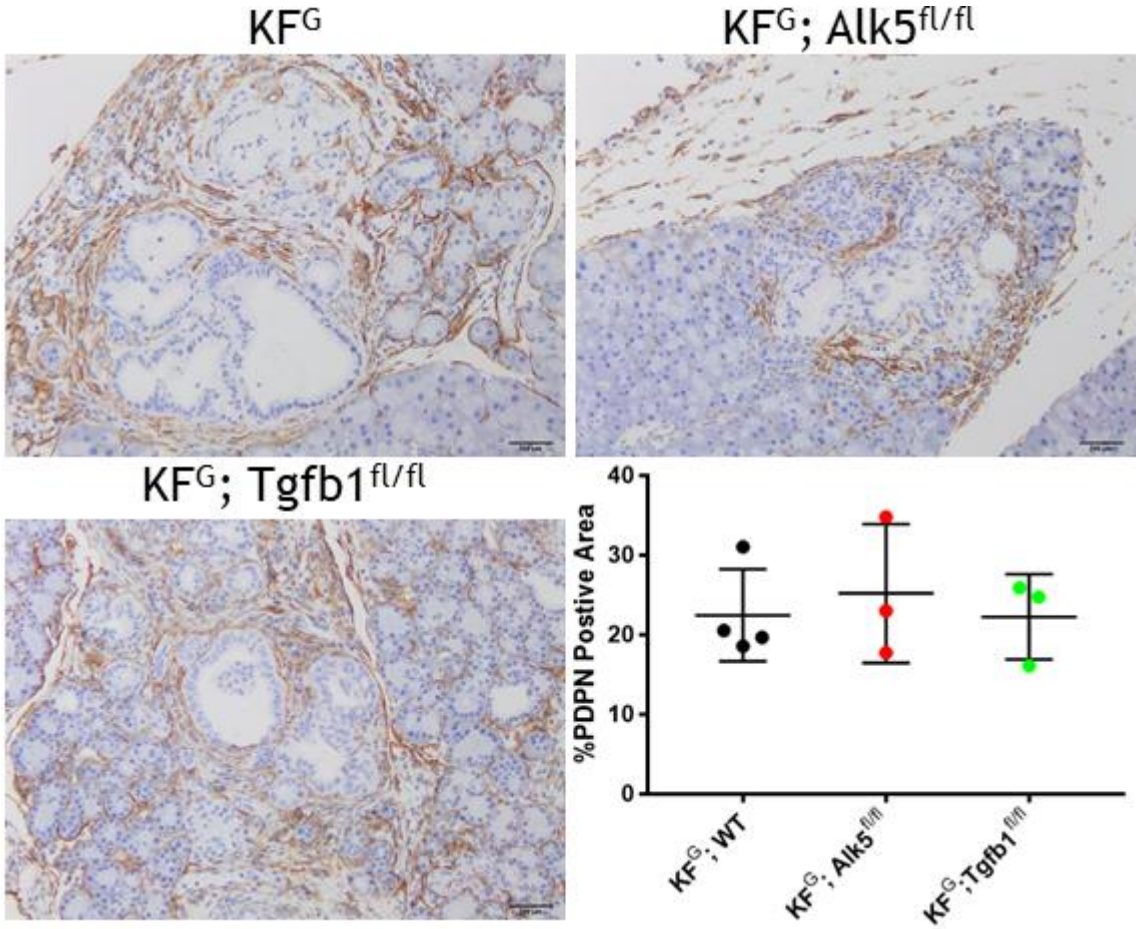

Figure 82 Fibroblast abundance in PanIN regions was unchanged in the KF^G mouse models
Representative images of podoplanin (PDPN) IHC stained tissue sections (Scale bar = 500μm). Fibroblasts accumulate around the PanIN lesion across all indicated models. HALO software quantification of the area of PDPN$^+$ staining in the adjacent PanIN stroma is shown. (n= 4, 3, 3, respectively, Mann Whitney Test used, significant P-values indicated).

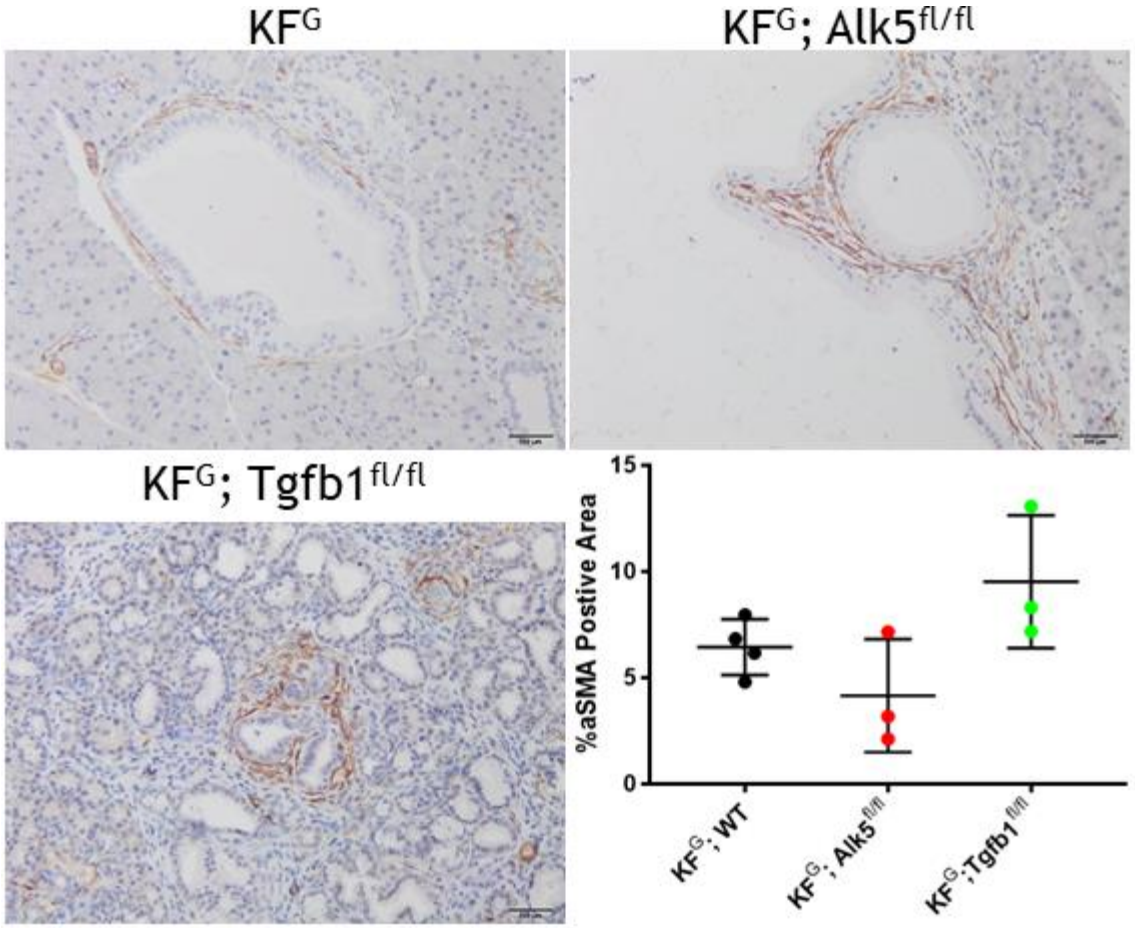

Figure 83 αSMA fibroblasts abundance around PanINs was unchanged between KF^{G}; KF^{G}; *Alk5$^{fl/fl}$* and KF^{G}; *Tgfb1$^{fl/fl}$* mice
Representative images of αSMA IHC stained tissue sections (Scale bars = 500μm). Infiltrating fibroblasts accumulate around the PanIN lesions across all indicated models. HALO software quantification of the area of αSMA^{+} staining in the adjacent PanIN stroma is shown. (n= 4, 3, 3, respectively, Mann Whitney Test used, significant P-Value indicated).

Therefore, I concluded that deletion of *Alk5* within Gli1 positive fibroblasts decreased senescence within PanIN epithelia but this did not accelerate PanIN progression. However, the Gli1 driven deletion of *Tgfb1$^{fl/fl}$* increased the number of PanIN-II lesions, which were more proliferative, without altering senescence. The survival of tumour bearing KPF^{G} mice was unchanged upon deletion of either *Alk5* or *Tgfb1* with metastatic dissemination to the liver elevated in the KPF^{G}; *Tgfb1$^{fl/fl}$* mouse model, although not significantly.

5.3.4 Gli1 driven deletion of *Alk5* or *Tgfb1* does not affect the PDAC TME in the KPF mouse model

With the deletion of *Alk5* or *Tgfb1* from established tumours found to have no significant effect on survival, I sought to investigate the impact it had upon the TME. Staining was performed on end-point KPF^{G} tumours, post tamoxifen induction, for fibroblast markers. The total abundance of CAFs was measured via staining with podoplanin; a pan-fibroblast marker proposed to mark all fibroblast populations within PDAC (Elyada et al., 2019). There was no change to the total abundance of CAFs within the end-point tumours following Gli1 driven deletion of *Alk5* or *Tgfb1* (**Figure 84)**. Published work from the Tuveson lab highlighted that high αSMA expressing fibroblast denote the 'myCAF' subpopulation of CAFs, which are dependent on TGFß signalling (Biffi et al., 2019). With Gli1 predominantly expressed within this 'myCAF' population (Steele et al., 2021), I stained for αSMA within the KPF tumours to determine if abrogation of TGFß signalling within the CAFs would reduce this subpopulation. Staining showed that the αSMA fibroblast abundance was reduced, but not significantly, when *Alk5* was deleted in Gli1 fibroblasts, although there was significant reduction in KPF; $Alk5^{fl/+}$ tumours (**Figure 85**). Interestingly, the Gli1 driven deletion of *Tgfb1* culminated in a significantly reduced αSMA positive area in end-point tumours. This was subsequently shown to increase the ratio of podoplanin to αSMA indicative of altered fibroblast populations within the TME (**Figure 86**). The ratio was also increased when *Alk5* was deleted in Gli1 fibroblasts, but not significantly.

TGFß signalling has been shown to be a potent driver of ECM accumulation and 'myCAFs' are the predominant ECM re-modellers. I therefore examined the deposition of collagen via staining with Sirius red, but no change in collagen deposition was detected across the cohorts even in the KPF^{G}; $Tgfb1^{fl/fl}$ tumours which had reduced αSMA positive area (**Figure 87**).

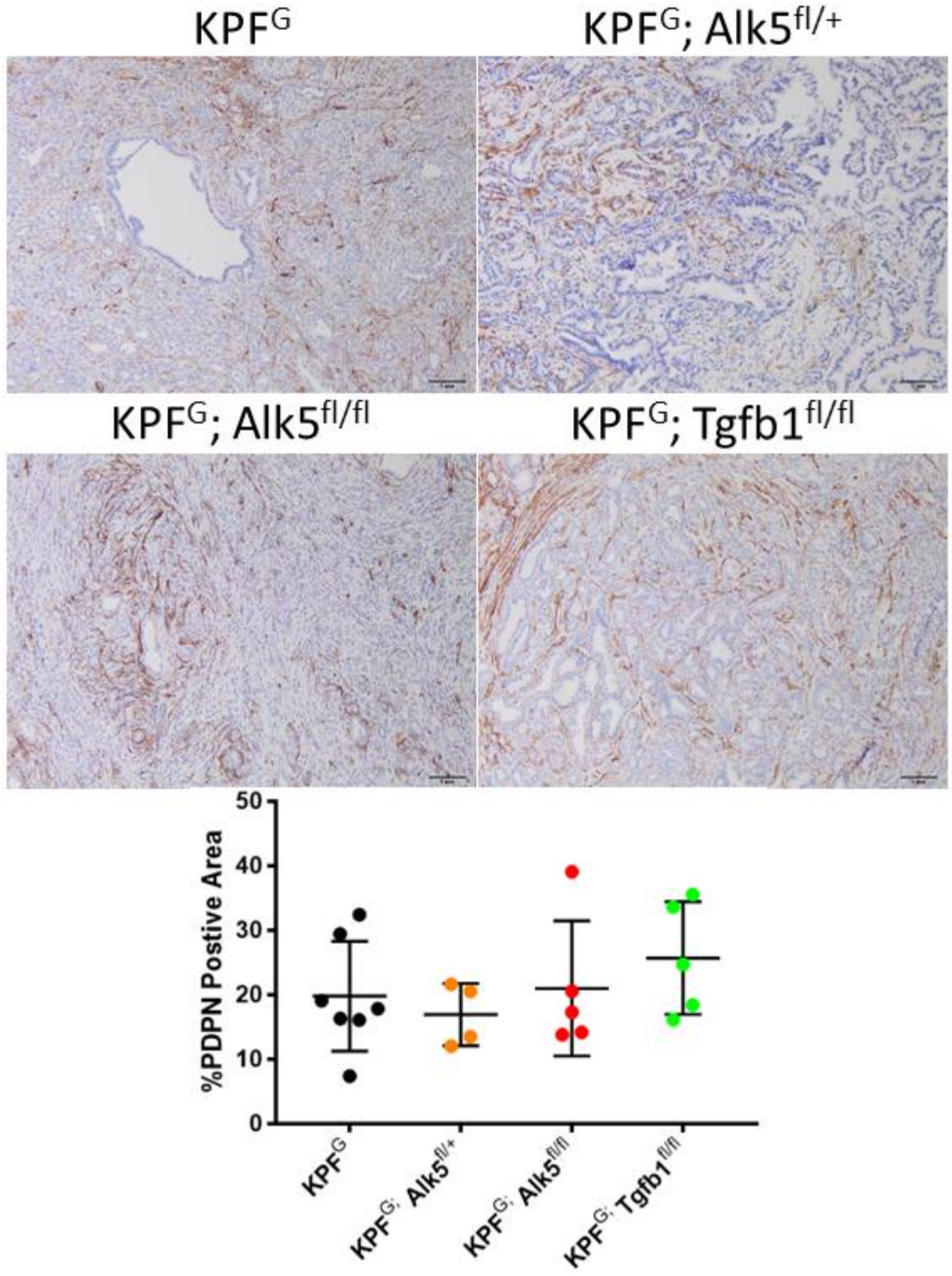

Figure 84 Deletion of *Alk5* or *Tgfb1* from Gli1^{+} fibroblasts does not affect fibroblast abundance in end-point PDAC
Representative images of podoplanin IHC stained end-point KPF^{G} tumours of the indicated genotypes (Scale bars = 1mm). Quantification of total area of PDPN staining, calculated via HALO software, is shown in the bottom panel. (n=7, 4, 5, 5, respectively. Mann Whitney test used, significant P-Values indicated).

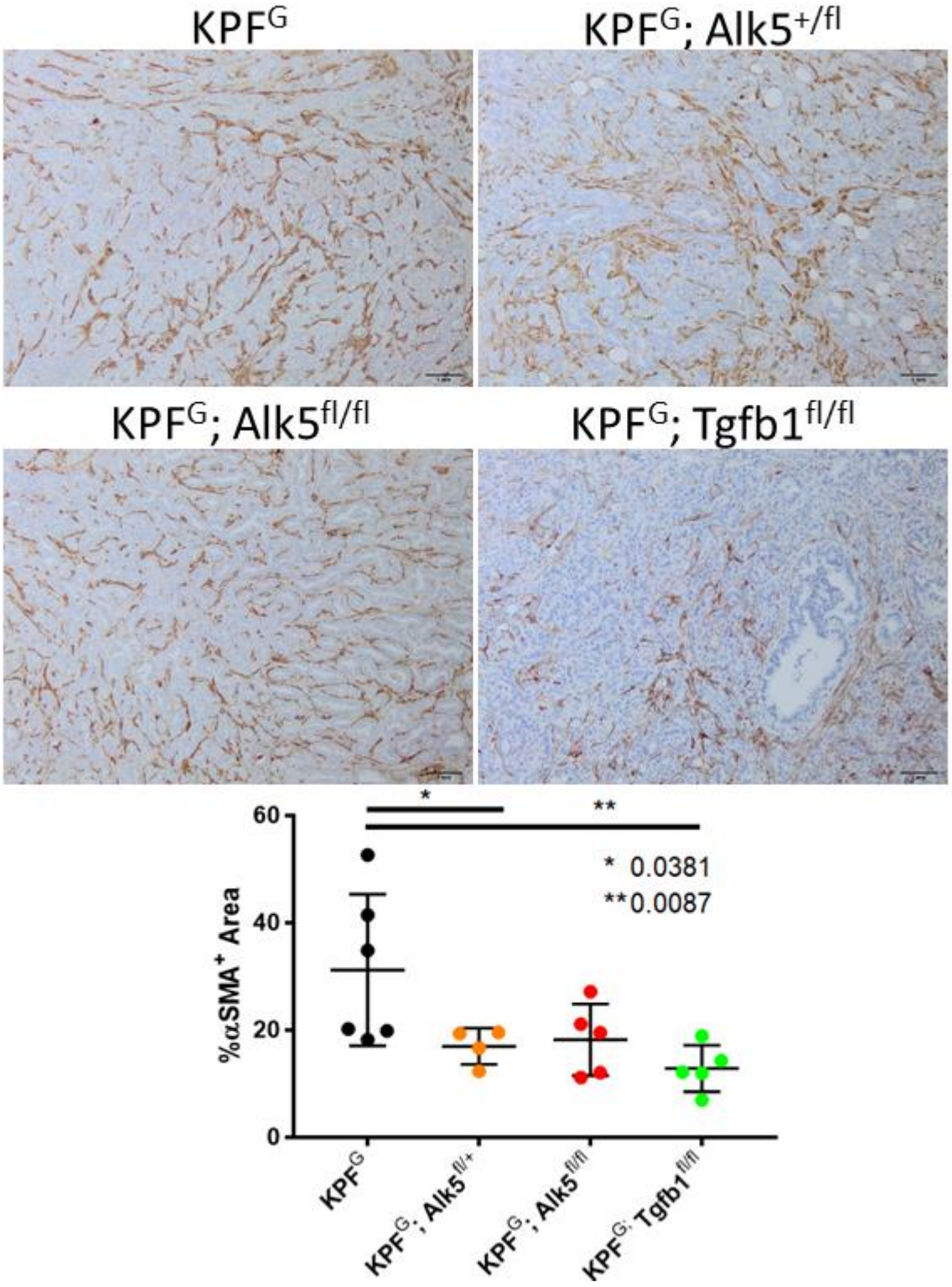

Figure 85 Gli1^{+} cell depletion of *Tgfb1,* and to a lesser extent *Alk5,* reduces αSMA^{+} fibroblasts within end-point tumours
Representative images of αSMA IHC stained end-point KPF^{G} tumours of the indicated genotypes (Scale bars = 1mm). Quantification, via HALO software, of total αSMA positive area as percentage of total tumour area is shown. (n=6, 4, 5, 5, respectively, Mann Whitney used, significant P-values indicated).

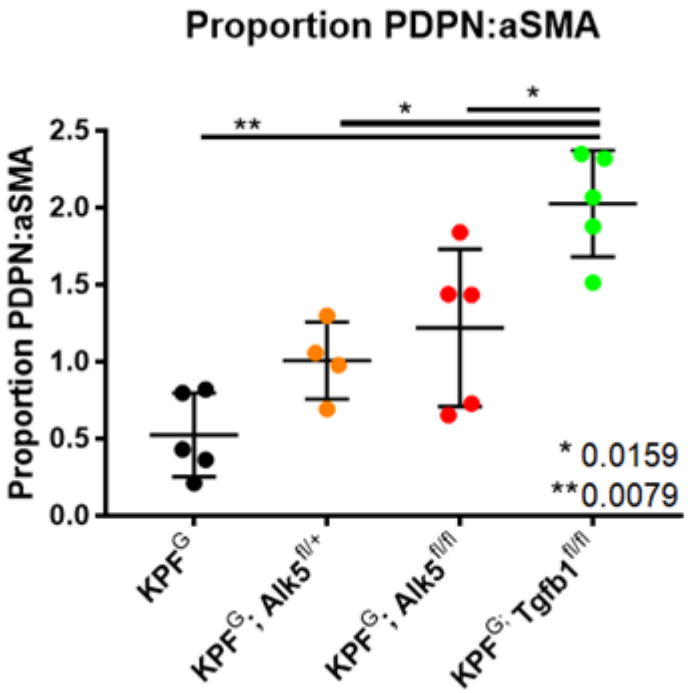

Figure 86 KPF^{G}; *Tgfb1$^{fl/fl}$* tumours had a greater ratio of podoplanin to αSMA positive fibroblasts compared to KPF^{G} tumours
From the HALO analysis the total are of podoplanin positive staining was divided by the total area of αSMA staining to generate a PDPN: αSMA ratio. The KPF^{G}; *Tgfb$^{fl/fl}$* mice had a significantly increased PDPN: αSMA ratio compared to the KPF^{G} mouse tumours (n=5, 4, 5, 5, respectively, Mann Whitney test used, significant P-values indicated).

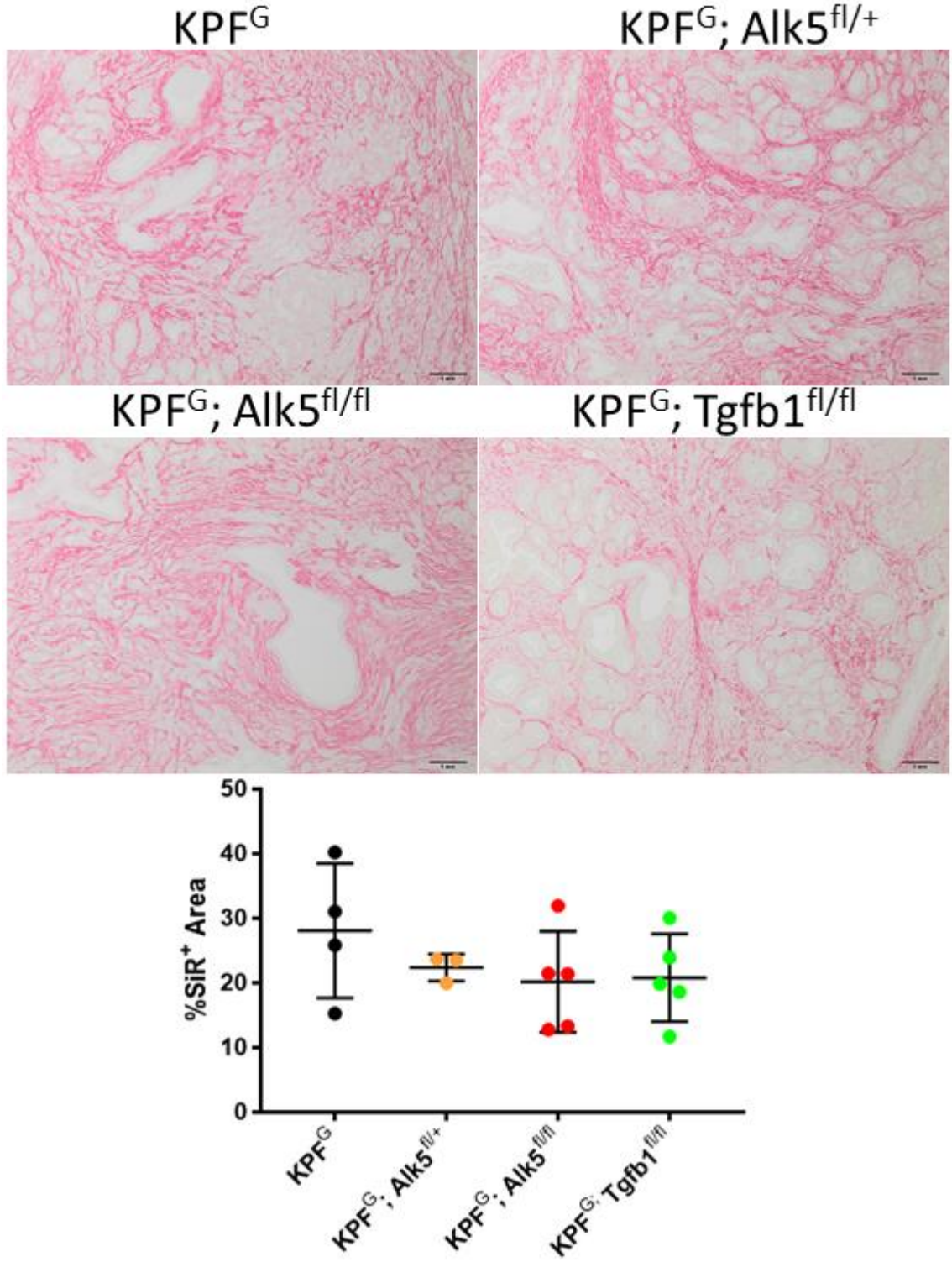

Figure 87 Collagen deposition in end-point KPF^{G} tumours was unchanged when either *Alk5* or *Tgfb1* was deleted in Gli1^{+} fibroblasts
Representative images of Sirius red staining in end-point tumours across the KPF^{G} genotypes are shown in the upper panel (Scale bars = 1mm). Quantification of Sirius red positive area as a percentage of total tumour area is shown in the bottom panel. (n=4, 3, 5, 5, respectively, Mann Whitney test used, significant P-Values indicated).

With multiple recent studies highlighting a link between fibroblasts and the immune infiltrate in PDAC (Hutton et al., 2021; Steele et al., 2021), I sought to elucidate if alterations in immune cell populations were detected in the KPF^{G}; *Alk5*$^{fl/fl}$ or KPF^{G}; *Tgfb1*$^{fl/fl}$ tumours. Macrophage infiltration was measured by staining for F4/80 and scoring the total area of positive staining (**Figure 88**), with T cell infiltration measured by staining for CD3 and counting the number of positive cells (**Figure 89**). However, both were unchanged in the either Gli1 driven *Alk5*$^{fl/fl}$ or *Tgfb1*$^{fl/fl}$ tumours in comparison to the KPF^{G} controls. Altogether, the data show that deletion of *Alk5* in Gli1^{+} fibroblasts did not have a significant impact on the TME in end-point KPF tumours, however deletion of *Tgfb1* affected the fibroblast populations, reducing the proportion of 'myCAFs' although the immune infiltrate and collagen deposition remained unchanged.

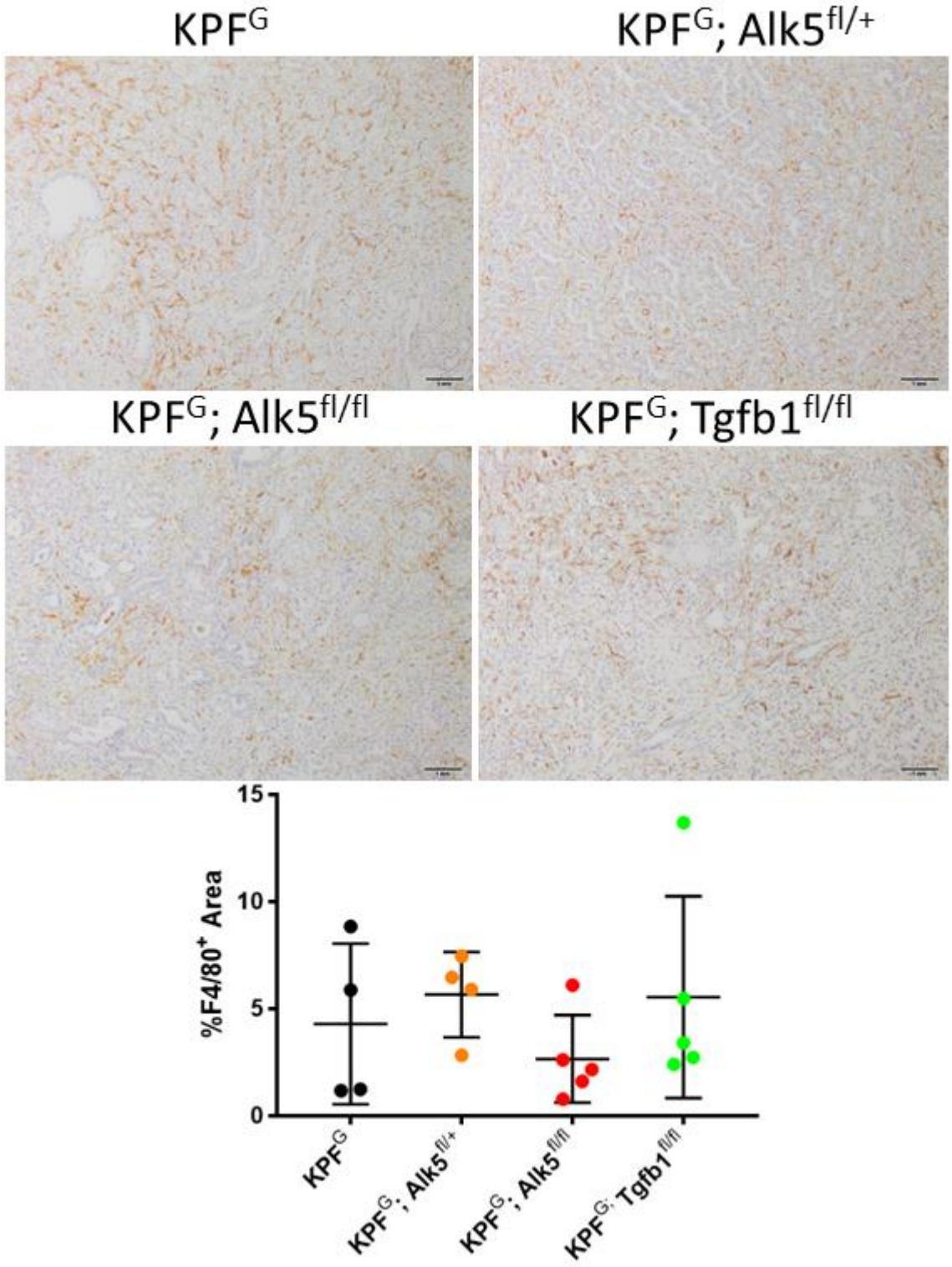

Figure 88 Gli1 driven deletion of *Alk5* or *Tgfb1* did not affect macrophage infiltration in end-point KPF^{G} tumours

Representative images of F4/80 IHC stained end-point tumour tissue across the genotypes are shown in the top panel (Scale bars = 1mm). Quantification, via HALO software, of the total area of F4/80 positive staining as a proportion of the whole tumour is shown in the bottom figure. (n= 4, 4, 5, 5, respectively, Mann Whitney test used, significant P-values indicated).

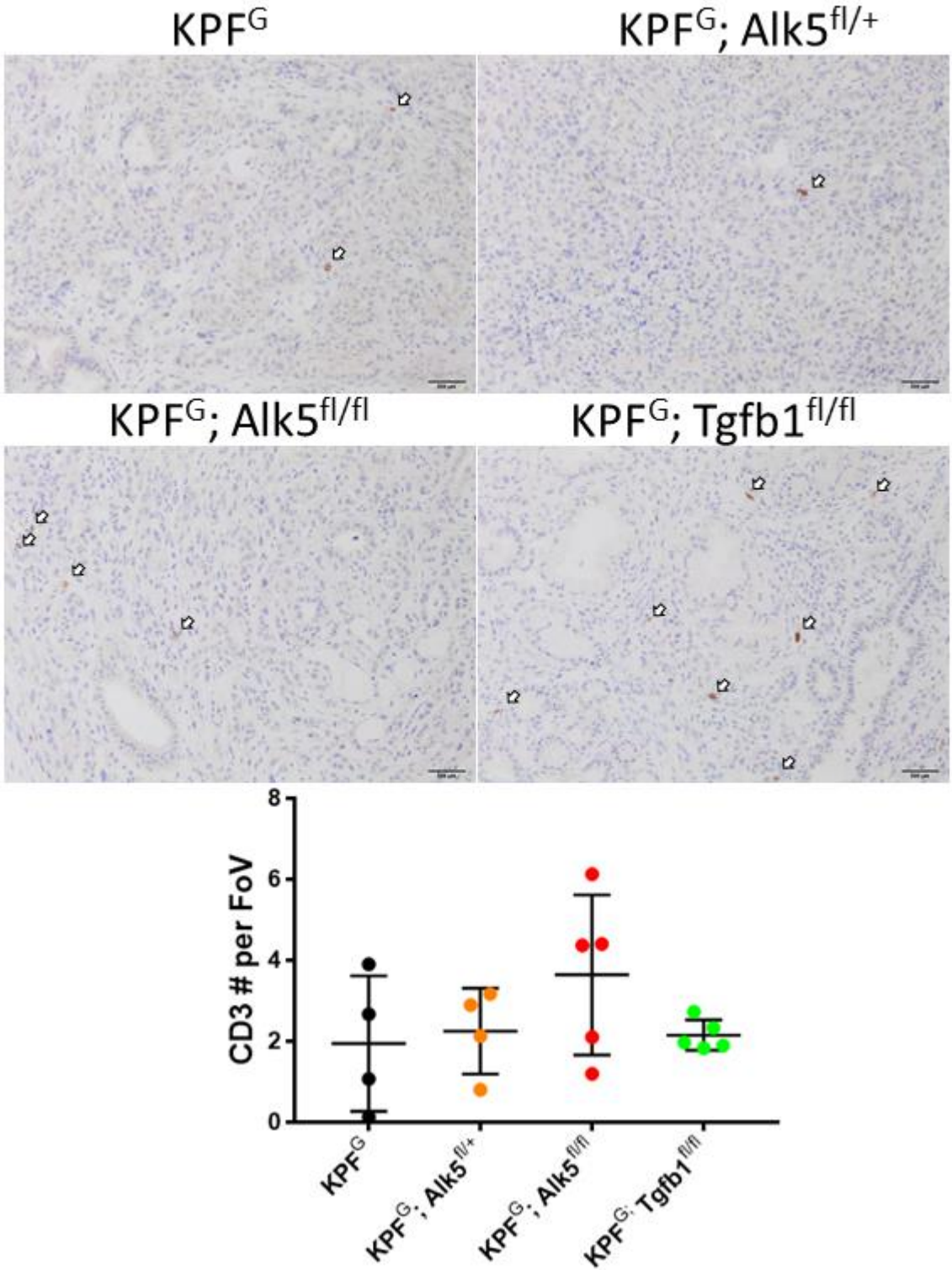

Figure 89 CD3^{+} T cell infiltration was unchanged in KPF^{G} tumours when either *Alk5* or *Tgfb1* was deleted in Gli1 fibroblasts
Representative images of CD3 IHC stained tissue in end-point tumours across the indicated genotypes are shown, upper panel (Scale bars = 500μm). Positive cells were counted across 30x Fields of view for each tumour and the average count per mouse (Per FoV) is shown in the graphs. (n= 4, 4, 5, 5, respectively, Mann Whitney test used, significant P-Values indicated).

5.3.5 Investigating TGFβ signalling in the TME of KPF^{G} *Alk5*$^{fl/fl}$ and *Tgfb1*$^{fl/fl}$ models

With no measurable change in the TME in either end-point tumours or in PanIN precursor lesions in the Gli1-Cre^{ER} driven *Alk5* deleted model I aimed to determine which fibroblasts had lost active TGFß signalling. In order to interrogate this, I performed multi immunofluorescence staining on both end-point and PanIN lesion tissue. I stained for pSMAD3, podoplanin and αSMA and then counted fibroblast specific nuclear positive staining for pSMAD3, which indicated active TGFß signalling in the fibroblasts.

Representative images of end-point tumour tissue showed high infiltration of fibroblasts positive for both podoplanin and αSMA (**Figure 90**). Quantification of the pSMAD3 positive fibroblasts showed that there was a slight reduction in pSMAD3 positive fibroblasts in the *Tgfb1* knockout model but not the *Alk5* knockout when compared to the controls (**Figure 91**), although this did not reach significance. This was perhaps further justification of a reduction in 'myCAF' populations within the KPF^{G}; *Tgfb1*$^{fl/fl}$ end-point tumours, with 'myCAFs' proposed to be αSMA^{hi} and pSMAD positive (Biffi et al., 2019), although it should be noted that there is significant heterogeneity between tumours of the same genotypes.

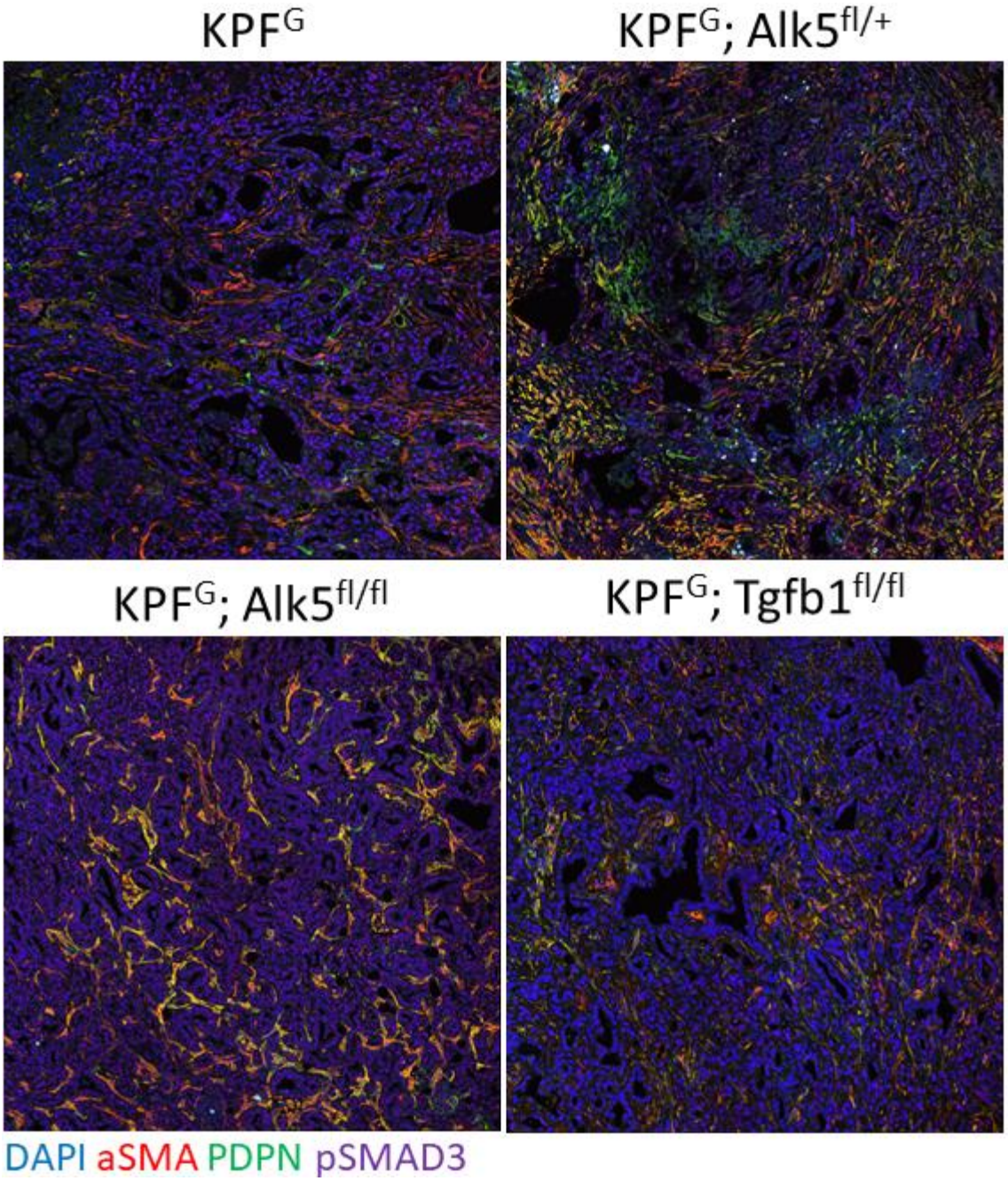

Figure 90 Representative images of immunofluorescent staining on end-point KPF^{G} tumours
Representative images of immunofluorescence staining on tissue from KPF^{G}; KPF^{G}; *Alk5$^{fl/+}$*, KPF^{G}; *Alk5$^{fl/fl}$* and KPF^{G}; *Tgfb1$^{fl/fl}$* tumours. Nuclei are in blue, stained with DAPI, pSMAD3 positive staining is indicated in magenta, and fibroblasts are marked in green for podoplanin and red for αSMA. Florescence images were taken on the Nikon A1R at 40x with 4 adjacent images stitched together shown.

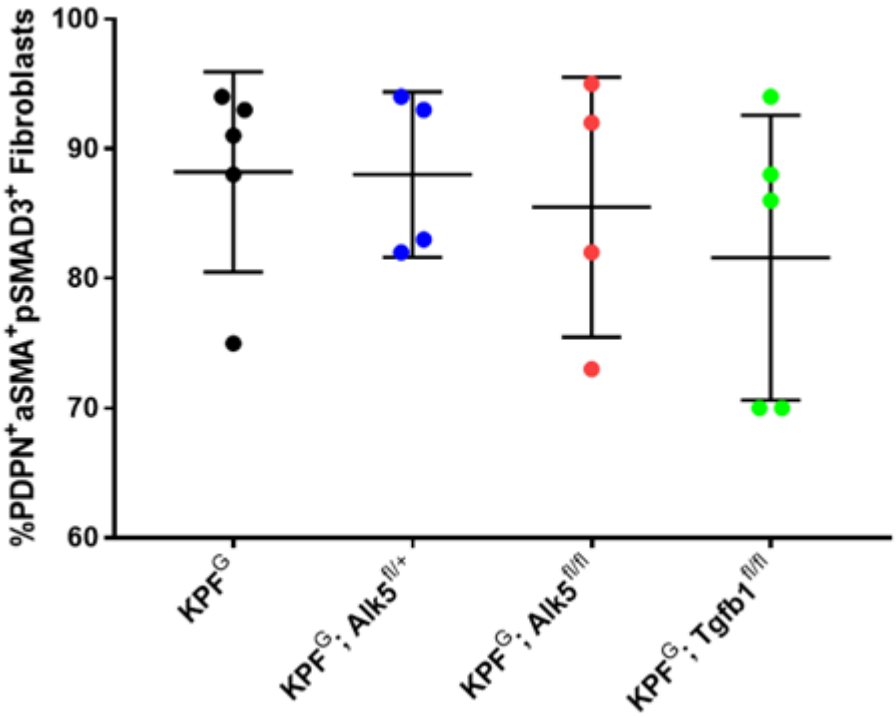

Figure 91 pSMAD3 positive fibroblast numbers are unchanged upon Gli1 driven *Alk5* deletion
Quantification of the percentage of PDPN$^+$αSMA$^+$pSMAD3$^+$ fibroblasts as a proportion of all PDPN$^+$ and αSMA$^+$ fibroblasts. 5x 40x images were taken for each tissue sample and all fibroblasts were counted across these images and the proportion of PDPN$^+$αSMA$^+$pSMAD3$^+$ fibroblasts is shown (n=5, 4, 4, 5, respectively, Mann Whitney test used, Significant P-values indicated).

Staining within the PanIN bearing tissue also showed a very similar pattern with the majority of fibroblasts being dual positive for both αSMA and podoplanin regardless of the *Gli1-Cre^{ER}* driven gene knockout (**Figure 92**). Further, the pSMAD3 positive fibroblasts were again decreased when *Tgfb1* was deleted in the Gli1$^+$ fibroblasts when compared to the controls, but not when *Alk5* was deleted, although it should be noted that numbers are low in this experiment (**Figure 93**). The 'myCAF' fibroblasts population also appear reduced in the *Gli1-Cre^{ER}* driven *Tgfb1* deleted mice, however, this was not noted in the αSMA IHC stained samples with perhaps an increase in αSMA positive area apparent.

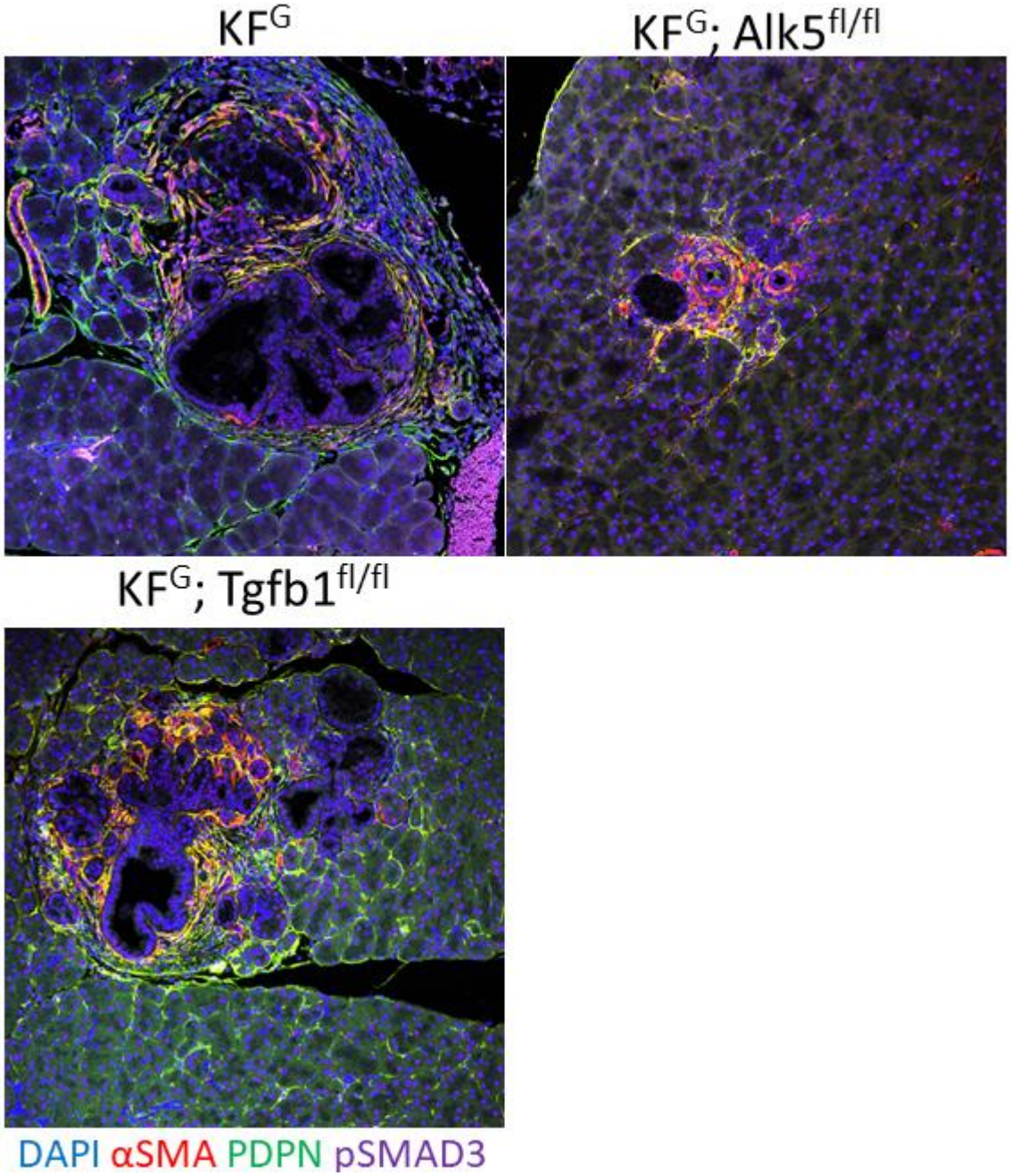

Figure 92 Representative images of immunofluorescence staining on PanIN-bearing tissue from KF^{G} mice
Representative images of immunofluorescence staining on tissue from KF^{G}; KF^{G}; *Alk5$^{fl/fl}$* and KF^{G}; *Tgfb1$^{fl/fl}$* mice at 7 weeks (1 week post induction). Nuclei are in blue, stained with DAPI, pSMAD3 positive staining is indicated in magenta, and fibroblasts are marked in green for podoplanin and red for αSMA. Fluorescence images were taken on the Nikon A1R at 20x.

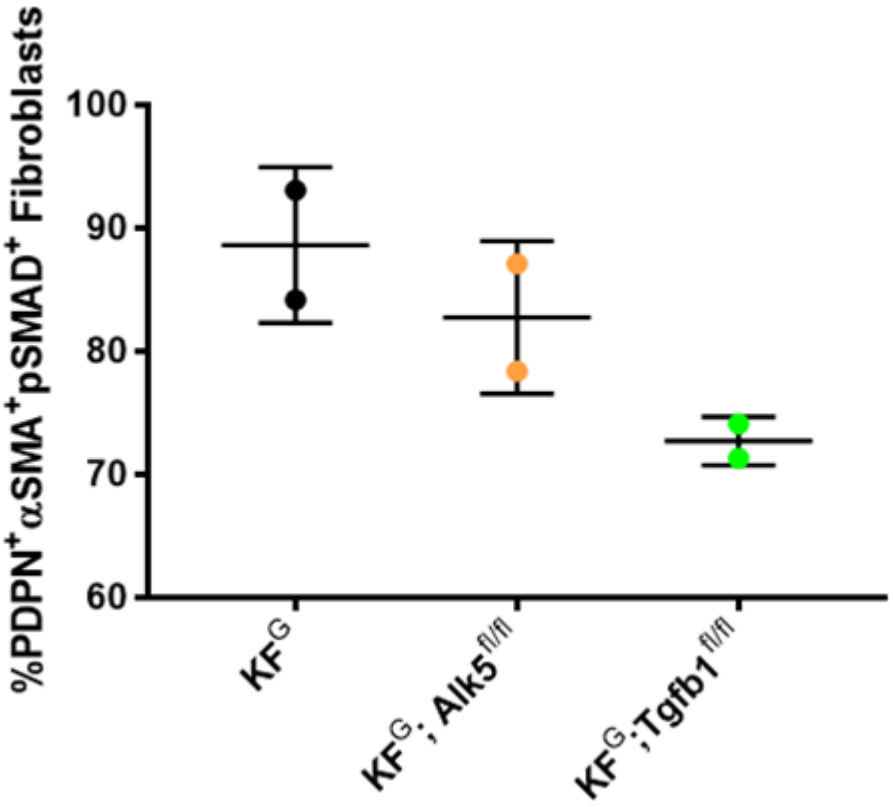

Figure 93 Gli1 driven deletion of *Tgfb1* results in a non-significant decreased in pSMAD3 positive fibroblasts in PanIN lesions
Quantification of the percentage of PDPN$^+$αSMA$^+$pSMAD3$^+$ fibroblasts as a proportion of all PDPN$^+$ and αSMA$^+$ fibroblasts. Each PanIN lesion on the slide was imaged at 20x and all fibroblasts counted within the lesion area. (n=2, 2, 2, respectively, Mann Whitney test used, Significant P-Values indicated).

These data, therefore, suggested that Gli1$^+$ fibroblast production of TGFß1 was required to maintaining a high level active TGFß signalling in the adjacent fibroblasts within developed PDAC, with further clarification required on their function within PanIN lesions, and increased numbers required for the study. However, in agreement with an unaltered TME and unchanged survival, Gli1 deletion of *Alk5* does not affect the active TGFß signalling in the fibroblast populations. Whether *Alk5* expression was essential for the maintenance of the Gli1$^+$ fibroblast population was not investigated, but loss and replenishment of these cells with non-recombined fibroblasts could have occurred as tumours progressed to end-point. This could differ from the *Tgfb1* deleted Gli1$^+$ fibroblast which lose ligand production but retain the receptor which may be

required for their persistence in the TME. Alternatively, if there is no paracrine effect of Alk5 deletion from Gli1^{+} fibroblasts on the surrounding Gli1-fibroblasts, the low number of Gli1^{+} cells, as a proportion of total fibroblasts might preclude observation of significant cell intrinsic changes.

5.3.6 Pan-fibroblast deletion of *Alk5* or *Tgfb1*

With *Gli1* expressed in a restricted population of 'myCAFs' (Steele et al., 2021), I sought to target all fibroblasts within the TME to elucidate the wider control TGFβ signalling exerts within PDAC. Therefore, mice expressing CRE-recombinase driven by the *Col1a2* promoter (Zheng et al., 2002a) were crossed with the KPF mice (KPF^C) with either floxed *Alk5* or *Tgfb1* alleles (**Figure 94**). It has recently been shown that expression of *Col1a2* is equivalent across both the 'iCAF' and 'myCAF' subtypes and therefore represents a pan-fibroblast marker (Elyada et al., 2019). Subsequently, these mice were enrolled in a survival cohort with detection of a palpable tumours confirmed via US followed by tamoxifen induction over 4 days and monitoring until mice reached clinical end-points. Either heterozygous or homozygous deletion of *Alk5* or *Tgfb1* did not influence survival of the KPF^C mice compared to the controls, with no significant changes noted, although additional numbers are still required (**Figure 95**).

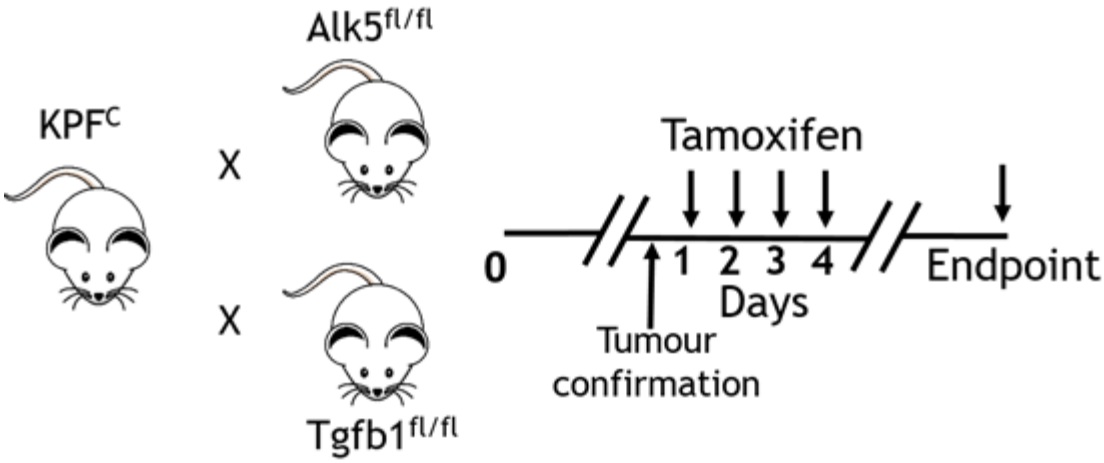

Figure 94 Pan-fibroblast deletion of *Alk5* or *Tgfb1* driven by expression of *Col1a2*-driven CRE-recombinase
The KPF mouse model was crossed to mice expressing a *Col1a2* driven tamoxifen inducible CRE recombinase allele. This allele contains an upstream Col1a2 enhancer and therefore drives CRE-recombinase expression specifically in fibroblasts. KPF^C mice were then crossed with mice expressing either the $Alk5^{fl/fl}$ or $Tgfb1^{fl/fl}$ alleles to drive deletion of these genes in fibroblasts only

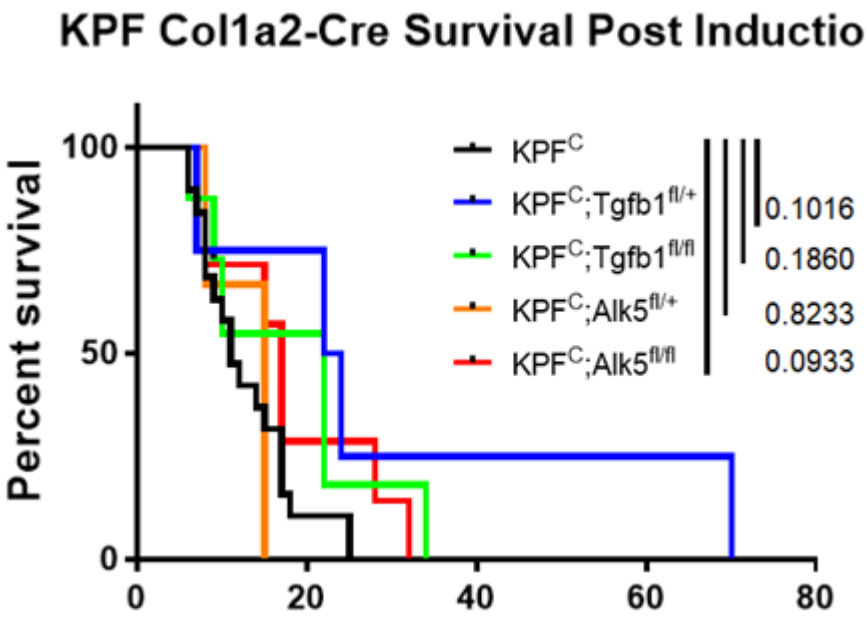

Figure 95 Col1a2 driven deletion of *Alk5* or *Tgfb1* does not alter survival of KPF^C mice
Kaplan-Meier survival analysis of KPF^C, KPF^C; *Alk5*$^{fl/+}$; KPF^C; *Alk5*$^{fl/fl}$, KPF; *Tgfb1*$^{fl/+}$ and KPF^C; *Tgfb1*$^{fl/fl}$ mice. Upon detection of a palpable tumour, and confirmation via ultrasound KPF^C mice were induced with tamoxifen. Heterozygous or homozygous deletion of *Alk5* or *Tgfb1* alleles did not alter survival in comparison to the KPF^C controls. (N=19, 4, 6, 3 and 7, respectively) (Median Survival=11, 23, 22, 15 and 17 days post induction respectively).

With the KPF^G models presenting with similar findings in the survival cohorts, I sought to interrogate if alterations to the TME, in particular to the fibroblast populations, were present in the KPF^C mice. Therefore, IHC staining for podoplanin and αSMA was conducted in end-point tumour tissue, with area of positive staining across the tumour tissue measured by HALO software. Representative images of podoplanin staining highlight abundant fibroblast infiltration across the models, with no significant alteration in fibroblast accumulation noted (**Figure 96**). The infiltration of αSMA positive fibroblasts was also unchanged in the KPF^C mouse models (**Figure 97**). This is particularly interesting in the KPF^C; *Tgfb1*$^{fl/fl}$ mice due to the significant decrease in αSMA staining noted previously in the KPF^G; *Tgfb1*$^{fl/fl}$ tumours. It would be expected that depletion of *Tgfb1* in the Col1a2 driven model would also ablate ligand production in the Gli1 positive fibroblasts and therefore a similar or more pronounced phenotype would be expected to be observed. The proportion of podoplanin to αSMA fibroblasts was also unchanged across the models (**Figure 98**), suggesting that there was no skew in fibroblast subtype within the TME

upon Col1a2 driven deletion of *Alk5* or *Tgfb1*, although additional numbers are required for some genotypes.

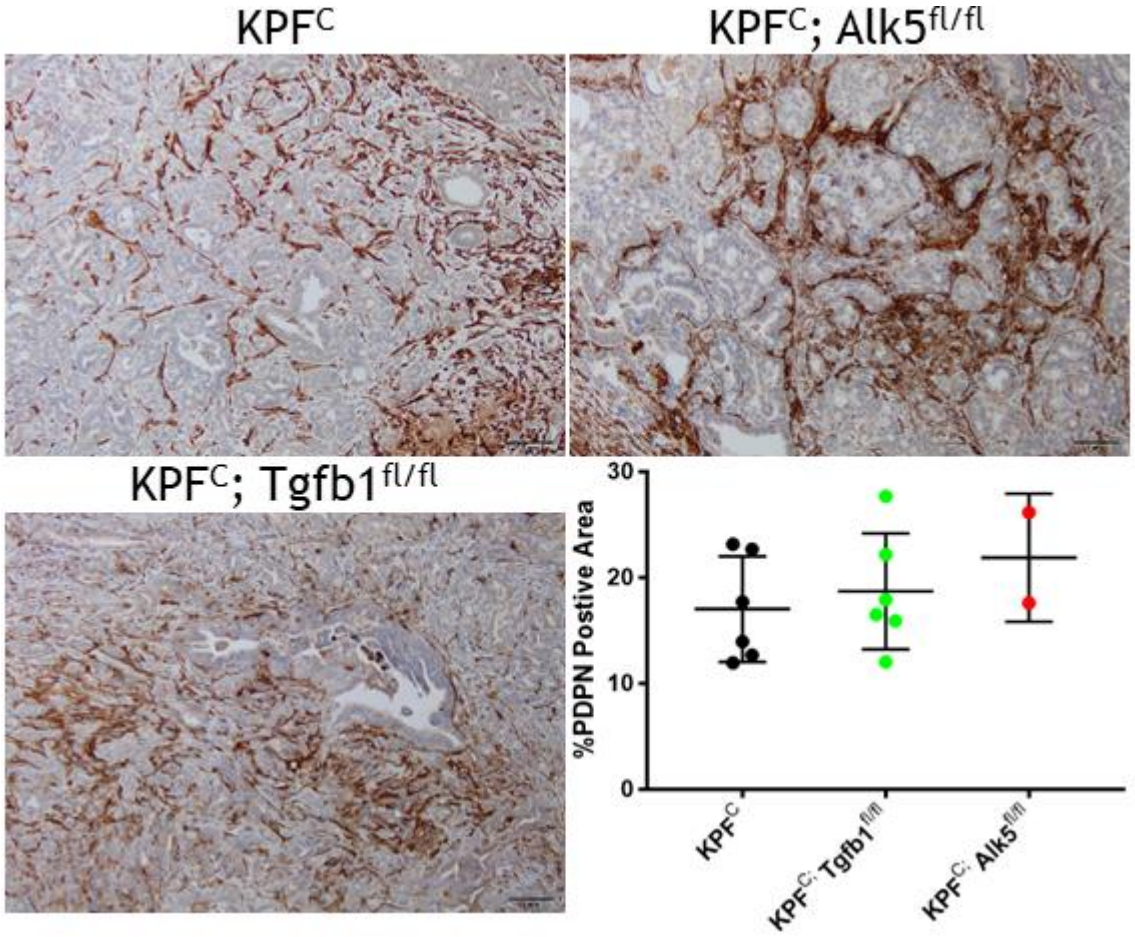

Figure 96 Col1a2-Cre^{ER} driven deletion of *Alk5* or *Tgfb1* did not affect fibroblast accumulation in end-point KPF^{C} tumours
Representative images of podoplanin IHC stained end-point KPF^{C} tumours of the indicated genotypes (Scale bars = 1mm). Quantification of total area of PDPN staining, calculated via HALO software, is shown in the bottom right panel. (n=5, 6, 2, respectively. Mann Whitney test used, significant P-Values indicated).

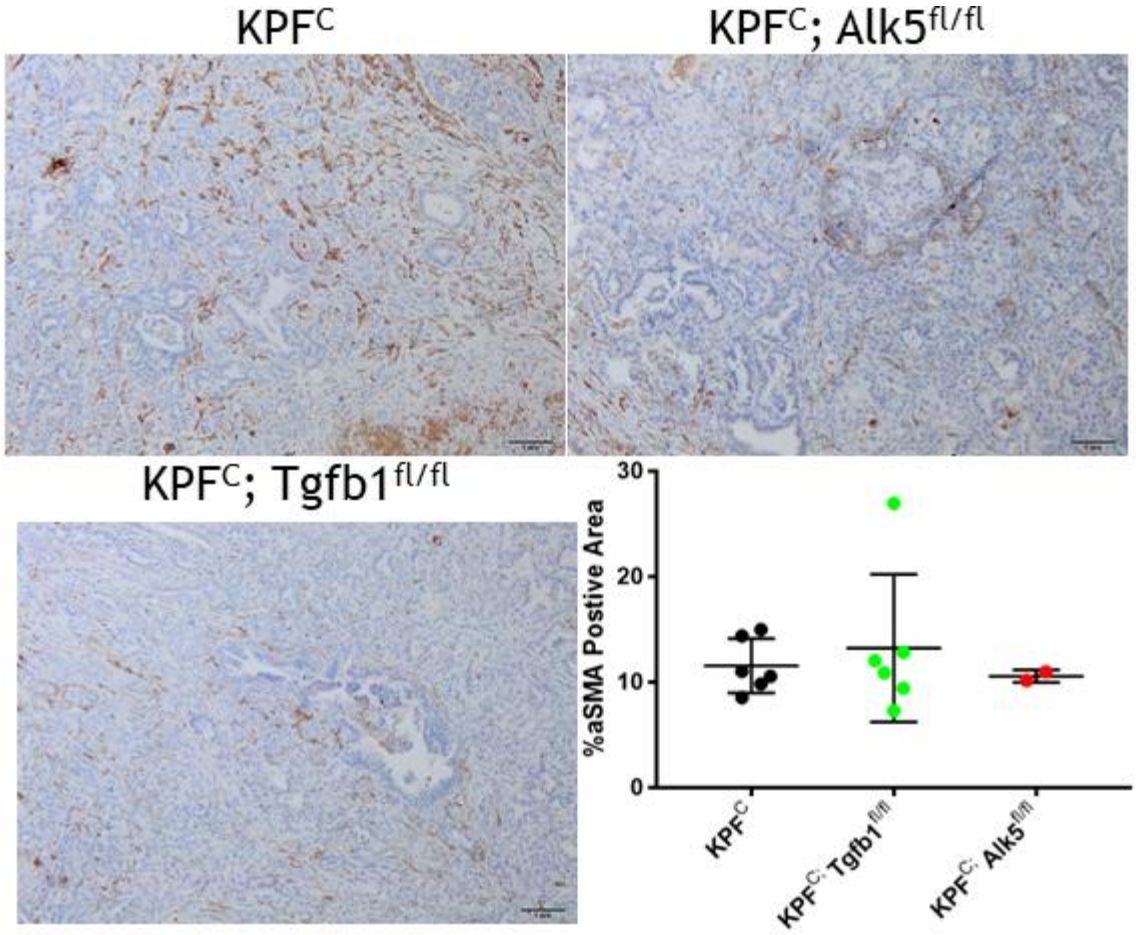

Figure 97 Col1a2-Cre^{ER} driven deletion of Alk5 or Tgfb1 did not affect αSMA positive fibroblast accumulation in end-point KPF^{C} tumours
Representative images of αSMA IHC stained end-point KPF^{C} tumours of the indicated genotypes (Scale bars = 1mm). Quantification of total area of αSMA staining, calculated via HALO software, is shown in the bottom right panel. (n=5, 6, 2, respectively. Mann Whitney test used, significant P-Values indicated).

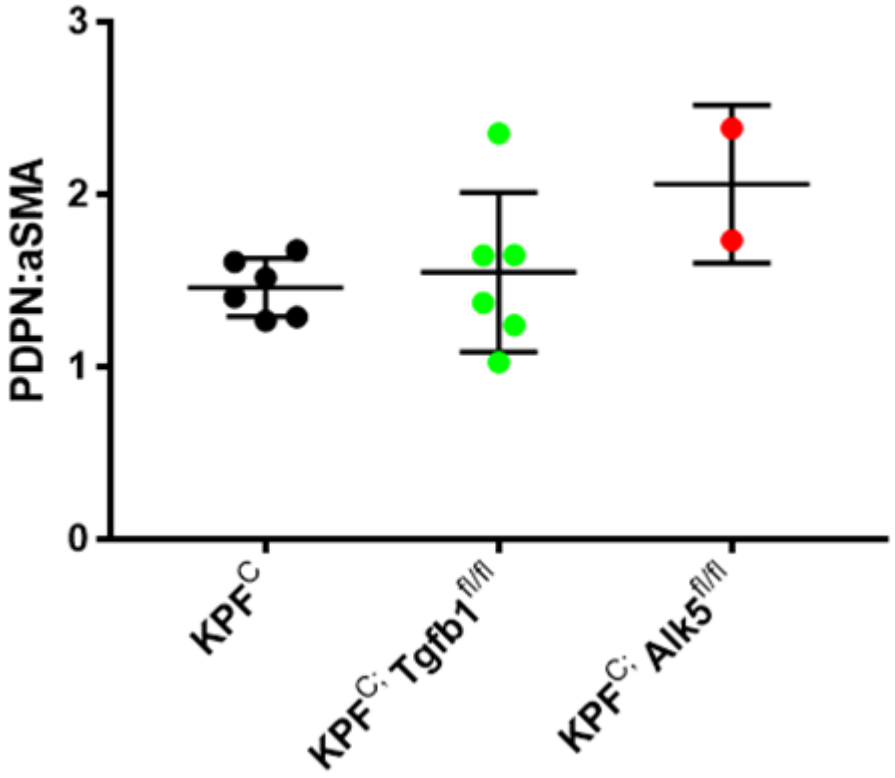

Figure 98 KPF^{C}; *Tgfb1*$^{fl/fl}$ and KPF^{C}; *Alk5*$^{fl/fl}$ tumours had an unchanged ratio of podoplanin to αSMA positive fibroblasts compare to KPF^{C} tumours
From the HALO analysis the total are of podoplanin positive staining was divided by the total area of αSMA staining to generate a PDPN: αSMA ratio. The KPF^{C}; *Tgfb*$^{fl/fl}$ and KPF^{C}; *Alk5*$^{fl/fl}$ mice had an unchanged PDPN: αSMA ratio compared to the KPF^{C} mouse tumours. (n=5, 6, 2, respectively, Mann Whitney test used, significant P-values indicated).

Collectively, this highlights a divergent function of fibroblast populations within PDAC, with pan-fibroblasts deletion of *Tgfb1* exhibiting an altered TME response compared to Gli1-Cre^{ER} driven deletion. Further work is required in the KPF^{C} model to elucidate differences across all stages of PDAC development.

5.4 Discussion

Collectively I have demonstrated that fibroblast-targeted deletion of *Alk5* or *Tgfb1* within established tumours, either in a restricted population or across all fibroblasts, does not affect long-term survival. However, Gli1 driven deletion of *Tgfb1* in 6 week old KF^G mice increases PanIN proliferation and the accumulation of more progressed PanIN lesions, while deletion in established tumours alters the podoplanin to αSMA ratio, with a reduction in 'myCAFs' potentially observed.

Although I have shown both positive staining for CRE-recombinase and RFP in the stromal regions of the KPF^G tumours, denoting stromal specific CRE recombination, it would be important to confirm if this was targeted to fibroblasts specifically. This could be proven through dual staining, for instance with podoplanin and RFP or podoplanin and CRE-recombinase. Further with the $Gli1^+$ fibroblasts enriched within the 'myCAF' subpopulation (Steele et al., 2021), defining the proportion of αSMA-recombined cells would also be enlightening. Definitive proof of deletion of *Alk5* or *Tgfb1* within these cells is also required. Although there was a decrease in the $pSMAD3^+$ fibroblasts in the KPG^G; $Tgfb1^{fl/fl}$ tumours, this was not significant and decreased activation of downstream signalling was not observed in the *Alk5* deleted fibroblasts. ISH for *Alk5* in the KAF mice detected a limited number of stromal cells, so this may not prove the most effective mechanism for interrogating loss of *Alk5*. ISH for *Tgfb1* could also be informative, however, RNA quality is a potential limiting factor in intact tissue because of the very high level of RNase in the pancreas. Therefore, it would be useful to sort fibroblasts from established tumours post tamoxifen induction and perform a qPCR on RNA extracted from the sorted cells to determine deletion of *Alk5* or *Tgfb1*. Although this would not give insight into the proportion of fibroblasts which has undergone recombination, it would be possible to determine whether 'iCAFs' or 'myCAFs' exhibit similar or differential gene expression, as they can be separated with a flow cytometry panel (Elyada et al., 2019). This is of course also applicable to the *Col1a2-Cre* driven deletion of *Alk5* or *Tgfb1* and will be essential in determining pan-fibroblast deletion. Further, CAF specific recombination could be determined by the expression of RFP, and examination of where this population resides within the iCAF/myCAF flow cytometry panel would reveal the specificity of targeting across both models.

Whole body heterozygous deletion of *Alk5* in a mouse model expressing pancreas specific oncogenic Kras reduced PanIN development (Principe et al., 2016). However, when I deleted *Alk5* in the Gli1$^+$ fibroblasts, PanIN abundance and progression was unchanged in comparison to the controls, although there was an indication of slightly increased senescence within PanIN epithelium. Whether, ageing of mice for longer post induction would result in slowed PanIN progression could prove interesting. Intriguingly, the Gli1 driven deletion of *Tgfb1* increased PanIN proliferation and increased the number of more advanced PanIN-2 lesions. TGFβ was shown to be a mediator of the senescence associated secretory phenotype, able to repress PanIN progression (Acosta et al., 2013), therefore, it is possible that Gli1$^+$ fibroblasts are important producers of TGFβ1 ligand and abolition of their capacity to produce ligand could relieve TGFβ induced PanIN suppression.

With SHH responsive genes shown to be enriched within a subset of 'myCAFs' (Steele et al., 2021) and Gli1 positive fibroblasts observed to expand upon oncogenic transformation of the pancreas (Garcia et al., 2020), I examined the dependence of this population of fibroblasts on TGFβ signalling. The 'myCAF' population has been shown, both *in vitro* and *in vivo,* to be driven by TGFβ signalling, with TGFβ receptor inhibition decreasing αSMA positive fibroblasts within KPC tumours (Biffi et al., 2019). Therefore, it was surprising to observe that deletion of *Alk5* in Gli1$^+$ fibroblasts in the KPF model was unable to even partly replicate findings in the receptor inhibitor treated KPC mice. Inhibitor treatment would target the whole TME with genetic deletion restricted to a subset of fibroblast cells. Whether TGFβ signalling is only one part of a wider network of signalling molecules, that can dictate 'myCAF' fate and, thus, signalling redundancy in CAFs was able to compensate for loss of TGFβ signalling is unclear. Further, the receptor inhibitor would continuously block TGFβ signalling, and with fibroblasts evolving throughout disease progression (Dominguez et al., 2020) the inhibitor may be able to block the development of subsequent 'myCAFs'. Tamoxifen administration promotes a time-restricted depletion of *Alk5* in Gli1$^+$ fibroblasts and *Garcia et al,* have suggested that *de novo* generation of Gli1$^+$ fibroblasts occurs during PanIN development (Garcia et al., 2020). Therefore, it would be useful to know whether these *Alk5* depleted fibroblasts persist to end-point within tumours or whether they can be

replenished or replaced by other CAF populations and finally, if they are reliant on TGFß signalling and therefore depleted upon tamoxifen induced *Alk5* deletion. With these open questions remaining it would be pertinent to investigate alterations to the TME, particularly fibroblast populations, at early time-points post tamoxifen induction.

Intriguingly, the Gli1 driven deletion of *Tgfb1* was able to alter fibroblast populations, significantly reducing the αSMA levels as well as lowering the number of pSMAD3 positive CAFs. Although TGFß signalling has been shown to induce the 'myCAF' subtype while suppressing the 'iCAF' subtype within tumours (Biffi et al., 2019), the source of ligand has not been fully appreciated. With fibroblasts able to produce TGFß1 (Shek et al., 2002), and its expression enriched in 'myCAFs' (Elyada et al., 2019), this perhaps indicates that paracrine and autocrine fibroblast signalling is important for maintenance of these subtypes.

With the αSMA high 'myCAFs' proposed to be the predominant producers of ECM components (Ohlund et al., 2017) and TGFß signalling demonstrated to increase ECM molecule production in fibroblasts (Schneider et al., 2001; Shek et al., 2002), I expected to note a decrease in collagen deposition within the αSMA low KPF^{G}; *Tgfb1*$^{fl/fl}$ tumours. However, no change in Sirius red positivity was observed. Whether the decreased ligand availability was capable of suppressing αSMA but sufficient to maintain ECM levels was unclear. Alternatively, TGFß1 has been shown to inhibit IL-1R expression (Biffi et al., 2019; Tjomsland et al., 2016) and perhaps the decreased availability of ligands creates a permissive environment for the expansion of αSMA low 'iCAFs'. The pan-fibroblast marker podoplanin was slightly, although not significantly, elevated in the KPF^{G}; *Tgfb1*$^{fl/fl}$ tumours, indicative of an increase in non-myCAF populations.

Depletion of CAFs has been shown to be tumour promoting in some circumstances (Lee et al., 2014; Oezdemir et al., 2014; Rhim et al., 2014), with these studies predominantly targeting markers or signalling pathways promoting the 'myCAF' subtype. Inhibition of TGFß receptor has been shown to have no effect on tumour growth in the KPC model, whereas inhibition of 'iCAFs' through a JAK/STAT inhibitor resulted in reduced tumour growth, although in both situations the impact on the full TME could explain the divergent response (Biffi

et al., 2019). However, these studies predict that Gli1 targeted deletion of *Alk5* would be worse for tumour prognosis as 'myCAFs' are thought to be the most tumour suppressive subtype. Further, the Gli1^{+} fibroblasts compose less than 50% of the fibroblasts within KPF tumours, although they are enriched within the αSMA positive populations (Garcia et al., 2020). Therefore, it was also essential to examine the wider CAF population. Thus, using a tamoxifen inducible *Cre-recombinase* allele driven by the pan-fibroblast marker Col1a2 (Elyada et al., 2019), I deleted both *Alk5* and *Tgfb1* in the CAFs of established KPF tumours. With the observed alterations in fibroblasts in the tumours of the KPF^{G}; *Tgfb1*$^{fl/fl}$ model, I expected to see a similar or even more pronounced effect upon pan-fibroblast depletion of *Tgfb1*$^{fl/fl}$, however, this was not the case. Divergent functions of different populations of fibroblasts have been highlighted previously (Chen et al., 2021; Garcia et al., 2020), although the difference between the Gli1 and Col1a2 models shown here will require further investigation. Whether the pan-fibroblast deletion culminates in more compensation across the TME, which ultimately retains all fibroblast population is possible. In addition, the Gli1^{+} fibroblasts are located adjacent to cancer cell beds (Biffi et al., 2019; Garcia et al., 2020) with location perhaps playing a role. The wider Col1a2 driven deletion of *Tgfb1* could result in a feedback loop to restore TGFβ signalling through upregulation of other TGFβ ligands. This may not be observed in the KPF^{G}; *Tgfb1*$^{fl/fl}$ mice due to Gli1 expression being restricted to a subset of 'myCAFs' (Steele et al., 2021), with sufficient alternate sources of ligand potentially blocking increased production of other ligands. Therefore, investigation of ligand levels within both the KPF^{C} and KPF^{G} tumour would be of interest.

Immune cell infiltration has been shown to be altered upon short term SHH inhibition, with this treatment resulting in a reduced αSMA^{+} fibroblast population (Steele et al., 2021). Further, TGFβ has a potent immunosuppressive function across multiple cell types (Batlle and Massague, 2019), with blockade of TGFβ signalling enhancing anti-PD-L1 treatment in KPC mice (Principe et al., 2019). Aberrations to the TME, for instance reduction in collagen, was shown to be worse for prognosis due to recruitment of suppressive myeloid cells (Chen et al., 2021). Therefore, I examined the immune infiltration in the KPF^{G} models by counting T cell and macrophage infiltration. However, the immune infiltration

was unchanged. The highlighted studies have investigated in more detail the reciprocal alterations to immune cell populations caused by altering fibroblasts in the TME. With expanding developments in immunotherapy, understanding of the immune cell alterations within the fibroblast targeted depletion models shown in this chapter could provide new avenues for therapy.

In conclusion, I have generated two models, which can be utilised to delete either *Alk5* or *Tgfb1* in a pan-fibroblast or restricted fibroblast manner at different stages across PDAC development. Although survival is unchanged in these models, *Tgfb1* deletion in Gli1^{+} fibroblasts alters fibroblast populations within the TME. Open questions remain as to the dependence of fibroblasts on TGFß signalling driven through *Alk5,* and the importance of fibroblast-to-fibroblast communication through TGFß ligand availability.

Chapter 6 The role of TGFβ signalling within neutrophils in PDAC

6.1 Introduction

Neutrophils are an important component of the innate immune system through their ability to rapidly infiltrate into damaged tissue and induce cytotoxic effects via degranulation (Cowland and Borregaard, 2016; Hager et al., 2010).This response is required to dampen and restrict the spread of infectious particles within the body (Lekstrom-Himes and Gallin, 2000). However, in situations of chronic disease, specifically in this case cancer, systemic alterations to the immune system can cause egress of less mature neutrophils from the bone marrow (Evrard et al., 2018; Zhu et al., 2018). These immature neutrophils can exhibit pro-tumorigenic functions, with tumour education influencing their capabilities (Fridlender et al., 2012; Mishalian et al., 2013). Further, studies have indicated that neutrophils are involved in the metastatic cascade, potentially through their ability to inhibit the cytotoxic T cell response (Coffelt et al., 2015; Jackstadt et al., 2019; Steele et al., 2016). With a high neutrophil to lymphocyte ratio recently being shown to indicate poor prognosis of pancreatic cancer (Nywening et al., 2018; Piciucchi et al., 2017), understanding neutrophils function in PDAC is required. Work has indicated that TGFß signalling may function to repress the cytotoxic activity of neutrophils and thereby increase their pro-tumorigenic function (Fridlender et al., 2009). However, this has not yet been properly interrogated in autochthonous models of disease. The generation of the 'Catchup' mouse model allowed for targeted gene deletion in neutrophils through a Ly6G-Cre recombinase (Hasenberg et al., 2015), providing the basis to examine the effect of TGFß signalling in neutrophils.

6.2 Experimental Aims

Through use of the KPF mouse model of PDAC, I aimed to examine the effects of neutrophil specific ablation of TGFß signalling through the Ly6g-Cre driven deletion of *Alk5*. I sought to investigate how this deletion would affect the survival of the PDAC mice, as well as investigating the influence on metastatic disease. Further, I aimed to dissect the neutrophil activation and maturity and

understand whether deletion of *Alk5* would translate into increased activated neutrophils within the circulation, in PDAC, and at metastatic sites.

6.3 Results

6.3.1 Generation of a next generation mouse model of PDAC with neutrophil specific deletion of *Alk5*

The KPF mouse, as described in **figure 6,** was crossed with mice expressing Cre recombinase driven by the neutrophil specific Ly6G gene (KPF^{L}) (Hasenberg et al., 2015). The *Cre* was inserted into the first exon of the *Ly6g* this gene thereby rendering the allele non-functional. The KPF^{L} mouse was then crossed with $Alk5^{fl/fl}$ mice to obtain KPF^{L} mice bearing either heterozygous or homozygous *Alk5* floxed alleles, culminating in deletion of *Alk5* in Ly6G positive cells only (**Figure 99**).

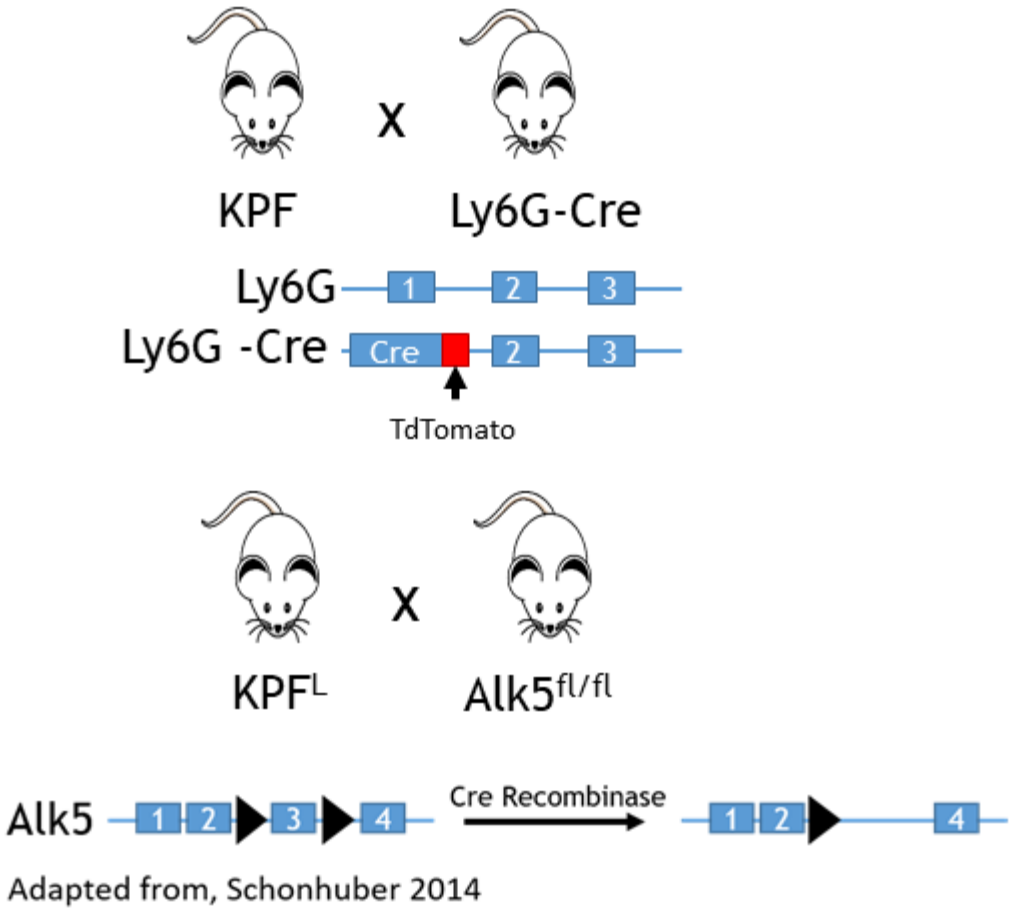

Figure 99 Generation of a mouse model with neutrophil specific deletion of *Alk5*
The KPF mouse described by *Schonhuber et al* was crossed with the 'Catch-up' mouse described by *Hasenberg et al.* The first exon of Ly6G was replaced with a Cre-recombinase and a TdTomato construct. The KPF^{L} mouse was then crossed to $Alk5^{fl/fl}$ mice to generate a colony with neutrophil specific deletion of *Alk5*.

In order to confirm neutrophil specific *Alk5* deletion I sorted and collected neutrophils using fluorescence-activated cell sorting (FACS). Blood was collected through cardiac puncture of aged *Pdx1-Flp; Kras^{WT}; Trp53^{WT}; Ly6g-Cre; Alk5$^{+/+}$* and *Pdx1-Flp; Kras^{WT}; Trp53^{WT}; Ly6g-Cre; Alk5$^{fl/fl}$* mice. I gated for single cells and those alive, denoted by the lack of expression of the live/dead marker, zombie yellow. Neutrophils were defined as CD45^{+}CD11b^{+}Ly6G^{+} cells, with CD45 a marker of immune cells, CD11b a marker of the monocyte lineage and Ly6G a bona fide neutrophil marker (**Figure 100**). From these sorted neutrophils, I performed RTqPCR for *Alk5 (***Figure 101**) and showed that expression of *Alk5* was reduced in the neutrophils collected from the *Ly6g-Cre; Alk5$^{fl/fl}$* mouse in comparison with the *Ly6g-Cre* mice.

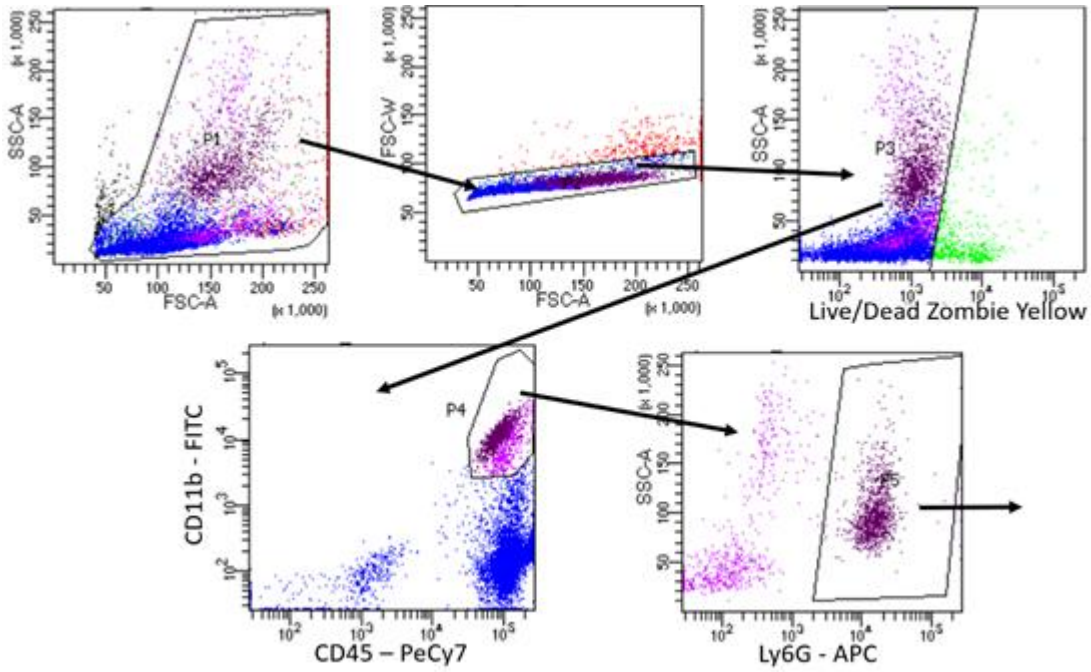

Figure 100 FACS neutrophil gating strategy
Neutrophils were sorted from the circulating blood of aged *Pdx1-Flp; Kras^{WT}; Trp53^{WT}; Ly6g-Cre; Alk5$^{+/+}$* and *Pdx1-Flp; Kras^{WT}; Trp53^{WT}; Ly6g-Cre; Alk5$^{fl/fl}$* mice. Neutrophils were defined as live single cells that were positive for CD45, CD11b and Ly6G. Representative flow plots of the gating used for isolating neutrophils.

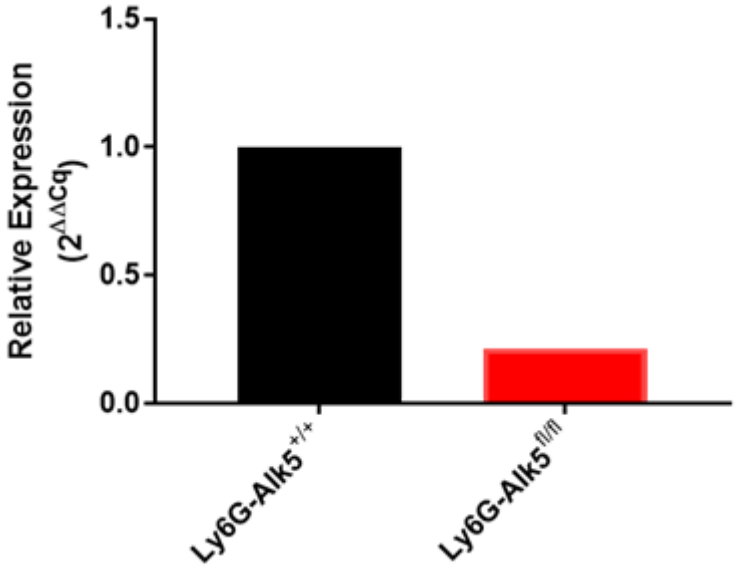

Figure 101 Expression of *Alk5* is reduced in neutrophils from *Ly6G-Cre; Alk5$^{f/fl}$* mice
Expression of *Alk5* was analysed in neutrophils obtained from the circulating blood via FACS. Neutrophils from the *Ly6g-Cre; Alk5$^{fl/fl}$* mouse had reduced expression of *Alk5* in comparison to the wild-type controls, as determined by RTqPCR (n=1).

I next examined the composition of cells in the blood of the mice through utilisation of the IDEXX ProCyte Haematology Analyser. The IDEXX is essentially a mini flow cytometer that examines the composition of the blood by side scatter and side scatter fluorescence, which determines the granularity and nuclear content to cell size ratio, allowing for the separation of distinct white blood cell populations.. I collected blood through cardiac puncture from 6wk old and 8wk old *Ly6g-Cre; Alk5$^{+/+}$*, *Ly6g-Cre; Alk5$^{fl/+}$* or *Ly6g-Cre; Alk5$^{fl/fl}$* mice, which were otherwise WT, as well as from tumour bearing KPF^{L} mice of the various *Alk5* genotypes. At both the 6-week and 8-week time points there was no significant change in total number of white blood cells (WBCs) counted across any of the genotypes. In the KPF tumour bearing mice there was an elevated number of WBCs when compared to the blood taken from WT mice with healthy pancreas, however, WBC numbers were again unaffected by the neutrophil-specific deletion of *Alk5* (**Figure 102**).

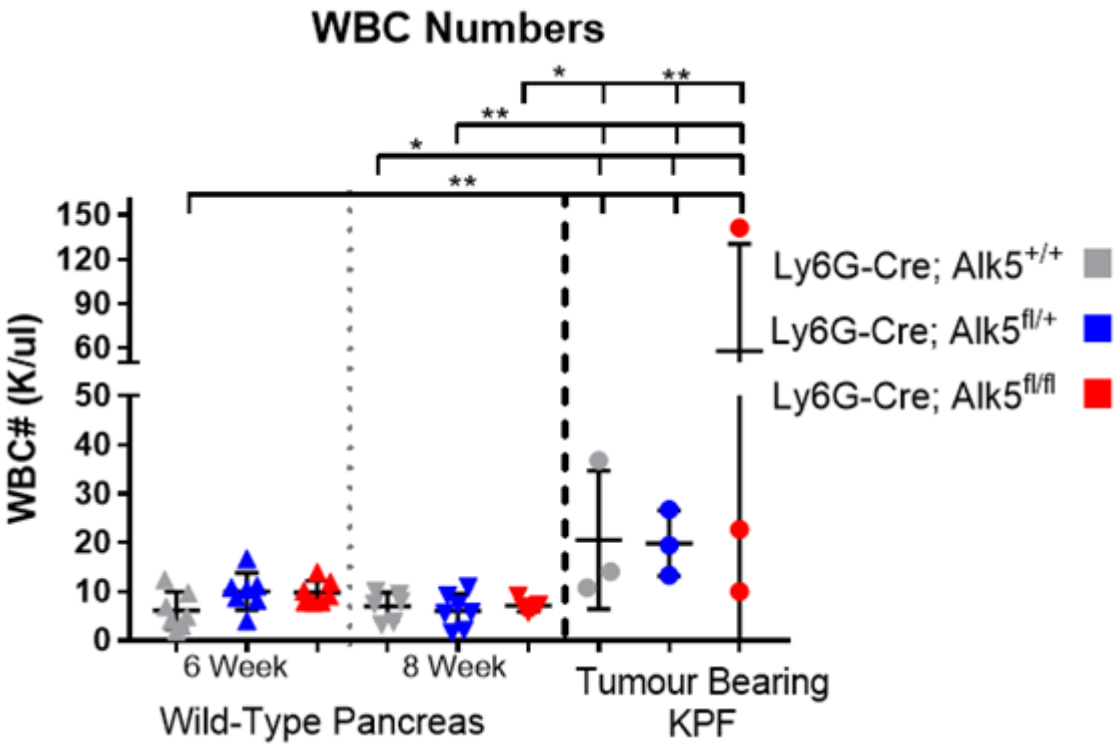

Figure 102 Circulating WBC levels are unaffected by deletion of *Alk5* but are elevated in tumour bearing mice
Total WBCs were counted from the blood of both wild type and tumour bearing mice using the IDEXX analyser. Neutrophil-specific heterozygous or homozygous deletion of *Alk5* did not affect the levels of circulating WBC at either the 6-week, or 8-week timepoint, or in tumour bearing KPF mice. WBC numbers were significantly elevated in the tumour bearing mice in comparison to their wild type pancreas controls (1 way ANOVA with uncorrected Dunn's Test for multiple comparisons). n=6-7 in Wild-Type pancreas samples, n=3 in KPF samples)

The increase in WBC numbers was accounted for by a significant increase in both monocyte and neutrophil numbers in the tumour-bearing mice. However, this was again unaffected by the deletion of *Alk5* in neutrophils, and there was no change noted at either the 6-week or 8-week time points. The lymphocyte numbers were unchanged across all genotypes regardless of the time point taken or the presence of a tumour in the KPF models (**Figure 103**). This is indicative of the chronic disease state promoting the egress of BM derived cells into the circulation, with lymphocytes unchanged due to their effector/priming sites existing in lymph nodes and tumour sites.

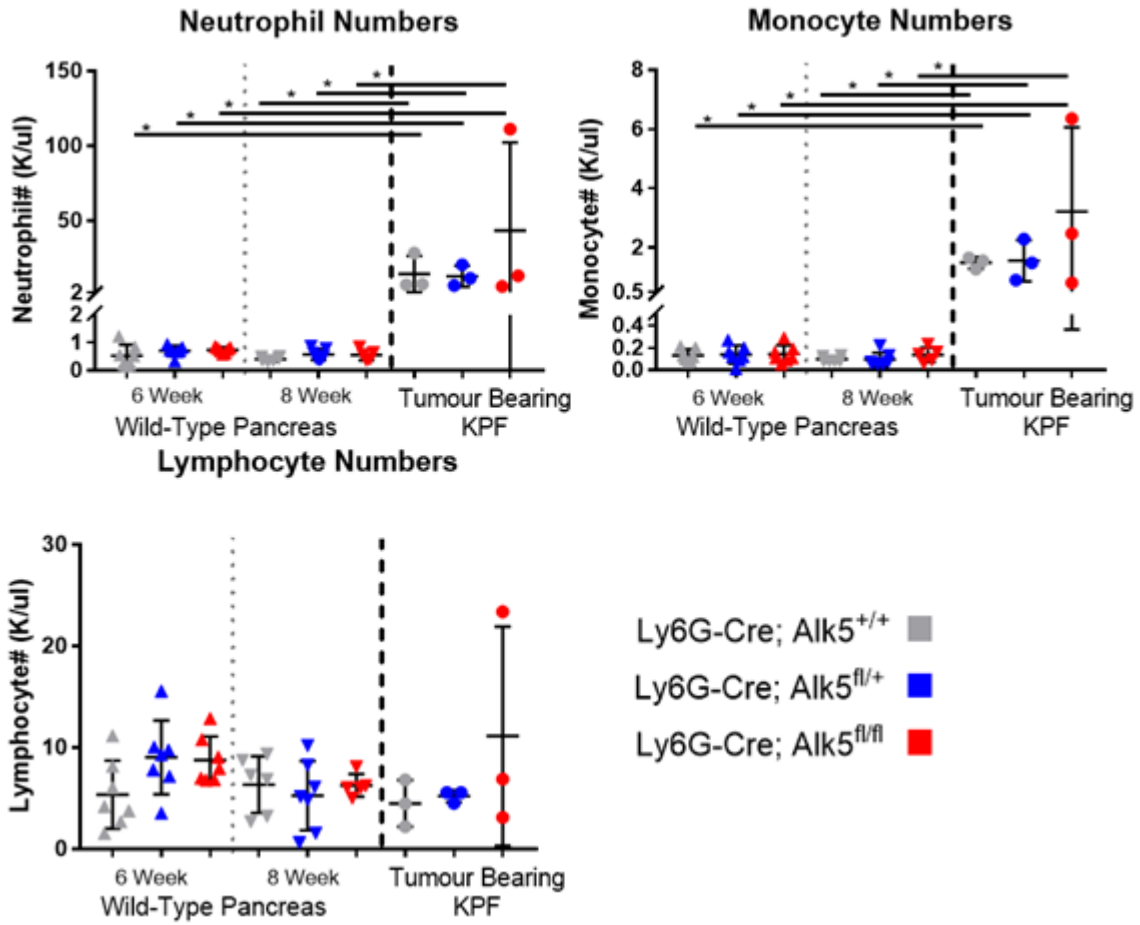

Figure 103 Neutrophils and monocytes, but not lymphocytes, are increased in the circulating blood of tumour-bearing animals, independent of neutrophil specific deletion of *Alk5*
The number of circulating neutrophils was unaffected by the neutrophil specific deletion of *Alk5* in wild-type tissue, however, in tumour bearing mice blood neutrophil numbers are elevated although *Alk5* deletion on neutrophils did not affect their numbers. Monocyte numbers were elevated in the tumour bearing mice in comparison to their wild-type controls and this was unaffected by *Alk5* deletion on neutrophils. Blood lymphocyte numbers were unaffected by the neutrophil deletion of *Alk5* or by the presence of a tumour. Neutrophil, monocyte and lymphocyte numbers were measured using the IDEXX ProCyte Haematology Analyser. (Mann Whitney test used, n=6-7 in Wild-Type pancreas samples, n=3 in KPF samples).

This is further embodied by the alteration of neutrophil and lymphocyte numbers as a proportion of WBCs. The proportion of lymphocytes was significantly reduced in the tumour-bearing mice when compared to the early time points, but was unaffected by the status of *Alk5* in the neutrophils. The opposite was true for the proportion of neutrophils, with a significant increase seen in the tumour bearing mice compared with the early time points; however, neutrophil specific *Alk5* deletion did not affect this change. Finally, as expected from the increase in numbers in the blood, there was also an increased proportion of monocytes in tumour bearing mice compared with healthy wild-type mice, in an

Alk5 independent manner (**Figure 104**). Ultimately, this demonstrated that deletion of *Alk5* in neutrophils does not affect the blood cell composition in normal or tumour bearing states. However, neutrophil numbers are significantly increased in the circulating blood upon development of PDAC.

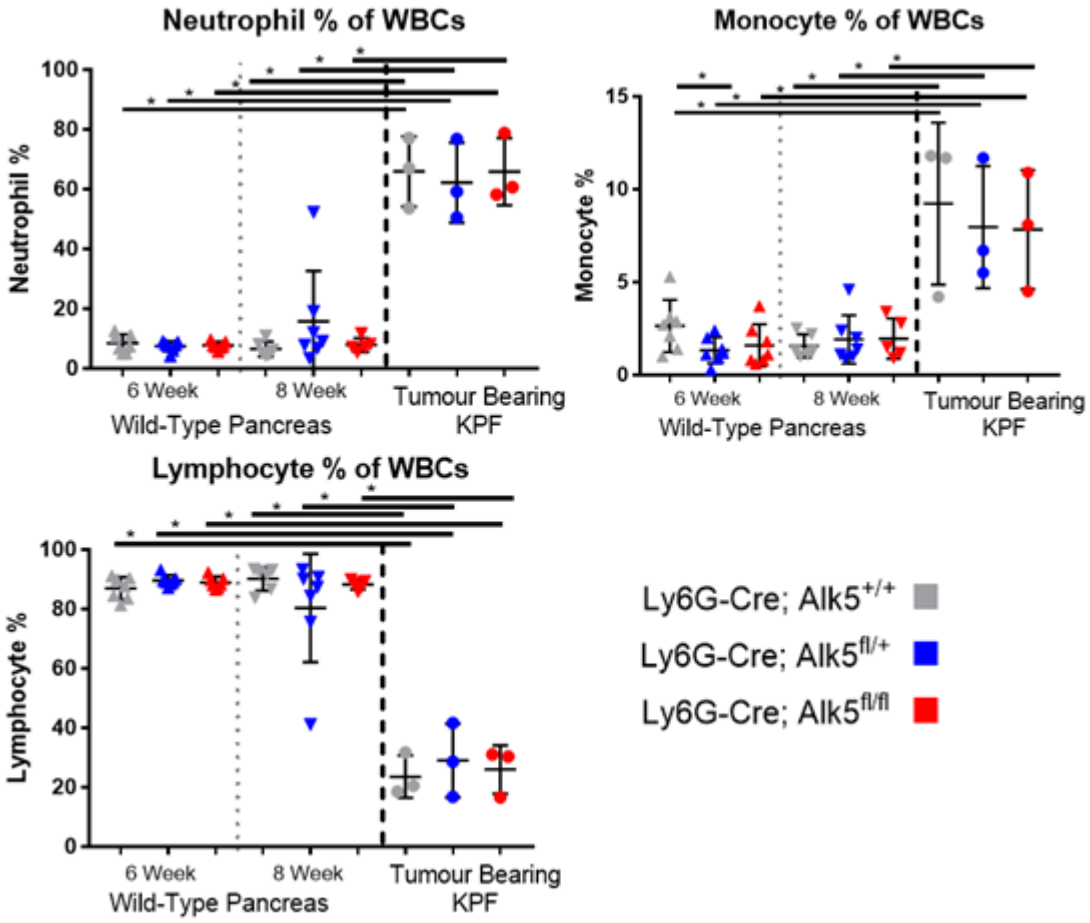

Figure 104 The proportion of neutrophils increases in the circulating blood in tumour bearing mice independent of *Alk5* deletion from neutrophils
The proportion of neutrophils as a % of total WBCs was increased in tumour bearing mice, but was not affected either in steady state or in tumour conditions by the neutrophil specific deletion of *Alk5*. Monocyte proportion increased in tumour bearing mice, but not wild-type mice independently of Alk5 status of neutrophils. Lymphocyte proportion decreased in tumour bearing mice, but still composed the majority of cells in the wild-type circulating blood and was unaffected by *Alk5* deletion in neutrophils. Neutrophil, monocyte and lymphocyte proportions were measured using the IDEXX ProCyte Haematology Analyser. (Mann-Whitney test, p-value <0.05 = *, n=6-7 in Wild-Type pancreas samples, n=3 in KPF samples).

6.3.2 Neutrophil deletion of *Alk5* does not affect survival but limits metastasis.

With the blood cell composition unchanged upon neutrophil specific deletion of *Alk5,* I sought to investigate the impact on survival in ageing cohorts of tumour-prone mice. As shown in **Figure 105** the heterozygous or homozygous deletion of *Alk5* in neutrophils had no impact on the survival of KPF mice in comparison to *Alk5* wild type controls. These mice were sampled at clinical end-point due to PDAC related phenotypes, and as can be seen in representative images of the end-point tumours (**Figure 106**), present with broadly similar tumour morphology.

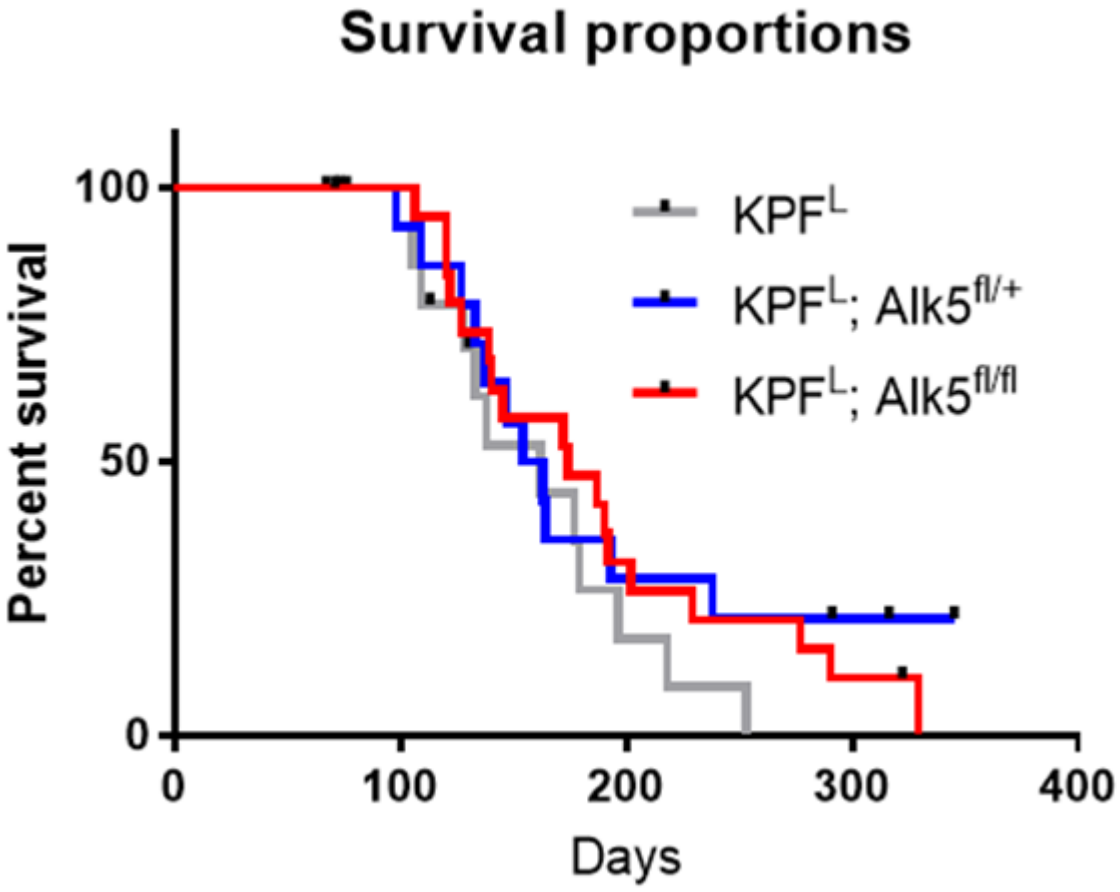

Figure 105 Survival of KPF mice is unaffected by neutrophil-specific deletion of *Alk5*
Kaplan-Meier survival analysis of KPF mice with either wild type neutrophils, or heterozygous or homozygous neutrophil-specific deletion of *Alk5,* showing no differences in survival. (n=16,15, 21 respectively, median survival KPF^{L}=162days, KPF^{L}; Alk5$^{fl/+}$=159days, KPF^{L}; Alk5$^{fl/fl}$ =174days)

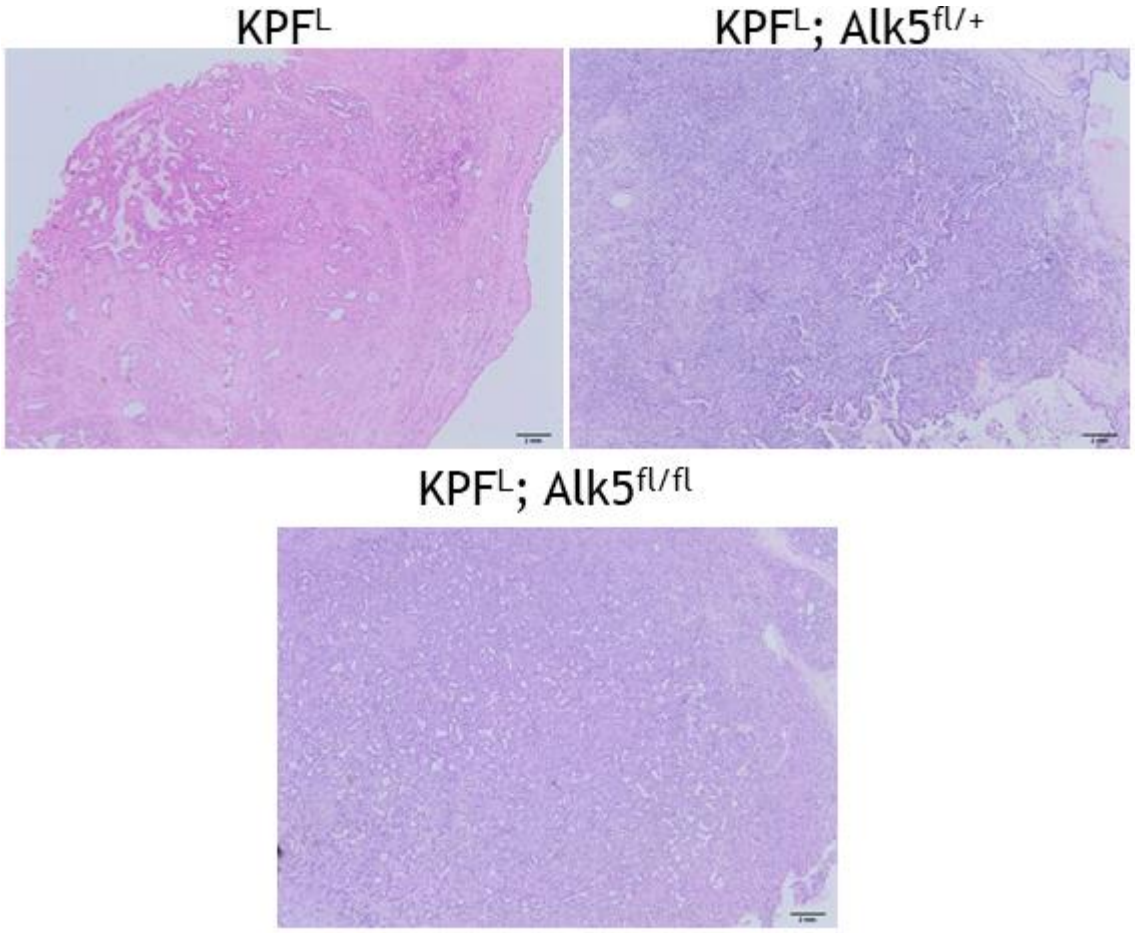

Figure 106 Representative images of KPF^{L} end-point tumours
Representative images of H&E stained sections of end-point tumours sampled from KPF^{L}; Alk5$^{+/+}$, KPF^{L}; Alk5$^{fl/+}$, and KPF^{L}; Alk5$^{fl/fl}$ models. Tumours across the cohorts presented with broadly similar morphology. (Scale bars = 2mm).

Subsequently I investigated the infiltration of neutrophils into the tumours by staining for myeloperoxidase (MPO) in end-point tumours. MPO positive cells infiltrating the tumour site were counted across the cohorts. Representative images of MPO staining (**Figure 107**) indicate that neutrophils penetrate into central tumour areas, regardless of *Alk5* deletion. Quantification of the MPO staining demonstrated that neutrophil infiltration into end-point KPF^{L} tumours was unchanged when they lack *Alk5* expression (**Figure 107**). Thus, I conclude that deletion of *Alk5* in neutrophils did not affect their infiltration into tumours.

With neutrophils known to inhibit T cell responses (Pillay et al., 2012; Zea et al., 2005) I counted the number of infiltrating CD3^{+} T cells in end point tumours. Representative images of CD3 staining highlighted the low penetrance of T cells

infiltrating PDAC, as expected. The low abundance of T cells was similar across all cohorts, with quantification highlighting no significant change in T cell infiltration across the cohorts (**Figure 108**). These data collectively demonstrate that neutrophil-specific depletion of *Alk5* did not impact neutrophil or T cell infiltration into tumours in these models.

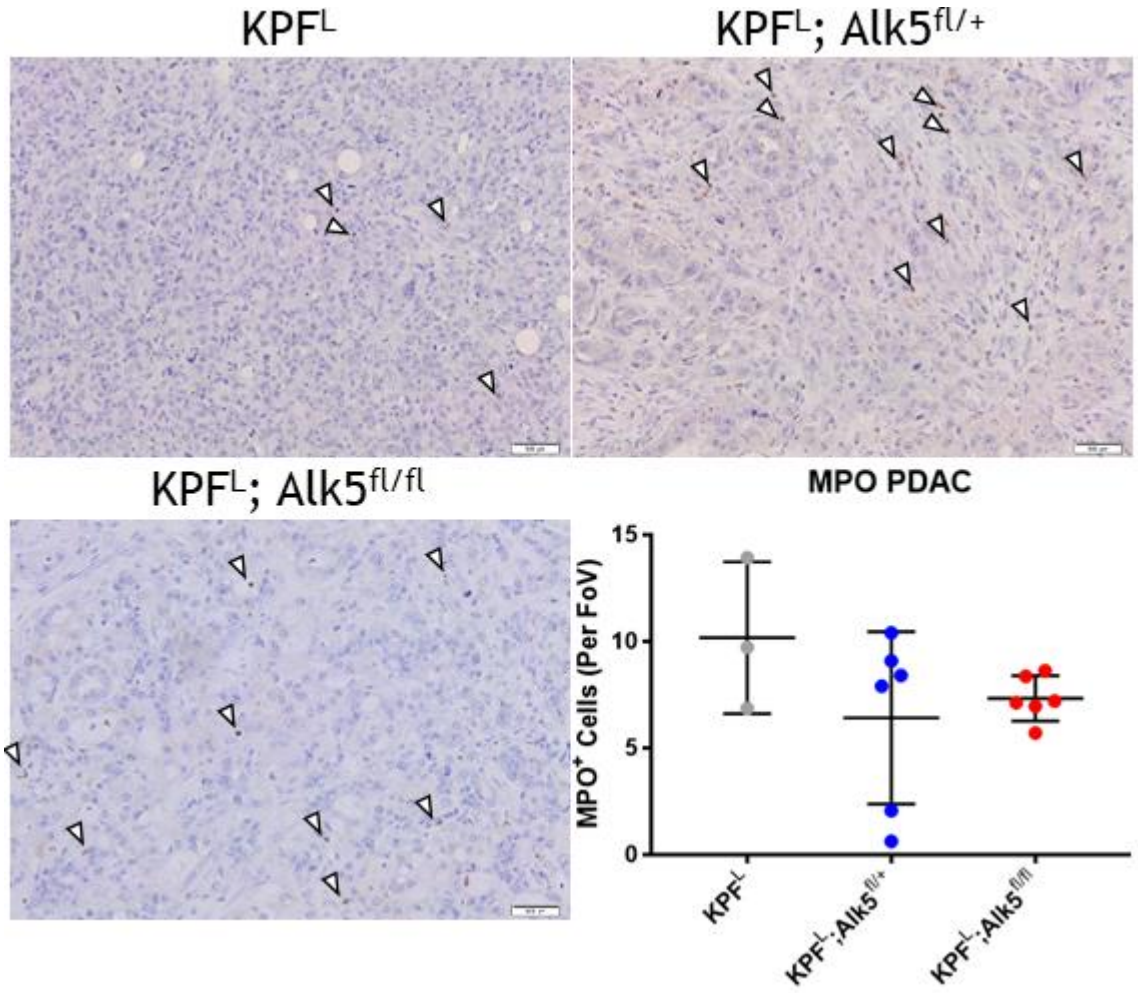

Figure 107 Neutrophil infiltration into end-point KPF^{L} tumours is unchanged when *Alk5* is deleted.
Representative images of immunohistochemical staining for the neutrophil marker MPO within end-point KPF^{L} tumours of the genotypes shown (Scale bars = 500μm). Arrowheads denote positive cells infiltrating the tumour beds. Quantification of MPO staining across the cohorts is shown in the bottom right quadrant. No significant difference in neutrophil infiltration was observed between the cohorts. (n=3,6, 6, average count of 30x field of view) (Mann-Whitney test used)

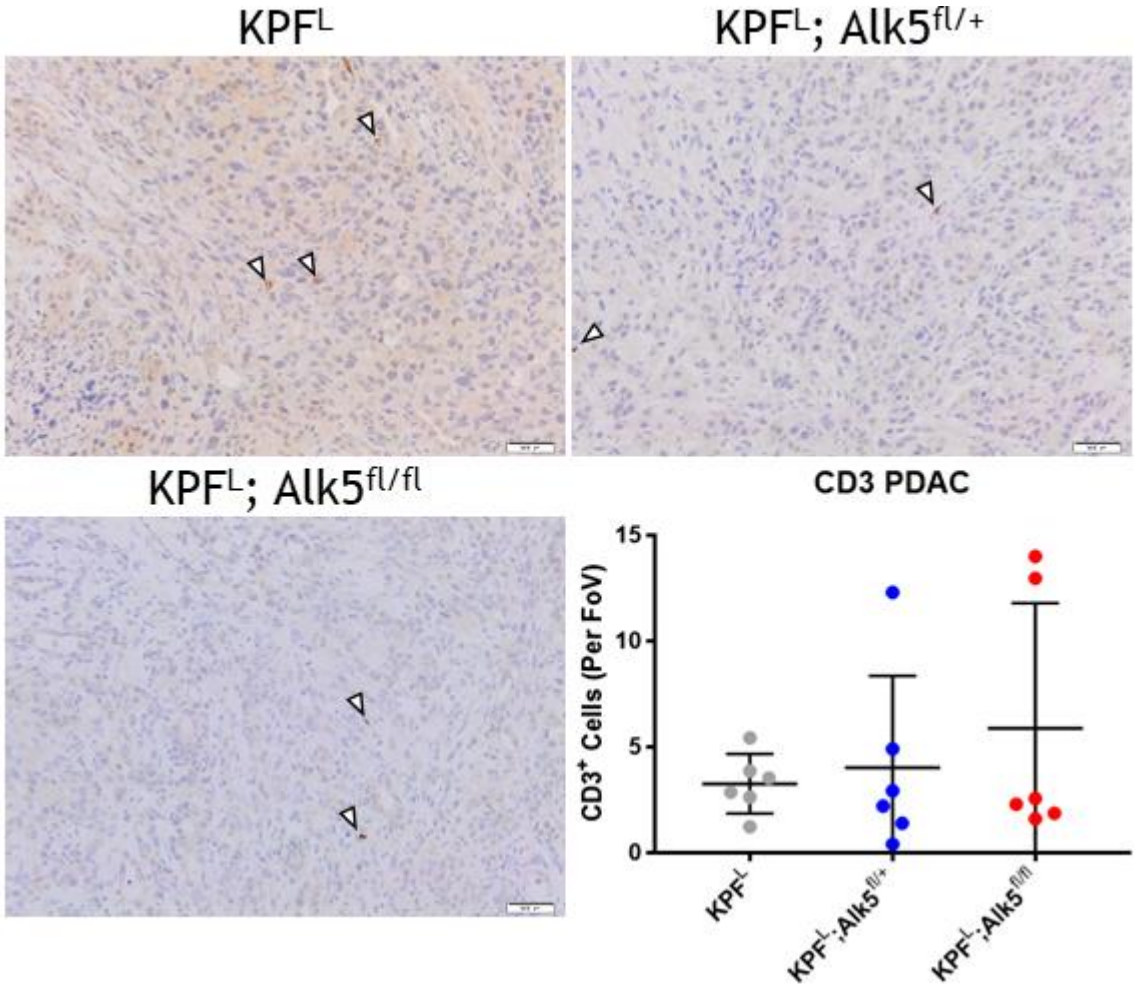

Figure 108 Tumour infiltration by CD3+ T cells was unaffected by neutrophil-specific deletion of Alk5
End-point tumour sections were stained by IHC for the T cell marker CD3, with representative images shown (Scale bars = 500μm). T cells infiltrated in low number into tumour regions. Quantification shown in the bottom right quadrant demonstrating no significant change in T cell infiltration between the cohorts (N= 6, 6, 6, average count of 30x field of view) (Mann-Whitney test used).

With multiple studies highlighting a link between neutrophils and metastasis (Coffelt et al., 2015; Jackstadt et al., 2019; Steele et al., 2016), I next assessed the metastatic burden in these cohorts (**Figure 109**). Representative images of both liver and lung metastasis are shown in **Figure 111.** Metastases are distinguishable from the normal tissue due to their ductal morphology. Although there was a slight decrease in the percentage of mice presenting with metastasis at any site in the KPF^{L}; Alk5$^{fl/fl}$ cohort in comparison to both the KPF^{L}; Alk5$^{+/+}$ and KPF^{L}; Alk5$^{fl/+}$ mice, this was not significant. Interestingly, the proportion of

mice presenting with liver metastasis was lower in the KPF^{L} mice than was expected, with over 70% of mice presenting with liver metastasis in the original KPF study (Schonhuber et al., 2014). KPF^{L}; $Alk5^{fl/fl}$ mice presented with reduced metastasis to the lung in comparison with the KPF^{L}; $Alk5^{fl/+}$ and KPF^{L}; $Alk5^{+/+}$ mice, and with decreased liver metastasis compared to the KPF^{L}; $Alk5^{fl/+}$, but not the KPF^{L}; $Alk5^{+/+}$ mice. However, significance was not reached in either case. The mice also presented with metastasis to the diaphragm, which has not been reported previously in this model. However, rates were unchanged when comparing the KPF^{L}; $Alk5^{+/+}$ to KPF^{L}; $Alk5^{fl/fl}$ mice. The number of mice presenting with metastasis to multiple sites concurrently was also examined. Although KPF^{L}; $Alk5^{fl/fl}$ mice present with a reduced percentage of multi-site metastasis in comparison to the KPF^{L}; $Alk5^{fl/+}$ mice, this was unchanged in comparison to the KPF^{L}; $Alk5^{+/+}$ mice (**Figure 109**). Further the number of metastasis present within either the liver or the lung of the KPF^{L}; $Alk5^{fl/fl}$, KPF^{L}; $Alk5^{fl/+}$ and KPF^{L}; $Alk5^{+/+}$ was counted from a single H&E stained slide of the relevant tissue type. Notably there was no significant change in the number of metastatic lesions detected in either the liver or lung of the models examined (**Figure 110**). Together, these data indicate that deletion of neutrophil *Alk5* may influence the metastasis of PDAC, however, increased cohort numbers are required to draw any firm conclusions.

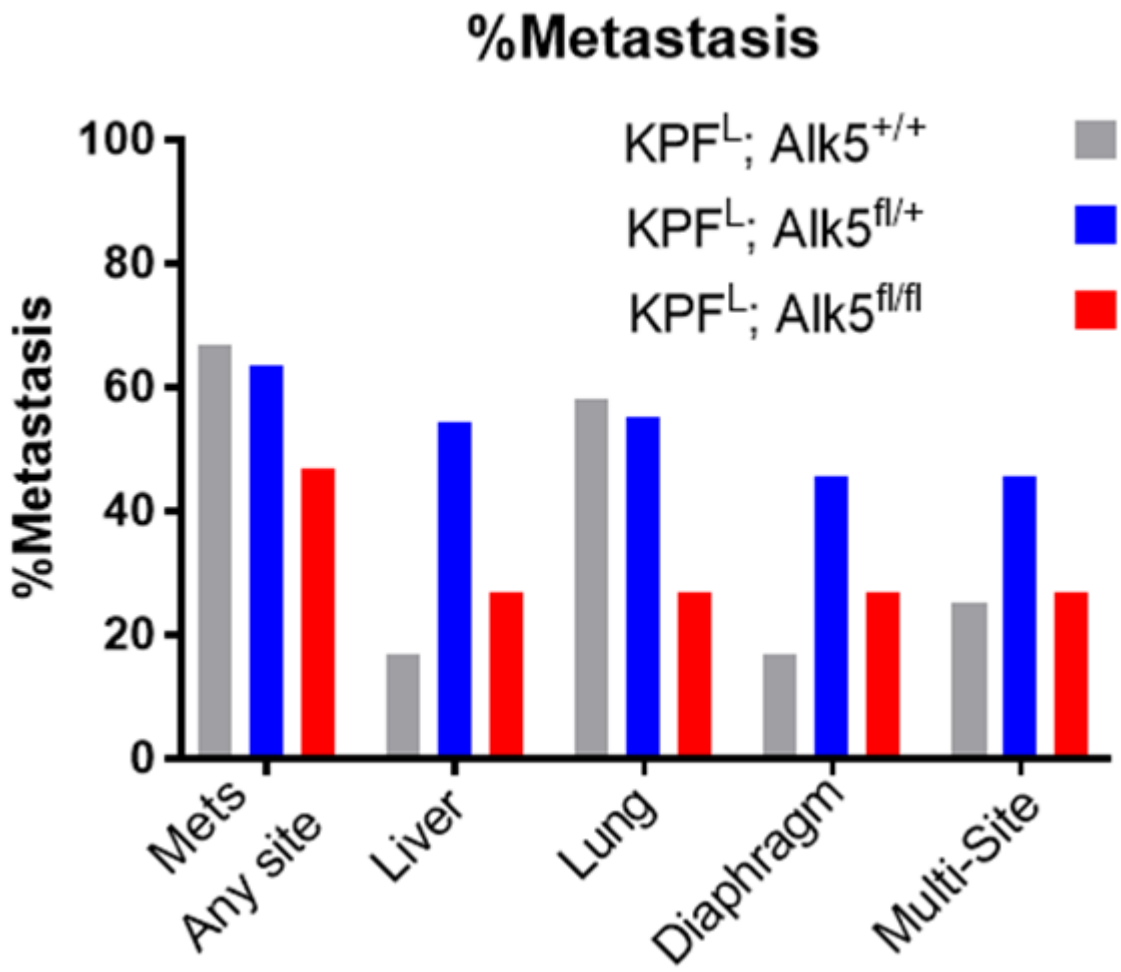

Figure 109 Metastatic burden in the KPF^{L} model
The percentage of mice presenting with macro- or micro-metastasis to the various sites is shown. Mets at any site denotes the presence of any evidence of metastasis, with liver, lung and diaphragm reporting the presence of organ specific metastasis. Multi-site metastasis denotes mice presenting with concurrent metastasis to multiple sites. (n=12, 11, 15 respectively) (Fisher's exact Test used).

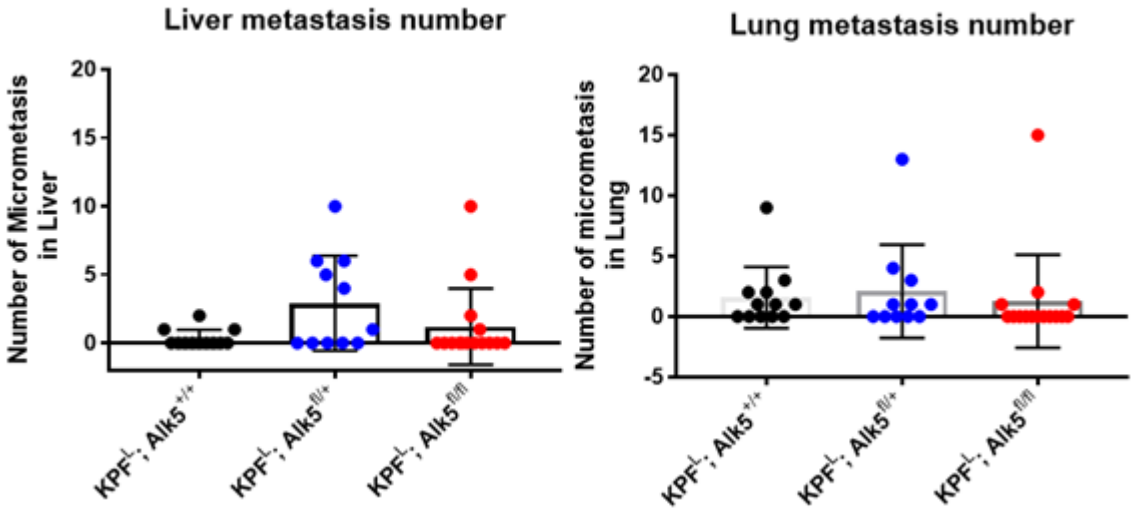

Figure 110 The number of metastatic nodules detected in the liver and lung was unchanged between KPF^{L} models

The number of metastasis present within the liver and lungs of the indicated mouse models was counted across a single H&E stained tissue slide. The was no significant difference in the number of liver metastasis counted across the models in the liver, or in the lung. (n=12, 11, 15 respectively) (Mann Whitney test used).

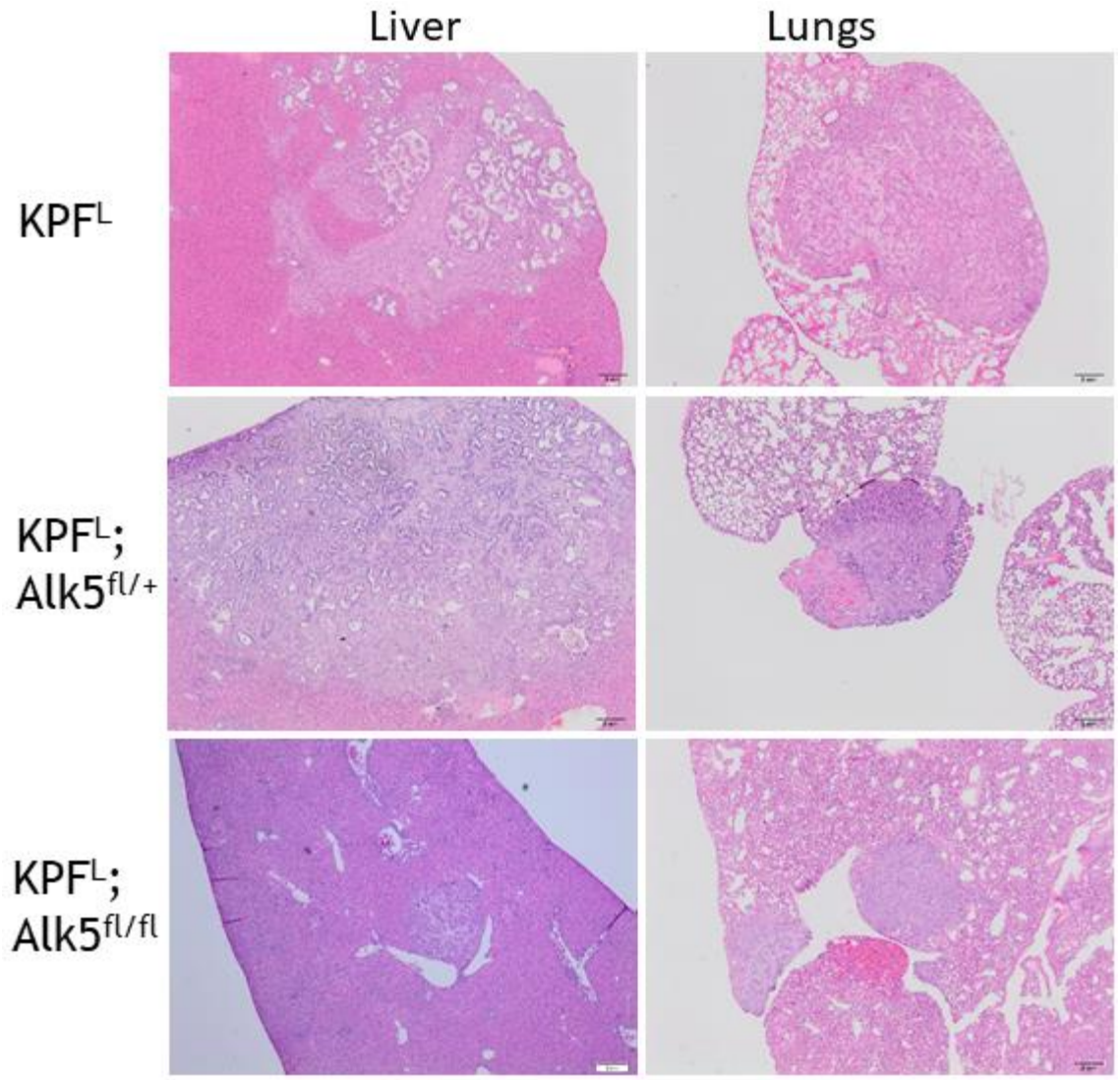

Figure 111 Representative images of liver and lung metastasis in the KPF^{L} mice. Representative images of H&E stained sections of liver and lung metastasis in the KPF^{L} mice of the indicated genotypes. Metastasis present with a ductal morphology and are easily distinguishable from the normal organ architecture. (Scale bars = 2mm).

Subsequently, with these slight changes in metastasis detected in the liver, and with neutrophil-specific deletion of *Alk5* shown to reduce liver infiltrating neutrophils while increasing T cells in a metastatic colorectal cancer model (Jackstadt et al., 2019), I investigated both neutrophils and T cell infiltration into this site. MPO staining was counted across the liver tissue with representative images shown in **Figure 112**. Quantification of MPO^{+} cells demonstrated that neutrophil infiltration into the liver was unchanged, with CD3 T cell infiltration into the liver also unchanged. Representative images and quantification are shown in **Figure 113**. Therefore, neutrophil-specific loss of

Alk5 in a metastatic PDAC model does not exclude neutrophils from infiltrating the liver, nor does it alter neutrophil T cell numbers via their crosstalk.

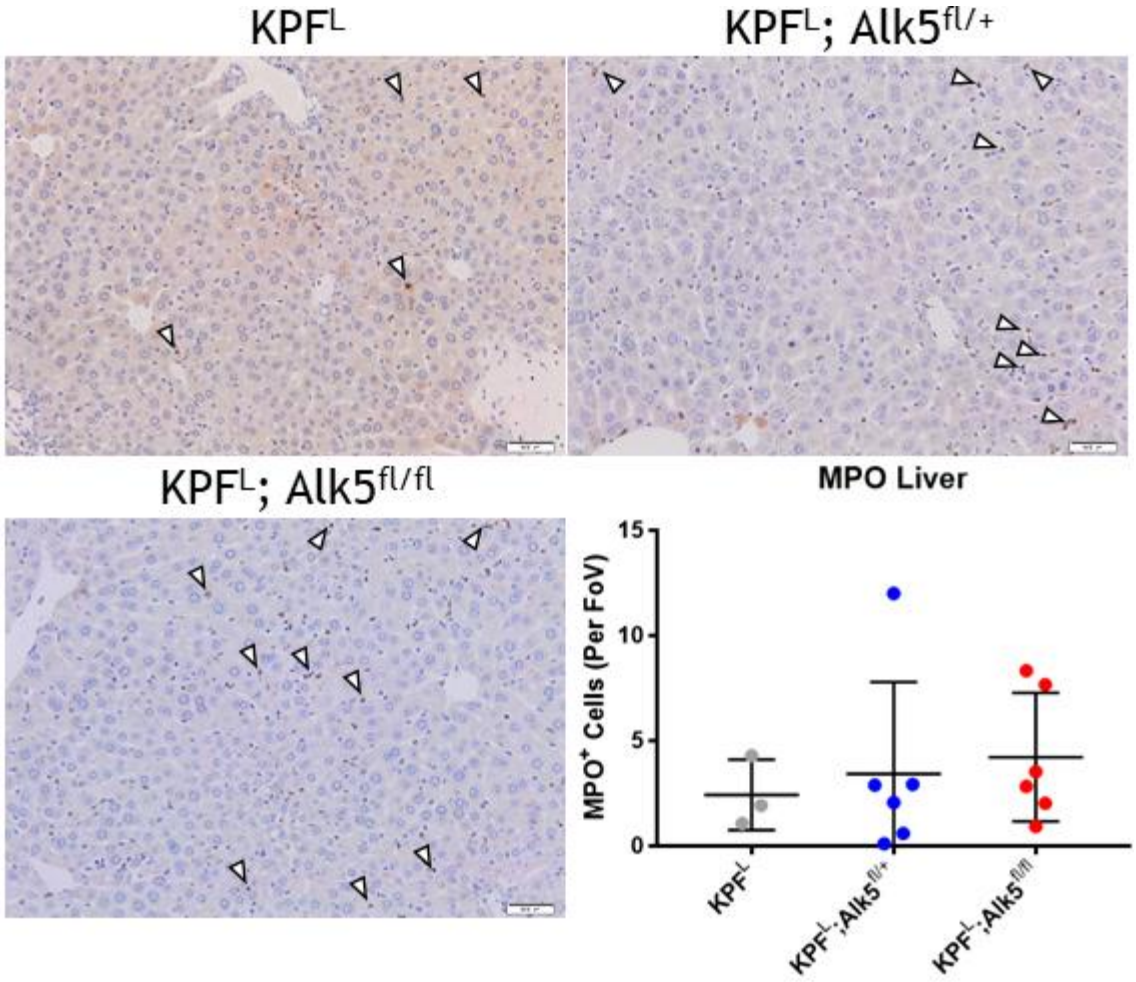

Figure 112 Neutrophil infiltration into the liver is not affected by neutrophil specific deletion of *Alk5*
MPO IHC staining was conducted on sections of livers from end-point tumour-bearing KPF^{L} mice of the indicated genotypes (Scale bars = 500μm). Representative images are shown with MPO^{+} cells highlighted with white arrowheads. Quantification of MPO^{+} cells showed no significant changes across the cohorts. (N= 3, 6, 6, average count of 30x field of view) (Mann-Whitney Test used).

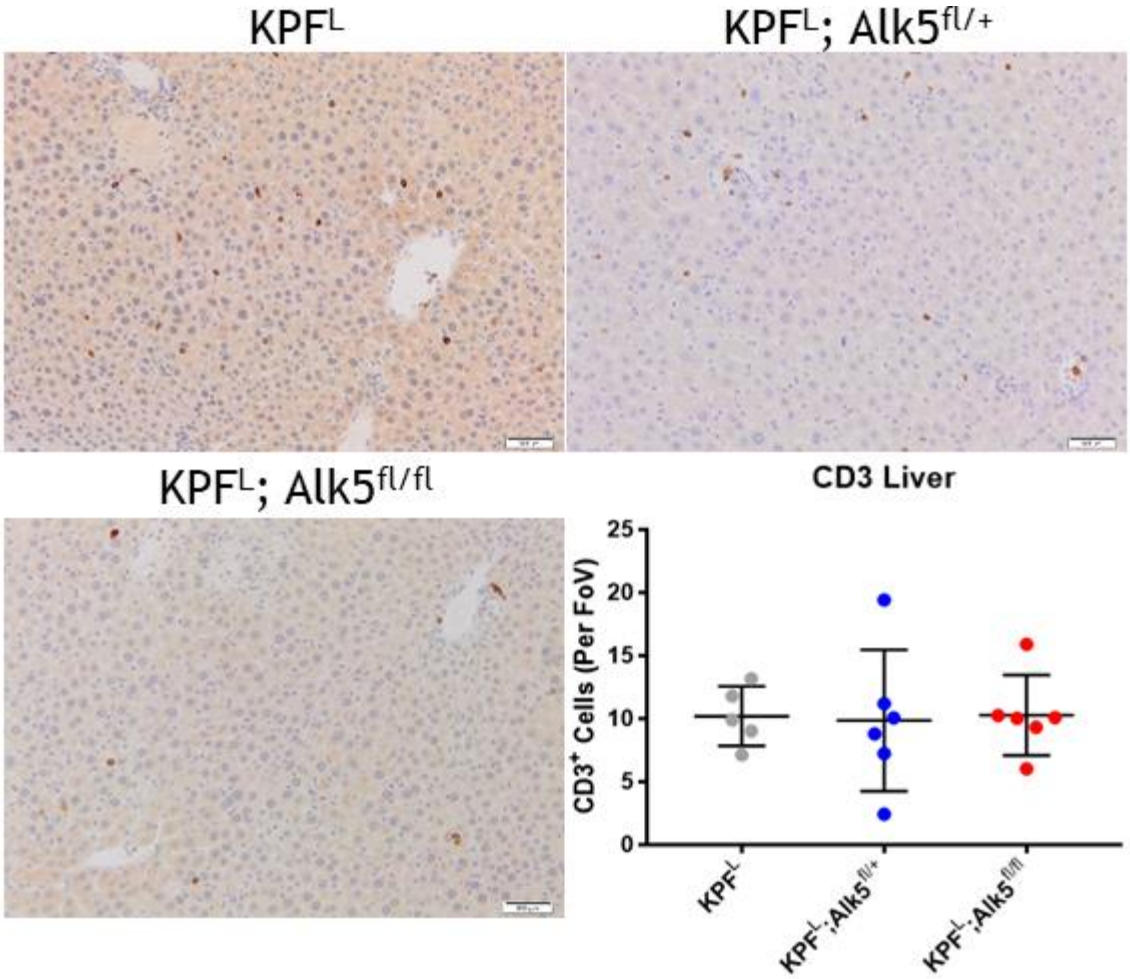

Figure 113 CD3^{+} T cell infiltration into the liver is not affected by neutrophil-specific deletion of *Alk5*

CD3 IHC staining was conducted on liver tissue from end-point tumour bearing KPF^{L} mice of the indicated genotypes (Scale bars = 500μm). Representative images of CD3 stained livers are shown. Quantification of CD3 positive cells shows no significant change across the cohorts. (N=6, 6, 6, average count of 30x field of view) (Mann-Whitney Test Used).

6.3.3 Neutrophil maturity

With no change in survival, but some potentially interesting effects on metastasis, and with TGFβ signalling predicted to dictate pro-/anti-tumourigenic potential of neutrophils (Fridlender et al., 2009), I sought to characterise the circulating, tumour infiltrating and metastatic site infiltrating neutrophils in wild-type compared to *Alk5* deficient neutrophil models. To do so I used a flow cytometry panel to interrogate multiple markers, which have previously been shown in the literature to denote more activated or mature neutrophils (**Figure 114**). The panel initially identified neutrophils as $CD45^{+}Lineage^{-}CD11b^{+}Ly6G^{+}$ cells as shown in the gating strategy in **Figure 115**. Lineage negative cells were those defined as not expressing T cell (CD3), B cell (CD19), macrophage (CSF1R), eosinophil (Siglec-F), natural killer (NKp46) or red blood cell (Ter119) markers. CD45 is a definitive marker for immune cells, with CD11b expressed on myeloid cells. Ly6G is the prototypical marker used for neutrophils in flow cytometry, and therefore this denotes a pure neutrophil population. This population was visible within the spleen, liver, and lung of wild-type mice (**Figure 116)**, but not in the pancreas, which was sparsely infiltrated with immune cells in general in steady state (**Figure 117**). I therefore conducted a pilot study across a small number of mice to elucidate any tumour-induced and Alk5 specific alterations in neutrophil maturity.

Marker	Type
CD45	Immune Cell populations
CD11b	Myeloid Cell marker
Ly6G	Neutrophil marker $Ly6G^{hi}$ = mature
ICAM-1	Adherence $ICAM^{+}$ = increased ROS
CD62L	Adherence $CD62L^{lo}$ = Inhibit T cells
CD101	Maturity $CD101^{+}$ = mature neutrophils
c-Kit	Stem marker $cKit^{+}$ = increased in metastasis
CXCR4	Bone Marrow $CXCR4^{+}$ = Old or immature
CXCR2	Blood $CXCR2^{+}$ = mature neutrophils

Figure 114 Neutrophil maturity panel
Selected neutrophil markers were used in a flow cytometry panel to assess neutrophil maturity across multiple tissue types in the *Ly6g-Cre* model. Neutrophils were defined as $CD45^{+}Lin^{-}CD11b^{+}Ly6G^{+}$ cells. From this population the markers listed were utilised to determine neutrophil maturity and effector function.

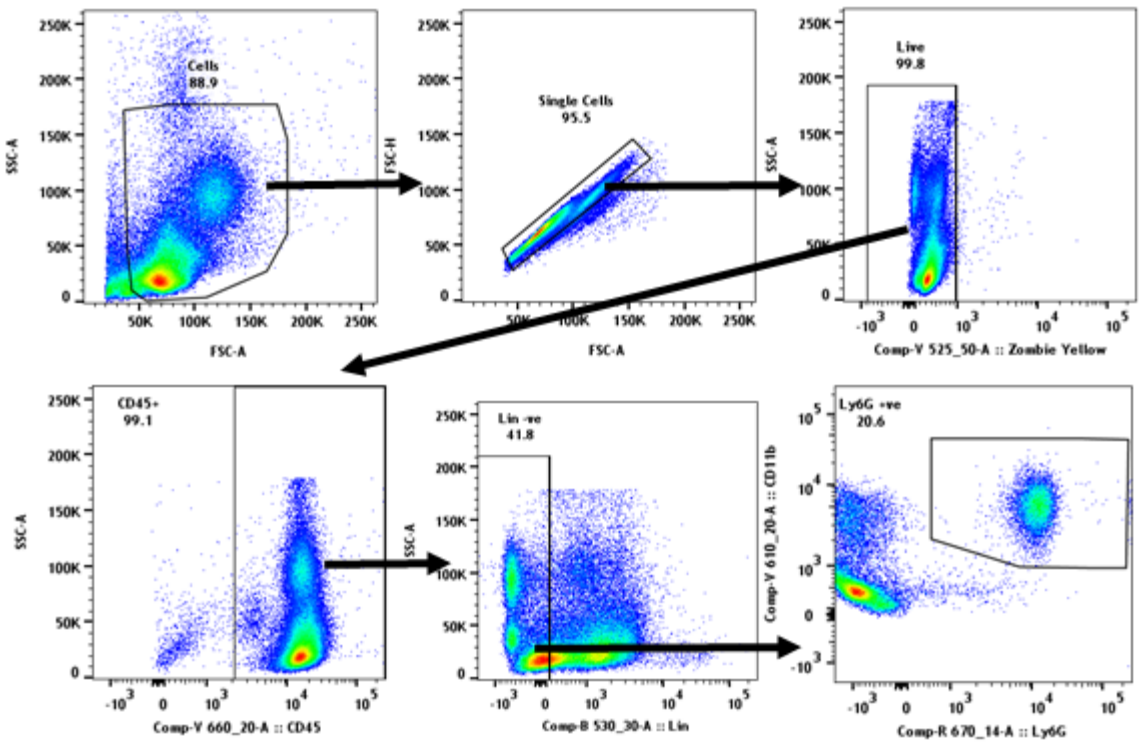

Figure 115 Gating strategy for identifying neutrophil populations
The gating strategy above was used to identify neutrophils. The top left panel selects all cells, the top centre panel shows the gate to exclude any doublets, with the top right panel selecting cells negative for the live dead marker zombie yellow. From this live population immune cells ($CD45^+$) cells were selected, bottom left, and those negative for the lineage markers (bottom middle) were finally selected as a pure neutrophil population by expression of markers CD11b and Ly6G (bottom right). Representative data is shown from blood taken from a wild-type mouse.

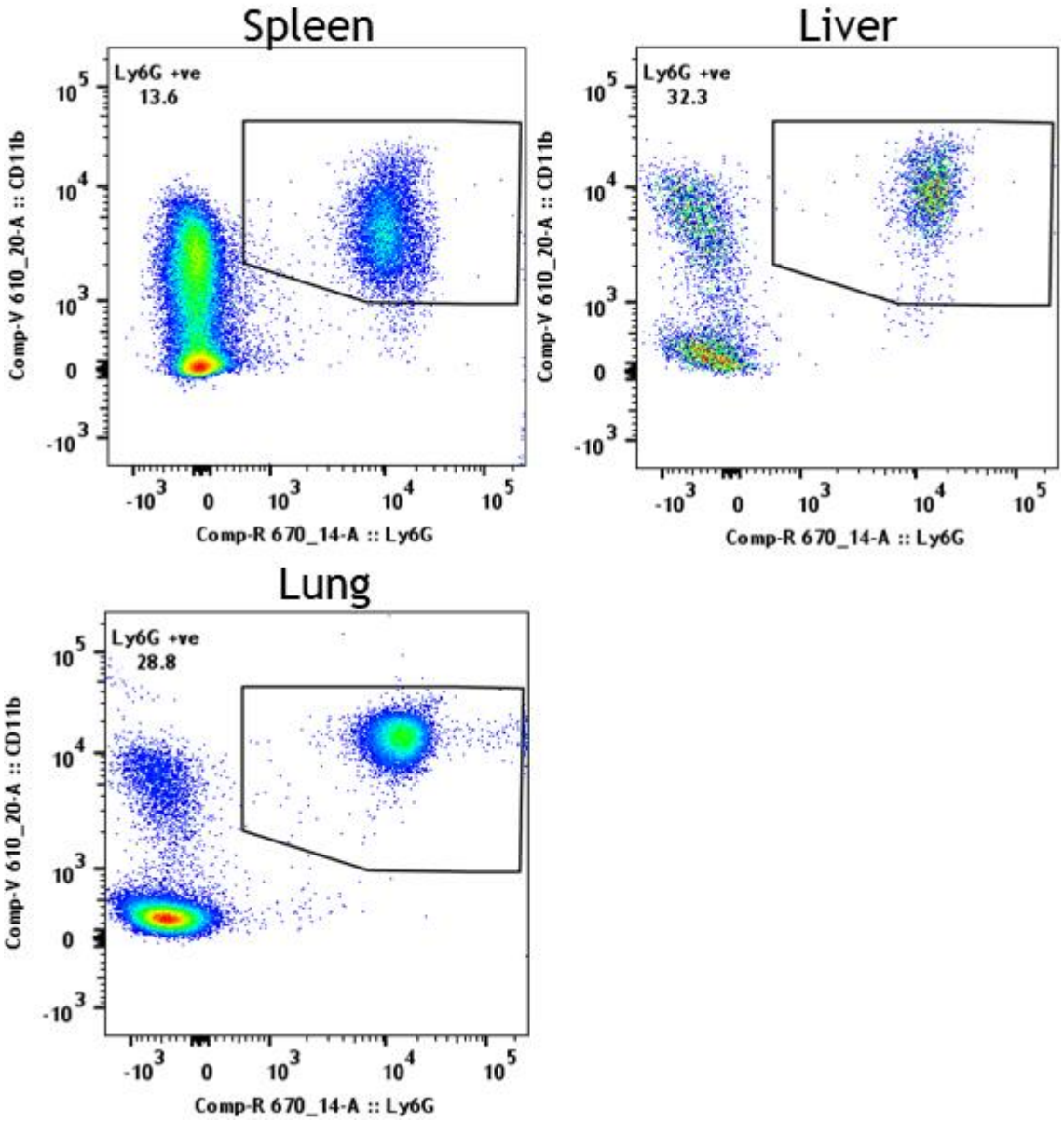

Figure 116 Neutrophils are found in the spleen, liver and lung of wild-type mice
Representative flow plots of the $CD45^+Lineage^-CD11b^+Ly6G^+$ neutrophil population in the spleen, liver and lung of wild-type mice.

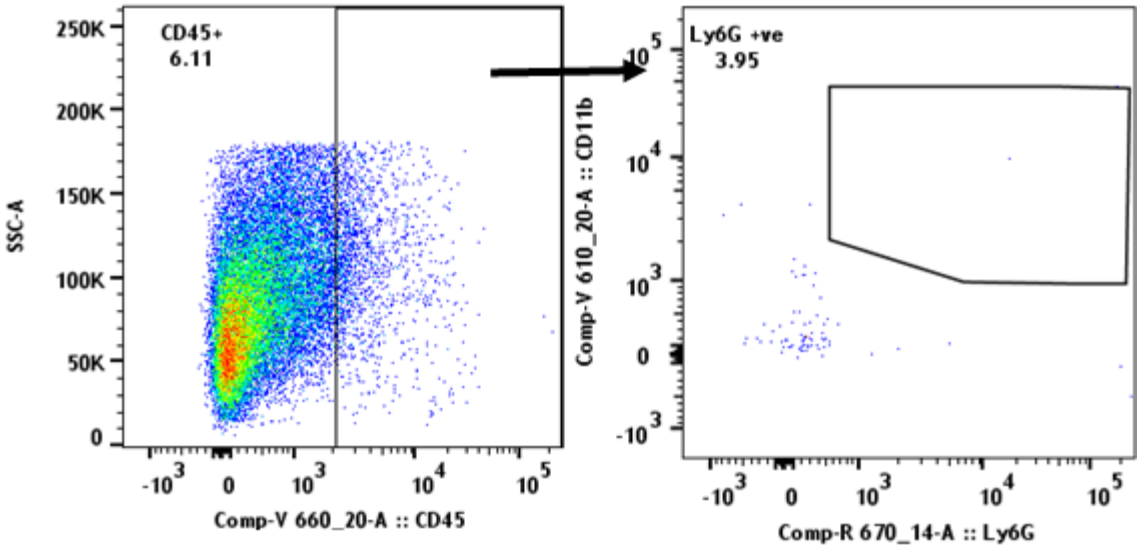

Figure 117 normal pancreas is sparsely infiltrated by neutrophils
Normal pancreata from wild-type mice were dissociated and flow cytometry was performed on the stained cells. $CD45^+$ cells composed a small proportion of the total cells in the pancreas (Left panel), with neutrophils being almost non-existent in the pancreas at steady state (right panel).

With neutrophils present within the different tissues, to varying extents, and able to be analysed by flow cytometry, I next sought to interogate the maturity of these cells. Initially I considered the expression of Ly6G, with high expression shown to mark more activated and effector neutrophil populations (Deniset et al., 2017). Ly6G high and intermediate gating was defined by the wild-type blood sample, as in steady state neutrophils in the cicrulating blood are fully mature (Rice et al., 2018; Xie et al., 2020). Therefore, 99.5% of the $CD45^+Lin^-CD11b^+Ly6G^+$ neutrophils in the wildtype blood were $Ly6G^{hi}$ (**Figure 118**). Interestingly, in blood samples from the tumour bearing KPF mice, the percentage of $Ly6G^{int}$ neutrophils was greatly increased in the KPF^L; $Alk5^{fl/fl}$ sample in comparison to the KPF $Alk5^{+/+}$ sample. This was surprising given that the prescence of tumour was expected to cause the chronic egress of immature neutrophils, with deletion of *Alk5* hypothesised to increase their maturity. Of course, this experiment is caveated by the fact that it is a preliminary study with a sample size of just 1 per cohort.

When examining the proportion of $Ly6G^{hi}$ cells from the total $Ly6G^+$ cells across the various tissue types, there was a trend towards decreased $Ly6^{hi}$ cells in all

tissues from the tumour bearing KPF^{L}; *Alk5*$^{fl/fl}$ mice, however, the Ly6G^{hi} proportion in other models remained largely unaltered (**Figure 119**). It is important to note that Ly6G allele imbalance may have played a role in this decrease. The wildype control and KPF mouse did not express Ly6G-Cre, and therefore retained two intract alleles of Ly6g, whereas in the *Alk5* deleted models one copy of *Ly6g* was replaced with *Ly6g-Cre*, which was noted in the original publication to result in a decrease in Ly6G expression (Hasenberg et al., 2015). This is particulalry pertinent given the Ly6G^{hi} gating was defined by the wild type blood sample Ly6G^{+} population. Nevertheless, the same switch in ratio towards Ly6G^{int} neutrophils was not evident in any of the tissue samples from the Ly6G; *Alk5*$^{fl/fl}$ control mice, suggesting this finding is worthy of follow up. Unfortunately, in this small pilot experiment the blood sample from the Ly6G-Cre; *Alk5*$^{fl/fl}$ mouse was of inadequate quality for flow cytometry analysis, so gating could not be based on blood from the same model.

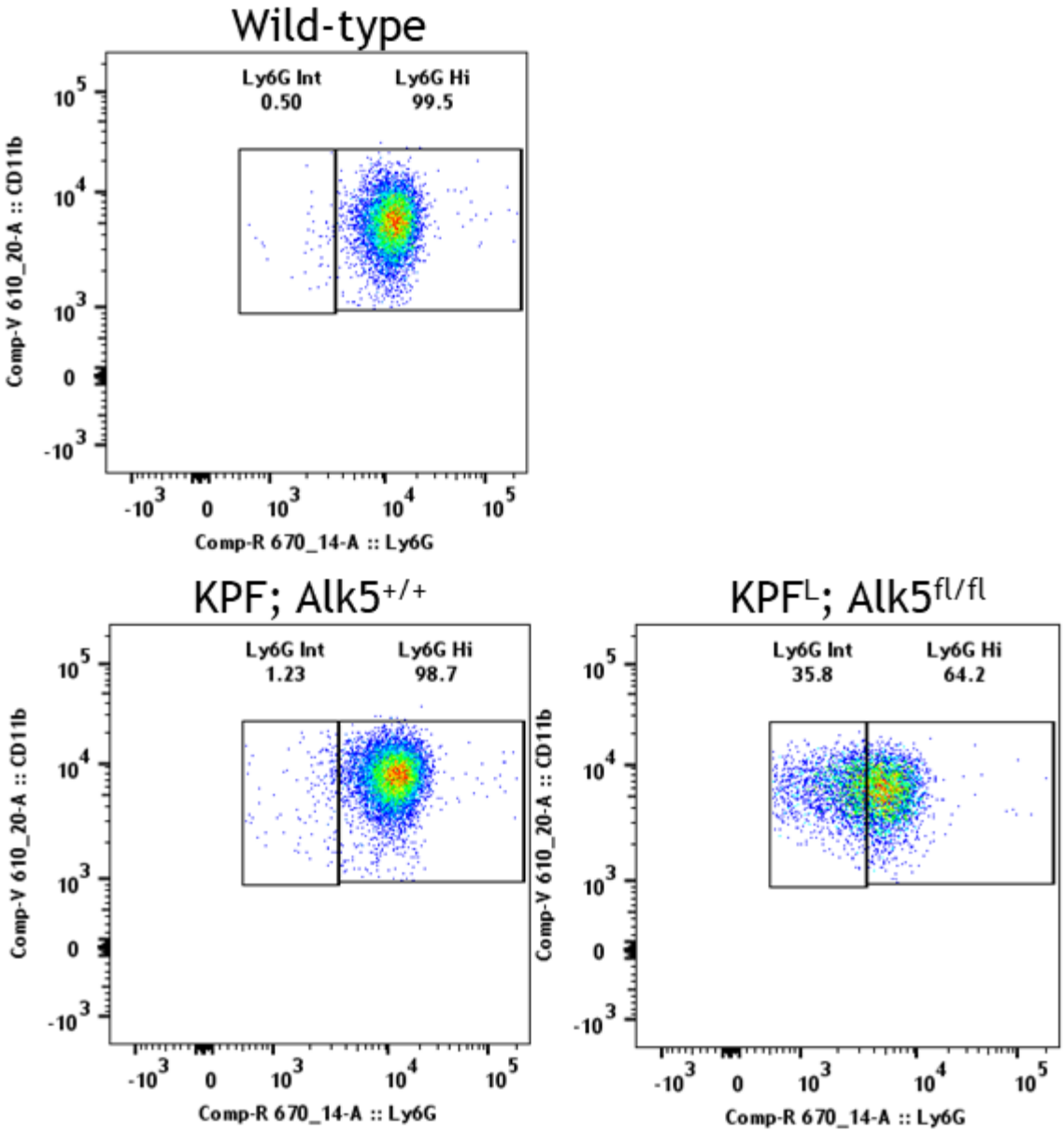

Figure 118 Reduced Ly6G^{hi} neutrophils in circulating blood from KPF^{L}; Alk5$^{fl/fl}$ tumour bearing models
The presence of Ly6G^{hi} and Ly6G^{int} neutrophils was examined as a proportion of all CD45^{+}Lin^{-} CD11b^{+}Ly6G^{+} cells. Ly6G^{hi} gating was defined by the Ly6G^{+} population in blood from a wild-type healthy mouse (top panel) with all Ly6G neutrophils marked as Ly6G^{hi}. There was no difference in the proportion of Ly6G^{hi} neutrophils in the KPF sample, however, Ly6G^{hi} neutrophils were reduced in the KPF^{L}; Alk5$^{fl/fl}$ circulating blood, with increased Ly6G^{int} neutrophils noted.

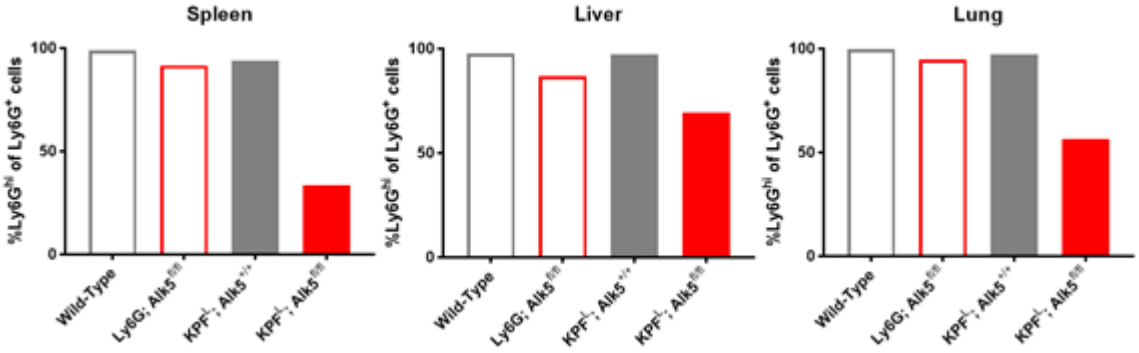

Figure 119 The KPF^{L}; Alk5$^{fl/fl}$ model exhibits a reduced proportion of Ly6G^{hi} neutrophils across all tissues examined
The Ly6G^{hi} population of CD45^{+}Lin^{-}CD11b^{+}Ly6G^{+} neutrophils was examined across the spleen, liver, and lung of the models of the genotype indicated. There was a very slight decrease in the percentage of Ly6G^{hi} neutrophils in the Ly6G; *Alk5$^{fl/fl}$* control tissue compared to the wild-type control tissue, however, tissue from the tumour bearing KPF^{L}; Alk5$^{fl/fl}$ mouse exhibited a substantial decrease in the proportion of Ly6G^{hi} neutrophils (n=1).

Although high/intermediate Ly6G expression has been proposed as the definitive measurement of neutrophil maturity (MacKay, bioRxiv), I also sought to interrogate various molecules proposed to denote neutrophils with differential function. Therefore, I examined their expression on the total neutrophil population (Ly6G^{+}) as well as the Ly6G^{hi} and Ly6G^{int} populations across the samples. As demonstrated in **Figure 120** the expression levels of the markers vary in neutrophils in wild-type blood. It was evident in the flow plots for the detection of CD62L and CXCR2 that two populations were present which fall into the overall negative population (**Figure 120**), and this was seen across all samples (not shown). This was perhaps indicative of a low antibody availability and the positive cells therefore having a low fluorescent intensity. The gates were all defined by the fluorescence minus one (FMO) controls, which take into account samples stained for all antibodies minus the one of interest. This allowed a threshold to be set above which cells were deemed positive. Future experiments should therefore have increased antibody concentrations to definitively mark the positive cell populations.

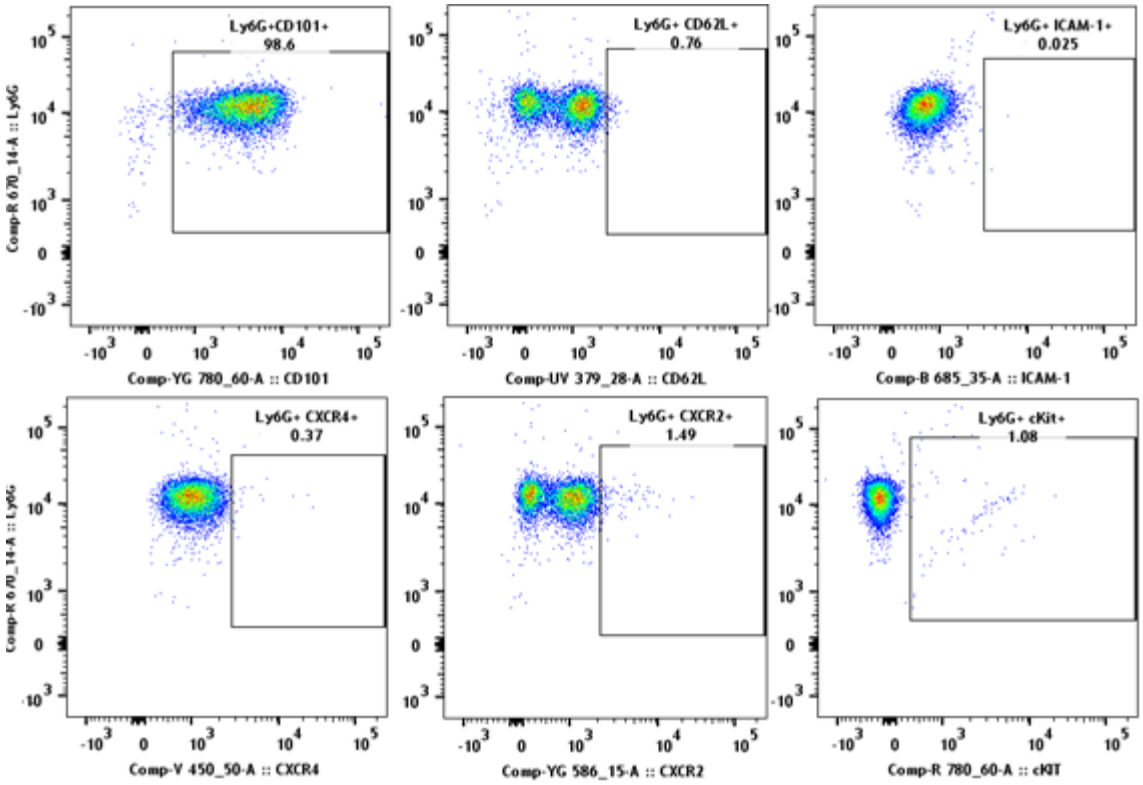

Figure 120 Expression of neutrophil maturity markers in blood from healthy mice
The expression of CD101, CD62L, ICAM-1, CXCR4, CXCR2 and cKIT was examined on the $CD45^{+}Lin^{-}CD11b^{+}Ly6G^{+}$ neutrophil population. Representative flow cytometry plots from the blood of a wild-type mouse are shown.

$CD101^{+}$ neutrophils represented the highest proportion of $Ly6G^{+}$ cells across all tissue types (**Figure 121**). Within the liver and blood, the percentage of $CD101^{+}$ cells was reduced in tumour-bearing mice, with perhaps a more prominent decrease in the KPF^{L}; $Alk5^{fl/fl}$ model. In the lungs, this trend was also visible, although the decrease was less obvious. In the spleen, $CD101^{+}$ percentage was decreased in the Ly6G; $Alk5^{fl/fl}$ and KPF $Alk5^{fl/fl}$ model, with the KPF^{L}; $Alk5^{fl/fl}$ model presenting with a similar $CD101^{+}$ percentage to the wild-type control. Together, although preliminary, the data suggest that mature neutrophils ubiquitously express CD101, with the presence of a tumour potentially causing a decrease in this population in the blood and liver. TGFß signalling may have influenced this population, since there was an elevated splenic neutrophil $CD101^{+}$ population in the KPF^{L}; $Alk5^{fl/fl}$ model. The other markers generally showed a low expression across all tissue types. Within the spleen, the proportion of $cKIT^{+}$ neutrophils appeared decreased in the tumour bearing mice, which could prove interesting with the spleen a site for extramedullary

haematopoiesis. There was also detectable cKIT^{+} neutrophils in the tumour bearing mice but not in the steady state in the circulating blood, perhaps indicative of immature egress of pre-neutrophils.

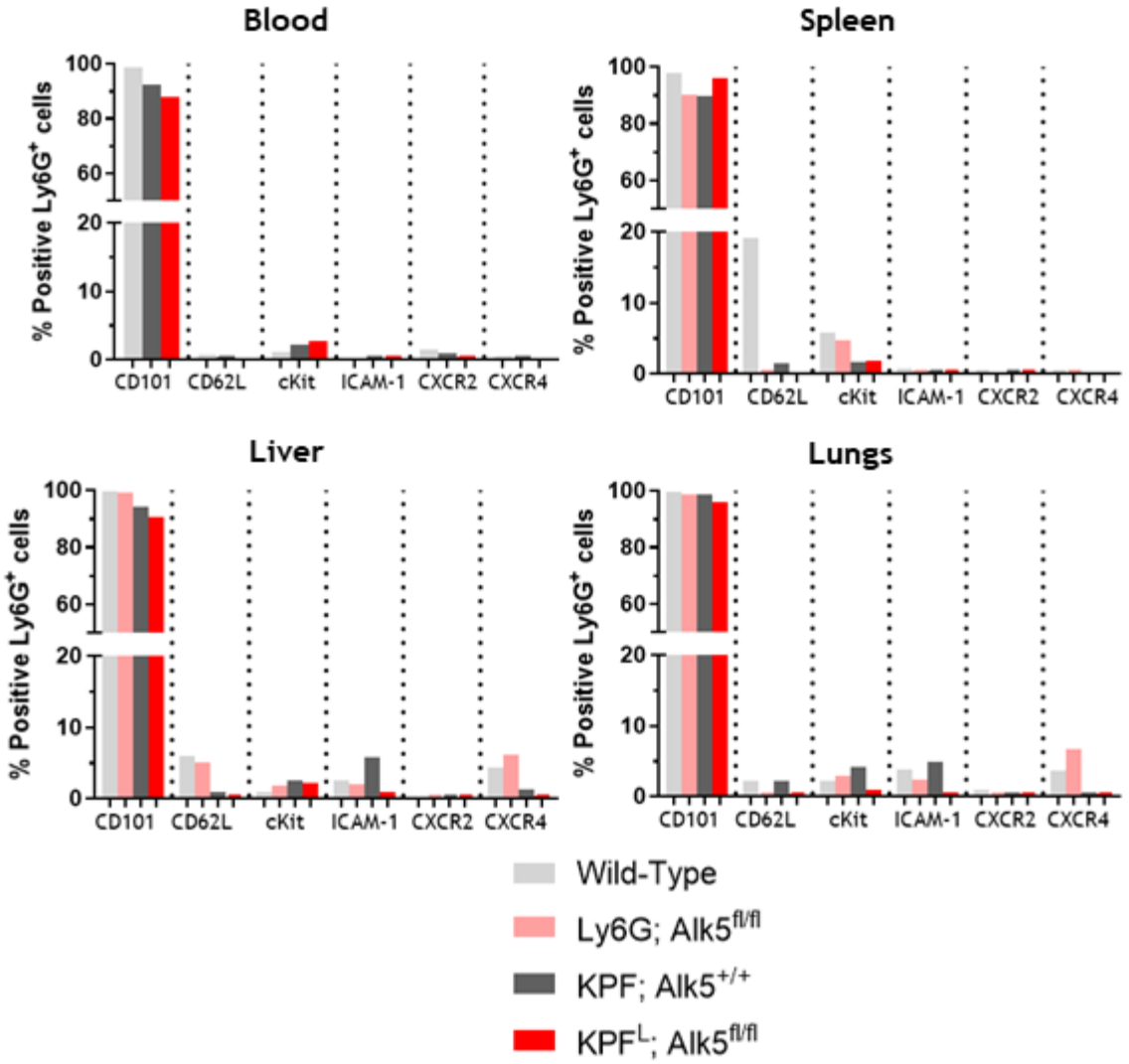

Figure 121 Neutrophil maturity marker expression across organs
The expression of CD101, CD62L, ICAM-1, CXCR4, CXCR2 and cKIT was determined on the neutrophil (CD45^{+}Lin^{-}CD11b^{+}Ly6G^{+}) population across the various organs examined in mice of the indicated genotypes. CD101 was the most widely and highest expressed of the markers with the other markers detecting a much smaller proportion of neutrophils. (n=1)

Investigating differential expression of the various markers on Ly6G^{hi} compared with Ly6G^{int} neutrophils was only possible in the KPF^{L}; *Alk5$^{fl/fl}$* samples, as the tissue from the other models presented with negligible Ly6G^{int} cells. However, there was no noticeable alteration in the markers in any tissue type when comparing between the immature and mature neutrophils. As can be seen in **Figure 122,** CD101 was expressed in most neutrophils, while expression of the other markers was generally low. Expression of CD101 was similar in both the Ly6G^{hi} and Ly6G^{int} populations across all tissues, with the exception of the liver, in which CD101^{+} cells represented a lower proportion of Ly6G^{int} neutrophils.

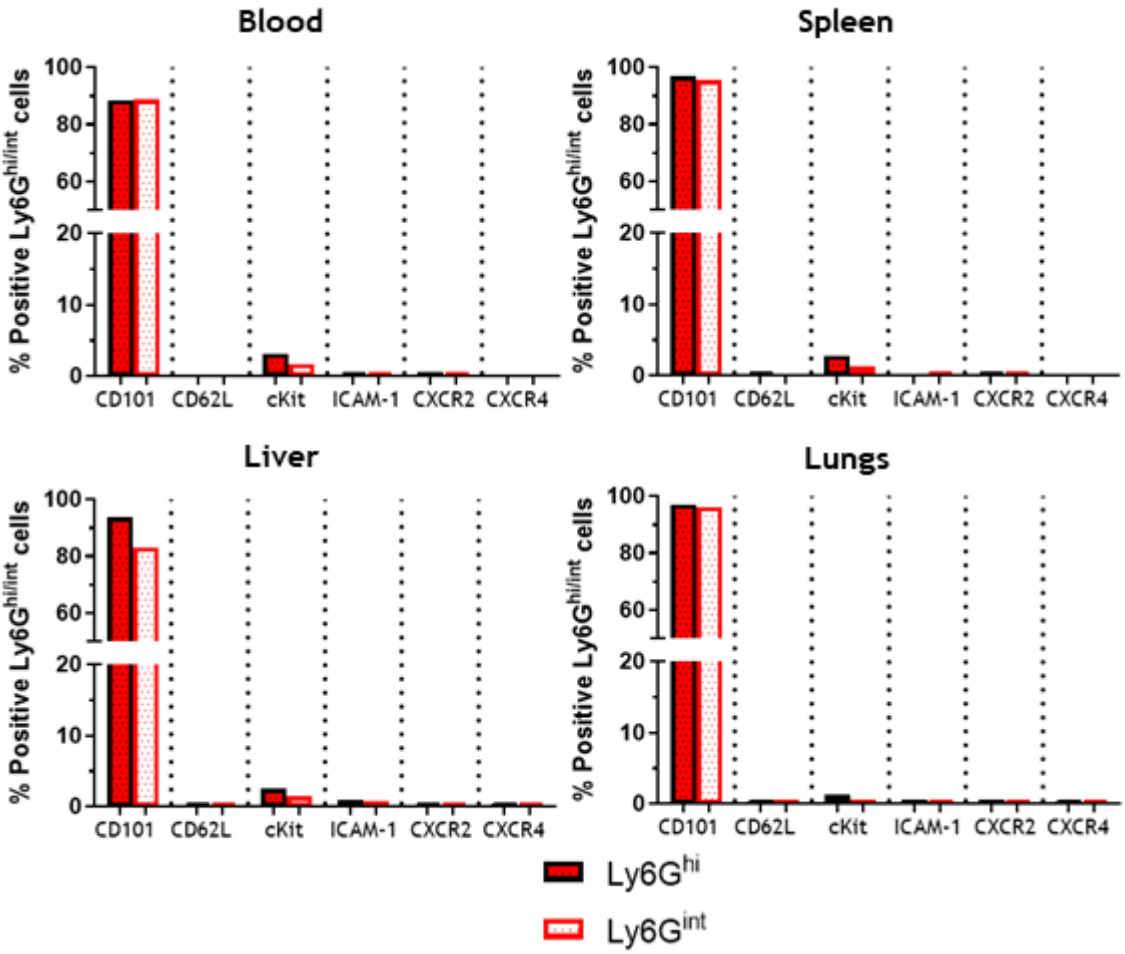

Figure 122 Maturity markers are largely unchanged in Ly6Ghi vs Ly6Gint neutrophils
The expression of CD101, CD62L, cKIT, ICAM-1, CXCR2 and CXCR4 was measured in the Ly6G^{hi} and Ly6G^{int} populations of neutrophils in KPF^{L}; *Alk5$^{fl/fl}$* tissues. CD101 was expressed in the majority of neutrophils across both populations, with only the liver Ly6G^{int} neutrophils demonstrating a decrease in the proportion of CD101^{+} cells. The other markers were expressed in a vanishingly low proportion of cells.

Ultimately, as a pilot experiment multiple repeats will be required to acquire robust neutrophil maturity data. However, from this preliminary data the intermediate or high expression of Ly6G appears to represent the best method to distinguish between neutrophils, with a clearly elevated proportion of Ly6G^{int} neutrophils detected in multiple sites in the KPF^{L}; *Alk5*$^{fl/fl}$ tumour bearing model in comparison to controls, in agreement with *Mackey et al,*. CD101 was expressed in the majority of neutrophils and there was no obvious pattern for altered expression detected, with only slight changes observed. The low level of expression of other markers hindered all analysis on their capacity to mark neutrophils of different maturity levels.

6.4 Discussion

As the understanding of neutrophils in chronic disease states has increased, the idea of neutrophils existing in polarized states has materialized (Grieshaber-Bouyer et al., 2021; Xie et al., 2020). It is no longer thought that neutrophils in diseases such as cancer exist as a homogenous population (Evrard et al., 2018), with more clarity on the systemic effects of diseases states on the immune system becoming apparent. With the suggestion that TGFß signalling inhibition resulted in decreased tumour growth in a neutrophil dependent manner (Fridlender et al., 2009), and that tumour site education of neutrophils alongside TGFß signalling can drive a pro-tumorigenic neutrophil phenotype (Fridlender et al., 2012; Mishalian et al., 2013), I sought to investigate this in an autochthonous PDAC model.

Although TGFß inhibition was shown to reduce the tumour growth in a neutrophil dependent manner in the subcutaneous model (Fridlender et al., 2009), this was not apparent in the spontaneous PDAC model used here, with neutrophil specific deletion of *Alk5* having no impact on survival. The KPF^{L}; *Alk5*$^{fl/fl}$ model exhibits no delay in tumorigenesis nor alteration in the morphology of end-point tumours. Mice presented with large primary tumours and reached end-point due to PDAC related phenotypes in the majority of cases. There are relevant disparities between the two model systems that would explain the alternate results. The spontaneous KPF PDAC model better recapitulates the site of disease and the relevant stromal infiltration in comparison to the subcutaneous model. Subcutaneous models have shown responsiveness to gemcitabine for instance, yet the autochthonous KPC model is resistant (Olive et al., 2009). Further, the inhibitor used, although shown to mediate an effect even when administered intratumourally, would inhibit TGFß signalling in a non-neutrophil specific manner as well as inhibiting Alk4. Even though, neutrophils isolated from the treated tumour sites had increased cytotoxic function, the question of whether this increased activation of neutrophils occurred via direct inhibition or in a paracrine manner through modulation of stromal and cancer cell signalling was not interrogated. In the model used in this chapter, the Ly6G specific deletion of *Alk5* allowed me to focus on the specific function of TGFß signalling on neutrophils. I did not examine neutrophil cytotoxicity or ROS function, which may have provided insight into neutrophil activity; however, neutrophil specific

deletion of *Alk5* did not delay disease progression. A caveat of the model, however, would be the lack of neutrophil *Alk5* expression prior to tumour initiation. Therefore, any potential enhanced anti-tumorigenic function of neutrophils could have been overcome during tumorigenesis. Insight into pre-neoplastic lesions would be interesting to detect any delay on onset or direct cytolytic effects of infiltrating neutrophils.

The role of neutrophils within the metastatic cascade has also been widely described (Coffelt et al., 2015; Jackstadt et al., 2019; Spiegel et al., 2016; Steele et al., 2016). Therefore, I sought to interrogate this in the metastatic KPF model (Schonhuber et al., 2014). The blockage of neutrophil infiltration, or depletion of circulating neutrophils has been shown to reduce metastasis (Coffelt et al., 2015; Spiegel et al., 2016) even in the metastatic KPC model (Steele et al., 2016) with neutrophil specific *Alk5* deletion in an orthotopic model of metastatic CRC reducing metastasis (Jackstadt et al., 2019). Neutrophil-specific deletion of *Alk5* in the KPF model used here resulted in a non-significant reduction in the percentage of mice exhibiting metastasis, but increased numbers would be required to determine if this observation is statistically meaningful.

The metastatic CRC model was shown to exhibit high expression of TGFß2, which was proposed to promote neutrophil penetrance into tumour and metastatic sites (Jackstadt et al., 2019). The apparent chemoattractant role of TGFß2 in the metastatic CRC model may explain why such a clear drop in metastasis is noted. Whether the PDAC model I investigated exhibits this elevated expression is currently unknown, however, there was no appreciable increase in neutrophils in either the primary site or metastatic organs in comparison to tumours arising in control mice. Further, the CRC model presents with multiple smaller sites of metastasis per organ, whereas, our model has a tendency to develop a lower number of larger metastasis.

With evidence suggesting that immature neutrophils are elevated in the blood in cancer models (Evrard et al., 2018), and pro-tumorigenic neutrophils suggested to enhance circulating cancer cell proliferation (Szczerba et al., 2019), it is unsurprising that total ablation or blockade of neutrophils reduces metastasis (Coffelt et al., 2015; Steele et al., 2016). However, with TGFß signalling

purported to polarize pro-tumorigenic neutrophils (Fridlender et al., 2009), deletion of *Alk5* in neutrophils may support a more mature neutrophil population, even in disease states. Therefore, I utilised a flow cytometry panel to interrogate various neutrophil markers that have been shown to denote neutrophil activation. Ly6G expression has recently been shown to be the most universal marker for neutrophil maturity (Mackey et al., 2021). Although, my data is preliminary, the trend of increased levels of $Ly6G^{int}$ immature neutrophils was noted in the tumour bearing models as expected, but particularly in the KPF^{L} $Alk5^{fl/fl}$ model, caveats regarding sample size and *Ly6g* allelic loss notwithstanding.

CD101 expression was clearly detected in the majority of neutrophils within the models although there was no obvious correlation with neutrophil maturity. This contrasted with the elevated CD101 negative population, described in the orthotopic pancreatic tumour models utilised by *Evrard et al.* Interestingly, *MacKey et al.*, suggests that CD101 is an ineffective marker of tumour maturity, with *Jackstadt et al.*, showing no change in CD101 expression in neutrophils in the CRC bearing Ly6G; $Alk5^{fl/fl}$ model (Evrard et al., 2018; Jackstadt et al., 2019). Therefore, the tumour site, and perhaps specifically PDAC, may be the key influencer of CD101 expression on neutrophils. For instance, *Evrard et al.*, propose that CXCR2 makers all mature neutrophils in the circulation with $CXCR4^{hi}$ neutrophils denoted immature (Evrard et al., 2018) or aged neutrophils (Martin et al., 2003). Meanwhile, $cKIT^{+}$ neutrophils were shown to compose a small proportion of circulating and splenic neutrophils in steady state (Rice et al., 2018), which we observe, although the increased $cKIT^{+}$ population noted in tumour models (Evrard et al., 2018) was not apparent. Although we were unable to draw any conclusions on the other markers due to low-level expression, it remains pertinent to conduct further study as they may provide further insight into neutrophil maturity.

Chapter 7 Conclusions and Future Directions

The data presented in this thesis describes a cell context and tumour staging specific function for the TGFß signalling pathway. The deletion of *Alk5* in the epithelium of KF mice culminates in accelerated tumorigenesis and development of frank PDAC within a short time frame. This model better recapitulates the acquisition of genetic permutations in human disease, as well as improving on previous models which present with squamous stomach and skin tumours (Acosta et al., 2013).

This model also recapitulates the genetics of 2% of PDAC patients but likely also represents a larger subsection of patients with other TGFß signalling component mutations, thereby providing a potential pre-clinical model for the stratified investigation of therapeutic targets. For instance, GSEA highlighted enriched p53 pathway in the KAF tumours compared to the KPF, which was unsurprising given p53 was deleted in the KPF model. However, this opens a therapeutic window for targeted therapy, with p53 restored cell lines shown to be more sensitive to radiation or chemotherapy, such as cisplatin with synergy with nutlin3a (Candido et al., 2019). Staining for p53 and p21 should be performed in KAF and KPF tumours with the hypothesis that KAF tumours retain functional p53, whereas KPF tumours do not, thereby proving KAF tumours remain p53 proficient. Continued investigation of *in vitro* vulnerability of the KAF derived cell lines would be useful to determine if the cancer cells are sensitive to other therapies. For instance, p53 proficient cells overexpressing Ccng1, which is upregulated at the RNA levels in KAF mice tumours, have increased vulnerability to cisplatin (Smith et al., 1997). Therefore, further *in silico* investigation should be done, followed by *in vitro* assays to screen potential drugs and provide a solid platform of evidence before transitioning to *in vivo* work.

The importance of Ccng1 as a negative regulator of p53 function (Okamoto et al., 1996) also warrants further investigation. Patients with high levels of CCNG1 have a worse prognosis than those with lower levels, and a high *CCNG1* expression was seen in mutant *KRAS*-driven tumours that also carried TGFß signalling aberrations (*TGFBR1, TGFBR2* and *SMAD4* mutants) (**Figure 123**). Knockdown studies of *Ccng1* within cell lines would prove interesting to determine how essential a role this protein plays in maintaining carcinogenesis.

This is especially relevant given the capacity to target Ccng1 through inhibitors, which have shown some promise in patient trials (Chawla et al., 2019; Morse et al., 2021). It would also be of interest to examine if there is TGFß induced control of *Ccng1* or whether the elevated expression is purely driven by p53.

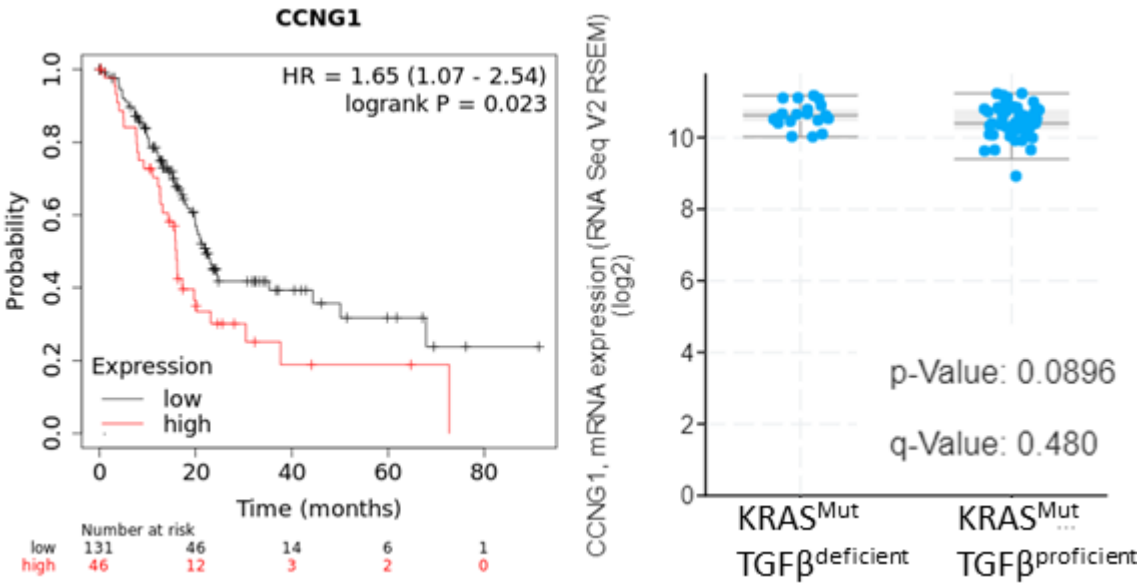

Figure 123 High levels of CCNG1 were associated with worse patient prognosis, with *CCNG1* expression enriched in TGFβ signalling pathway mutated patients
Kaplan-Meier survival analysis of PDAC patients stratified by high of low-level expression of CCNG1 (**Left**). Data generated from Kaplan Meier Plotter (Nagy et al., 2021). *CCNG1* mRNA expression from the TCGA data set on cBioPortal. Mutant *KRAS* patients were selected and stratified on their mutations in TGFβ signalling pathway components. *TGFBR1, TGFBR2* and *SMAD4* mutants that were *TP53* wild-type are represented in the $KRAS^{Mut}$ $TGFβ^{deficient}$ cohort, with the $KRAS^{Mut}$ $TGFβ^{proficient}$ representing all other KRAS mutant samples that have no mutations in the TGFβ signalling components *TGFβR1, TGFβR2* and *SMAD4*.

Further, the reduction in EMT-associated gene expression pathways that I observed in ALK5 deficient tumours may render tumour cells more sensitive to frontline therapy, since EMT has been shown to enhance resistance of cancer cells to, for instance, cisplatin and gemcitabine (Arumugam et al., 2009; Zheng et al., 2015). Therefore, cisplatin represents a key potential treatment option with sensitivity previously noted in *Ccng1* overexpressing cells and p53 proficient cells, and with EMT potentially driving resistance.

Interrogation of the human data sets, particularly the *ALK5* mutated samples, but also those with mutations in other TGFß signalling pathway components, as well as the p53 proficient tumour subset, will confirm whether these alterations in gene expression translate into patients. This would be a key part in proving the value of the KAF mouse as a good pre-clinical model in which to examine stratified therapeutics.

Other differentially expressed genes from the RNA sequencing that I have not yet investigated could also provide interesting avenues either for investigating the biology of tumour development in the setting of TGFß signalling loss in epithelial cells or for therapeutic targeting (**Figure 124**). The almost complete loss of expression of *Eif5al3-ps* is interesting, especially given it is the top downregulated gene in KAF tumours compared to KPF tumours, and while there are no publications on its function, it seems likely that it plays a role in translational initiation. The opposite is true for with *Zfp750,* with almost no expression detected in KPF tumours and elevated expression in KAF tumours. This protein has been shown to inhibit EMT through repression of SNAI1 (Kong et al., 2020), and through epigenetic suppression of LAMB3 and CTNNAL1 in oesophageal squamous cell carcinoma and breast cancer, respectively (Cassandri et al., 2020). Determining whether Znf750 is essential in modulating the reduced EMT noted in the KAF tumours would be of interest, in addition to investigating the expression of the drivers of EMT.

The upregulation of *Slc2a2,* also known as GLUT2, could also be of relevance, with cancer cells known to have an altered metabolism to suit their hyper-proliferative needs. Therefore, investigation of KAF cell metabolism could be useful in delineating additional therapeutic targets. Further, high levels of SLC2A2 have been shown to be poorly prognostic in hepatocellular carcinoma (Kim et al., 2017) with inhibitors to SLC2A also improving response to frontline therapy in mouse models of glioma (Azzalin et al., 2017).

CTGF inhibition through monoclonal antibodies was previously shown to synergise with gemcitabine, extending the survival of tumour bearing KPC mice (Neesse et al., 2013). Interestingly, CTGF is induced by TGFß signalling (Gao and Brigstock, 2005), with the upregulation I observed in the KAF model perhaps suggesting an altered activation of fibroblasts. It has been shown that stromal

TGFβ1 ligand is increased in a *Tgfbr2* deficient PDAC mouse model (Principe et al., 2016), with TGFβ known to activate fibroblasts and increase ECM production (Shek et al., 2002). Therefore, examination of the ligand level within KAF tumours would be of interest, especially with collagen deposition, as measured by Sirius red staining, increased in end-point KAF tumours compare to KPF tumours.

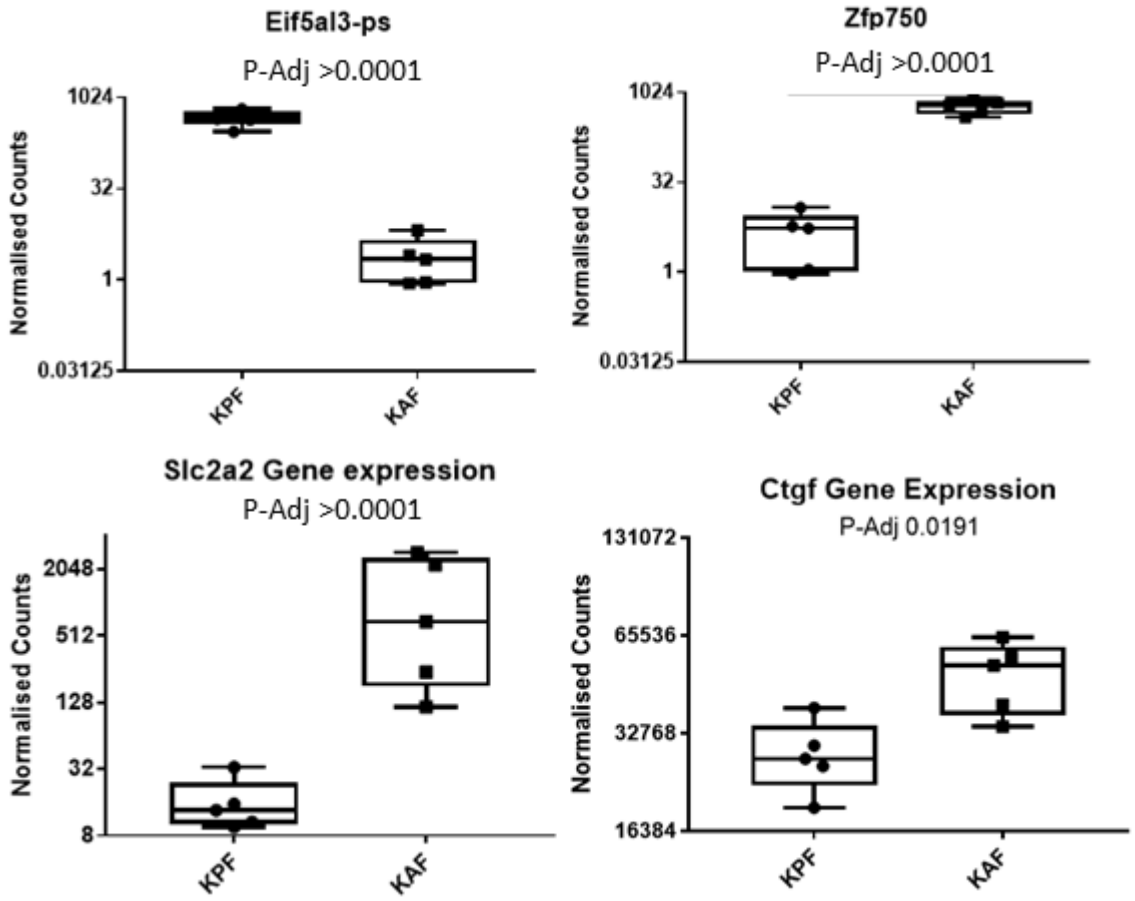

Figure 124 Differentially expressed genes in the KAF tumours for potential further investigation
The expression of *Eifal3-ps* was reduced, while expression of *Zfp750, Slc2a2* and *Ctgf* was enhanced in the KAF tumour samples compared to KPF tumour samples. (P-adjusted values indicated).

Although KAF tumours were driven by the loss of TGFβ signalling, dissecting TGFβ specific alterations that drive carcinogenesis was complicated by the comparison to KPF tumours, which have p53 loss. Future work could be undertaken to examine TGFβ signalling specific effects through deletion of *Alk5*

in KPF mice at the pre-neoplastic stages. I would hypothesis that this model would have a rapid onset similar to the KAF model, however, whether, the mice would retain their second copy of *Trp53* would be interesting as the homozygous deletion of *Alk5* was sufficient to overcome the senescent block of PanIN progression and drives invasive carcinoma. Therefore, comparison could ultimately be similar to the data shown in this thesis, with KPF mice lacking p53 and KPF; *Alk5*$^{fl/fl}$ retaining one copy.

It may therefore be of more interest to examine the alterations noted upon *Alk5* deletion in established tumours, although in this scenario, loss of pro-tumourigenic functions driven by tumour cell intrinsic TGFß signalling may be revealed. I have highlighted that survival was unchanged in these mice, however metastasis was reduced (**Figure 125**). IHC staining for mesenchymal and epithelial cell markers showed no obvious alteration in EMT markers when comparing KPF and KPF; *Alk5*$^{fl/fl}$ tumours, although KAF tumours had a more epithelial phenotype. Further staining for *bona fide* functional drivers of EMT such as Snail1, Zeb and Twist would provide further elucidation of cells undergoing EMT. The reporter locus expression would assist with this investigation, with those cells expressing eGFP likely to have retained *Alk5* and those expressing tomato having *Alk5* deleted. This could lend itself to dual IF staining, investigating EMT marker expression on either eGFP^{+} or tomato^{+} cells, or to sorting of these populations and examining RNA level expression alterations. It could also provide a mechanism for tracking metastatic dissemination, with the hypothesis that all cancer cells in metastatic lesions would express eGFP. Further, it would aid in tracking circulating cancer cells, which may give an indication of the effect either *Alk5* or *Tgfb1* gene deletion has on cancer cell escape and dissemination. Additionally the deletion of *Tgfb1* in established KPF tumours also reduced metastasis, without affecting survival. Whether this suggests that autocrine signalling through TGFß drives metastasis or perhaps that lack of TGFß1 impinges on metastatic cells capability to remodel the metastatic site would be two interesting avenues to interrogate, especially within larger metastases that have an altered stroma in comparison to smaller metastases (Aiello et al., 2016). It would also be important to interrogate the effect gene deletion has upon cancer cells at the metastatic site. For instance, examination of the number and size of metastases in these models would give an

indication of whether cancer cell deletion of *Alk5* or *Tgfb1* influences metastatic growth. A greater proportion of smaller metastases to larger metastases would propose a stunting of metastatic growth, for instance. However, the added complexity of when metastasis has occurred will complicate these analyses, with mouse models of PDAC shown to have very early dissemination of metastatic cells (Rhim et al., 2012), and therefore potentially harbouring metastatic lesions prior to detection of a palpable tumour and tamoxifen induced gene deletion.

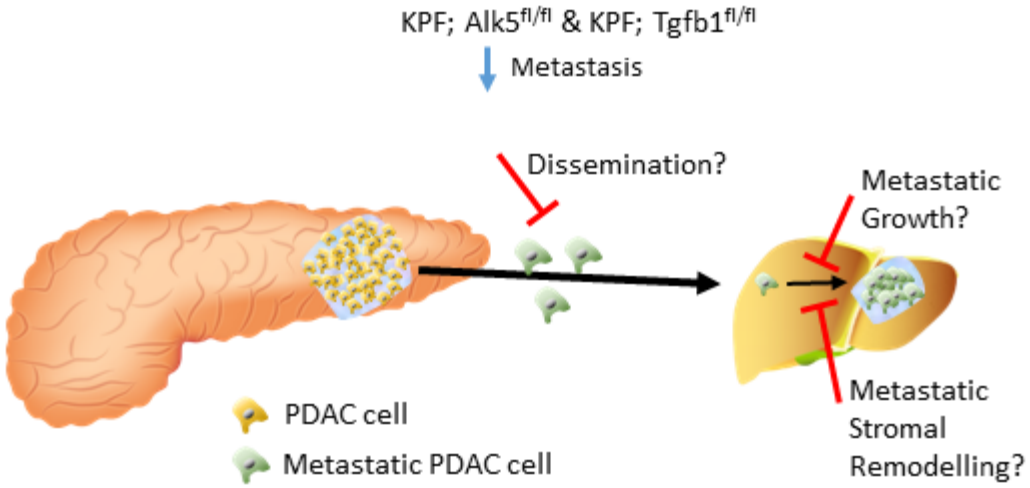

Figure 125 Exploring the mechanisms of reduced metastasis in the *KPF; Alk5$^{fl/fl}$* and *KPF; Tgfb1$^{fl/fl}$* mouse models
Cancer cell specific deletion of *Alk5* or *Tgfb1* within established KPF tumours reduces the percentage of mice presenting with metastasis with the mechanism not yet clarified. Further work should be undertaken to establish whether deletion of these genes effects the dissemination and egress of the cancer cells from the tumours, or whether deletion effects the ability of these cells to seed and grow at metastatic sites. It would also be of interest to establish whether mice have pre-existing metastases before tamoxifen induced gene deletion.

Fibroblasts have been shown to become activated and increase ECM matrix deposition upon TGFß stimulation (Schneider et al., 2001; Shek et al., 2002). Further, TGFß signalling has been implicated as a regulator of CAF subtypes within PDAC (Biffi et al., 2019; Dominguez et al., 2020; Elyada et al., 2019; Hutton et al., 2021; Ohlund et al., 2017). I have shown that deletion of *Alk5* across all fibroblasts (KPF^{C}; *Alk5$^{fl/fl}$*) or in a restricted population of 'myCAFs' (KPG^{G}; *Alk5$^{fl/fl}$*) does not affect survival significantly. There was also no notable changes in fibroblast populations, with expression of αSMA, a 'myCAF' marker, unchanged in end-point and pre-neoplastic lesions (**Figure 126**). This was surprising given the reported role of TGFß in driving the 'myCAFs' phenotype

while inhibiting 'iCAFs', with TGFß inhibitor treatment shown to reduce αSMA$^+$ CAFs (Biffi et al., 2019). I hypothesised that the pan-fibroblast *Alk5* deletion would mimic these findings, and perhaps with increased numbers in the study, a similar phenotype could emerge. Examination of *Gli1* driven deletion of *Alk5* at earlier timepoints post induction could also help in elucidating whether these *Alk5* deficient cells are retained in the tumour or whether they are replaced with *Alk5* proficient fibroblasts.

Intriguingly the *Gli1* driven but not *Col1a2* driven deletion of *Tgfb1*$^{fl/fl}$ skewed the fibroblast population, with less αSMA$^+$ fibroblasts measured. The 'myCAFs' were previously shown to be enriched in *Tgfb1* expression (Elyada et al., 2019) and with Gli1$^+$ fibroblasts composing a subsection of 'myCAFs' (Steele et al., 2021), perhaps this subset are important for maintaining 'myCAFs' through CAF-CAF crosstalk via paracrine signalling. This contrasts with Gli1 driven deletion of *Alk5,* perhaps providing insight into the difference between paracrine and autocrine TGFß signalling in dictating CAF fate. To interrogate this further, it would be interesting *in vivo* to delineate the proportion of Gli1$^+$ cells within the Gli1 driven *Alk5* and *Tgfb1* deletion models, through ISH of Gli1, and thereby elucidate whether these fibroblasts depend on TGFß signalling to persist. Further, 3-D culturing of sorted CAF populations from KPF tumours utilising the reporter locus to collect Gli1$^+$ and Gli$^-$ CAFs, specifically, would enhance the interrogation of paracrine and autocrine effects of TGFß signalling. This would allow for clarification as to which CAF population is the major producer of TGFß ligand, as well as determine whether medium conditioned by CAFs following *in vitro* deletion of *Tgfb1,* was able to influence 'myCAF' or 'iCAF' subtype switching in either Gli1$^+$ or Gli$^-$ CAFs which expressed or lacked *Alk5*. Examination of the ligand availability within the TME may also provide insight into whether the Gli1$^+$ population are essential producers of TGFß1.

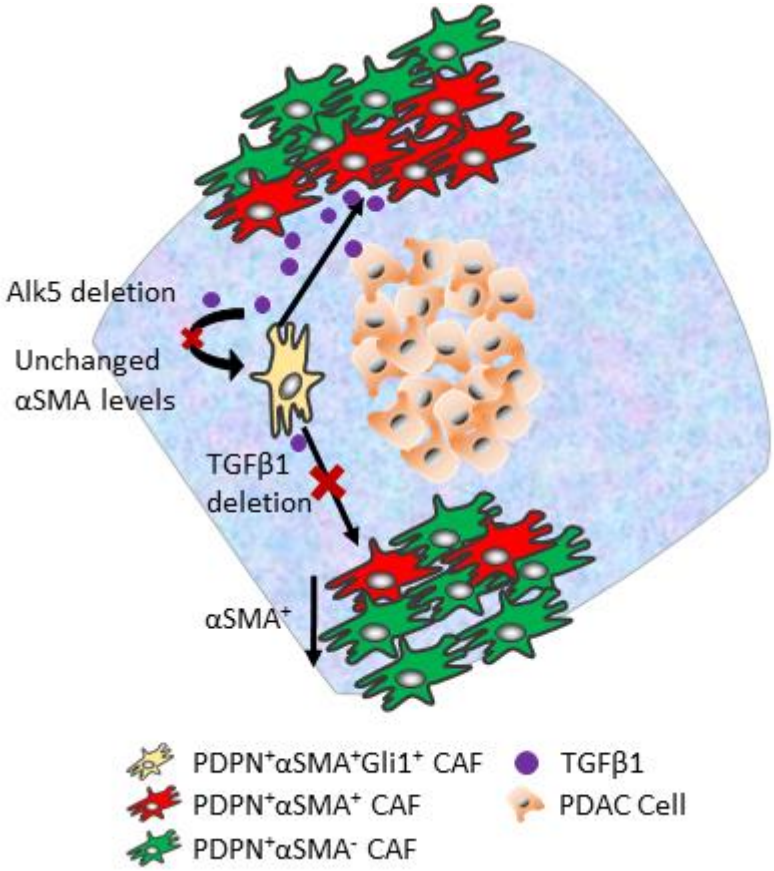

Figure 126 TGFβ1 production by Gli1 positive fibroblasts may sustain αSMA positive CAFs
The deletion of *Alk5* from Gli1^{+} fibroblasts does not affect the levels of αSMA or podoplanin positive fibroblasts in endpoint KPF tumours. However, deletion of *Tgfb1* from Gli1^{+} fibroblasts reduces the levels of αSMA positive CAFs in endpoint tumours.

In terms of determining CAF subtypes, CyTOF and scRNAseq have been the two most convincing methods used. Alternatively, flow cytometry has been used to distinguish between 'myCAF', 'iCAF' and 'apCAF' populations (Elyada et al., 2019; Steele et al., 2021). Therefore, examination of fibroblast populations within the KPG^{G} and KPF^{C} cohorts with either *Alk5* or *Tgfb1* deletion through this method would provide further insight into fibroblast subtype composition. It would also be of interest to examine CD105 and LRRC15 levels within the tumours across these cohorts, with both linked to TGFß signalling and marking subsets of fibroblasts (Dominguez et al., 2020; Hutton et al., 2021).

Regarding the effects of TGFß signalling in neutrophils, further examination of neutrophil maturity would be key to interpret the effects that deletion of *Alk5* has upon these cells, especially with the alterations to metastasis but not survival noted in this model. The flow cytometry experiment should be expanded to determine if neutrophils have an altered phenotype. It would also be useful to

examine neutrophil morphology with ring shaped nuclei indicative of immature neutrophils (Andzinski et al., 2016) and TGFß inhibitor treatment altering their morphology (Fridlender et al., 2009). Functional assays such as co-culturing neutrophils with cancer cells to determine cytotoxic efficacy could be investigated with mature neutrophils proposed to have an enhanced cytotoxic effect (Fridlender et al., 2009). Further, neutrophils appear to be important for suppressing T cell effector function, particularly CD8 T cells (Coffelt et al., 2015), with TGFß inhibition reducing this activity (Fridlender et al., 2009). Therefore, interrogation of T cell activation within the primary tumour and at metastatic sites should also be conducted to elucidate the effects of the *Alk5* deficient neutrophils on T cell populations. A recent study in a model of metastatic colorectal cancer showed that increased cancer cell production of *Tgfb2* was responsible for neutrophil driven metastasis (Jackstadt et al., 2019). Thus, expression of TGFß ligands within KPF tumours and metastases at different sites would an interesting avenue to explore. This would potentially explain the dramatic decrease in metastasis observed in the CRC model compared to the more subtle effects observed in the KPF.

Collectively I have highlighted that TGFß signalling is a potent tumour suppressor pathway, however, in established tumours deletion across multiple cell types does not appear to accelerate tumour progression. Survival was not significantly affected by the deletion of *Alk5* from cancer cells, fibroblasts or neutrophils, although reduced metastasis and stromal reprogramming are apparent. Therefore, TGFß inhibitor therapy may be an effective option in the treatment of PDAC, although most likely in combination with other therapeutics. For instance with the known function of TGFß signalling as a potent tumour suppressor, combination with anti-PD1 has shown promise in other cancers (Mariathasan et al., 2018; Tauriello et al., 2018) and in a cohort of PDAC patients (Strauss et al., 2018). Overall, however, more work is required to extend our understanding of TGFß signalling in the difference cell types in PDAC and to identify more refined targets for therapy.

List of References

Abbassi, O., T. K. Kishimoto, L. V. McIntire, D. C. Anderson, and C. W. Smith, 1993, E-SELECTIN SUPPORTS NEUTROPHIL ROLLING IN-VITRO UNDER CONDITIONS OF FLOW: Journal of Clinical Investigation, v. 92, p. 2719-2730.

Abdollah, S., M. MaciasSilva, T. Tsukazaki, H. Hayashi, L. Attisano, and J. L. Wrana, 1997, T beta RI phosphorylation of Smad2 on Ser(465) and Ser(467) is required for Smad2-Smad4 complex formation and signaling: Journal of Biological Chemistry, v. 272, p. 27678-27685.

Acosta, J. C., A. Banito, T. Wuestefeld, A. Georgilis, P. Janich, J. P. Morton, D. Athineos, T. W. Kang, F. Lasitschka, M. Andrulis, G. Pascual, K. J. Morris, S. Khan, H. Jin, G. Dharmalingam, A. P. Snijders, T. Carroll, D. Capper, C. Pritchard, G. J. Inman, T. Longerich, O. J. Sansom, S. A. Benitah, L. Zender, and J. Gil, 2013, A complex secretory program orchestrated by the inflammasome controls paracrine senescence: Nature Cell Biology, v. 15, p. 978-U221.

Adorno, M., M. Cordenonsi, M. Montagner, S. Dupont, C. Wong, B. Hann, A. Solari, S. Bobisse, M. B. Rondina, V. Guzzardo, A. R. Parenti, A. Rosato, S. Bicciato, A. Balmain, and S. Piccolo, 2009, A Mutant-p53/Smad Complex Opposes p63 to Empower TGF beta-Induced Metastasis: Cell, v. 137, p. 87-98.

Adrian, K., M. J. Strouch, Q. H. Zeng, M. R. Barron, E. C. Cheon, A. Honasoge, Y. F. Xu, S. Phukan, M. Sadim, D. J. Bentrem, B. Pasche, and P. J. Grippo, 2009, Tgfbr1 Haploinsufficiency Inhibits the Development of Murine Mutant Kras-Induced Pancreatic Precancer: Cancer Research, v. 69, p. 9169-9174.

Aguirre, A. J., N. Bardeesy, M. Sinha, L. Lopez, D. A. Tuveson, J. Horner, M. S. Redston, and R. A. DePinho, 2003, Activated Kras and Ink4a/Arf deficiency cooperate to produce metastatic pancreatic ductal adenocarcinoma: Genes & Development, v. 17, p. 3112-3126.

Aguirre, A. J., R. H. Hruban, B. J. Raphael, and N. Canc Genome Atlas Res, 2017, Integrated Genomic Characterization of Pancreatic Ductal Adenocarcinoma: Cancer Cell, v. 32, p. 185-+.

Ahn, S., and A. L. Joyner, 2004, Dynamic changes in the response of cells to positive hedgehog signaling during mouse limb patterning: Cell, v. 118, p. 505-516.

Aiello, N. M., D. L. Bajor, R. J. Norgard, A. Sahmoud, N. Bhagwat, M. N. Pham, T. C. Cornish, C. A. Iacobuzio-Donahue, R. H. Vonderheide, and B. Z. Stanger, 2016, Metastatic progression is associated with dynamic changes in the local microenvironment: Nature Communications, v. 7.

Andzinski, L., N. Kasnitz, S. Stahnke, C. F. Wu, M. Gereke, M. von Kockritz-Blickwede, B. Schilling, S. Brandau, S. Weiss, and J. Jablonska, 2016, Type I IFNs induce anti-tumor polarization of tumor associated neutrophils in mice and human: International Journal of Cancer, v. 138, p. 1982-1993.

Annes, J. P., Y. Chen, J. S. Munger, and D. B. Rifkin, 2004, Integrin alpha(v)beta(6)-mediated activation of latent TGF-beta requires the latent TGF-beta binding protein-1: Journal of Cell Biology, v. 165, p. 723-734.

Anzano, M. A., A. B. Roberts, C. A. Meyers, A. Komoriya, L. C. Lamb, J. M. Smith, and M. B. Sporn, 1982a, SYNERGISTIC INTERACTION OF 2 CLASSES OF TRANSFORMING GROWTH-FACTORS FROM MURINE SARCOMA-CELLS: Cancer Research, v. 42, p. 4776-4778.

Anzano, M. A., A. B. Roberts, J. M. Smith, L. C. Lamb, and M. B. Sporn, 1982b, PURIFICATION BY REVERSE-PHASE HIGH-PERFORMANCE LIQUID-CHROMATOGRAPHY OF AN EPIDERMAL GROWTH FACTOR-DEPENDENT TRANSFORMING GROWTH-FACTOR: Analytical Biochemistry, v. 125, p. 217-224.

Apte, M. V., P. S. Haber, T. L. Applegate, I. D. Norton, G. W. McCaughan, M. A. Korsten, R. C. Pirola, and J. S. Wilson, 1998, Periacinar stellate shaped cells in rat pancreas: identification, isolation, and culture: Gut, v. 43, p. 128-133.

Apte, M. V., P. S. Haber, S. J. Darby, S. C. Rodgers, G. W. McCaughan, M. A. Korsten, R. C. Pirola, and J. S. Wilson, 1999, Pancreatic stellate cells are activated by proinflammatory cytokines: implications for pancreatic fibrogenesis: Gut, v. 44, p. 534-541.

Apte, M. V., S. Park, P. A. Phillips, N. Santucci, D. Goldstein, R. K. Kumar, G. A. Ramm, M. Buchler, H. Friess, J. A. McCarroll, G. Keogh, N. Merrett, R. Pirola, and J. S. Wilson, 2004, Desmoplastic reaction in pancreatic cancer - Role of pancreatic stellate cells: Pancreas, v. 29, p. 179-187.

Arumugam, T., V. Ramachandran, K. F. Fournier, H. M. Wang, L. Marquis, J. L. Abbruzzese, G. E. Gallick, C. D. Logsdon, D. J. McConkey, and W. Choi, 2009, Epithelial to Mesenchymal Transition Contributes to Drug Resistance in Pancreatic Cancer: Cancer Research, v. 69, p. 5820-5828.

Assi, M., Y. Achouri, A. Loriot, N. Dauguet, H. Dahou, J. Baldan, M. Libert, J. S. Fain, C. Guerra, L. Bouwens, M. Barbacid, F. P. Lemaigre, and P. Jacquemin, 2021, Dynamic Regulation of Expression of KRAS and Its Effectors Determines the Ability to Initiate Tumorigenesis in Pancreatic Acinar Cells: Cancer Research, v. 81, p. 2679-2689.

Assoian, R. K., A. Komoriya, C. A. Meyers, D. M. Miller, and M. B. Sporn, 1983, TRANSFORMING GROWTH FACTOR-BETA IN HUMAN-PLATELETS - IDENTIFICATION OF A MAJOR STORAGE SITE, PURIFICATION, AND CHARACTERIZATION: Journal of Biological Chemistry, v. 258, p. 7155-7160.

Azhar, M., M. Yin, R. Bommireddy, J. J. Duffy, J. Q. Yang, S. A. Pawlowski, G. P. Boivin, S. J. Engle, L. P. Sanford, C. Grisham, R. R. Singh, G. F. Babcock, and T. Doetschman, 2009, Generation of Mice With a Conditional Allele for Transforming Growth Factor beta 1 Gene: Genesis, v. 47, p. 423-431.

Azzalin, A., G. Nato, E. Parmigiani, F. Garello, A. Buffo, and L. Magrassi, 2017, Inhibitors of GLUT/SLC2A Enhance the Action of BCNU and Temozolomide against High-Grade Gliomas: Neoplasia, v. 19, p. 364-373.

Bachem, M. G., M. Schunemann, M. Ramadani, M. Siech, H. Beger, A. Buck, S. X. Zhou, A. Schmid-Kotsas, and G. Adler, 2005, Pancreatic carcinoma cells induce fibrosis by stimulating proliferation and matrix synthesis of stellate cells: Gastroenterology, v. 128, p. 907-921.

Bailey, J. M., B. J. Swanson, T. Hamada, J. P. Eggers, P. K. Singh, T. Caffery, M. M. Ouellette, and M. A. Hollingsworth, 2008, Sonic Hedgehog Promotes Desmoplasia in Pancreatic Cancer: Clinical Cancer Research, v. 14, p. 5995-6004.

Bailey, P., D. K. Chang, K. Nones, A. L. Johns, A. M. Patch, M. C. Gingras, D. K. Miller, A. N. Christ, T. J. C. Bruxner, M. C. Quinn, C. Nourse, L. C. Murtaugh, I. Harliwong, S. Idrisoglu, S. Manning, E. Nourbakhsh, S. Wani, L. Fink, O. Holmes, V. Chin, M. J. Anderson, S. Kazakoff, C. Leonard, F. Newell, N. Waddell, S. Wood, Q. Y. Xu, P. J. Wilson, N. Cloonan, K. S. Kassahn, D. Taylor, K. Quek, A. Robertson, L. Pantano, L. Mincarelli, L. N. Sanchez, L. Evers, J. M. Wu, M. Pinese, M. J. Cowley, M. D. Jones, E. K.

Colvin, A. M. Nagrial, E. S. Humphrey, L. A. Chantrill, A. Mawson, J. Humphris, A. Chou, M. Pajic, C. J. Scarlett, A. V. Pinho, M. Giry-Laterriere, I. Rooman, J. S. Samra, J. G. Kench, J. A. Lovell, N. D. Merrett, C. W. Toon, K. Epari, N. Q. Nguyen, A. Barbour, N. Zeps, K. Moran-Jones, N. B. Jamieson, J. S. Graham, F. Duthie, K. Oien, J. Hair, R. Grutzmann, A. Maitra, C. A. Iacobuzio-Donahue, C. L. Wolfgang, R. A. Morgan, R. T. Lawlor, V. Corbo, C. Bassi, B. Rusev, P. Capelli, R. Salvia, G. Tortora, D. Mukhopadhyay, G. M. Petersen, D. M. Munzy, W. E. Fisher, S. A. Karim, J. R. Eshleman, R. H. Hruban, C. Pilarsky, J. R. Morton, O. J. Sansom, A. Scarpa, E. A. Musgrove, U. M. H. Bailey, O. Hofmann, R. L. Sutherland, D. A. Wheeler, A. J. Gill, R. A. Gibbs, J. V. Pearson, A. V. Biankin, et al., 2016, Genomic analyses identify molecular subtypes of pancreatic cancer: Nature, v. 531, p. 47-+.

Bainton, D. F., J. L. Ullyot, and M. G. Farquhar, 1971, DEVELOPMENT OF NEUTROPHILIC POLYMORPHONUCLEAR LEUKOCYTES IN HUMAN BONE MARROW - ORIGIN AND CONTENT OF AZUROPHIL AND SPECIFIC GRANULES: Journal of Experimental Medicine, v. 134, p. 907-+.

Barak, Y., T. Juven, R. Haffner, and M. Oren, 1993, MDM2 EXPRESSION IS INDUCED BY WILD TYPE-P53 ACTIVITY: Embo Journal, v. 12, p. 461-468.

Bardeesy, N., K. H. Cheng, J. H. Berger, G. C. Chu, J. Pahler, P. Olson, A. F. Hezel, J. Horner, G. Y. Lauwers, D. Hanahan, and R. A. DePinho, 2006, Smad4 is dispensable for normal pancreas development yet critical in progression and tumor biology of pancreas cancer: Genes & Development, v. 20, p. 3130-3146.

Bardeesy, N., and R. A. DePinho, 2002, Pancreatic cancer biology and genetics: Nature Reviews Cancer, v. 2, p. 897-909.

Batlle, E., and J. Massague, 2019, Transforming Growth Factor-beta Signaling in Immunity and Cancer: Immunity, v. 50, p. 924-940.

Begum, A., R. H. McMillan, Y. T. Chang, V. R. Penchev, N. V. Rajeshkumar, A. Maitra, M. G. Goggins, J. R. Eshelman, C. L. Wolfgang, Z. A. Rasheed, and W. Matsui, 2019, Direct Interactions With Cancer-Associated Fibroblasts Lead to Enhanced Pancreatic Cancer Stem Cell Function: Pancreas, v. 48, p. 329-334.

Bengtsson, A., R. Andersson, and D. Ansari, 2020, The actual 5-year survivors of pancreatic ductal adenocarcinoma based on real-world data: Scientific Reports, v. 10.

Bevilacqua, M. P., S. Stengelin, M. A. Gimbrone, and B. Seed, 1989, ENDOTHELIAL LEUKOCYTE ADHESION MOLECULE-1 - AN INDUCIBLE RECEPTOR FOR NEUTROPHILS RELATED TO COMPLEMENT REGULATORY PROTEINS AND LECTINS: Science, v. 243, p. 1160-1165.

Biankin, A. V., N. Waddell, K. S. Kassahn, M. C. Gingras, L. B. Muthuswamy, A. L. Johns, D. K. Miller, P. J. Wilson, A. M. Patch, J. M. Wu, D. K. Chang, M. J. Cowley, B. B. Gardiner, S. Song, I. Harliwong, S. Idrisoglu, C. Nourse, E. Nourbakhsh, S. Manning, S. Wani, M. Gongora, M. Pajic, C. J. Scarlett, A. J. Gill, A. V. Pinho, I. Rooman, M. Anderson, O. Holmes, C. Leonard, D. Taylor, S. Wood, Q. Y. Xu, K. Nones, J. L. Fink, A. Christ, T. Bruxner, N. Cloonan, G. Kolle, F. Newell, M. Pinese, R. S. Mead, J. L. Humphris, W. Kaplan, M. D. Jones, E. K. Colvin, A. M. Nagrial, E. S. Humphrey, A. Chou, V. T. Chin, L. A. Chantrill, A. Mawson, J. S. Samra, J. G. Kench, J. A. Lovell, R. J. Daly, N. D. Merrett, C. Toon, K. Epari, N. Q. Nguyen, A. Barbour, N. Zeps, N. Kakkar, F. M. Zhao, Y. Q. Wu, M. Wang, D. M. Muzny, W. E. Fisher, F. C. Brunicardi, S. E. Hodges, J. G. Reid, J. Drummond, K.

Chang, Y. Han, L. R. Lewis, H. Dinh, C. J. Buhay, T. Beck, L. Timms, M. Sam, K. Begley, A. Brown, D. Pai, A. Panchal, N. Buchner, R. De Borja, R. E. Denroche, C. K. Yung, S. Serra, N. Onetto, D. Mukhopadhyay, M. S. Tsao, P. A. Shaw, G. M. Petersen, S. Gallinger, R. H. Hruban, A. Maitra, C. A. Iacobuzio-Donahue, R. D. Schulick, C. L. Wolfgang, R. A. Morgan, et al., 2012, Pancreatic cancer genomes reveal aberrations in axon guidance pathway genes: Nature, v. 491, p. 399-405.

Biffi, G., T. E. Oni, B. Spielman, Y. Hao, E. Elyada, Y. Park, J. Preall, and D. A. Tuveson, 2019, IL1-Induced JAK/STAT Signaling Is Antagonized by TGF beta to Shape CAF Heterogeneity in Pancreatic Ductal Adenocarcinoma: Cancer Discovery, v. 9, p. 282-301.

Bird, T. G., M. Muller, L. Boulter, D. F. Vincent, R. A. Ridgway, E. Lopez-Guadamillas, W. Y. Lu, T. Jamieson, O. Govaere, A. D. Campbell, S. Ferreira-Gonzalez, A. M. Cole, T. Hay, K. J. Simpson, W. Clark, A. Hedley, M. Clarke, P. Gentaz, C. Nixon, S. Bryce, C. Kiourtis, J. Sprangers, R. J. B. Nibbs, N. Van Rooijen, L. Bartholin, S. R. McGreal, U. Apte, S. T. Barry, J. P. Iredale, A. R. Clarke, M. Serrano, T. A. Roskams, O. J. Sansom, and S. J. Forbes, 2018, TGF beta inhibition restores a regenerative response in acute liver injury by suppressing paracrine senescence: Science Translational Medicine, v. 10.

Block, H., A. Stadtmann, D. Riad, J. Rossaint, C. Sohlbach, G. Germena, D. Q. Wu, S. I. Simon, K. Ley, and A. Zarbock, 2016, Gnb isoforms control a signaling pathway comprising Rac1, Plc beta 2, and Plc beta 3 leading to LFA-1 activation and neutrophil arrest in vivo: Blood, v. 127, p. 314-324.

Bockhorn, M., F. G. Uzunoglu, M. Adham, C. Imrie, M. Milicevic, A. A. Sandberg, H. J. Asbun, C. Bassi, M. Buchler, R. M. Charnley, K. Conlon, L. F. Cruz, C. Dervenis, A. Fingerhutt, H. Friess, D. J. Gouma, W. Hartwig, K. D. Lillemoe, M. Montorsi, J. P. Neoptolemos, S. V. Shrikhande, K. Takaori, W. Traverso, Y. K. Vashist, C. Vollmer, C. J. Yeo, J. R. Izbicki, and S. Int Study Grp Pancreatic, 2014, Borderline resectable pancreatic cancer: A consensus statement by the International Study Group of Pancreatic Surgery (ISGPS): Surgery, v. 155, p. 977-988.

Bosetti, C., E. Lucenteforte, D. T. Silverman, G. Petersen, P. M. Bracci, B. T. Ji, E. Negri, D. Li, H. A. Risch, S. H. Olson, S. Gallinger, A. B. Miller, H. B. Bueno-de-Mesquita, R. Talamini, J. Polesel, P. Ghadirian, P. A. Baghurst, W. Zatonski, E. Fontham, W. R. Bamlet, E. A. Holly, P. Bertuccio, Y. T. Gao, M. Hassan, H. Yu, R. C. Kurtz, M. Cotterchio, J. Su, P. Maisonneuve, E. J. Duell, P. Boffetta, and C. La Vecchia, 2012, Cigarette smoking and pancreatic cancer: an analysis from the International Pancreatic Cancer Case-Control Consortium (Panc4): Annals of Oncology, v. 23, p. 1880-1888.

Boyd, F. T., and J. Massague, 1989, TRANSFORMING GROWTH FACTOR-BETA INHIBITION OF EPITHELIAL-CELL PROLIFERATION LINKED TO THE EXPRESSION OF A 53-KDA MEMBRANE-RECEPTOR: Journal of Biological Chemistry, v. 264, p. 2272-2278.

Brinkmann, V., U. Reichard, C. Goosmann, B. Fauler, Y. Uhlemann, D. S. Weiss, Y. Weinrauch, and A. Zychlinsky, 2004, Neutrophil extracellular traps kill bacteria: Science, v. 303, p. 1532-1535.

Brown, K. F., H. Rumgay, C. Dunlop, M. Ryan, F. Quartly, A. Cox, A. Deas, L. Elliss-Brookes, A. Gavin, L. Hounsome, D. Huws, N. Ormiston-Smith, J. Shelton, C. White, and D. M. Parkin, 2018, The fraction of cancer attributable to modifiable risk factors in England, Wales, Scotland, Northern

Ireland, and the United Kingdom in 2015: British Journal of Cancer, v. 118, p. 1130-1141.

Burlison, J. S., Q. M. Long, Y. Fujitani, C. V. E. Wright, and M. A. Magnuson, 2008, Pdx-1 and Ptf1a concurrently determine fate specification of pancreatic multipotent progenitor cells: Developmental Biology, v. 316, p. 74-86.

Burris, H. A., M. J. Moore, J. Andersen, M. R. Green, M. L. Rothenberg, M. R. Madiano, M. C. Cripps, R. K. Portenoy, A. M. Storniolo, P. Tarassoff, R. Nelson, F. A. Dorr, C. D. Stephens, and D. D. VanHoff, 1997, Improvements in survival and clinical benefit with gemcitabine as first-line therapy for patients with advanced pancreas cancer: A randomized trial: Journal of Clinical Oncology, v. 15, p. 2403-2413.

Buscail, L., B. Bournet, and P. Cordelier, 2020, Role of oncogenic KRAS in the diagnosis, prognosis and treatment of pancreatic cancer: Nature Reviews Gastroenterology & Hepatology, v. 17, p. 153-168.

Buscemi, L., D. Ramonet, F. Klingberg, A. Formey, J. Smith-Clerc, J. J. Meister, and B. Hinz, 2011, The Single-Molecule Mechanics of the Latent TGF-beta 1 Complex: Current Biology, v. 21, p. 2046-2054.

Campbell, F., and C. S. Verbeke, 2013, Pathology of The Pancreas: A Practical Approach, Springer.

Campbell, M. G., A. Cormier, S. Ito, R. I. Seed, A. J. Bondesson, J. Lou, J. D. Marks, J. L. Baron, Y. F. Cheng, and S. L. Nishimura, 2020, Cryo-EM Reveals Integrin-Mediated TGF-beta Activation without Release from Latent TGF-beta: Cell, v. 180, p. 490-+.

CancerResearchUK, https://www.cancerresearchuk.org/health-professional/cancer-statistics/statistics-by-cancer-type/pancreatic-cancer/survival#heading-Zero.

CancerResearchUK, 2018, Pancreatic Cancer Risk, Cancer Reasearch UK.

Candido, J. B., J. P. Morton, P. Bailey, A. D. Campbell, S. A. Karim, T. Jamieson, L. Lapienyte, A. Gopinathan, W. Clark, E. J. McGhee, J. Wang, M. Escorcio-Correia, R. Zollinger, R. Roshani, L. Drew, L. Rishi, R. Arkell, T. R. J. Evans, C. Nixon, D. I. Jodrell, R. W. Wilkinson, A. V. Biankin, S. T. Barry, F. R. Balkwill, and O. J. Sansom, 2018, CSF1R(+) Macrophages Sustain Pancreatic Tumor Growth through T Cell Suppression and Maintenance of Key Gene Programs that Define the Squamous Subtype: Cell Reports, v. 23, p. 1448-1460.

Candido, S., S. L. Abrams, L. S. Steelman, K. Lertpiriyapong, A. M. Martelli, L. Cocco, S. Ratti, M. Y. Follo, R. M. Murata, P. L. Rosalen, B. Bueno-Silva, S. M. de Alencar, P. Lombardi, W. Mao, G. Montalto, M. Cervello, D. Rakus, A. Gizak, H.-L. Lin, M. Libra, S. M. Akula, and J. A. McCubrey, 2019, Effects of the MDM-2 inhibitor Nutlin-3a on PDAC cells containing and lacking WT-TP53 on sensitivity to chemotherapy, signal transduction inhibitors and nutraceuticals: Advances in Biological Regulation, v. 72, p. 22-40.

Canon, J., K. Rex, A. Y. Saiki, C. Mohr, K. Cooke, D. Bagal, K. Gaida, T. Holt, C. G. Knutson, N. Koppada, B. A. Lanman, J. Werner, A. S. Rapaport, T. San Miguel, R. Ortiz, T. Osgood, J. R. Sun, X. C. Zhu, J. D. McCarter, L. P. Volak, B. E. Houk, M. G. Fakih, B. H. O'Neil, T. J. Price, G. S. Falchook, J. Desai, J. Kuo, R. Govindan, D. S. Hong, W. J. Ouyang, H. Henary, T. Arvedson, V. J. Cee, and J. R. Lipford, 2019, The clinical KRAS(G12C) inhibitor AMG 510 drives anti-tumour immunity: Nature, v. 575, p. 217-+.

Carretero, R., I. M. Sektioglu, N. Garbi, O. C. Salgado, P. Beckhove, and G. J. Hammerling, 2015, Eosinophils orchestrate cancer rejection by normalizing

tumor vessels and enhancing infiltration of CD8(+) T cells: Nature Immunology, v. 16, p. 609-+.

Cassandri, M., A. Butera, I. Amelio, A. M. Lena, M. Montanaro, A. Mauriello, L. Anemona, E. Candi, R. A. Knight, M. Agostini, and G. Melino, 2020, ZNF750 represses breast cancer invasion via epigenetic control of prometastatic genes: Oncogene, v. 39, p. 4331-4343.

Chauhan, V. P., J. D. Martin, H. Liu, D. A. Lacorre, S. R. Jain, S. V. Kozin, T. Stylianopoulos, A. S. Mousa, X. X. Han, P. Adstamongkonkul, Z. Popovic, P. G. Huang, M. G. Bawendi, Y. Boucher, and R. K. Jain, 2013, Angiotensin inhibition enhances drug delivery and potentiates chemotherapy by decompressing tumour blood vessels: Nature Communications, v. 4.

Chawla, S. P., H. Bruckner, M. A. Morse, N. Assudani, F. L. Hall, and E. M. Gordon, 2019, A Phase I-II Study Using Rexin-G Tumor-Targeted Retrovector Encoding a Dominant-Negative Cyclin G1 Inhibitor for Advanced Pancreatic Cancer: Molecular Therapy-Oncolytics, v. 12, p. 56-67.

Cheifetz, S., T. Bellon, C. Cales, S. Vera, C. Bernabeu, J. Massague, and M. Letarte, 1992, ENDOGLIN IS A COMPONENT OF THE TRANSFORMING GROWTH-FACTOR-BETA RECEPTOR SYSTEM IN HUMAN ENDOTHELIAL-CELLS: Journal of Biological Chemistry, v. 267, p. 19027-19030.

Chen, W. J., W. W. Jin, N. Hardegen, K. J. Lei, L. Li, N. Marinos, G. McGrady, and S. M. Wahl, 2003, Conversion of peripheral CD4(+)CD25(-) naive T cells to CD4(+)CD25(+) regulatory T cells by TGF-beta induction of transcription factor Foxp3: Journal of Experimental Medicine, v. 198, p. 1875-1886.

Chen, X., M. J. Rubock, and M. Whitman, 1996, A transcriptional partner for MAD proteins in TGF-beta signalling: Nature, v. 383, p. 691-696.

Chen, Y., J. Kim, S. J. Yang, H. M. Wang, C. J. Wu, H. Sugimoto, V. S. LeBleu, and R. Kalluri, 2021, Type I collagen deletion in alpha SMA(+) myofibroblasts augments immune suppression and accelerates progression of pancreatic cancer: Cancer Cell, v. 39, p. 548-+.

Chuvin, N., D. F. Vincent, R. M. Pommier, L. B. Alcaraz, J. Gout, C. Caligaris, K. Yacoub, V. Cardot, E. Roger, B. Kaniewski, S. Martel, C. Cintas, S. Goddard-Leon, A. Colombe, J. Valantin, N. Gadot, E. Servoz, J. Morton, I. Goddard, A. Couvelard, V. Rebours, J. Guillermet, O. J. Sansom, I. Treilleux, U. Valcourt, S. Sentis, P. Dubus, and L. Bartholin, 2017, Acinar-to-Ductal Metaplasia Induced by Transforming Growth Factor Beta Facilitates KRAS(G12D)-driven Pancreatic Tumorigenesis: Cellular and Molecular Gastroenterology and Hepatology, v. 4, p. 263-282.

Coffelt, S. B., K. Kersten, C. W. Doornebal, J. Weiden, K. Vrijland, C. S. Hau, N. J. M. Verstegen, M. Ciampricotti, L. Hawinkels, J. Jonkers, and K. E. de Visser, 2015, IL-17-producing gamma delta T cells and neutrophils conspire to promote breast cancer metastasis: Nature, v. 522, p. 345-+.

Cohen, M., A. Giladi, A. D. Gorki, D. G. Solodkin, M. Zada, A. Hladik, A. Miklosi, T. M. Salame, K. B. Halpern, E. David, S. Itzkovitz, T. Harkany, S. Knapp, and I. Amit, 2018, Lung Single-Cell Signaling Interaction Map Reveals Basophil Role in Macrophage Imprinting: Cell, v. 175, p. 1031-+.

Cohen, S. J., R. K. Alpaugh, I. Palazzo, N. J. Meropol, A. Rogatko, Z. H. Xu, J. P. Hoffman, L. M. Weiner, and J. D. Cheng, 2008, Fibroblast activation protein and its relationship to clinical outcome in pancreatic adenocarcinoma: Pancreas, v. 37, p. 154-158.

Collins, M. A., F. Bednar, Y. Q. Zhang, J. C. Brisset, S. Galban, C. J. Galban, S. Rakshit, K. S. Flannagan, N. V. Adsay, and M. P. di Magliano, 2012,

Oncogenic Kras is required for both the initiation and maintenance of pancreatic cancer in mice: Journal of Clinical Investigation, v. 122, p. 639-653.

Collisson, E. A., P. Bailey, D. K. Chang, and A. V. Biankin, 2019, Molecular subtypes of pancreatic cancer: Nature Reviews Gastroenterology & Hepatology, v. 16, p. 207-220.

Collisson, E. A., A. Sadanandam, P. Olson, W. J. Gibb, M. Truitt, S. D. Gu, J. Cooc, J. Weinkle, G. E. Kim, L. Jakkula, H. S. Feiler, A. H. Ko, A. B. Olshen, K. L. Danenberg, M. A. Tempero, P. T. Spellman, D. Hanahan, and J. W. Gray, 2011, Subtypes of pancreatic ductal adenocarcinoma and their differing responses to therapy: Nature Medicine, v. 17, p. 500-U140.

Colotta, F., F. Re, N. Polentarutti, S. Sozzani, and A. Mantovani, 1992, MODULATION OF GRANULOCYTE SURVIVAL AND PROGRAMMED CELL-DEATH BY CYTOKINES AND BACTERIAL PRODUCTS: Blood, v. 80, p. 2012-2020.

Conroy, T., F. Desseigne, M. Ychou, O. Bouche, R. Guimbaud, Y. Becouarn, A. Adenis, J. L. Raoul, S. Gourgou-Bourgade, C. de la Fouchardiere, J. Bennouna, J. B. Bachet, F. Khemissa-Akouz, D. Pere-Verge, C. Delbaldo, E. Assenat, B. Chauffert, P. Michel, C. Montoto-Grillot, M. Ducreux, U. Grp Tumeurs Digestives, and P. Intergrp, 2011, FOLFIRINOX versus Gemcitabine for Metastatic Pancreatic Cancer: New England Journal of Medicine, v. 364, p. 1817-1825.

Conroy, T., P. Hammel, M. Hebbar, M. Ben Abdelghani, A. C. Wei, J. L. Raoul, L. Chone, E. Francois, P. Artru, J. J. Biagi, T. Lecomte, E. Assenat, R. Faroux, M. Ychou, J. Volet, A. Sauvanet, G. Breysacher, F. Di Fiore, C. Cripps, P. Kavan, P. Texereau, K. Bouhier-Leporrier, F. Khemissa-Akouz, J. L. Legoux, B. Juzyna, S. Gourgou, C. J. O'Callaghan, C. Jouffroy-Zeller, P. Rat, D. Malka, F. Castan, J. B. Bachet, G. Canadian Canc Trials, and G. I. P. G. Unicanc, 2018, FOLFIRINOX or Gemcitabine as Adjuvant Therapy for Pancreatic Cancer: New England Journal of Medicine, v. 379, p. 2395-2406.

Cowland, J. B., and N. Borregaard, 2016, Granulopoiesis and granules of human neutrophils: Immunological Reviews, v. 273, p. 11-28.

Crisan, M., S. Yap, L. Casteilla, C. W. Chen, M. Corselli, T. S. Park, G. Andriolo, B. Sun, B. Zheng, L. Zhang, C. Norotte, P. N. Teng, J. Traas, R. Schugar, B. M. Deasy, S. Badylak, H. J. Buhring, J. P. Giacobino, L. Lazzari, J. Huard, and B. Peault, 2008, A perivascular origin for mesenchymal stem cells in multiple human organs: Cell Stem Cell, v. 3, p. 301-313.

Cunningham, D., I. Chau, D. D. Stocken, J. W. Valle, D. Smith, W. Steward, P. G. Harper, J. Dunn, C. Tudur-Smith, J. West, S. Falk, A. Crellin, F. Adab, J. Thompson, P. Leonard, J. Ostrowski, M. Eatock, W. Scheithauer, R. Herrmann, and J. P. Neoptolemos, 2009, Phase III Randomized Comparison of Gemcitabine Versus Gemcitabine Plus Capecitabine in Patients With Advanced Pancreatic Cancer: Journal of Clinical Oncology, v. 27, p. 5513-5518.

Danielian, P. S., D. Muccino, D. H. Rowitch, S. K. Michael, and A. P. McMahon, 1998, Modification of gene activity in mouse embryos in utero by a tamoxifen-inducible form of Cre recombinase: Current Biology, v. 8, p. 1323-1326.

Daopin, S., K. A. Piez, Y. Ogawa, and D. R. Davies, 1992, CRYSTAL-STRUCTURE OF TRANSFORMING GROWTH-FACTOR-BETA-2 - AN UNUSUAL FOLD FOR THE SUPERFAMILY: Science, v. 257, p. 369-373.

David, C. J., Y. H. Huang, M. Chen, J. Su, Y. L. Zou, N. Bardeesy, C. A. Iacobuzio-Donahue, and J. Massague, 2016, TGF-beta Tumor Suppression through a Lethal EMT: Cell, v. 164, p. 1015-1030.

De Monte, L., S. Wormann, E. Brunetto, S. Heltai, G. Magliacane, M. Reni, A. M. Paganoni, H. Recalde, A. Mondino, M. Falconi, F. Aleotti, G. Balzano, H. A. Ul, C. Doglioni, and M. P. Protti, 2016, Basophil Recruitment into Tumor-Draining Lymph Nodes Correlates with Th2 Inflammation and Reduced Survival in Pancreatic Cancer Patients: Cancer Research, v. 76, p. 1792-1803.

Dekoninck, S., and C. Blanpain, 2019, Stem cell dynamics, migration and plasticity during wound healing: Nature Cell Biology, v. 21, p. 18-24.

Delarco, J. E., and G. J. Todaro, 1978, GROWTH-FACTORS FROM MURINE SARCOMA VIRUS-TRANSFORMED CELLS: Proceedings of the National Academy of Sciences of the United States of America, v. 75, p. 4001-4005.

Deniset, J. F., B. G. Surewaard, W. Y. Lee, and P. Kubes, 2017, Splenic Ly6G(high) mature and Ly6G(int) immature neutrophils contribute to eradication of S-pneumoniae: Journal of Experimental Medicine, v. 214, p. 1333-1350.

Dennler, S., S. Itoh, D. Vivien, P. ten Dijke, S. Huet, and J. M. Gauthier, 1998, Direct binding of Smad3 and Smad4 to critical TGF beta-inducible elements in the promoter of human plasminogen activator inhibitor-type 1 gene: Embo Journal, v. 17, p. 3091-3100.

Derynck, R., J. A. Jarrett, E. Y. Chen, D. H. Eaton, J. R. Bell, R. K. Assoian, A. B. Roberts, M. B. Sporn, and D. V. Goeddel, 1985, HUMAN TRANSFORMING GROWTH FACTOR-BETA COMPLEMENTARY-DNA SEQUENCE AND EXPRESSION IN NORMAL AND TRANSFORMED-CELLS: Nature, v. 316, p. 701-705.

Ding, L., T. L. Saunders, G. Enikolopov, and S. J. Morrison, 2012, Endothelial and perivascular cells maintain haematopoietic stem cells: Nature, v. 481, p. 457-U65.

Diop-Frimpong, B., V. P. Chauhan, S. Krane, Y. Boucher, and R. K. Jain, 2011, Losartan inhibits collagen I synthesis and improves the distribution and efficacy of nanotherapeutics in tumors: Proceedings of the National Academy of Sciences of the United States of America, v. 108, p. 2909-2914.

Dominguez, C. X., S. Muller, S. Keerthivasan, H. Koeppen, J. Hung, S. Gierke, B. Breart, O. Foreman, T. W. Bainbridge, A. Castiglioni, Y. Senbabaoglu, Z. Modrusan, Y. X. Liang, M. R. Junttila, C. Klijn, R. Bourgon, and S. J. Turley, 2020, Single-Cell RNA Sequencing Reveals Stromal Evolution into LRRC15(+) Myofibroblasts as a Determinant of Patient Response to Cancer Immunotherapy: Cancer Discovery, v. 10, p. 232-253.

Dreyer, S. B., N. B. Jamieson, S. L. Cooke, J. W. Valle, C. J. McKay, A. V. Biankin, and D. K. Chang, 2020a, PRECISION-Panc: the Next Generation Therapeutic Development Platform for Pancreatic Cancer: Clinical Oncology, v. 32, p. 1-4.

Dreyer, S. B., N. B. Jamieson, J. P. Morton, O. J. Sansom, A. V. Biankin, and D. K. Chang, 2020b, Pancreatic Cancer: From Genome Discovery to PRECISION-Panc: Clinical Oncology, v. 32, p. 5-8.

Dreyer, S. B., R. Upstill-Goddard, V. Paulus-Hock, C. Paris, E. M. Lampraki, E. Dray, B. Serrels, G. Caligiuri, S. Rebus, D. Plenker, Z. Galluzzo, H. Brunton, R. Cunningham, M. Tesson, C. Nourse, U. M. Bailey, M. Jones, K. Moran-Jones, D. W. Wright, F. Duthie, K. Oien, L. Evers, C. J. McKay, G. A. McGregor, A. Gulati, R. Brough, I. Bajrami, S. Pettitt, M. L. Dziubinski, J.

Candido, F. Balkwill, S. T. Barry, R. Grutzmann, L. Rahib, A. Johns, M. Pajic, F. E. M. Froeling, P. Beer, E. A. Musgrove, G. M. Petersen, A. Ashworth, M. C. Frame, H. C. Crawford, D. M. Simeone, C. Lord, D. Mukhopadhyay, C. Pilarsky, D. A. Tuveson, S. L. Cooke, N. B. Jamieson, J. P. Morton, O. J. Sansom, P. J. Bailey, A. V. Biankin, D. K. Chang, L. Glasgow Precision Oncology, and G. Australian Pancreatic Canc, 2021, Targeting DNA Damage Response and Replication Stress in Pancreatic Cancer: Gastroenterology, v. 160, p. 362-+.

Drissen, R., N. Buza-Vidas, P. Woll, S. Thongjuea, A. Gambardella, A. Giustacchini, E. Mancini, A. Zriwil, M. Lutteropp, A. Grover, A. Mead, E. Sitnicka, S. E. W. Jacobsen, and C. Nerlov, 2016, Distinct myeloid progenitor-differentiation pathways identified through single-cell RNA sequencing: Nature Immunology, v. 17, p. 666-+.

Eash, K. J., J. M. Means, D. W. White, and D. C. Link, 2009, CXCR4 is a key regulator of neutrophil release from the bone marrow under basal and stress granulopoiesis conditions: Blood, v. 113, p. 4711-4719.

Elyada, E., M. Bolisetty, P. Laise, W. F. Flynn, E. T. Courtois, R. A. Burkhart, J. A. Teinor, P. Belleau, G. Biffi, M. S. Lucito, S. Sivajothi, T. D. Armstrong, D. D. Engle, K. H. Yu, Y. Hao, C. L. Wolfgang, Y. Park, J. Preall, E. M. Jaffee, A. Califano, P. Robson, and D. A. Tuveson, 2019, Cross-Species Single-Cell Analysis of Pancreatic Ductal Adenocarcinoma Reveals Antigen-Presenting Cancer-Associated Fibroblasts: Cancer Discovery, v. 9, p. 1102-1123.

Evrard, M., I. W. H. Kwok, S. Z. Chong, K. W. W. Teng, E. Becht, J. M. Chen, J. L. Sieow, H. L. Penny, G. C. Ching, S. Devi, J. P. M. Adrover, J. L. Y. Li, K. H. Liong, L. Tan, Z. Poon, S. Foo, J. W. Chua, I. H. Su, K. Balabanian, F. Bachelerie, S. K. Biswas, A. Larbi, W. Y. K. Hwang, V. Madan, H. P. Koeffler, S. C. Wong, E. W. Newell, A. Hidalgo, F. Ginhoux, and L. G. Ng, 2018, Developmental Analysis of Bone Marrow Neutrophils Reveals Populations Specialized in Expansion, Trafficking, and Effector Functions: Immunity, v. 48, p. 364-+.

Eyres, M., S. Lanfredini, H. N. Xu, A. Burns, A. Blake, F. Willenbrock, R. Goldin, D. Hughes, S. Hughes, A. Thapa, D. Vavoulis, A. Hubert, Z. D'Costa, A. Sabbagh, A. G. Abraham, C. Blancher, S. Jones, C. Verrill, M. Silva, Z. Soonawalla, T. Maughan, A. Schuh, S. Mukherjee, and E. O'Neill, 2021, TET2 Drives 5hmc Marking of GATA6 and Epigenetically Defines Pancreatic Ductal Adenocarcinoma Transcriptional Subtypes: Gastroenterology, v. 161, p. 653-+.

Feig, L. A., 1999, Tools of the trade: use of dominant-inhibitory mutants of Ras-family GTPases: Nature Cell Biology, v. 1, p. E25-E27.

Feldmann, G., R. Beaty, R. H. Hruban, and A. Maitra, 2007, Molecular genetics of pancreatic intraepithelial neoplasia: Journal of Hepato-Biliary-Pancreatic Surgery, v. 14, p. 224-232.

Ferlay, J., C. Partensky, and F. Bray, 2016, More deaths from pancreatic cancer than breast cancer in the EU by 2017: Acta Oncologica, v. 55, p. 1158-1160.

Franzen, P., P. Tendijke, H. Ichijo, H. Yamashita, P. Schulz, C. H. Heldin, and K. Miyazono, 1993, CLONING OF A TGF-BETA TYPE-I RECEPTOR THAT FORMS A HETEROMERIC COMPLEX WITH THE TGF-BETA TYPE-II RECEPTOR: Cell, v. 75, p. 681-692.

Fridlender, Z. G., J. Sun, S. Kim, V. Kapoor, G. Cheng, L. Ling, G. S. Worthen, and S. M. Albelda, 2009, Polarization of Tumor-Associated Neutrophil Phenotype by TGF-beta: "N1" versus "N2" TAN: Cancer Cell, v. 16, p. 183-194.

Fridlender, Z. G., J. Sun, I. Mishalian, S. Singhal, G. J. Cheng, V. Kapoor, W. Horng, G. Fridlender, R. Bayuh, G. S. Worthen, and S. M. Albelda, 2012, Transcriptomic Analysis Comparing Tumor-Associated Neutrophils with Granulocytic Myeloid-Derived Suppressor Cells and Normal Neutrophils: Plos One, v. 7, p. 13.

Frolik, C. A., L. M. Wakefield, D. M. Smith, and M. B. Sporn, 1984, CHARACTERIZATION OF A MEMBRANE-RECEPTOR FOR TRANSFORMING GROWTH FACTOR-BETA IN NORMAL RAT-KIDNEY FIBROBLASTS: Journal of Biological Chemistry, v. 259, p. 995-1000.

Galli, S. J., N. Gaudenzio, and M. Tsai, 2020, Mast Cells in Inflammation and Disease: Recent Progress and Ongoing Concerns: Annual Review of Immunology, Vol 38, v. 38, p. 49-77.

Gao, R. P., and D. R. Brigstock, 2005, Connective tissue growth factor (CCN2) in rat pancreatic stellate cell function: Integrin zeta(5)beta(1) as a novel CCN2 receptor: Gastroenterology, v. 129, p. 1019-1030.

Gao, Z. J., X. P. Wang, K. Wu, Y. Zhao, and G. Y. Hu, 2010, Pancreatic Stellate Cells Increase the Invasion of Human Pancreatic Cancer Cells through the Stromal Cell-Derived Factor-1/CXCR4 Axis: Pancreatology, v. 10, p. 186-193.

Garcia, P. E., M. Adoumie, E. C. Kim, Y. Q. Zhang, M. K. Scales, Y. S. El-Tawi, A. Z. Shaikh, H. J. Wen, F. Bednar, B. Allen, D. M. Wellik, H. C. Crawford, and M. P. D. Magliano, 2020, Differential Contribution of Pancreatic Fibroblast Subsets to the Pancreatic Cancer Stroma: Cellular and Molecular Gastroenterology and Hepatology, v. 10, p. 581-599.

Gentry, L. E., and B. W. Nash, 1990, THE PRO DOMAIN OF PRE-PRO-TRANSFORMING GROWTH FACTOR-BETA-1 WHEN INDEPENDENTLY EXPRESSED IS A FUNCTIONAL BINDING-PROTEIN FOR THE MATURE GROWTH-FACTOR: Biochemistry, v. 29, p. 6851-6857.

Girbl, T., T. Lenn, L. Perez, L. Rolas, A. Barkaway, A. Thiriot, C. del Fresno, E. Lynam, E. Hub, M. Thelen, G. Graham, R. Alon, D. Sancho, U. H. von Andrian, M. B. Voisin, A. Rot, and S. Nourshargh, 2018, Distinct Compartmentalization of the Chemokines CXCL1 and CXCL2 and the Atypical Receptor ACKR1 Determine Discrete Stages of Neutrophil Diapedesis: Immunity, v. 49, p. 1062-+.

Goetze, R. G., S. M. Buchholz, S. Patil, G. Petzold, V. Ellenrieder, E. Hessmann, and A. Neesse, 2018, Utilizing High Resolution Ultrasound to Monitor Tumor Onset and Growth in Genetically Engineered Pancreatic Cancer Models: Jove-Journal of Visualized Experiments.

Goldstein, D., R. H. El-Maraghi, P. Hammel, V. Heinemann, V. Kunzmann, J. Sastre, W. Scheithauer, S. Siena, J. Tabernero, L. Teixeira, G. Tortora, J. L. Van Laethem, R. Young, D. N. Penenberg, B. Lu, A. Romano, and D. D. Von Hoff, 2015, nab-Paclitaxel Plus Gemcitabine for Metastatic Pancreatic Cancer: Long-Term Survival From a Phase III Trial: Jnci-Journal of the National Cancer Institute, v. 107, p. 10.

Gomis, R. R., C. Alarcon, C. Nadal, C. Van Poznak, and J. Massague, 2006, C/EBP beta at the core of the TGF beta cytostatic response and its evasion in metastatic breast cancer cells: Cancer Cell, v. 10, p. 203-214.

Gopinathan, A., J. P. Morton, D. I. Jodrell, and O. J. Sansom, 2015, GEMMs as preclinical models for testing pancreatic cancer therapies: Disease Models & Mechanisms, v. 8, p. 1185-1200.

Gougos, A., and M. Letarte, 1990, PRIMARY STRUCTURE OF ENDOGLIN, AN RGD-CONTAINING GLYCOPROTEIN OF HUMAN ENDOTHELIAL-CELLS: Journal of Biological Chemistry, v. 265, p. 8361-8364.

Granot, Z., E. Henke, E. A. Comen, T. A. King, L. Norton, and R. Benezra, 2011, Tumor Entrained Neutrophils Inhibit Seeding in the Premetastatic Lung: Cancer Cell, v. 20, p. 300-314.

Grieshaber-Bouyer, R., F. A. Radtke, P. Cunin, G. Stifano, A. Levescot, B. Vijaykumar, N. Nelson-Maney, R. B. Blaustein, P. A. Monach, P. A. Nigrovic, and C. ImmGen, 2021, The neutrotime transcriptional signature defines a single continuum of neutrophils across biological compartments: Nature Communications, v. 12.

Gu, G. Q., J. R. Brown, and D. A. Melton, 2003, Direct lineage tracing reveals the ontogeny of pancreatic cell fates during mouse embryogenesis: Mechanisms of Development, v. 120, p. 35-43.

Gu, G. Q., J. Dubauskaite, and D. A. Melton, 2002, Direct evidence for the pancreatic lineage: NGN3+cells are islet progenitors and are distinct from duct progenitors: Development, v. 129, p. 2447-2457.

Habbe, N., G. L. Shi, R. A. Meguid, V. Fendrich, F. Esni, H. P. Chen, G. Feldmann, D. A. Stoffers, S. F. Konieczny, S. D. Leach, and A. Maitra, 2008, Spontaneous induction of murine pancreatic intraepithelial neoplasia (mPanIN) by acinar cell targeting of oncogenic Kras in adult mice: Proceedings of the National Academy of Sciences of the United States of America, v. 105, p. 18913-18918.

Haddad, A., G. C. Kowdley, T. M. Pawlik, and S. C. Cunningham, 2011, Hereditary pancreatic and hepatobiliary cancers: International journal of surgical oncology, v. 2011, p. 154673.

Hafner, A., M. L. Bulyk, A. Jambhekar, and G. Lahav, 2019, The multiple mechanisms that regulate p53 activity and cell fate: Nature Reviews Molecular Cell Biology, v. 20, p. 199-210.

Hager, M., J. B. Cowland, and N. Borregaard, 2010, Neutrophil granules in health and disease: Journal of Internal Medicine, v. 268, p. 25-34.

Hahn, S. A., M. Schutte, A. Hoque, C. A. Moskaluk, L. T. daCosta, E. Rozenblum, C. L. Weinstein, A. Fischer, C. J. Yeo, R. H. Hruban, and S. E. Kern, 1996, DPC4, a candidate tumor suppressor gene at human chromosome 18q21.1: Science, v. 271, p. 350-353.

Haigis, K. M., 2017, KRAS Alleles: The Devil Is in the Detail: Trends in Cancer, v. 3, p. 686-697.

Handler, J., J. Cullis, A. Avanzi, E. A. Vucic, and D. Bar-Sagi, 2018, Pre-neoplastic pancreas cells enter a partially mesenchymal state following transient TGF-beta exposure: Oncogene, v. 37, p. 4334-4342.

Hasenberg, A., M. Hasenberg, L. Mann, F. Neumann, L. Borkenstein, M. Stecher, A. Kraus, D. R. Engel, A. Klingberg, P. Seddigh, Z. Abdullah, S. Klebow, S. Engelmann, A. Reinhold, S. Brandau, M. Seeling, A. Waisman, B. Schraven, J. R. Gothert, F. Nimmerjahn, and M. Gunzer, 2015, Catchup: a mouse model for imaging-based tracking and modulation of neutrophil granulocytes: Nature Methods, v. 12, p. 445-+.

Haupt, Y., R. Maya, A. Kazaz, and M. Oren, 1997, Mdm2 promotes the rapid degradation of p53: Nature, v. 387, p. 296-299.

Hayashi, H., S. Abdollah, Y. B. Qiu, J. X. Cai, Y. Y. Xu, B. W. Grinnell, M. A. Richardson, J. N. Topper, M. A. Gimbrone, J. L. Wrana, and D. Falb, 1997, The MAD-related protein Smad7 associates with the TGF beta receptor and functions as an antagonist of TGF beta signaling: Cell, v. 89, p. 1165-1173.

Hertel, L. W., G. B. Boder, J. S. Kroin, S. M. Rinzel, G. A. Poore, G. C. Todd, and G. B. Grindey, 1990, EVALUATION OF THE ANTITUMOR-ACTIVITY OF GEMCITABINE (2',2'-DIFLUORO-2'-DEOXYCYTIDINE): Cancer Research, v. 50, p. 4417-4422.

Hezel, A. F., A. C. Kimmelman, B. Z. Stanger, N. Bardeesy, and R. A. DePinho, 2006, Genetics and biology of pancreatic ductal adenocarcinoma: Genes & Development, v. 20, p. 1218-1249.

Hingorani, S. R., E. F. Petricoin, A. Maitra, V. Rajapakse, C. King, M. A. Jacobetz, S. Ross, T. P. Conrads, T. D. Veenstra, B. A. Hitt, Y. Kawaguchi, D. Johann, L. A. Liotta, H. C. Crawford, M. E. Putt, T. Jacks, C. V. E. Wright, R. H. Hruban, A. M. Lowy, and D. A. Tuveson, 2003, Preinvasive and invasive ductal pancreatic cancer and its early detection in the mouse: Cancer Cell, v. 4, p. 437-450.

Hingorani, S. R., L. F. Wang, A. S. Multani, C. Combs, T. B. Deramaudt, R. H. Hruban, A. K. Rustgi, S. Chang, and D. A. Tuveson, 2005, Trp53(R172H) and KraS(G12D) cooperate to promote chromosomal instability and widely metastatic pancreatic ductal adenocarcinoma in mice: Cancer Cell, v. 7, p. 469-483.

Horne, M. C., G. L. Goolsby, K. L. Donaldson, D. Tran, M. Neubauer, and A. F. Wahls, 1996, Cyclin G1 and cyclin G2 comprise a new family of cyclins with contrasting tissue-specific and cell cycle-regulated expression: Journal of Biological Chemistry, v. 271, p. 6050-6061.

Hosein, A. N., H. C. Huang, Z. N. Wang, K. Parmar, W. T. Du, J. Huang, A. Maitra, E. Olson, U. Verma, and R. A. Brekken, 2019, Cellular heterogeneity during mouse pancreatic ductal adenocarcinoma progression at single-cell resolution: Jci Insight, v. 4, p. 16.

Hotz, B., M. Arndt, S. Dullat, S. Bhargava, H. J. Buhr, and H. G. Hotz, 2007, Epithelial to mesenchymal transition: Expression of the regulators snail, slug, and twist in pancreatic cancer: Clinical Cancer Research, v. 13, p. 4769-4776.

Hruban, R. H., A. Maitra, and M. Goggins, 2008, Update on Pancreatic Intraepithelial Neoplasia: International Journal of Clinical and Experimental Pathology, v. 1, p. 306-316.

Huang, H. C., Y. Q. Zhang, V. Gallegos, N. Sorrelle, M. M. Zaid, J. Toombs, W. T. Du, S. Wright, M. Hagopian, Z. N. Wang, A. N. Hosein, A. A. Sathe, C. Xing, E. J. Koay, K. E. Driscoll, and R. A. Brekken, 2019, Targeting TGF beta R2-mutant tumors exposes vulnerabilities to stromal TGF beta blockade in pancreatic cancer: Embo Molecular Medicine, v. 11, p. 20.

Huang, Y. H., J. Hu, F. Chen, N. Lecomte, H. Basnet, C. J. David, M. D. Witkin, P. J. Allen, S. D. Leach, T. J. Hollmann, C. A. Iacobuzio-Donahue, and J. Massague, 2020, ID1 Mediates Escape from TGF beta Tumor Suppression in Pancreatic Cancer: Cancer Discovery, v. 10, p. 142-157.

Hutton, C., F. Heider, A. Blanco-Gomez, A. Banyard, A. Kononov, X. Zhang, S. Karim, V. Paulus-Hock, D. Watt, N. Steele, S. Kemp, E. K. J. Hogg, J. Kelly, R.-F. Jackstadt, F. Lopes, M. Menotti, L. Chisholm, A. Lamarca, J. Valle, O. J. Sansom, C. Springer, A. Malliri, R. Marais, M. Pasca di Magliano, S. Zelenay, J. P. Morton, and C. Jorgensen, 2021, Single-cell analysis defines a pancreatic fibroblast lineage that supports anti-tumor immunity: Cancer cell.

Hwang, R. F., T. Moore, T. Arumugam, V. Ramachandran, K. D. Amos, A. Rivera, B. Ji, D. B. Evans, and C. D. Logsdon, 2008, Cancer-associated stroma fibroblasts promote pancreatic tumor progression: Cancer Research, v. 68, p. 918-926.

Hyun, Y. M., Y. H. Choe, S. A. Park, and M. Kim, 2019, LFA-1 (CD11a/CD18) and Mac-1 (CD11b/CD18) distinctly regulate neutrophil extravasation through hotspots I and II: Experimental and Molecular Medicine, v. 51.

Iacobuzio-Donahue, C. A., B. Ryu, R. H. Hruban, and S. E. Kern, 2002, Exploring the host desmoplastic response to pancreatic carcinoma - Gene expression of stromal and neoplastic cells at the site of primary invasion: American Journal of Pathology, v. 160, p. 91-99.

Ijichi, H., A. Chytil, A. E. Gorska, M. E. Aakre, B. Bierie, M. Tada, D. Mohri, K. Miyabayashi, Y. Asaoka, S. Maeda, T. Ikenoue, K. Tateishi, C. V. E. Wright, K. Koike, M. Omata, and H. L. Moses, 2011, Inhibiting Cxcr2 disrupts tumor-stromal interactions and improves survival in a mouse model of pancreatic ductal adenocarcinoma: Journal of Clinical Investigation, v. 121, p. 4106-4117.

Ijichi, H., A. Chytil, A. E. Gorska, M. E. Aakre, Y. Fujitani, S. Fujitani, C. V. E. Wright, and H. L. Moses, 2006, Aggressive pancreatic ductal adenocarcinoma in mice caused by pancreas-specific blockade of transforming growth factor-beta signaling in cooperation with active Kras expression: Genes & Development, v. 20, p. 3147-3160.

Indra, A. K., X. Warot, J. Brocard, J. M. Bornert, J. H. Xiao, P. Chambon, and D. Metzger, 1999, Temporally-controlled site-specific mutagenesis in the basal layer of the epidermis: comparison of the recombinase activity of the tamoxifen-inducible Cre-ERT and Cre-ERT2 recombinases: Nucleic Acids Research, v. 27, p. 4324-4327.

Inman, G. J., F. J. Nicolas, and C. S. Hill, 2002, Nucleocytoplasmic shuttling of Smads 2, 3, and 4 permits sensing of TGF-beta receptor activity: Molecular Cell, v. 10, p. 283-294.

Isaji, S., S. Mizuno, J. A. Windsor, C. Bassi, C. Fernandez-del Castillo, T. Hackert, A. Hayasaki, M. H. G. Katz, S. W. Kim, M. Kishiwada, H. Kitagawa, C. W. Michalski, and C. L. Wolfgang, 2018, International consensus on definition and criteria of borderline resectable pancreatic ductal adenocarcinoma 2017: Pancreatology, v. 18, p. 2-11.

Ischenko, I., S. D'Amico, M. Rao, J. Y. Li, M. J. Hayman, S. Powers, O. Petrenko, and N. C. Reich, 2021, KRAS drives immune evasion in a genetic model of pancreatic cancer: Nature Communications, v. 12.

Iwamoto, C., K. Ohuchida, T. Shinkawa, S. Okuda, Y. Otsubo, T. Okumura, A. Sagara, K. Koikawa, Y. Ando, K. Shindo, N. Ikenaga, K. Nakata, T. Moriyama, Y. Miyasaka, T. Ohtsuka, M. Eto, K. Akashi, and M. Nakamura, 2021, Bone marrow-derived macrophages converted into cancer-associated fibroblast-like cells promote pancreatic cancer progression: Cancer Letters, v. 512, p. 15-27.

Jackstadt, R., S. R. van Hooff, J. D. Leach, X. Cortes-Lavaud, J. O. Lohuis, R. A. Ridgway, V. M. Wouters, J. Roper, T. J. Kendall, C. S. Roxburgh, P. G. Horgan, C. Nixon, C. Nourse, M. Gunzer, W. Clark, A. Hedley, O. H. Yilmaz, M. Rashid, P. Bailey, A. V. Biankin, A. D. Campbell, D. J. Adams, S. T. Barry, C. W. Steele, J. P. Medema, and O. J. Sansom, 2019, Epithelial NOTCH Signaling Rewires the Tumor Microenvironment of Colorectal Cancer to Drive Poor-Prognosis Subtypes and Metastasis: Cancer Cell, v. 36, p. 319-+.

Jacobetz, M. A., D. S. Chan, A. Neesse, T. E. Bapiro, N. Cook, K. K. Frese, C. Feig, T. Nakagawa, M. E. Caldwell, H. I. Zecchini, M. P. Lolkema, P. Jiang, A. Kultti, C. B. Thompson, D. C. Maneval, D. I. Jodrell, G. I. Frost, H. M. Shepard, J. N. Skepper, and D. A. Tuveson, 2013, Hyaluronan impairs vascular function and drug delivery in a mouse model of pancreatic cancer: Gut, v. 62, p. 112-U153.

Jacobs, E. J., S. J. Chanock, C. S. Fuchs, A. LaCroix, R. R. McWilliams, E. Steplowski, R. Z. Stolzenberg-Solomon, A. A. Arslan, H. B. Bueno-de-

Mesquita, M. Gross, K. Helzlsouer, G. Petersen, W. Zheng, I. Agalliu, N. E. Allen, L. Amundadottir, M. C. Boutron-Ruault, J. E. Buring, F. Canzian, S. Clipp, M. Dorronsoro, J. M. Gaziano, E. L. Giovannucci, S. E. Hankinson, P. Hartge, R. N. Hoover, D. J. Hunter, K. B. Jacobs, M. Jenab, P. Kraft, C. Kooperberg, S. M. Lynch, M. Sund, J. B. Mendelsohn, T. Mouw, C. C. Newton, K. Overvad, D. Palli, P. H. M. Peeters, A. Rajkovic, X. O. Shu, G. Thomas, G. S. Tobias, D. Trichopoulos, J. Virtamo, J. Wactawski-Wende, B. M. Wolpin, K. Yu, and A. Zeleniuch-Jacquotte, 2010, Family history of cancer and risk of pancreatic cancer: a pooled analysis from the Pancreatic Cancer Cohort Consortium (PanScan): International Journal of Cancer, v. 127, p. 1421-1428.

Jang, C. W., C. H. Chen, C. C. Chen, J. Y. Chen, Y. H. Su, and R. H. Chen, 2002, TGF-beta induces apoptosis through Smad-mediated expression of DAP-kinase: Nature Cell Biology, v. 4, p. 51-58.

Jean-Paul, D., L. L. Emerson, J. L. Goodman, S. C. Froebe, B. E. Illum, A. B. Curtis, and L. C. Murtaugh, 2008, Notch and Kras reprogram pancreatic acinar cells to ductal intraepithelial neoplasia: Proceedings of the National Academy of Sciences of the United States of America, v. 105, p. 18907-18912.

Jonk, L. J. C., S. Itoh, C. H. Heldin, P. ten Dijke, and W. Kruijer, 1998, Identification and functional characterization of a Smad binding element (SBE) in the JunB promoter that acts as a transforming growth factor-beta, activin, and bone morphogenetic protein-inducible enhancer: Journal of Biological Chemistry, v. 273, p. 21145-21152.

Jonsson, J., L. Carlsson, T. Edlund, and H. Edlund, 1994, INSULIN-PROMOTER-FACTOR-1 IS REQUIRED FOR PANCREAS DEVELOPMENT IN MICE: Nature, v. 371, p. 606-609.

Kandoth, C., M. D. McLellan, F. Vandin, K. Ye, B. F. Niu, C. Lu, M. C. Xie, Q. Y. Zhang, J. F. McMichael, M. A. Wyczalkowski, M. D. M. Leiserson, C. A. Miller, J. S. Welch, M. J. Walter, M. C. Wendl, T. J. Ley, R. K. Wilson, B. J. Raphael, and L. Ding, 2013, Mutational landscape and significance across 12 major cancer types: Nature, v. 502, p. 333-+.

Kang, Y. B., C. R. Chen, and J. Massague, 2003, A self-enabling TGF beta response coupled to stress signaling: Smad engages stress response factor ATF3 for Id1 repression in epithelial cells: Molecular Cell, v. 11, p. 915-926.

Katsuno, Y., D. S. Meyer, Z. Y. Zhang, K. M. Shokat, R. J. Akhurst, K. Miyazono, and R. Derynck, 2019, Chronic TGF-beta exposure drives stabilized EMT, tumor stemness, and cancer drug resistance with vulnerability to bitopic mTOR inhibition: Science Signaling, v. 12.

Kavsak, P., R. K. Rasmussen, C. G. Causing, S. Bonni, H. T. Zhu, G. H. Thomsen, and J. L. Wrana, 2000, Smad7 binds to Smurf2 to form an E3 ubiquitin ligase that targets the TGF beta receptor for degradation: Molecular Cell, v. 6, p. 1365-1375.

Kennedy, A. L., J. P. Morton, I. Manoharan, D. M. Nelson, N. B. Jamieson, J. S. Pawlikowski, T. McBryan, B. Doyle, C. McKay, K. A. Oien, G. H. Enders, R. G. Zhang, O. J. Sansom, and P. D. Adams, 2011, Activation of the PIK3CA/AKT Pathway Suppresses Senescence Induced by an Activated RAS Oncogene to Promote Tumorigenesis: Molecular Cell, v. 42, p. 36-49.

Kikuta, K., A. Masamune, T. Watanabe, H. Ariga, H. Itoh, S. Hamada, K. Satoh, S. Egawa, M. Unno, and T. Shimosegawa, 2010, Pancreatic stellate cells promote epithelial-mesenchymal transition in pancreatic cancer cells: Biochemical and Biophysical Research Communications, v. 403, p. 380-384.

Kim, E. J., V. Sahai, E. V. Abel, K. A. Griffith, J. K. Greenson, N. Takebe, G. N. Khan, J. L. Blau, R. Craig, U. G. Balis, M. M. Zalupski, and D. M. Simeone, 2014, Pilot Clinical Trial of Hedgehog Pathway Inhibitor GDC-0449 (Vismodegib) in Combination with Gemcitabine in Patients with Metastatic Pancreatic Adenocarcinoma: Clinical Cancer Research, v. 20, p. 5937-5945.

Kim, H. K., M. D. Sierra, C. K. Williams, A. V. Gulino, and G. Tosato, 2006, G-CSF down-regulation of CXCR4 expression identified as a mechanism for mobilization of myeloid cells: Blood, v. 108, p. 812-820.

Kim, Y. H., D. C. Jeong, K. Pak, M. E. Han, J. Y. Kim, L. Liangwen, H. J. Kim, T. W. Kim, T. H. Kim, D. W. Hyun, and S. O. Oh, 2017, SLC2A2 (GLUT2) as a novel prognostic factor for hepatocellular carcinoma: Oncotarget, v. 8, p. 68381-68392.

Kimura, S. H., M. Ikawa, A. Ito, M. Okabe, and H. Nojima, 2001, Cyclin G1 is involved in G2/M arrest in response to DNA damage and in growth control after damage recovery: Oncogene, v. 20, p. 3290-3300.

Kimura, S. H., and H. Nojima, 2002, Cyclin G1 associates with MDM2 and regulates accumulation and degradation of p53 protein: Genes to Cells, v. 7, p. 869-880.

Kirkegard, J., F. V. Mortensen, and D. Cronin-Fenton, 2017, Chronic Pancreatitis and Pancreatic Cancer Risk: A Systematic Review and Meta-analysis: American Journal of Gastroenterology, v. 112, p. 1366-1372.

Kleeff, J., M. Korc, M. Apte, C. La Vecchia, C. D. Johnson, A. V. Biankin, R. E. Neale, M. Tempero, D. A. Tuveson, R. H. Hruban, and J. P. Neoptolemos, 2016, Pancreatic cancer: Nature Reviews Disease Primers, v. 2.

Klein, A. P., 2012, Genetic susceptibility to pancreatic cancer: Molecular Carcinogenesis, v. 51, p. 14-24.

Kohler, A., K. De Filippo, M. Hasenberg, C. van den Brandt, E. Nye, M. P. Hosking, T. E. Lane, L. Mann, R. M. Ransohoff, A. E. Hauser, O. Winter, B. Schraven, H. Geiger, N. Hogg, and M. Gunzer, 2011, G-CSF-mediated thrombopoietin release triggers neutrophil motility and mobilization from bone marrow via induction of Cxcr2 ligands: Blood, v. 117, p. 4349-4357.

Kong, P. Z., E. W. Xu, Y. H. Bi, X. Q. Xu, X. Liu, B. Song, L. Zhang, C. X. Cheng, T. Yan, Y. Qian, J. Yang, Y. C. Ma, H. Y. Cui, Y. F. Zhai, B. B. Zou, X. C. Liu, Y. K. Cheng, S. P. Guo, X. L. Cheng, and Y. P. Cui, 2020, Novel ESCC-related gene ZNF750 as potential Prognostic biomarker and inhibits Epithelial-Mesenchymal Transition through directly depressing SNAI1 promoter in ESCC: Theranostics, v. 10, p. 1798-1813.

Krapp, A., M. Knofler, B. Ledermann, K. Burki, C. Berney, N. Zoerkler, O. Hagenbuchle, and P. K. Wellauer, 1998, The bHLH protein PTF1-p48 is essential for the formation of the exocrine and the correct spatial organization of the endocrine pancreas: Genes & Development, v. 12, p. 3752-3763.

Krystel-Whittemore, M., K. N. Dileepan, and J. G. Wood, 2016, Mast Cell: A Multi-Functional Master Cell: Frontiers in Immunology, v. 6, p. 1-12.

Kuonen, F., J. Laurent, C. Secondini, G. Lorusso, J. C. Stehle, T. Rausch, E. Faes-van't Hull, G. Bieler, G. C. Alghisi, R. Schwendener, S. Andrejevic-Blant, R. O. Mirimanoff, and C. Ruegg, 2012, Inhibition of the Kit Ligand/c-Kit Axis Attenuates Metastasis in a Mouse Model Mimicking Local Breast Cancer Relapse after Radiotherapy: Clinical Cancer Research, v. 18, p. 4365-4374.

Kyrgiou, M., I. Kalliala, G. Markozannes, M. J. Gunter, E. Paraskevaidis, H. Gabra, P. Martin-Hirsch, and K. K. Tsilidis, 2017, Adiposity and cancer at major

anatomical sites: umbrella review of the literature: Bmj-British Medical Journal, v. 356.

Labibi, B., M. Bashkurov, J. L. Wrana, and L. Attisano, 2020, Modeling the Control of TGF-beta/Smad Nuclear Accumulation by the Hippo Pathway Effectors, Taz/Yap: Iscience, v. 23.

Lahoz-Beneytez, J., M. Elemans, Y. Zhang, R. Ahmed, A. Salam, M. Block, C. Niederalt, B. Asquith, and D. Macallan, 2016, Human neutrophil kinetics: modeling of stable isotope labeling data supports short blood neutrophil half-lives: Blood, v. 127, p. 3431-3438.

Laiho, M., F. M. B. Weis, and J. Massague, 1990, CONCOMITANT LOSS OF TRANSFORMING GROWTH-FACTOR (TGF)-BETA RECEPTOR TYPE-I AND TYPE-II IN TGF-BETA-RESISTANT CELL MUTANTS IMPLICATES BOTH RECEPTOR TYPES IN SIGNAL TRANSDUCTION: Journal of Biological Chemistry, v. 265, p. 18518-18524.

Laklai, H., Y. A. Miroshnikova, M. W. Pickup, E. A. Collisson, G. E. Kim, A. S. Barrett, R. C. Hill, J. N. Lakins, D. D. Schlaepfer, J. K. Mouw, V. S. LeBleu, N. Roy, S. V. Novitskiy, J. S. Johansen, V. Poli, R. Kalluri, C. A. Iacobuzio-Donahue, L. D. Wood, M. Hebrok, K. Hansen, H. L. Moses, and V. M. Weaver, 2016, Genotype tunes pancreatic ductal adenocarcinoma tissue tension to induce matricellular fibrosis and tumor progression: Nature Medicine, v. 22, p. 497-505.

Larsson, J., M. J. Goumans, L. J. Sjostrand, M. A. van Rooijen, D. Ward, P. Leveen, X. F. Xu, P. ten Dijke, C. L. Mummery, and S. Karlsson, 2001, Abnormal angiogenesis but intact hematopoietic potential in TGF-beta type I receptor-deficient mice: Embo Journal, v. 20, p. 1663-1673.

Lasorella, A., R. Benezra, and A. Iavarone, 2014, The ID proteins: master regulators of cancer stem cells and tumour aggressiveness: Nature Reviews Cancer, v. 14, p. 77-91.

Lazarova, M., and A. Steinle, 2019, Impairment of NKG2D-Mediated Tumor Immunity by TGF-beta: Frontiers in Immunology, v. 10.

Lee, J. J., R. M. Perera, H. Wang, D. C. Wu, X. S. Liu, S. Han, J. Fitamant, P. D. Jones, K. S. Ghanta, S. Kawano, J. M. Nagle, V. Deshpande, Y. Boucher, T. Kato, J. K. Chen, J. K. Willmann, N. Bardeesy, and P. A. Beachy, 2014, Stromal response to Hedgehog signaling restrains pancreatic cancer progression: Proceedings of the National Academy of Sciences of the United States of America, v. 111, p. E3091-E3100.

Lee, J. W., C. A. Komar, F. Bengsch, K. Graham, and G. L. Beatty, 2016, Genetically Engineered Mouse Models of Pancreatic Cancer: The KPC Model (LSL-Kras(G12D/+) ;LSL-Trp53(R172H/+) ;Pdx-1-Cre), Its Variants, and Their Application in Immuno-oncology Drug Discovery: Current protocols in pharmacology, v. 73, p. 14.39.1-14.39.20.

Lekstrom-Himes, J. A., and J. I. Gallin, 2000, Immunodeficiency diseases caused by defects in phagocytes: New England Journal of Medicine, v. 343, p. 1703-1714.

Ley, K., P. Gaehtgens, C. Fennie, M. S. Singer, L. A. Lasky, and S. D. Rosen, 1991, LECTIN-LIKE CELL-ADHESION MOLECULE-1 MEDIATES LEUKOCYTE ROLLING IN MESENTERIC VENULES INVIVO: Blood, v. 77, p. 2553-2555.

Lienart, S., R. Merceron, C. Vanderaa, F. Lambert, D. Colau, J. Stockis, B. van der Woning, H. De Haard, M. Saunders, P. G. Coulie, S. N. Savvides, and S. Lucas, 2018, Structural basis of latent TGF-beta 1 presentation and activation by GARP on human regulatory T cells: Science, v. 362, p. 952-+.

Lin, H. Y., X. F. Wang, E. Ngeaton, R. A. Weinberg, and H. F. Lodish, 1992, EXPRESSION CLONING OF THE TGF-BETA TYPE-II RECEPTOR, A FUNCTIONAL TRANSMEMBRANE SERINE THREONINE KINASE: Cell, v. 68, p. 775-785.

Liu, X. D., Y. Sun, S. N. Constantinescu, E. Karam, R. A. Weinberg, and H. F. Lodish, 1997, Transforming growth factor beta-induced phosphorylation of Smad3 is required for growth inhibition and transcriptional induction in epithelial cells: Proceedings of the National Academy of Sciences of the United States of America, v. 94, p. 10669-10674.

Lood, C., L. P. Blanco, M. M. Purmalek, C. Carmona-Rivera, S. S. De Ravin, C. K. Smith, H. L. Malech, J. A. Ledbetter, K. B. Elkon, and M. J. Kaplan, 2016, Neutrophil extracellular traps enriched in oxidized mitochondrial DNA are interferogenic and contribute to lupus-like disease: Nature Medicine, v. 22, p. 146-153.

Lopezcasillas, F., S. Cheifetz, J. Doody, J. L. Andres, W. S. Lane, and J. Massague, 1991, STRUCTURE AND EXPRESSION OF THE MEMBRANE PROTEOGLYCAN BETAGLYCAN, A COMPONENT OF THE TGF-BETA RECEPTOR SYSTEM: Cell, v. 67, p. 785-795.

Lu, J. L., L. L. Wang, X. L. Liang, X. G. Liu, H. W. Wu, and Z. Y. Liang, 2019, High-molecular-weight hyaluronan produced by activated pancreatic stellate cells promotes pancreatic cancer cell migration via paracrine signaling: Biochemical and Biophysical Research Communications, v. 515, p. 493-498.

Lukasova, E., Z. Koristek, M. Klabusay, V. Ondrej, S. Grigoryev, A. Bacikova, M. Rezacova, M. Falk, J. Vavrova, V. Kohutova, and S. Kozubek, 2013, Granulocyte maturation determines ability to release chromatin NETs and loss of DNA damage response; these properties are absent in immature AML granulocytes: Biochimica Et Biophysica Acta-Molecular Cell Research, v. 1833, p. 767-779.

Mackey, J. B. G., A. J. McFarlane, T. Jamieson, R. Jackstadt, X. L. Raffo-Iraolagoitia, J. Secklehner, X. Cortes-Lavaud, F. Fercoq, W. Clarke, A. Hedley, K. Gilroy, S. Lilla, J. Vuononvirta, G. J. Graham, K. De Filippo, D. J. Murphy, C. W. Steele, J. C. Norman, T. G. Bird, D. A. Mann, J. P. Morton, S. Zanivan, O. J. Sansom, and L. M. Carlin, 2021, Maturation, developmental site, and pathology dictate murine neutrophil function: bioRxiv, p. 2021.07.21.453108.

Maddalena, M., G. Mallel, N. B. Nataraj, M. Shreberk-Shaked, O. Hassin, S. Mukherjee, S. Arandkar, R. Rotkopf, A. Kapsack, G. Lambiase, B. Pellegrino, E. Ben-Isaac, O. Golani, Y. Addadi, E. Hajaj, R. Eilam, R. Straussman, Y. Yarden, M. Lotem, and M. Oren, 2021, TP53 missense mutations in PDAC are associated with enhanced fibrosis and an immunosuppressive microenvironment: Proceedings of the National Academy of Sciences of the United States of America, v. 118.

Mann, K. M., H. Q. Ying, J. Juan, N. A. Jenkins, and N. G. Copeland, 2016, KRAS-related proteins in pancreatic cancer: Pharmacology & Therapeutics, v. 168, p. 29-42.

Mariathasan, S., S. J. Turley, D. Nickles, A. Castiglioni, K. Yuen, Y. L. Wang, E. E. Kadel, H. Koeppen, J. L. Astarita, R. Cubas, S. Jhunjhunwala, R. Banchereau, Y. G. Yang, Y. H. Guan, C. Chalouni, J. Ziai, Y. Senbabaoglu, S. Santoro, D. Sheinson, J. Hung, J. M. Giltnane, A. A. Pierce, K. Mesh, S. Lianoglou, J. Riegler, R. A. D. Carano, P. Eriksson, M. Hoglund, L. Somarriba, D. L. Halligan, M. S. van der Heijden, Y. Loriot, J. E. Rosenberg, L. Fong, I. Mellman, D. S. Chen, M. Green, C. Derleth, G. D.

Fine, P. S. Hegde, R. Bourgon, and T. Powles, 2018, TGF beta attenuates tumour response to PD-L1 blockade by contributing to exclusion of T cells: Nature, v. 554, p. 544-+.

Marone, G., J. T. Schroeder, F. Mattei, S. Loffredo, A. R. Gambardella, R. Poto, A. de Paulis, G. Schiavoni, and G. Varricchi, 2020, Is There a Role for Basophils in Cancer?: Frontiers in Immunology, v. 11.

Martin, C., P. C. E. Burdon, G. Bridger, J. C. Gutierrez-Ramos, T. J. Williams, and S. M. Rankin, 2003, Chemokines acting via CXCR2 and CXCR4 control the release of neutrophils from the bone marrow and their return following senescence: Immunity, v. 19, p. 583-593.

Martinez-Reyes, I., and N. S. Chandel, 2021, Cancer metabolism: looking forward: Nature Reviews Cancer, v. 21, p. 669-680.

Massague, J., 1985, SUBUNIT STRUCTURE OF A HIGH-AFFINITY RECEPTOR FOR TYPE BETA-TRANSFORMING GROWTH-FACTOR - EVIDENCE FOR A DISULFIDE-LINKED GLYCOSYLATED RECEPTOR COMPLEX: Journal of Biological Chemistry, v. 260, p. 7059-7066.

Massague, J., M. P. Czech, K. Iwata, J. E. Delarco, and G. J. Todaro, 1982, AFFINITY LABELING OF A TRANSFORMING GROWTH-FACTOR RECEPTOR THAT DOES NOT INTERACT WITH EPIDERMAL GROWTH-FACTOR: Proceedings of the National Academy of Sciences of the United States of America-Biological Sciences, v. 79, p. 6822-6826.

Massague, J., and B. Like, 1985, CELLULAR RECEPTORS FOR TYPE-BETA TRANSFORMING GROWTH-FACTOR - LIGAND-BINDING AND AFFINITY LABELING IN HUMAN AND RODENT CELL-LINES: Journal of Biological Chemistry, v. 260, p. 2636-2645.

Mathew, E., A. L. Brannon, A. Del Vecchio, P. E. Garcia, M. K. Penny, K. T. Kane, A. Vinta, R. J. Buckanovich, and M. P. di Magliano, 2016, Mesenchymal Stem Cells Promote Pancreatic Tumor Growth by Inducing Alternative Polarization of Macrophages: Neoplasia, v. 18, p. 142-151.

Maurer, C., S. R. Holmstrom, J. He, P. Laise, T. Su, A. Ahmed, H. Hibshoosh, J. A. Chabot, P. E. Oberstein, A. R. Sepulveda, J. M. Genkinger, J. P. Zhang, A. C. Iuga, M. Bansal, A. Califano, and K. P. Olive, 2019, Experimental microdissection enables functional harmonisation of pancreatic cancer subtypes: Gut, v. 68, p. 1034-1043.

McCarroll, J. A., S. Naim, G. Sharbeen, N. Russia, J. Lee, M. Kavallaris, D. Goldstein, and P. A. Phillips, 2014, Role of pancreatic stellate cells in chemoresistance in pancreatic cancer: Frontiers in Physiology, v. 5.

McCarthy, A. J., and R. Chetty, 2018, Smad4/DPC4: Journal of Clinical Pathology, v. 71, p. 661-664.

Melisi, D., R. Garcia-Carbonero, T. Macarulla, D. Pezet, G. Deplanque, M. Fuchs, J. Trojan, H. Oettle, M. Kozloff, A. Cleverly, C. Smith, S. T. Estrem, I. Gueorguieva, M. M. F. Lahn, A. Blunt, K. A. Benhadji, and J. Tabernero, 2018, Galunisertib plus gemcitabine vs. gemcitabine for first-line treatment of patients with unresectable pancreatic cancer: British Journal of Cancer, v. 119, p. 1208-1214.

Miettinen, P. J., R. Ebner, A. R. Lopez, and R. Derynck, 1994, TGF-BETA INDUCED TRANSDIFFERENTIATION OF MAMMARY EPITHELIAL-CELLS TO MESENCHYMAL CELLS - INVOLVEMENT OF TYPE-I RECEPTORS: Journal of Cell Biology, v. 127, p. 2021-2036.

Mishalian, I., R. Bayuh, L. Levy, L. Zolotarov, J. Michaeli, and Z. G. Fridlender, 2013, Tumor-associated neutrophils (TAN) develop pro-tumorigenic properties during tumor progression: Cancer Immunology Immunotherapy, v. 62, p. 1745-1756.

Miyazono, K., S. Moriwaki, T. Ito, A. Kurisaki, M. Asashima, and M. Tanokura, 2018, Hydrophobic patches on SMAD2 and SMAD3 determine selective binding to cofactors: Science Signaling, v. 11.

Moffitt, R. A., R. Marayati, E. L. Flate, K. E. Volmar, S. G. H. Loeza, K. A. Hoadley, N. U. Rashid, L. A. Williams, S. C. Eaton, A. H. Chung, J. K. Smyla, J. M. Anderson, H. J. Kim, D. J. Bentrem, M. S. Talamonti, C. A. Iacobuzio-Donahue, M. A. Hollingsworth, and J. J. Yeh, 2015, Virtual microdissection identifies distinct tumor- and stroma-specific subtypes of pancreatic ductal adenocarcinoma: Nature Genetics, v. 47, p. 1168-+.

Moletta, L., S. Serafini, M. Valmasoni, E. S. Pierobon, A. Ponzoni, and C. Sperti, 2019, Surgery for Recurrent Pancreatic Cancer: Is It Effective?: Cancers, v. 11.

Momand, J., G. P. Zambetti, D. C. Olson, D. George, and A. J. Levine, 1992, THE MDM-2 ONCOGENE PRODUCT FORMS A COMPLEX WITH THE P53 PROTEIN AND INHIBITS P53-MEDIATED TRANSACTIVATION: Cell, v. 69, p. 1237-1245.

Morse, M., S. Chawla, T. Wong, H. Bruckner, F. Hall, and E. Gordon, 2021, Tumor protein p53 mutation in archived tumor samples from a 12-year survivor of stage 4 pancreatic ductal adenocarcinoma may predict long-term survival with DeltaRex-G: A case report and literature review: Molecular and Clinical Oncology, v. 15.

Morton, J. P., Unpublished, Unpublised.

Morton, J. P., P. Timpson, S. A. Karim, R. A. Ridgway, D. Athineos, B. Doyle, N. B. Jamieson, K. A. Oien, A. M. Lowy, V. G. Brunton, M. C. Frame, T. R. J. Evans, and O. J. Sansom, 2010, Mutant p53 drives metastasis and overcomes growth arrest/senescence in pancreatic cancer: Proceedings of the National Academy of Sciences of the United States of America, v. 107, p. 246-251.

Moses, H. L., E. L. Branum, J. A. Proper, and R. A. Robinson, 1981, TRANSFORMING GROWTH-FACTOR PRODUCTION BY CHEMICALLY TRANSFORMED-CELLS: Cancer Research, v. 41, p. 2842-2848.

Moustakas, A., H. Y. Lin, Y. I. Henis, J. Plamondon, M. D. Oconnormccourt, and H. F. Lodish, 1993, THE TRANSFORMING GROWTH-FACTOR BETA-RECEPTORS TYPE-I, TYPE-II, AND TYPE-III FORM HETEROOLIGOMERIC COMPLEXES IN THE PRESENCE OF LIGAND: Journal of Biological Chemistry, v. 268, p. 22215-22218.

Murphy, J. E., J. Y. Wo, D. P. Ryan, J. W. Clark, W. Q. Jiang, B. Y. Yeap, L. C. Drapek, L. Ly, C. V. Baglini, L. S. Blaszkowsky, C. R. Ferrone, A. R. Parikh, C. D. Weekes, R. D. Nipp, E. L. Kwak, J. N. Allen, R. B. Corcoran, D. T. Ting, J. E. Faris, A. X. Zhu, L. Goyal, D. L. Berger, M. Qadan, K. D. Lillemoe, N. Talele, R. K. Jain, T. F. DeLaney, D. G. Duda, Y. Boucher, C. Fernandez-Del Castillo, and T. S. Hong, 2019, Total Neoadjuvant Therapy With FOLFIRINOX in Combination With Losartan Followed by Chemoradiotherapy for Locally Advanced Pancreatic Cancer A Phase 2 Clinical Trial: Jama Oncology, v. 5, p. 1020-1027.

Nagasawa, T., K. Tachibana, and T. Kishimoto, 1998, A novel CXC chemokine PBSF/SDF-1 and its receptor CXCR4: their functions in development, hematopoiesis and HIV infection: Seminars in Immunology, v. 10, p. 179-185.

Nagy, A., G. Munkacsy, and B. Gyorffy, 2021, Pancancer survival analysis of cancer hallmark genes: Scientific Reports, v. 11.

Neesse, A., K. K. Frese, T. E. Bapiro, T. Nakagawa, M. D. Sternlicht, T. W. Seeley, C. Pilarsky, D. I. Jodrell, S. M. Spong, and D. A. Tuveson, 2013,

CTGF antagonism with mAb FG-3019 enhances chemotherapy response without increasing drug delivery in murine ductal pancreas cancer: Proceedings of the National Academy of Sciences of the United States of America, v. 110, p. 12325-12330.

Neoptolemos, J. P., D. H. Palmer, P. Ghaneh, E. E. Psarelli, J. W. Valle, C. M. Halloran, O. Faluyi, D. A. O'Reilly, D. Cunningham, J. Wadsley, S. Darby, T. Meyer, R. Gillmore, A. Anthoney, P. Lind, B. Glimelius, S. Falk, J. R. Izbicki, G. W. Middleton, S. Cummins, P. J. Ross, H. Wasan, A. McDonald, T. Crosby, Y. T. Ma, K. Patel, D. Sherriff, R. Soomal, D. Borg, S. Sothi, P. Hammel, T. Hackert, R. Jackson, M. W. Buchler, and C. European Study Grp Pancreat, 2017, Comparison of adjuvant gemcitabine and capecitabine with gemcitabine monotherapy in patients with resected pancreatic cancer (ESPAC-4): a multicentre, open-label, randomised, phase 3 trial: Lancet, v. 389, p. 1011-1024.

Neuzillet, C., A. Tijeras-Raballand, C. Ragulan, J. Cros, Y. Patil, M. Martinet, M. Erkan, J. Kleeff, J. Wilson, M. Apte, M. Tosolini, A. S. Wilson, F. R. Delvecchio, C. Bousquet, V. Paradis, P. Hammel, A. Sadanandam, and H. M. Kocher, 2019, Inter- and intra-tumoural heterogeneity in cancer-associated fibroblasts of human pancreatic ductal adenocarcinoma: Journal of Pathology, v. 248, p. 51-65.

Ntala, C., S. Debernardi, R. M. Feakins, and T. Crnogorac-Jurcevic, 2018, Demographic, clinical, and pathological features of early onset pancreatic cancer patients: Bmc Gastroenterology, v. 18.

Nywening, T. M., B. A. Belt, D. R. Cullinan, R. Z. Panni, B. J. Han, D. E. Sanford, R. C. Jacobs, J. Ye, A. A. Patel, W. E. Gillanders, R. C. Fields, D. G. DeNardo, W. G. Hawkins, P. Goedegebuure, and D. C. Linehan, 2018, Targeting both tumour-associated CXCR2(+) neutrophils and CCR2(+) macrophages disrupts myeloid recruitment and improves chemotherapeutic responses in pancreatic ductal adenocarcinoma: Gut, v. 67, p. 1112-+.

Oezdemir, B. C., T. Pentcheva-Hoang, J. L. Carstens, X. Zheng, C.-C. Wu, T. R. Simpson, H. Laklai, H. Sugimoto, C. Kahlert, S. V. Novitskiy, A. De Jesus-Acosta, P. Sharma, P. Heidari, U. Mahmood, L. Chin, H. L. Moses, V. M. Weaver, A. Maitra, J. P. Allison, V. S. LeBleu, and R. Kalluri, 2014, Depletion of Carcinoma-Associated Fibroblasts and Fibrosis Induces Immunosuppression and Accelerates Pancreas Cancer with Reduced Survival: Cancer Cell, v. 25, p. 719-734.

Oft, M., K. H. Heider, and H. Beug, 1998, TGF beta signaling is necessary for carcinoma cell invasiveness and metastasis: Current Biology, v. 8, p. 1243-1252.

Ohgushi, M., S. Kuroki, H. Fukamachi, L. A. O'Reilly, K. Kuida, A. Strasser, and S. Yonehara, 2005, Transforming growth factor beta-dependent sequential activation of Smad, Bim, and caspase-9 mediates physiological apoptosis in gastric epithelial cells: Molecular and Cellular Biology, v. 25, p. 10017-10028.

Ohlund, D., A. Handly-Santana, G. Biffi, E. Elyada, A. S. Almeida, M. Ponz-Sarvise, V. Corbo, T. E. Oni, S. A. Hearn, E. J. Lee, I. I. C. Chio, C. I. Hwang, H. Tiriac, L. A. Baker, D. D. Engle, C. Feig, A. Kultti, M. Egeblad, D. T. Fearon, J. M. Crawford, H. Clevers, Y. Park, and D. A. Tuveson, 2017, Distinct populations of inflammatory fibroblasts and myofibroblasts in pancreatic cancer: Journal of Experimental Medicine, v. 214, p. 579-596.

Okamoto, K., and D. Beach, 1994, CYCLIN-G IS A TRANSCRIPTIONAL TARGET OF THE P53 TUMOR-SUPPRESSOR PROTEIN: Embo Journal, v. 13, p. 4816-4822.

Okamoto, K., C. Kamibayashi, M. Serrano, C. Prives, M. C. Mumby, and D. Beach, 1996, p53-dependent association between cyclin G and the B' subunit of protein phosphatase 2A: Molecular and Cellular Biology, v. 16, p. 6593-6602.

Oliner, J. D., J. A. Pietenpol, S. Thiagalingam, J. Gvuris, K. W. Kinzler, and B. Vogelstein, 1993, ONCOPROTEIN MDM2 CONCEALS THE ACTIVATION DOMAIN OF TUMOR SUPPRESSOR-P53: Nature, v. 362, p. 857-860.

Olive, K. P., M. A. Jacobetz, C. J. Davidson, A. Gopinathan, D. McIntyre, D. Honess, B. Madhu, M. A. Goldgraben, M. E. Caldwell, D. Allard, K. K. Frese, G. DeNicola, C. Feig, C. Combs, S. P. Winter, H. Ireland-Zecchini, S. Reichelt, W. J. Howat, A. Chang, M. Dhara, L. Wang, F. Rueckert, R. Gruetzmann, C. Pilarsky, K. Izeradjene, S. R. Hingorani, P. Huang, S. E. Davies, W. Plunkett, M. Egorin, R. H. Hruban, N. Whitebread, K. McGovern, J. Adams, C. Iacobuzio-Donahue, J. Griffiths, and D. A. Tuveson, 2009, Inhibition of Hedgehog Signaling Enhances Delivery of Chemotherapy in a Mouse Model of Pancreatic Cancer: Science, v. 324, p. 1457-1461.

Orecchioni, M., Y. Ghosheh, A. B. Pramod, and K. Ley, 2019, Macrophage Polarization: Different Gene Signatures in M1(LPS+) vs. Classically and M2(LPS-) vs. Alternatively Activated Macrophages: Frontiers in Immunology, v. 10.

Owen-Woods, C., R. Joulia, A. Barkaway, L. Rolas, B. Ma, A. F. Nottebaum, K. P. Arkill, M. Stein, T. Girbl, M. Golding, D. O. Bates, D. Vestweber, M. B. Voisin, and S. Nourshargh, 2020, Local microvascular leakage promotes trafficking of activated neutrophils to remote organs: Journal of Clinical Investigation, v. 130, p. 2301-2318.

Ozanne, B., R. J. Fulton, and P. L. Kaplan, 1980, KIRSTEN MURINE SARCOMA-VIRUS TRANSFORMED-CELL LINES AND A SPONTANEOUSLY TRANSFORMED RAT CELL-LINE PRODUCE TRANSFORMING FACTORS: Journal of Cellular Physiology, v. 105, p. 163-180.

Ozdamar, B., R. Bose, M. Barrios-Rodiles, H. R. Wang, Y. Zhang, and J. L. Wrana, 2005, Regulation of the polarity protein Par6 by TGF beta receptors controls epithelial cell plasticity: Science, v. 307, p. 1603-1609.

PCUK, Signs & Symptoms of Pancreatic Cancer, PCUK.

Peng, J. Y., B. F. Sun, C. Y. Chen, J. Y. Zhou, Y. S. Chen, H. Chen, L. L. Liu, D. Huang, J. L. Jiang, G. S. Cui, Y. Yang, W. Z. Wang, D. Guo, M. H. Dai, J. C. Guo, T. P. Zhang, Q. Liao, Y. Liu, Y. L. Zhao, D. L. Han, Y. P. Zhao, Y. G. Yang, and W. M. Wu, 2019, Single-cell RNA-seq highlights intra-tumoral heterogeneity and malignant progression in pancreatic ductal adenocarcinoma: Cell Research, v. 29, p. 725-738.

Permuth-Wey, J., and K. M. Egan, 2009, Family history is a significant risk factor for pancreatic cancer: results from a systematic review and meta-analysis: Familial Cancer, v. 8, p. 109-117.

Pettazzoni, P., A. Viale, P. Shah, A. Carugo, H. Q. Ying, H. M. Wang, G. Genovese, S. Seth, R. Minelli, T. Green, E. Huang-Hobbs, D. Corti, N. Sanchez, L. Nezi, M. Marchesini, A. Kapoor, W. T. Yao, M. E. Di Francesco, A. Petrocchi, A. K. Deem, K. Scott, S. Colla, G. B. Mills, J. B. Fleming, T. P. Heffernan, P. Jones, C. Toniatti, R. A. DePinho, and G. F. Draetta, 2015, Genetic Events That Limit the Efficacy of MEK and RTK Inhibitor Therapies in a Mouse Model of KRAS-Driven Pancreatic Cancer: Cancer Research, v. 75, p. 1091-1101.

Phillipson, M., B. Heit, P. Colarusso, L. X. Liu, C. M. Ballantyne, and P. Kubes, 2006, Intraluminal crawling of neutrophils to emigration sites: a molecularly

distinct process from adhesion in the recruitment cascade: Journal of Experimental Medicine, v. 203, p. 2569-2575.

Piciucchi, M., S. Stigliano, L. Archibugi, G. Zerboni, M. Signoretti, V. Barucca, R. Valente, G. Delle Fave, and G. Capurso, 2017, The Neutrophil/Lymphocyte Ratio at Diagnosis Is Significantly Associated with Survival in Metastatic Pancreatic Cancer Patients: International Journal of Molecular Sciences, v. 18.

Pickup, M. W., P. Owens, A. E. Gorska, A. Chytil, F. Ye, C. J. Shi, V. M. Weaver, R. Kalluri, H. L. Moses, and S. V. Novitskiy, 2017, Development of Aggressive Pancreatic Ductal Adenocarcinomas Depends on Granulocyte Colony Stimulating Factor Secretion in Carcinoma Cells: Cancer Immunology Research, v. 5, p. 718-729.

Picozzi, V. J., J. M. Pipas, A. Koong, A. Giaccia, N. Bahary, S. S. Krishnamurthi, C. D. Lopez, P. J. O'Dwyer, K. Modelska, M. Carney, H. Hernandez, J. Chou, T. Lee, M. Zhong, S. Porter, T. Neff, and F. Valone, 2014, FG-3019, a human monoclonal antibody to connective tissue growth factor (CTGF), with gemcitabine/erlotinib (G/E) in patients with locally advanced or metastatic pancreatic ductal adenocarcinoma (PDAC): Journal of Clinical Oncology, v. 32.

Pierreux, C. E., F. J. Nicolas, and C. S. Hill, 2000, Transforming growth factor beta-independent shuttling of Smad4 between the cytoplasm and nucleus: Molecular and Cellular Biology, v. 20, p. 9041-9054.

Pillay, J., I. den Braber, N. Vrisekoop, L. M. Kwast, R. J. de Boer, J. A. M. Borghans, K. Tesselaar, and L. Koenderman, 2010, In vivo labeling with (H2O)-H-2 reveals a human neutrophil lifespan of 5.4 days: Blood, v. 116, p. 625-627.

Pillay, J., V. M. Kamp, E. van Hoffen, T. Visser, T. Tak, J. W. Lammers, L. H. Ulfman, L. P. Leenen, P. Pickkers, and L. Koenderman, 2012, A subset of neutrophils in human systemic inflammation inhibits T cell responses through Mac-1: Journal of Clinical Investigation, v. 122, p. 327-336.

Pinho, A. V., M. Van Bulck, L. Chantrill, M. Arshi, T. Sklyarova, D. Herrmann, C. Vennin, D. Gallego-Ortega, A. Mawson, M. Giry-Laterriere, A. Magenau, G. Leuckx, L. Baeyens, A. J. Gill, P. Phillips, P. Timpson, A. V. Biankin, J. M. Wu, and I. Rooman, 2018, ROBO2 is a stroma suppressor gene in the pancreas and acts via TGF-beta signalling: Nature Communications, v. 9.

Pircher, R., P. Jullien, and D. A. Lawrence, 1986, BETA-TRANSFORMING GROWTH-FACTOR IS STORED IN HUMAN-BLOOD PLATELETS AS A LATENT HIGH-MOLECULAR-WEIGHT COMPLEX: Biochemical and Biophysical Research Communications, v. 136, p. 30-37.

Potts, J. D., and R. B. Runyan, 1989, EPITHELIAL MESENCHYMAL CELL-TRANSFORMATION IN THE EMBRYONIC HEART CAN BE MEDIATED, IN PART, BY TRANSFORMING GROWTH FACTOR-BETA: Developmental Biology, v. 134, p. 392-401.

Principe, D. R., B. DeCant, E. Mascarinas, E. A. Wayne, A. M. Diaz, N. Akagi, R. Hwang, B. Pasche, D. W. Dawson, D. Y. Fang, D. J. Bentrem, H. G. Munshi, B. Jung, and P. J. Grippo, 2016, TGF beta Signaling in the Pancreatic Tumor Microenvironment Promotes Fibrosis and Immune Evasion to Facilitate Tumorigenesis: Cancer Research, v. 76, p. 2525-2539.

Principe, D. R., M. Narbutis, S. Kumar, A. Park, N. Viswakarma, M. J. Dorman, S. D. Kamath, P. J. Grippo, M. L. Fishel, R. F. Hwang, D. Thummuri, P. W. Underwood, H. G. Munshi, J. G. Trevino, and A. Rana, 2020, Long-Term Gemcitabine Treatment Reshapes the Pancreatic Tumor Microenvironment

and Sensitizes Murine Carcinoma to Combination Immunotherapy: Cancer Research, v. 80, p. 3101-3115.

Principe, D. R., A. Park, M. J. Dorman, S. Kumar, N. Viswakarma, J. Rubin, C. Torres, R. McKinney, H. G. Munshi, P. J. Grippo, and A. Rana, 2019, TGF beta Blockade Augments PD-1 Inhibition to Promote T-Cell-Mediated Regression of Pancreatic Cancer: Molecular Cancer Therapeutics, v. 18, p. 613-620.

Principe, D. R., and A. Rana, 2020, Updated risk factors to inform early pancreatic cancer screening and identify high risk patients: Cancer Letters, v. 485, p. 56-65.

Provenzano, P. P., C. Cuevas, A. E. Chang, V. K. Goel, D. D. Von Hoff, and S. R. Hingorani, 2012, Enzymatic Targeting of the Stroma Ablates Physical Barriers to Treatment of Pancreatic Ductal Adenocarcinoma: Cancer Cell, v. 21, p. 418-429.

Puleo, F., R. Nicolle, Y. Blum, J. Cros, L. Marisa, P. Demetter, E. Quertinmont, M. Svrcek, N. Elarouci, J. Iovanna, D. Franchimont, L. Verset, M. G. Galdon, J. Deviere, A. de Reynies, P. Laurent-Puig, J. L. Van Laethem, J. B. Bachet, and R. Marechal, 2018, Stratification of Pancreatic Ductal Adenocarcinomas Based on Tumor and Microenvironment Features: Gastroenterology, v. 155, p. 1999-+.

Qin, H. W., L. F. Wang, T. Feng, C. O. Elson, S. A. Niyongere, S. J. Lee, S. L. Reynolds, C. T. Weaver, K. Roarty, R. Serra, E. N. Benveniste, and Y. Z. Cong, 2009, TGF-beta Promotes Th17 Cell Development through Inhibition of SOCS3: Journal of Immunology, v. 183, p. 97-105.

Rawla, P., T. Sunkara, and V. Gaduputi, 2019, Epidemiology of Pancreatic Cancer: Global Trends, Etiology and Risk Factors: World Journal of Oncology, v. 10, p. 10-27.

Rhim, A. D., E. T. Mirek, N. M. Aiello, A. Maitra, J. M. Bailey, F. McAllister, M. Reichert, G. L. Beatty, A. K. Rustgi, R. H. Vonderheide, S. D. Leach, and B. Z. Stanger, 2012, EMT and Dissemination Precede Pancreatic Tumor Formation: Cell, v. 148, p. 349-361.

Rhim, A. D., P. E. Oberstein, D. H. Thomas, E. T. Mirek, C. F. Palermo, S. A. Sastra, E. N. Dekleva, T. Saunders, C. P. Becerra, I. W. Tattersa, C. B. Westphalen, J. Kitajewski, M. G. Fernandez-Barrena, M. E. Fernandez-Zapico, C. Iacobuzio-Donahue, K. P. Olive, and B. Z. Stanger, 2014, Stromal Elements Act to Restrain, Rather Than Support, Pancreatic Ductal Adenocarcinoma: Cancer Cell, v. 25, p. 735-747.

Rice, C. M., L. C. Davies, J. J. Subleski, N. Maio, M. Gonzalez-Cotto, C. Andrews, N. L. Patel, E. M. Palmieri, J. M. Weiss, J. M. Lee, C. M. Annunziata, T. A. Rouault, S. K. Durum, and D. W. McVicar, 2018, Tumour-elicited neutrophils engage mitochondrial metabolism to circumvent nutrient limitations and maintain immune suppression: Nature Communications, v. 9.

Roberts, A. B., M. A. Anzano, L. C. Lamb, J. M. Smith, and M. B. Sporn, 1981, NEW CLASS OF TRANSFORMING GROWTH-FACTORS POTENTIATED BY EPIDERMAL GROWTH-FACTOR - ISOLATION FROM NON-NEOPLASTIC TISSUES: Proceedings of the National Academy of Sciences of the United States of America-Biological Sciences, v. 78, p. 5339-5343.

Roberts, A. B., L. C. Lamb, D. L. Newton, M. B. Sporn, J. E. Delarco, and G. J. Todaro, 1980, TRANSFORMING GROWTH-FACTORS - ISOLATION OF POLYPEPTIDES FROM VIRALLY AND CHEMICALLY TRANSFORMED-CELLS BY ACID-ETHANOL EXTRACTION: Proceedings of the National

Academy of Sciences of the United States of America-Biological Sciences, v. 77, p. 3494-3498.

Rupert, J. E., A. Narasimhan, D. H. A. Jengelley, Y. L. Jiang, J. G. Liu, E. N. Au, L. M. Silverman, G. Sandusky, A. Bonetto, S. Cao, X. Y. Lu, T. M. O'Connell, Y. L. Liu, L. G. Koniaris, and T. A. Zimmers, 2021, Tumor-derived IL-6 and trans-signaling among tumor, fat, and muscle mediate pancreatic cancer cachexia: Journal of Experimental Medicine, v. 218.

Satake, S., H. Hirai, Y. Hayashi, N. Shime, A. Tamura, H. Yao, S. Yoshioka, Y. Miura, T. Inaba, N. Fujita, E. Ashihara, J. Imanishi, T. Sawa, and T. Maekawa, 2012, C/EBP beta Is Involved in the Amplification of Early Granulocyte Precursors during Candidemia-Induced "Emergency" Granulopoiesis: Journal of Immunology, v. 189, p. 4546-4555.

Sawanobori, Y., S. Ueha, M. Kurachi, T. Shimaoka, J. E. Talmadge, J. Abe, Y. Shono, M. Kitabatake, K. Kakimi, N. Mukaida, and K. Matsushima, 2008, Chemokine-mediated rapid turnover of myeloid-derived suppressor cells in tumor-bearing mice: Blood, v. 111, p. 5457-5466.

Schneider, E., A. Schmid-Kotsas, J. S. Zhao, H. Weidenbach, R. M. Schmid, A. Menke, G. Adler, J. Waltenberger, A. Grunert, and M. G. Bachem, 2001, Identification of mediators stimulating proliferation and matrix synthesis of rat pancreatic stellate cells: American Journal of Physiology-Cell Physiology, v. 281, p. C532-C543.

Schonhuber, N., B. Seidler, K. Schuck, C. Veltkamp, C. Schachtler, M. Zukowska, S. Eser, T. B. Feyerabend, M. C. Paul, P. Eser, S. Klein, A. M. Lowy, R. Banerjee, F. Yang, C. L. Lee, E. J. Moding, D. G. Kirsch, A. Scheideler, D. R. Alessi, I. Varela, A. Bradley, A. Kind, A. E. Schnieke, H. R. Rodewald, R. Rad, R. M. Schmid, G. Schneider, and D. Saur, 2014, A next-generation dual-recombinase system for time- and host-specific targeting of pancreatic cancer: Nature Medicine, v. 20, p. 1340-1347.

Seeberger, K. L., J. M. Dufour, A. M. J. Shapiro, J. R. T. Lakey, R. V. Rajotte, and G. S. Korbutt, 2006, Expansion of mesenchymal stem cells from human pancreatic ductal epithelium: Laboratory Investigation, v. 86, p. 141-153.

SEER, 2018, Cancer Stat Facts: Pancreatic Cancer.

Semerad, C. L., M. J. Christopher, F. L. Liu, B. Short, P. J. Simmons, I. Winkler, J. P. Levesque, J. Chappel, F. P. Ross, and D. C. Link, 2005, G-CSF potently inhibits osteoblast activity and CXCL12 mRNA expression in the bone marrow: Blood, v. 106, p. 3020-3027.

Seoane, J., H. V. Le, L. J. Shen, S. A. Anderson, and J. Massague, 2004, Integration of Smad and Forkhead pathways in the control of neuroepithelial and glioblastoma cell proliferation: Cell, v. 117, p. 211-223.

Seoane, J., C. Pouponnot, P. Staller, M. Schader, M. Eilers, and J. Massague, 2001, TGF beta influences Myc, Miz-1 and Smad to control the CDK inhibitor p15(INK4b): Nature Cell Biology, v. 3, p. 400-408.

Shaw, S. K., S. Ma, M. B. Kim, R. M. Rao, C. U. Hartman, R. M. Froio, L. Yang, T. Jones, Y. Liu, A. Nusrat, C. A. Parkos, and F. W. Luscinskas, 2004, Coordinated redistribution of leukocyte LFA-1 and endothelial cell ICAM-1 accompany neutrophil transmigration: Journal of Experimental Medicine, v. 200, p. 1571-1580.

Shek, F. W. T., R. C. Benyon, F. M. Walker, P. R. McCrudden, S. L. F. Pender, E. J. Williams, P. A. Johnson, C. D. Johnson, A. C. Bateman, D. R. Fine, and J. P. Iredale, 2002, Expression of transforming growth factor-beta 1 by pancreatic stellate cells and its implications for matrix secretion and turnover in chronic pancreatitis: American Journal of Pathology, v. 160, p. 1787-1798.

Shi, Y. G., Y. F. Wang, L. Jayaraman, H. J. Yang, J. Massague, and N. P. Pavletich, 1998, Crystal structure of a Smad MH1 domain bound to DNA: Insights on DNA binding in TGF-beta signaling: Cell, v. 94, p. 585-594.

Shull, M. M., I. Ormsby, A. B. Kier, S. Pawlowski, R. J. Diebold, M. Y. Yin, R. Allen, C. Sidman, G. Proetzel, D. Calvin, N. Annunziata, and T. Doetschman, 1992, TARGETED DISRUPTION OF THE MOUSE TRANSFORMING GROWTH FACTOR-BETA-1 GENE RESULTS IN MULTIFOCAL INFLAMMATORY DISEASE: Nature, v. 359, p. 693-699.

Siegel, P. M., W. P. Shu, and J. Massague, 2003, Mad upregulation and Id2 repression accompany transforming growth factor (TGF)-beta-mediated epithelial cell growth suppression: Journal of Biological Chemistry, v. 278, p. 35444-35450.

Smith, M. L., H. U. Kontny, R. Bortnick, and A. J. Fornace, 1997, The p53-regulated cyclin G gene promotes cell growth: p53 downstream effectors cyclin G and GADD45 exert different effects on cisplatin chemosensitivity: Experimental Cell Research, v. 230, p. 61-68.

Smittenaar, C. R., K. A. Petersen, K. Stewart, and N. Moitt, 2016, Cancer incidence and mortality projections in the UK until 2035: British Journal of Cancer, v. 115, p. 1147-1155.

Soucek, L., E. R. Lawlor, D. Soto, K. Shchors, L. B. Swigart, and G. I. Evan, 2007, Mast cells are required for angiogenesis and macroscopic expansion of Myc-induced pancreatic islet tumors: Nature Medicine, v. 13, p. 1211-1218.

Spiegel, A., M. W. Brooks, S. Houshyar, F. Reinhardt, M. Ardolino, E. Fessler, M. B. Chen, J. A. Krall, J. DeCock, I. K. Zervantonakis, A. Iannello, Y. Iwamoto, V. Cortez-Retamozo, R. D. Kamm, M. J. Pittet, D. H. Raulet, and R. A. Weinberg, 2016, Neutrophils Suppress Intraluminal NK Cell-Mediated Tumor Cell Clearance and Enhance Extravasation of Disseminated Carcinoma Cells: Cancer Discovery, v. 6, p. 630-649.

Staller, P., K. Peukert, A. Kiermaier, J. Seoane, J. Lukas, H. Karsunky, T. Moroy, J. Bartek, J. Massague, F. Hanel, and M. Eilers, 2001, Repression of p15(INK4b) expression by Myc through association with Miz-1: Nature Cell Biology, v. 3, p. 392-399.

Steele, C. W., S. A. Karim, J. D. G. Leach, P. Bailey, R. Upstill-Goddard, L. Rishi, M. Foth, S. Bryson, K. McDaid, Z. Wilson, C. Eberlein, J. B. Candido, M. Clarke, C. Nixon, J. Connelly, N. Jamieson, C. R. Carter, F. Balkwill, D. K. Chang, T. R. J. Evans, D. Strathdee, A. V. Biankin, R. J. B. Nibbs, S. T. Barry, O. J. Sansom, and J. P. Morton, 2016, CXCR2 Inhibition Profoundly Suppresses Metastases and Augments Immunotherapy in Pancreatic Ductal Adenocarcinoma: Cancer Cell, v. 29, p. 832-845.

Steele, N. G., G. Biffi, S. B. Kemp, Y. Zhang, D. Drouillard, L. Syu, Y. Hao, T. E. Oni, E. Brosnan, E. Elyada, A. Doshi, C. Hansma, C. Espinoza, A. Abbas, S. The, V. Irizarry-Negron, C. J. Halbrook, N. E. Franks, M. T. Hoffman, K. Brown, E. S. Carpenter, Z. C. Nwosu, C. Johnson, F. Lima, M. A. Anderson, Y. Park, H. C. Crawford, C. A. Lyssiotis, T. L. Frankel, A. Rao, F. Bednar, A. A. Dlugosz, J. B. Preall, D. A. Tuveson, B. L. Allen, and M. P. di Magliano, 2021, Inhibition of Hedgehog Signaling Alters Fibroblast Composition in Pancreatic Cancer: Clinical Cancer Research, v. 27, p. 2023-2037.

Strauss, J., C. R. Heery, J. Schlom, R. A. Madan, L. Cao, Z. G. Kang, E. Lamping, J. L. Marte, R. N. Donahue, I. Grenga, L. Cordes, O. Christensen, L. Mahnke, C. Helwig, and J. L. Gulley, 2018, Phase I Trial of M7824 (MSB0011359C), a Bifunctional Fusion Protein Targeting PD-L1 and TGF beta, in Advanced Solid Tumors: Clinical Cancer Research, v. 24, p. 1287-1295.

Su, J., S. M. Morgani, C. J. David, Q. Wang, E. E. Er, Y. H. Huang, H. Basnet, Y. L. Zou, W. P. Shu, R. K. Soni, R. C. Hendrickson, A. K. Hadjantonakis, and J. Massague, 2020, TGF-beta orchestrates fibrogenic and developmental EMTs via the RAS effector RREB1: Nature, v. 577, p. 566-+.

Sugiyama, T., H. Kohara, M. Noda, and T. Nagasawa, 2006, Maintenance of the hematopoietic stem cell pool by CXCL12-CXCR4 chemokine signaling in bone marrow stromal cell niches: Immunity, v. 25, p. 977-988.

Sumagin, R., H. Prizant, E. Lomakina, R. E. Waugh, and I. H. Sarelius, 2010, LFA-1 and Mac-1 Define Characteristically Different Intralumenal Crawling and Emigration Patterns for Monocytes and Neutrophils In Situ: Journal of Immunology, v. 185, p. 7057-7066.

Sumagin, R., A. Z. Robin, A. Nusrat, and C. A. Parkos, 2014, Transmigrated neutrophils in the intestinal lumen engage ICAM-1 to regulate the epithelial barrier and neutrophil recruitment: Mucosal Immunology, v. 7, p. 905-915.

Sumagin, R., and I. H. Sarelius, 2006, TNF-alpha activation of arterioles and venules alters distribution and levels of ICAM-1 and affects leukocyte-endothelial cell interactions: American Journal of Physiology-Heart and Circulatory Physiology, v. 291, p. H2116-H2125.

Szczerba, B. M., F. Castro-Giner, M. Vetter, I. Krol, S. Gkountela, J. Landin, M. C. Scheidmann, C. Donato, R. Scherrer, J. Singer, C. Beisel, C. Kurzeder, V. Heinzelmann-Schwarz, C. Rochlitz, W. P. Weber, N. Beerenwinkel, and N. Aceto, 2019, Neutrophils escort circulating tumour cells to enable cell cycle progression: Nature, v. 566, p. 553-+.

Sznurkowska, M. K., E. Hannezo, R. Azzarelli, S. Rulands, S. Nestorowa, C. J. Hindley, J. Nichols, B. Gottgens, M. Huch, A. Philpott, and B. D. Simons, 2018, Defining Lineage Potential and Fate Behavior of Precursors during Pancreas Development: Developmental Cell, v. 46, p. 360-+.

Taipale, J., K. Miyazono, C. H. Heldin, and J. Keskioja, 1994, LATENT TRANSFORMING GROWTH-FACTOR-BETA-1 ASSOCIATES TO FIBROBLAST EXTRACELLULAR-MATRIX VIA LATENT TGF-BETA BINDING-PROTEIN: Journal of Cell Biology, v. 124, p. 171-181.

Tak, T., P. Wijten, M. Heeres, P. Pickkers, A. Scholten, A. J. R. Heck, N. Vrisekoop, L. P. Leenen, J. A. M. Borghans, K. Tesselaar, and L. Koenderman, 2017, Human CD62L(dim) neutrophils identified as a separate subset by proteome profiling and in vivo pulse-chase labeling: Blood, v. 129, p. 3476-3485.

Tape, C. J., S. Ling, M. Dimitriadi, K. M. McMahon, J. D. Worboys, H. S. Leong, I. C. Norrie, C. J. Miller, G. Poulogiannis, D. A. Lauffenburger, and C. Jorgensen, 2016, Oncogenic KRAS Regulates Tumor Cell Signaling via Stromal Reciprocation: Cell, v. 165, p. 910-920.

Tauriello, D. V. F., S. Palomo-Ponce, D. Stork, A. Berenguer-Llergo, J. Badia-Ramentol, M. Iglesias, M. Sevillano, S. Ibiza, A. Canellas, X. H. Momblona, D. Byrom, J. A. Matarin, A. Calon, E. I. Rivas, A. R. Nebreda, A. Riera, C. S. O. Attolini, and E. Batlle, 2018, TGF beta drives immune evasion in genetically reconstituted colon cancer metastasis: Nature, v. 554, p. 538-+.

Tian, C. X., K. R. Clauser, D. Ohlund, S. Rickelt, Y. Huang, M. Gupta, D. R. Mani, S. A. Carr, D. A. Tuveson, and R. O. Hynes, 2019, Proteomic analyses of ECM during pancreatic ductal adenocarcinoma progression reveal different contributions by tumor and stromal cells: Proceedings of the National Academy of Sciences of the United States of America, v. 116, p. 19609-19618.

Tjomsland, V., D. Sandnes, E. Pomianowska, S. T. Cizmovic, M. Aasrum, I. J. Brusevold, T. Christoffersen, and I. P. Gladhaug, 2016, The TGF beta-

SMAD3 pathway inhibits IL-1 alpha induced interactions between human pancreatic stellate cells and pancreatic carcinoma cells and restricts cancer cell migration: Journal of Experimental & Clinical Cancer Research, v. 35, p. 12.

Todaro, G. J., C. Fryling, and J. E. Delarco, 1980, TRANSFORMING GROWTH-FACTORS PRODUCED BY CERTAIN HUMAN-TUMOR CELLS - POLYPEPTIDES THAT INTERACT WITH EPIDERMAL GROWTH-FACTOR RECEPTORS: Proceedings of the National Academy of Sciences of the United States of America-Biological Sciences, v. 77, p. 5258-5262.

Tsuda, Y., H. Takahashi, M. Kobayashi, T. Hanafusa, D. N. Herndon, and F. Suzuki, 2004, Three different neutrophil subsets exhibited in mice with different susceptibilities to infection by methicillin-resistant Staphylococcus aureus: Immunity, v. 21, p. 215-226.

Tsukazaki, T., T. A. Chiang, A. F. Davison, L. Attisano, and J. L. Wrana, 1998, SARA, a FYVE domain protein that recruits Smad2 to the TGF beta receptor: Cell, v. 95, p. 779-791.

Tucker, R. F., E. L. Branum, G. D. Shipley, R. J. Ryan, and H. L. Moses, 1984a, SPECIFIC BINDING TO CULTURED-CELLS OF I-125-LABELED TYPE BETA-TRANSFORMING GROWTH-FACTOR FROM HUMAN-PLATELETS: Proceedings of the National Academy of Sciences of the United States of America-Biological Sciences, v. 81, p. 6757-6761.

Tucker, R. F., G. D. Shipley, H. L. Moses, and R. W. Holley, 1984b, GROWTH INHIBITOR FROM BSC-1 CELLS CLOSELY RELATED TO PLATELET TYPE-BETA TRANSFORMING GROWTH-FACTOR: Science, v. 226, p. 705-707.

Van Cutsem, E., M. A. Tempero, D. Sigal, D. Y. Oh, N. Fazio, T. Macarulla, E. Hitre, P. Hammel, A. E. Hendifar, S. E. Bates, C. P. Li, S. R. Hingorani, C. de la Fouchardiere, A. Kasi, V. Heinemann, A. Maraveyas, N. Bahary, L. Layos, V. Sahai, L. Zheng, J. Lacy, J. O. Park, F. Portales, P. Oberstein, W. Wu, D. Chondros, A. J. Bullock, and H. Investigators, 2020, Randomized Phase III Trial of Pegvorhyaluronidase Alfa With Nab-Paclitaxel Plus Gemcitabine for Patients With Hyaluronan-High Metastatic Pancreatic Adenocarcinoma: Journal of Clinical Oncology, v. 38, p. 3185-+.

Varelas, X., R. Sakuma, P. Samavarchi-Tehrani, R. Peerani, B. M. Rao, J. Dembowy, M. B. Yaffe, P. W. Zandstra, and J. L. Wrana, 2008, TAZ controls Smad nucleocytoplasmic shuttling and regulates human embryonic stem-cell self-renewal: Nature Cell Biology, v. 10, p. 837-848.

Varelas, X., P. Samavarchi-Tehrani, M. Narimatsu, A. Weiss, K. Cockburn, B. G. Larsen, J. Rossant, and J. L. Wrana, 2010, The Crumbs Complex Couples Cell Density Sensing to Hippo-Dependent Control of the TGF-beta-SMAD Pathway: Developmental Cell, v. 19, p. 831-844.

Vayrynen, S. A., J. M. Zhang, C. Yuan, J. P. Vayrynen, A. D. Costa, H. Williams, V. Morales-Oyarvide, M. C. Lau, D. A. Rubinson, R. F. Dunne, M. M. Kozak, W. J. Wang, D. Agostini-Vulaj, M. G. Drage, L. Brais, E. Reilly, O. Rahma, T. Clancy, J. P. Wang, D. C. Linehan, A. J. Aguirre, C. S. Fuchs, L. M. Coussens, D. T. Chang, A. C. Koong, A. F. Hezel, S. Ogino, J. A. Nowak, and B. M. Wolpin, 2021, Composition, Spatial Characteristics, and Prognostic Significance of Myeloid Cell Infiltration in Pancreatic Cancer: Clinical Cancer Research, v. 27, p. 1069-1081.

Vennin, C., P. Melenec, R. Rouet, M. Nobis, A. S. Cazet, K. J. Murphy, D. Herrmann, D. A. Reed, M. C. Lucas, S. C. Warren, Z. Elgundi, M. Pinese, G. Kalna, D. Roden, M. Samuel, A. Zaratzian, S. T. Grey, A. Da Silva, W. Leung, S. Mathivanan, Y. X. Wang, A. W. Braithwaite, D. Christ, A. Benda,

A. Parkin, P. A. Phillips, J. M. Whitelock, A. J. Gill, O. J. Sansom, D. R. Croucher, B. L. Parker, M. Pajic, J. P. Morton, T. R. Cox, P. Timpson, A. L. Johns, L. A. Chantrill, A. Chou, A. Steinmann, M. Arshi, T. Dwarte, D. Froio, B. Pereira, S. Ritchie, C. R. Chambers, X. Metcalf, N. Waddell, J. V. Pearson, A. M. Patch, K. Nones, F. Newell, P. Mukhopadhyay, V. Addala, S. Kazakoff, O. Holmes, C. Leonard, S. Wood, S. M. Grimmond, O. Hofmann, A. Christ, T. Bruxner, J. S. Samra, N. Pavlakis, H. A. High, R. Asghari, N. D. Merrett, D. Pavey, A. Das, P. H. Cosman, K. Ismail, C. O'Connnor, A. Stoita, D. Williams, A. Spigellman, V. W. Lam, D. McLeod, J. Kirk, J. G. Kench, P. Grimison, C. L. Cooper, C. Sandroussi, A. Goodwin, R. S. Mead, K. Tucker, L. Andrews, M. Texler, C. Forest, K. P. Epari, M. Ballal, D. R. Fletcher, S. Mukhedkar, N. Zeps, M. Beilin, K. Feeney, N. Q. Nguyen, A. R. Ruszkiewicz, C. Worthley, J. Chen, M. E. Brooke-Smith, V. Papangelis, et al., 2019, CAF hierarchy driven by pancreatic cancer cell p53-status creates a pro-metastatic and chemoresistant environment via perlecan: Nature Communications, v. 10, p. 22.

Vincent, T., E. P. A. Neve, J. R. Johnson, A. Kukalev, F. Rojo, J. Albanell, K. Pietras, I. Virtanen, L. Philipson, P. L. Leopold, R. G. Crystal, A. G. de Herreros, A. Moustakas, R. F. Pettersson, and J. Fuxe, 2009, A SNAIL1-SMAD3/4 transcriptional repressor complex promotes TGF-beta mediated epithelial-mesenchymal transition: Nature Cell Biology, v. 11, p. 943-U84.

Vizan, P., D. S. J. Miller, I. Gori, D. Das, B. Schmierer, and C. S. Hill, 2013, Controlling Long-Term Signaling: Receptor Dynamics Determine Attenuation and Refractory Behavior of the TGF-beta Pathway: Science Signaling, v. 6.

Von Hoff, D. D., T. Ervin, F. P. Arena, E. G. Chiorean, J. Infante, M. Moore, T. Seay, S. A. Tjulandin, W. W. Ma, M. N. Saleh, M. Harris, M. Reni, S. Dowden, D. Laheru, N. Bahary, R. K. Ramanathan, J. Tabernero, M. Hidalgo, D. Goldstein, E. Van Cutsem, X. Y. Wei, J. Iglesias, and M. F. Renschler, 2013, Increased Survival in Pancreatic Cancer with nab-Paclitaxel plus Gemcitabine: New England Journal of Medicine, v. 369, p. 1691-1703.

Vonderheide, R. H., and A. S. Bear, 2020, Tumor-Derived Myeloid Cell Chemoattractants and T Cell Exclusion in Pancreatic Cancer: Frontiers in Immunology, v. 11.

Vonlaufen, A., P. A. Phillips, L. Yang, Z. H. Xu, E. Fiala-Beer, X. G. Zhang, R. C. Pirola, J. S. Wilson, and M. V. Apte, 2010, Isolation of Quiescent Human Pancreatic Stellate Cells: A Promising in vitro Tool for Studies of Human Pancreatic Stellate Cell Biology: Pancreatology, v. 10, p. 434-443.

Waghray, M., M. Yalamanchili, M. Dziubinski, M. Zeinali, M. Erkkinen, H. B. Yang, K. A. Schradle, S. Urs, M. P. Di Magliano, T. H. Welling, P. L. Palmbos, E. V. Abel, V. Sahai, S. Nagrath, L. D. Wang, and D. M. Simeone, 2016, GM-CSF Mediates Mesenchymal-Epithelial Cross-talk in Pancreatic Cancer: Cancer Discovery, v. 6, p. 886-899.

Wang, H. C., J. Z. Liu, G. G. Xia, S. Z. Lei, and X. Y. Huang, 2020, Survival of pancreatic cancer patients is negatively correlated with age at diagnosis: a population-based retrospective study: Scientific Reports, v. 10.

Wang, J. X., A. M. Bair, S. L. King, R. Shnayder, Y. F. Huang, C. C. Shieh, R. J. Soberman, R. C. Fuhlbrigge, and P. A. Nigrovic, 2012, Ly6G ligation blocks recruitment of neutrophils via a beta 2-integrin-dependent mechanism: Blood, v. 120, p. 1489-1498.

Wang, X., L. P. Hu, W. T. Qin, Q. Yang, D. Y. Chen, Q. Li, K. X. Zhou, P. Q. Huang, C. J. Xu, J. Li, L. L. Yao, Y. H. Wang, G. A. Tian, J. Y. Yang, M. W.

Yang, D. J. Liu, Y. W. Sun, S. H. Jiang, X. L. Zhang, and Z. G. Zhang, 2021, Identification of a subset of immunosuppressive P2RX1-negative neutrophils in pancreatic cancer liver metastasis: Nature Communications, v. 12.

Wang, Y. T., Y. W. Gou, W. W. Jin, M. Xiao, and H. Y. Fang, 2016, Association between alcohol intake and the risk of pancreatic cancer: a dose-response meta-analysis of cohort studies: Bmc Cancer, v. 16.

Weller, P. F., and L. A. Spencer, 2017, Functions of tissue-resident eosinophils: Nature Reviews Immunology, v. 17, p. 746-760.

Wenger, C., V. Ellenrieder, B. Alber, U. Lacher, A. Menke, H. Hameister, M. Wilda, T. Iwamura, H. G. Beger, G. Adler, and T. M. Gress, 1999, Expression and differential regulation of connective tissue growth factor in pancreatic cancer cells: Oncogene, v. 18, p. 1073-1080.

Whipple, A. O., W. B. Parsons, and C. R. Mullins, 1935, Treatment of carcinoma of the ampulla of vater: Annals of Surgery, v. 102, p. 763-779.

Wiedenmann, B., W. W. Franke, C. Kuhn, R. Moll, and V. E. Gould, 1986, SYNAPTOPHYSIN - A MARKER PROTEIN FOR NEUROENDOCRINE CELLS AND NEOPLASMS: Proceedings of the National Academy of Sciences of the United States of America, v. 83, p. 3500-3504.

Wierup, N., H. Svensson, H. Mulder, and F. Sundler, 2002, The ghrelin cell: a novel developmentally regulated islet cell in the human pancreas: Regulatory Peptides, v. 107, p. 63-69.

Wojtowicz, S., S. Y. Lee, E. Chan, E. Ng, C. I. Campbell, and G. M. Di Guglielmo, 2020, SMURF2 and SMAD7 induce SARA degradation via the proteasome: Cellular Signalling, v. 72.

Woodfin, A., M. Beyrau, M. B. Voisin, B. Ma, J. R. Whiteford, P. L. Hordijk, N. Hogg, and S. Nourshargh, 2016, ICAM-1-expressing neutrophils exhibit enhanced effector functions in murine models of endotoxemia: Blood, v. 127, p. 898-907.

Woodfin, A., M. B. Voisin, M. Beyrau, B. Colom, D. Caille, F. M. Diapouli, G. B. Nash, T. Chavakis, S. M. Albelda, G. E. Rainger, P. Meda, B. A. Imhof, and S. Nourshargh, 2011, The junctional adhesion molecule JAM-C regulates polarized transendothelial migration of neutrophils in vivo: Nature Immunology, v. 12, p. 761-U145.

Wrana, J. L., L. Attisano, J. Carcamo, A. Zentella, J. Doody, M. Laiho, X. F. Wang, and J. Massague, 1992, TGF-BETA SIGNALS THROUGH A HETEROMERIC PROTEIN-KINASE RECEPTOR COMPLEX: Cell, v. 71, p. 1003-1014.

Wu, R. Y., Y. Zhang, X. H. Feng, and R. Derynck, 1997, Heteromeric and homomeric interactions correlate with signaling activity and functional cooperativity of Smad3 and Smad4/DPC4: Molecular and Cellular Biology, v. 17, p. 2521-2528.

Wu, X. W., J. H. Bayle, D. Olson, and A. J. Levine, 1993, THE P53 MDM-2 AUTOREGULATORY FEEDBACK LOOP: Genes & Development, v. 7, p. 1126-1132.

Xavier, G. D., 2018, The Cells of the Islets of Langerhans: Journal of Clinical Medicine, v. 7.

Xie, X. M., Q. Shi, P. Wu, X. Y. Zhang, H. Kambara, J. Y. Su, H. B. Yu, S. Y. Park, R. X. Guo, Q. Ren, S. D. Zhang, Y. F. Xu, L. E. Silberstein, T. Cheng, F. X. Ma, C. Li, and H. B. R. Luo, 2020, Single-cell transcriptome profiling reveals neutrophil heterogeneity in homeostasis and infection: Nature Immunology, v. 21, p. 1119-+.

Xu, L., Y. B. Kang, S. Col, and J. Massague, 2002, Smad2 nucleocytoplasmic shuttling by nucleoporins CAN/Nup214 and Nup153 feeds TGF beta signaling complexes in the cytoplasm and nucleus: Molecular Cell, v. 10, p. 271-282.

Yagi, K., D. Goto, T. Hamamoto, S. Takenoshita, M. Kato, and K. Miyazono, 1999, Alternatively spliced variant of Smad2 lacking exon 3 - Comparison with wild-type Smad2 and Smad3: Journal of Biological Chemistry, v. 274, p. 703-709.

Yamaguchi, T., S. Ikehara, Y. Akimoto, H. Nakanishi, M. Kume, K. Yamamoto, O. Ohara, and Y. Ikehara, 2019, TGF-beta signaling promotes tube-structure-forming growth in pancreatic duct adenocarcinoma: Scientific Reports, v. 9.

Yamanaka, R., C. Barlow, J. LekstromHimes, L. H. Castilla, P. P. Liu, M. Eckhaus, T. Decker, A. WynshawBoris, and K. G. Xanthopoulos, 1997, Impaired granulopoiesis, myelodysplasia, and early lethality in CCAAT/enhancer binding protein epsilon-deficient mice: Proceedings of the National Academy of Sciences of the United States of America, v. 94, p. 13187-13192.

Yang, J., P. Antin, G. Berx, C. Blanpain, T. Brabletz, M. Bronner, K. Campbell, A. Cano, J. Casanova, G. Christofori, S. Dedhar, R. Derynck, H. L. Ford, J. Fuxe, A. G. de Herreros, G. J. Goodall, A. K. Hadjantonakis, R. J. Y. Huang, C. Kalcheim, R. Kalluri, Y. B. Kang, Y. Khew-Goodall, H. Levine, J. S. Liu, G. D. Longmore, S. A. Mani, J. Massague, R. Mayor, D. McClay, K. E. Mostov, D. F. Newgreen, M. A. Nieto, A. Puisieux, R. Runyan, P. Savagner, B. Stanger, M. P. Stemmler, Y. Takahashi, M. Takeichi, E. Theveneau, J. P. Thiery, E. W. Thompson, R. A. Weinberg, E. D. Williams, J. H. Xing, B. H. P. Zhou, G. J. Sheng, and T. Emt Int Assoc, 2020, Guidelines and definitions for research on epithelial-mesenchymal transition: Nature Reviews Molecular Cell Biology, v. 21, p. 341-352.

Ying, H. Q., K. G. Elpek, A. Vinjamoori, S. M. Zimmerman, G. C. Chu, H. Y. Yan, E. Fletcher-Sananikone, H. L. Zhang, Y. C. Liu, W. Wang, X. J. Ren, H. W. Zheng, A. C. Kimmelman, J. H. Paik, C. Lim, S. R. Perry, S. Jiang, B. Malinn, A. Protopopov, S. Colla, Y. H. Xiao, A. F. Hezel, N. Bardeesy, S. J. Turley, Y. A. A. Wang, L. Chin, S. P. Thayer, and R. A. DePinho, 2011, PTEN Is a Major Tumor Suppressor in Pancreatic Ductal Adenocarcinoma and Regulates an NF-kappa B-Cytokine Network: Cancer Discovery, v. 1, p. 158-169.

Yipp, B. G., and P. Kubes, 2013, Antibodies against neutrophil LY6G do not inhibit leukocyte recruitment in mice in vivo: Blood, v. 121, p. 241-242.

Zea, A. H., P. C. Rodriguez, N. B. Atkins, C. Hernandez, S. Signoretti, J. Zabaleta, D. McDermott, D. Quiceno, A. Youmans, A. O'Neill, J. Mier, and A. C. Ochoa, 2005, Arginase-producing myeloid suppressor cells in renal cell carcinoma patients: A mechanism of tumor evasion: Cancer Research, v. 65, p. 3044-3048.

Zhang, D. E., P. Zhang, N. D. Wang, C. J. Hetherington, G. J. Darlington, and D. G. Tenen, 1997, Absence of granulocyte colony-stimulating factor signaling and neutrophil development in CCAAT enhancer binding protein alpha-deficient mice: Proceedings of the National Academy of Sciences of the United States of America, v. 94, p. 569-574.

Zhang, F., H. S. Wang, X. F. Wang, G. M. Jiang, H. Liu, G. Zhang, H. Wang, R. Fang, X. Z. Bu, S. H. Cai, and J. Du, 2016, TGF-beta induces M2-like macrophage polarization via SNAIL-mediated suppression of a pro-inflammatory phenotype: Oncotarget, v. 7, p. 52294-52306.

Zhang, Y., X. H. Feng, and R. Derynck, 1998, Smad3 and Smad4 cooperate with c-Jun/c-Fos to mediate TGF-beta-induced transcription: Nature, v. 394, p. 909-913.

Zhang, Y. Q., J. Lazarus, N. G. Steele, W. Yan, H. J. Lee, Z. C. Nwosu, C. J. Halbrook, R. E. Menjivar, S. B. Kemp, V. R. Sirihorachai, A. Velez-Delgado, K. Donahue, E. S. Carpenter, K. L. Brown, V. Irizarry-Negron, A. C. Nevison, A. Vinta, M. A. Anderson, H. C. Crawford, C. A. Lyssiotis, T. L. Frankel, F. Bednar, and M. P. di Magliano, 2020, Regulatory T-cell Depletion Alters the Tumor Microenvironment and Accelerates Pancreatic Carcinogenesis: Cancer Discovery, v. 10, p. 422-439.

Zhao, Z. W., Z. F. Yin, Z. S. Pu, and Q. C. Zhao, 2017, Association Between Consumption of Red and Processed Meat and Pancreatic Cancer Risk: A Systematic Review and Meta-analysis: Clinical Gastroenterology and Hepatology, v. 15, p. 486-+.

Zheng, B., Z. P. Zhang, C. M. Black, B. de Crombrugghe, and C. P. Denton, 2002a, Ligand-dependent genetic recombination in fibroblasts - A potentially powerful technique for investigating gene function in fibrosis: American Journal of Pathology, v. 160, p. 1609-1617.

Zheng, S. G., J. D. Gray, K. Ohtsuka, S. Yamagiwa, and D. A. Horwitz, 2002b, Generation ex vivo of TGF-beta-producing regulatory T cells from CD4(+)CD25(-) precursors: Journal of Immunology, v. 169, p. 4183-4189.

Zheng, X. F., J. L. Carstens, J. Kim, M. Scheible, J. Kaye, H. Sugimoto, C. C. Wu, V. S. LeBleu, and R. Kalluri, 2015, Epithelial-to-mesenchymal transition is dispensable for metastasis but induces chemoresistance in pancreatic cancer: Nature, v. 527, p. 525-+.

Zhu, Y., J. M. Herndon, D. K. Sojka, K. W. Kim, B. L. Knolhoff, C. Zuo, D. R. Cullinan, J. Q. Luo, A. R. Bearden, K. J. Lavine, W. M. Yokoyama, W. G. Hawkins, R. C. Fields, G. J. Randolph, and D. G. DeNardo, 2017, Tissue-Resident Macrophages in Pancreatic Ductal Adenocarcinoma Originate from Embryonic Hematopoiesis and Promote Tumor Progression: Immunity, v. 47, p. 323-+.

Zhu, Y., L. Padgett, H. Q. Dinh, P. Marcovecchio, A. Blatchley, R. P. Wu, E. Ehinger, C. Kim, Z. Mikulski, G. Seumois, A. Madrigal, P. Vijayanand, and C. C. Hedrick, 2018, Identification of an Early Unipotent Neutrophil Progenitor with Pro-tumoral Activity in Mouse and Human Bone Marrow: Cell Reports, v. 24, p. 2329-+.